Hepatocyte-specific drug delivery using active targeted nanomedicines - evaluation of targeting strategies *in vitro* and *in vivo*

Inauguraldissertation

zur

Erlangung der Würde eines Doktors der Philosophie

vorgelegt der

Philosophisch-Naturwissenschaftlichen Fakultät

der Universität Basel

von

Dominik Witzigmann

aus Deutschland

Basel, 2017

Genehmigt von der Philosophisch-Naturwissenschaftlichen Fakultät

auf Antrag von

Prof. Dr. Jörg Huwyler

Prof. Dr. Andreas Zumbühl

Basel, den 19. April 2016

Prof. Dr. Jörg Schibler (Dekan)

“Research is to see what everybody else has seen, and to think what nobody else has thought.”

Albert Szent-Gyorgyi

TABLE OF CONTENTS

ZUSAMMENFASSUNG FÜR LAIEN

Lebererkrankungen betreffen weltweit Millionen von Menschen und die Anzahl der Neuerkrankungen steigt stetig. Während sich die Überlebensraten für die meisten Krankheiten in den letzten Jahrzehnten verbessert haben, stellen Lebererkrankungen nach wie vor eine erhebliche Belastung für das Gesundheitssystem dar. Gegenwärtige Therapien bei Erkrankungen der Leberzellen (Hepatozyten) sind unzureichend und behandeln in den meisten Fällen nur die Symptome. Daher sind verbesserte Therapiemöglichkeiten dringend erforderlich. Der zielgerichtete Einsatz von Nanopartikeln für den Transport von Wirkstoffen oder genetischem Material zu einem bestimmten Zelltyp hat das Potenzial, den Mangel an zufriedenstellenden und alternativen Behandlungsmöglichkeiten zu überwinden. Diese Doktorarbeit hat sich auf die Entwicklung von neuartigen, nanomedizinischen Ansätzen für den gezielten Arzneimitteltransport zu Hepatozyten spezialisiert (Schlüssel-Schloss-Prinzip). Diese Technologien bieten die Möglichkeit, Medikamente spezifisch zu Leberzellen zu transportieren und damit einen bestimmten Zelltyp in der Leber anzusteuern. Das Projekt bestand aus zwei Hauptzielen, die wie folgt zusammengefasst werden können:

Erstens wurden Strategien für eine spezifische und hochselektive Arzneimittelabgabe an Hepatozyten über den Asialoglycoproteinrezeptor (Schloss) untersucht. Dieser Rezeptor wird in großem Ausmaß und fast ausschließlich auf Hepatozyten gebildet. Nach der spezifischen Bindung von Nanopartikeln (Arzneimittel-Transportsystem) an den Ziel-Rezeptor (Schlüssel-Schloss-Prinzip) werden die Nanopartikel in die Leberzellen aufgenommen. Um herauszufinden ob diese gezielte Therapie prinzipiell möglich ist, wurde die Häufigkeit des Zielrezeptors auf Hepatozyten untersucht.

Dazu wurden mehrere menschliche Leberzelllinien und Gewebeproben von Patienten, welche an verschiedenen Lebererkrankungen leiden, untersucht. Um die Durchführbarkeit einer zielgerichteten nanomedizinischen Therapie aufzuzeigen, wurden Nanopartikel auf der Oberfläche mit Glycoproteinen (Schlüssel) modifiziert und dann in menschlichen Zellen (*in vitro*) und in lebenden Organismen (*in vivo*) getestet. Um die Arzneimittel-Transport-Systeme weiter zu verbessern, wurden zusätzliche von Glycoproteinen abgeleitete Liganden (Schlüssel), wie z.B. komplexe Kohlenhydrate oder einfache Zucker, untersucht. Um zu untersuchen wie Nanopartikel in Zellen aufgenommen und dann weiter transportiert werden, wurden darüber hinaus neue Technologien entwickelt.

Zweitens wurden neuartige Nanopartikel für eine verbesserte Beladung mit genetischem Material (Erbgut) entwickelt um dieses gezielt zu bestimmten Zellen zu transportieren. Der Fokus dabei waren Nanomaterialien, die sich für eine intravenöse Verabreichung in Patienten eignen. Dazu wurden die physikalisch-chemischen Eigenschaften der mit Erbgut-beladenen-Nanopartikel charakterisiert und die effektive und sichere Einbringung von genetischem Material in menschlichen Zellen getestet.

Zusammengefasst war diese Doktorarbeit der erste Schritt zur Entwicklung neuartiger Hepatozyten-spezifischer Nanopartikel, welche die eingeschlossenen Wirkstoffe schützen und den zellspezifischen Transport effizient und ohne Nebenwirkungen ermöglichen. Diese Strategie ist von großem Interesse für diagnostische und therapeutische Anwendungen bei der Behandlung einer Vielzahl von Lebererkrankungen.

SUMMARY

Hepatic disorders affect millions of people around the globe and incidence rates are further increasing. While survival rates have improved for most diseases during recent decades, liver diseases still represent a considerable public health burden. Current therapies for diseases of hepatocytes are limited and in most cases only treat symptoms. Therefore, improved therapeutic technologies are urgently needed. Targeted nanomedicines for the delivery of small molecules or nucleic acids have the potential to overcome the lack of satisfactory and alternative treatment options. This PhD project focused on the development of novel nanomedicines for targeted drug delivery to liver parenchymal cells. These technologies offer the possibility to specifically target drugs to hepatocytes, thus giving access to a defined cell type within the liver. The project consisted of two major objectives, which can be summarized as follows:

First, targeting approaches for specific and highly selective drug delivery to hepatocytes via the asialoglycoprotein receptor (ASGPR) were evaluated. This receptor is abundantly and almost exclusively expressed on hepatocytes. After binding to its target, the drug delivery system is internalized by receptor-mediated endocytosis. The applicability of this targeting approach was evaluated by analysis of ASGPR expression. Human tissue samples from patients suffering from various liver diseases and several liver-derived cell lines were analyzed. As a proof-of-concept study, asialofetuin-conjugated liposomal drug carriers were designed and tested *in vitro* and *in vivo*. To further improve ASGPR-specific nanocarriers, glycoprotein derived targeting ligands including multiantennary glycans and monovalent sugars were evaluated. Furthermore, novel technologies were developed to investigate the uptake mechanisms and the intracellular fate of nanocarriers.

Second, in order to develop nucleic acid delivery systems, new nanomaterials for an optimized loading and retention of DNA expression plasmids were evaluated. The focus were nanomaterials applicable for a systemic administration *in vivo*. The physico-chemical properties were characterized and the plasmid DNA nanoparticles were screened for efficient and safe transfection activity *in vitro*.

In summary, this PhD project was the first step towards the development of novel hepatocyte-targeted nanocarriers, which protect encapsulated drugs and facilitate the cell-specific delivery efficiently and with low cytotoxicity. This strategy is of great interest for diagnostic and therapeutic medical applications in the treatment of liver disorders.

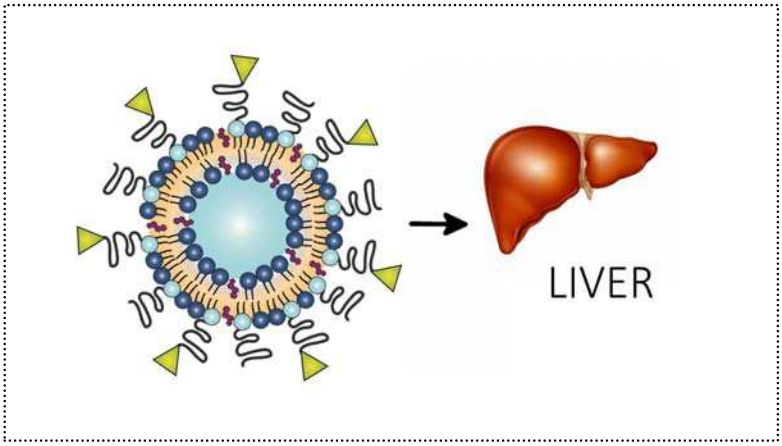

INTRODUCTION

I. LIVER

1. Liver Structure and Different Cell Types

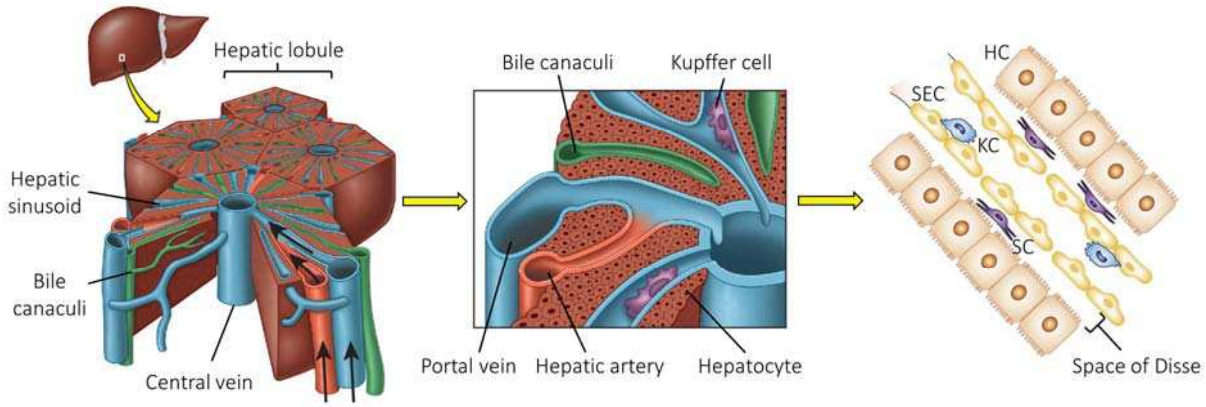

Figure 1: Structure of liver lobules. The hepatic lobule is the functional unit of the liver. Each lobule receives blood from the portal vein and the hepatic artery, which terminate in the hepatic sinusoids. The bile canaculi transport bile from the liver to the gut. Sinusoidal endothelial cells (SEC) line the blood vessels. Tissue-resident macrophages, i.e., Kupffer cells (KC), are interspersed in the lumen of hepatic sinusoids. Stellate cells (SC) are located in the perisinusoidal space of Disse. Hepatocytes (HC) form the liver parenchyma. Figures are adapted from Mosby and Lau *et al.* [1,2]

1.1. Liver

Due to its wide range of functions, the liver is one of the most interesting organs in the human body (estimated total number of 500 functions). [3–5] It is the key organ for metabolism and clearance of endo- and exogenous substances. In addition, the liver is responsible for storage (e.g., proteins, fats, vitamins, iron), protein production (e.g., clotting factors), cholesterol homeostasis

or immune responses. The hexagonal formed liver lobules are the functional units responsible for the different functions. [6] Liver lobules are supplied with oxygen and nutrients by peripheral blood from the hepatic artery and the portal vein, which is transported through liver capillaries (i.e., sinusoids) to the central vein (Figure 1). [7,8] Each liver lobule consists of parenchymal (i.e., hepatocytes, HC) and non-parenchymal liver cells including sinusoidal endothelial cells (SEC), hepatic macrophages (Kupffer cells, KC), and stellate cells (ito cells, SC). All cell types will be discussed in detail in the next sections.

1.2. Hepatocytes

Hepatocytes, also called liver parenchymal cells, are located behind the space of Disse separated from the blood by the sinusoids (Figure 1). They represent approximately 70–80% of all cells in the liver and have many essential functions including protein synthesis, transformation of carbohydrates or metabolism of xenobiotics. [9] The average lifespan of hepatocytes is around 150 days. Hepatocytes are highly differentiated and exhibit a polarized structure. They have a basolateral (sinusoidal) membrane facing the sinusoidal space, an apical side towards the bile canaliculi and a lateral surface connecting adjacent parenchymal cells. The basolateral membrane of hepatocytes has a large amount of microvilli, therefore increasing the perisinusoidal surface for absorptive processes (Figure 2). Besides the functional importance for the human body, the liver parenchymal cells are considered as key pro-pathogenic cell type for many disorders. A summary of different hepatic diseases, their frequencies, and the therapeutic strategies are discussed in "Section 2".

1.3. Sinusoidal Endothelial Cells

The endothelial wall of hepatic blood vessels consists of sinusoidal endothelial cells (SEC) (Figure 1). These cells have important morphological and physiological characteristics, which are

essential for hepatic metabolism as well as nanoparticulate drug delivery to hepatocytes. During the last three decades, Wisse and colleagues have revealed many of these structural and functional aspects. [10–14] Importantly, SEC form open pores in the sinusoidal wall, so-called liver fenestrae, which allow the exchange of various substances between the blood and parenchymal liver cells via the space of Disse. [12] These pores have a size of approximately 100–200 nm in diameter and they are arranged as groups of fenestrae, i.e., liver sieve plates (Figure 2). The precise diameter and number of hepatic fenestrae in different species are represented in Table 1 and compared to fenestrations in other organs/tissues. However, these fenestrae parameters might show inter- and intraindividual variations due to drug induced effects or pathological conditions. [15,16]

Table 1: Fenestrations of the vasculature. Fenestrations in hepatic blood vessels are given for different species. In addition, the fenestrations of vasculature in other organs or pathological tissues are given for comparison. The table is adapted from Braet *et al.* and Gaumet *et al.* [10,17]

Species / Organ	Diameter [nm]	Ref.
Hepatocytes		
. Human	50 – 300	18
. Rat	98.0 ± 13.0	19
. Mouse	99.0 ± 18.0	20
. Rabbit	59.4 ± 4.8	21
Other Organs/Tissues		
. Kidney (rat, rabbit, guinea pig)	20 – 30	22,23
. Spleen (mice)	150	24,25
. Bone marrow (rat, rabbit, guinea-pig)	85 – 150	26
. Skeletal, cardiac and smooth muscle (mice)	< 6	27
. Tumor (mice)	200 – 780	28,29
. Inflamed organs (hamster)	80 – 1400	30

In general, around 6–8% of the sinusoidal surface is fenestrated, therefore giving blood components, which are smaller than these pores, direct access to hepatocytes. Recently, among many other proposed mechanisms, elevated serum cholesterol levels leading to the development of

atherosclerosis have been related to decreased fenestrae size. [19,21,31] In general, chylomicron remnants can pass liver fenestrae, whereas large triglyceride-rich chylomicrons are held back in circulation. However, if the sieving capacity is impaired, the blood clearance of chylomicron remnants by hepatocytes is limited. Therefore, several compounds have been investigated to increase the pore size of fenestrae and thus influence the physiological access of lipoproteins to hepatocytes. [10] In case of hepatic drug targeting, these pore-opening substances offer interesting therapeutic possibilities to modulate the liver fenestration and thus enhance the delivery of nanoparticles to parenchymal liver cells.

1.4. Kupffer Cells

Resident liver macrophages were first described by Carl von Kupffer. [32] Circulating monocytes derived from bone marrow differentiate into liver resident macrophages, so-called Kupffer cells. These cells are members of the mononuclear phagocyte system (MPS) (or reticuloendothelial system, RES) and comprise more than 80% of the total population of tissue macrophages in the body. [7,33] They are located in the lumen of hepatic sinusoids in close proximity to sinusoidal endothelial cells (Figure 1/2). Due to their prominent location in the body, they are involved in various immunological and inflammatory processes. [34] Their endocytic activity is important for host defense and elimination of particulate and foreign materials including nanoparticles. Periportal-located Kupffer cells are more abundant, possess a greater phagocytic potential and have a higher lysosomal enzyme activity as compared to perivenous/midzonal-located Kupffer cells. [35] Kupffer cell uptake is mainly mediated by three mechanisms. [36] First, scavenger receptors are activated by several factors including highly charged nanoparticles, thus triggering endocytosis. Second, carbohydrate receptors including the mannose receptor initiate phagocytosis after ligand recognition. Third, nanoparticles, which have been coated in circulation by complement

factors (e.g., C3b or C1q) or serum opsonins such as fibronectin, will be cleared by Kupffer cells. In order to eliminate unwanted nanoparticle clearance, clodronate loaded liposomes can be injected *in vivo* for the eradication of Kupffer cells. [37,38]

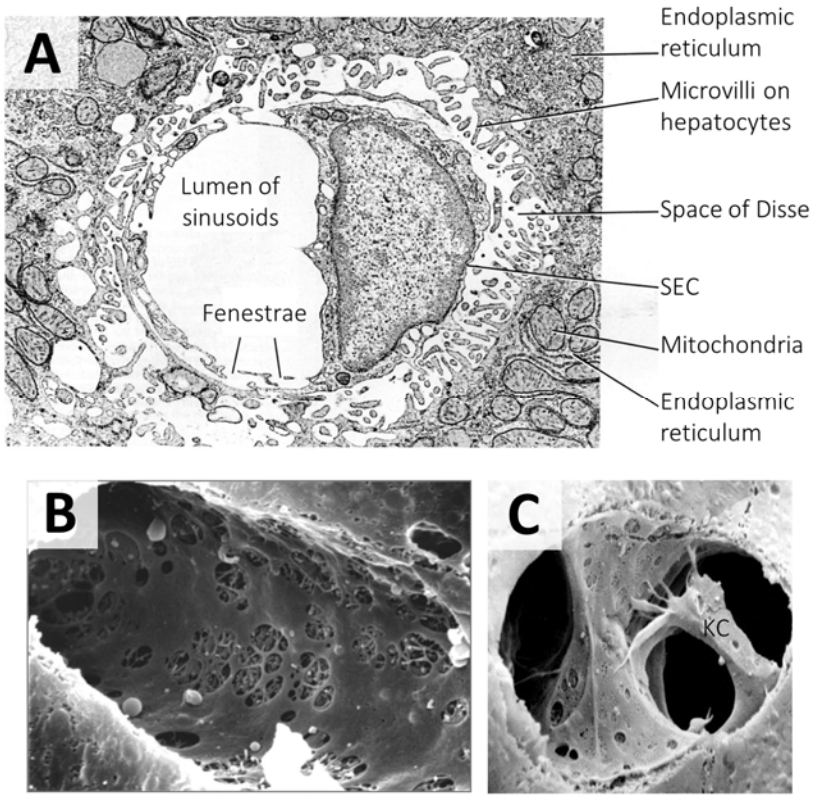

Figure 2: Liver Sinusoids. (A) Cross section of liver sinusoid, which is lined by sinusoidal endothelial cells (SEC). Microvilli on hepatocytes are exposed towards the space of Disse. (B) Lumen of hepatic sinusoid with fenestrated endothelium forming sieve plates. (C) Kupffer cell (KC) located in the lumen of hepatic sinusoids in close proximity to SEC. Figures are adapted from Cormack *et al.,* Vollmar *et al.* and missinglink.ucsf.edu. [39–41]

1.5. Stellate Cells

Hepatic stellate cells (SC) are star-shaped cells located in the perisinusoidal space of Disse between the sinusoidal endothelial cell wall and parenchymal liver cells (Figure 1). [8] In literature, there are several different names for this cell type including parasinusoidal cells, Ito cells, vitamin A

storing cells, or lipid-storing cells. [42] Two different types of stellate cells can be distinguished, a quiescent and an activated/transdifferentiated form. [43] In a normal and healthy liver the main function of stellate cells is the storage of vitamin A (retinol), which is essential for several growth and differentiation processes in the body. Upon liver damage, several mediators induce the differentiation of stellate cells into a myofibroblast-like cell type with diverse phenotypic changes. [44]

Platelet-derived growth factor (PDGF) and transforming growth factor beta (TGF-β) are the most important activators stimulating proliferation and fibrogenesis, respectively. The normal extracellular matrix remodeling changes qualitatively as well as quantitatively. Activated stellate cells produce excessive amounts of connective scar tissue (especially collagen type 1) and in addition secrete tissue inhibitors of matrix metalloproteinases (i.e., TIMP-1 and TIMP-2). The replacement of normal hepatic tissue with a scar-like matrix finally leads to fibrosis and therefore impairment of the physiological transendothelial transport in the liver (Figure 3).

2. Hepatocyte-related Diseases and Their Therapy

Hepatocytes are the key pro-pathogenic cell type within the liver implicated in various diseases. Hepatocellular carcinoma, viral and parasitic infections, or genetic disorders affect millions of people worldwide and incidence rates are further increasing (Figure 3). A list of hepatocyte-related liver diseases is shown in Table 2.

One example from each group is described in more detail in the following sections. These summaries also highlight the increasing need for alternative and improved treatment options. The targeted delivery of small molecules (e.g., with poor pharmacokinetic properties) or nucleic acids (where the pharmacological effect is dependent on cellular uptake) offers a promising strategy for therapeutic interventions of these diseases.

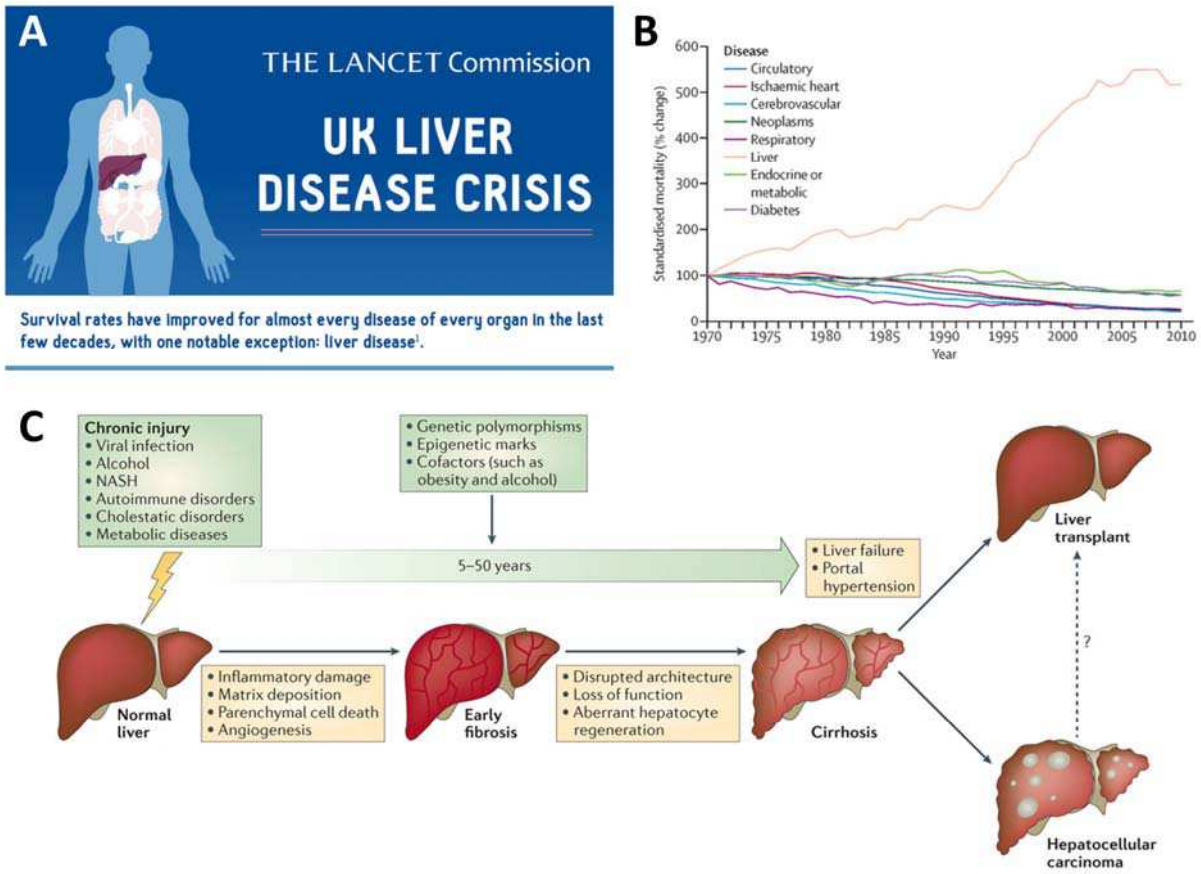

Figure 3: Liver diseases. (A) During the last decades, the lack of efficient therapeutic options has resulted in a strong increase in liver disease rates and mortality (exemplified for the UK). Cirrhosis, liver cancer and acute hepatitis caused more than 2 million deaths worldwide in 2010. (B) While survival rates have improved for most diseases during the last decades, liver diseases are on the rise and still represent a considerable public health burden. (C) The initiation and development of hepatocellular carcinoma is a multistep process occurring over years. Liver transplantation is still the only available option for many incurable or late-stage liver diseases. Figures are adapted from Williams *et al.* and Pellicoro *et al.* [45,46]

Table 2: Summary of hepatocyte-related diseases. Hepatocytes are the key pathogenic cell type for many liver disorders including liver cancer, viral or parasitic infections, and genetic diseases. Different diseases are summarized and current treatment options are indicated.

Disease	Pathophysiology / Mechanism	Symptoms	Treatment	Prevalence [47]	Ref.
Cancer					
Hepatocellular Carcinoma (HCC)	Chronic liver inflammation - cirrhosis - HCC	Liver damage, liver cancer	Curative or palliative treatment	16:100,000 and > 700,000 new cases per year	[48–50]
Viral Infections					
Hepatitis B	Hepatitis B Virus (HBV) infection	Liver damage, cirrhosis, HCC	Interferon α, nucleos(t)ide	350 million chronic carriers	[51–54]
Hepatitis C	Hepatitis C Virus (HCV) infection	Liver damage, cirrhosis, HCC	Interferon α, protease inhibitors	180 million chronic carriers	[51,55]
Parasitic Infections					
Malaria	Plasmodium vivax / Plasmodium ovale	Fever, severe anemia, renal failure	Primaquine, chloroquine	70–390 million cases per year	[56–59]
Genetic Disease (without parenchymal damage)					
Bilirubin metabolism disorders (e.g., Crigler-Najjar syndrome 1)	Uridine diphosphate glucuronosyltransferase (UGT1A1) deficiency - impairment of bilirubin conjugation	Neurological damage; kern-icterus (bilirubin encephalopathy)	Phototherapy (10–12h per day); Plasma exchange	< 1:1,000,000	[60,61]
Urea cycle disorders (e.g., OTC deficiency)	Ornithine transcarbamylase (OTC) deficiency [many other deficiencies such as Argininosuccinate synthetase (ASS; Citrullin-aemia), N-acetyl glutamate synthetase (NAGS), Carba-moylphosphate synthetase (CPS), Arginase (ARG)]	Hyperammo-nemia; neuro-logical damage	Nitrogen scavenger therapy, hemodialysis	OTC: 1:80,000	[62,63]
TTR Familial amyloid polyneuropathy (FAP)	Transthyretin mutation - deposition of insoluble protein	Neurodegene-ration, poly-neuropathy	Small mole-cule drugs (tafamidis)	< 1:100,000, >in some countries	[64,65]
Primary hyperoxaluria type 1	Alanine glyoxylate aminotransferase mutation	Calcium oxalate accumulation, kidney damage	High fluid intake, kid-ney trans-plantation	1:333,000–1,000,000	[62,66]
Familial Hyperchol-esterolemia (e.g., LDL receptor related)	LDL receptor protein mutation [also ApoB or PCSK9 mutations]	Coronary artery disease	Statins, LDL apheresis	Homozygous <10:1,000,000 Hetero: 1:500	[67,68]
Hemophilia disorders (e.g., Hemophilia B)	Factor IX deficiency [other coagulation factor mutations A and C]	Blood clotting disorder, hemorrhage	i.v. infusion of coagu-lation factor	1:20,000	[69,70]
Thrombotic disorders (e.g., Protein C deficiency type 1)	Thrombotic disease caused by PROC gene mutation [also other inherited thrombophilias]	Risk of thrombosis	Thrombo-embolism, protein C substitution	1:500,000–750,000	[71,72]

(continued on next page)

Table 2 (continued)

Disease	Pathophysiology / Mechanism	Symptoms	Treatment	Prevalence [47]	Ref.
Genetic Disease (with parenchymal damage)					
α1-antitrypsin deficiency	Mutations in the SERPINA1 gene; deficiency in protease inhibitor for neutrophil elastase	Lung and liver damage	Augmen-tation; replacement therapy	1–5:10,000	[73,74]
Wilson´s disease	Copper-transport P-type ATPase deficiency, Copper accumulation	Liver and neuro-logical damage	Copper complexation	1:30,000–100,000 individuals	[75,76]
Iron overload disorder (e.g., Hereditary hemo-chromatosis type 1)	HFE enzyme deficiency [other iron dysregulation; Type 2: HFE2 or HAMP (hepcidin); Type 3: TFR2 (transferrin receptor 2); Type 4: SLC40A1 (ferroportin)]	Liver cirrhosis, insulin resistance	Phlebotomy, iron-chelating	Type 1: >1:1,000 Type 2/3/4: < 1 : 1,000,000	[77,78]
Tyrosinemia disorders (e.g., Tyrosinemia type 1)	Fumarylacetoacetate hydrolase (FAH) deficiency - lack of tyrosine degra-dation [other types with enzyme deficiency in tyrosine metabolism]	Hepatomegaly, liver and kidney dysfunction	Nitisinone (inhibition of tyrosine degradation)	1:100,000	[79,80]
Glycogen storage diseases (GSD) (e.g., Pompe´s disease)	Various types of enzyme deficiencies in glycogen synthesis	Hepatomegaly, hypoglycemia	Treatments depending on type	1:50,000–1,000,000	[81,82]

2.1. Hepatocellular Carcinoma

Hepatocellular carcinoma (HCC) is one of the most common cancers worldwide. [7] More than 700´000 new cases are reported each year, with increasing incidence during the last two decades. [49,50] Due to its poor prognosis, HCC is the third most common cause of cancer-related deaths. The most frequent risk factors for HCC are chronic viral infections, i.e., HBV and HCV, which account for approximately 80% of all cases. [51] Patients with cirrhosis are at the highest risk to develop HCC. Other risk factors are alcohol abuse, toxins (e.g., aflatoxin B1), or genetic liver disorders including hereditary hemochromatosis, Wilson´s disease, or α1-antitrypsin deficiency. [48] The development of HCC is a complex multistep and multifactorial process (Figure 3C). [50]

Depending on the stage of HCC different curative or palliative treatment options are available. The Barcelona Clinic Liver Cancer (BCLC) strategy establishes treatment recommendations for all five stages of HCC. [50] In early stages three treatment options are recommended including surgical resection, liver transplantation, or ablation. The most frequently used form of local ablation therapy is radiofrequency ablation (RFA). Alternatively, injection of chemicals (e.g., ethanol) or other physical methods (e.g., microwave, cryoablation) can be used to induce tumor necrosis. For intermediate stages of HCC, only palliative treatment options are available. Transarterial chemoembolization (TACE) is the method of choice. Microparticles coated with chemotherapeutic agents are used to obstruct the arterial blood supply of the tumor and thus induce ischemic tumor necrosis. The multikinase inhibitor sorafenib is the only first-line therapeutic option for advanced stages of HCC. Many other antiproliferative and antiangiogenic compounds or biologicals are currently investigated in clinical trials. The discovery of biomarkers for early detection of HCC is an increasing field of research. Thus, therapeutic regimens could be personalized and clinical outcomes might be improved.

2.2. Infections

- *Viruses (Hepatitis B Virus)*

Hepatitis B virus (HBV) infection is one of the major causes for the development of cirrhosis and liver cancer. Approximately 50% of all HCC cases are caused by chronic HBV infection. [50] More than 350 million people are chronically infected worldwide and around 800´000 people die each year due to HBV infection. [54] There are three major modes of transmission: first, transmission from HBV-infected mothers to their newborn, second, sexual transmission, and third, transmission via blood caused by blood transfusions, dialysis, or contaminated needles (e.g., drug abuse). [53] HBV

infection can be prevented efficiently by avoidance of transmission or vaccination. However, the global vaccination coverage strongly varies. Thus, a total number of around 2 billion people have been infected worldwide (17.5% are still chronically infected) and almost 100´000 new cases are reported each year. [54] One of the reasons for these high numbers is the high infectious potential of the HBV. It has been reported that 1–10 virus particles are sufficient to infect a chimpanzee with hepatitis B. [83] After transmission, the HBV specifically enters hepatocytes via the sodium-taurocholate cotransporting polypeptide (NTCP/SLC10A1). [84,85]

The replication in parenchymal liver cells finally results in an immune system activation (i.e., cytotoxic T-lymphocytes) and induction of necroinflammatory liver disease. [52] This immune-mediated liver damage will further progress into its final stages of cirrhosis and liver cancer. For the treatment of HBV two therapeutic options are available: First, interferon α-2a is used owing to its antiviral and immunostimulatory activity. [86] Second, nucleoside (i.e., lamivudine, entecavir, telbivudine) and nucleotide analoga (i.e., adefovir, tenofovir) are used to inhibit the viral polymerase and reverse transcriptase activity. [53] Notably, both therapies are not curative. In addition, both therapeutic options suffer from significant drawbacks. Interferon therapy has severe side effects and nucleos(t)ide analoga show a high risk of developing resistance. [87] Several other strategies to treat HBV-infected patients are in clinical trials including the first HBV entry inhibitor Myrcludex B. [88]

- *Parasites (Malaria Vivax)*

Malaria is an infectious disease caused by Plasmodium parasites. After the bite of an infected female Anopheles mosquito, the Plasmodium sporozoites quickly enter the human body. [89] They migrate to the liver, cross the sinusoids and enter hepatocytes. Inside hepatocytes, sporozoites develop into thousands of merozoites, which will finally be released into the blood. After erythrocyte invasion, merozoites replicate until the red blood cells are disrupted and the erythrocytic cycle starts

again. This phenomenon causes the typical malaria symptom of recurrent paroxysmal fever at intervals of 48/72 hours. [90] In total, five different Plasmodium species can infect human beings, i.e., P. falciparum, P. vivax, P. ovale, P. malariae, and P. knowlesi. The most severe infection is caused by P. falciparum. All other forms are often assumed as benign, because they have a lower mortality and morbidity rate. However, this misleading view has changed in recent years for several reasons. [56] First, P. vivax is responsible for up to 40% of all malaria cases and causes up to 390 million new clinical cases each year, mainly in Southeast Asia and South America. [57,90] Second, P. vivax causes serious and life-threatening syndromes similar to P. falciparum including severe anemia, renal failure, and hepatic dysfunction. [90] Third, P. vivax (also P. ovale) has a special exoerythrocytic lifecycle. Some of the hepatic sporozoites do not develop into merozoites and thus result in dormant liver forms so-called hypnozoites. [89]

This reservoir of infectious parasites can cause disease relapses months and even years after the first infection. [58,91] The only treatment option against hypnozoites is the 8-aminoquinoline derivate primaquine. [59] However, high doses of primaquine (15 mg/day for 2 weeks or 45 mg/week for 8 weeks) are needed because of its poor pharmacokinetic properties. [91] In addition, primaquine can cause severe cytotoxic effects. The dose limiting hemolytic toxicity is especially pronounced in patients having a glucose-6-phosphate dehydrogenase (G6PD)-deficiency. [92] Unfortunately, G6PD-deficiency is most common in malaria vivax-endemic regions with 5–10% of all people having a decreased G6PD activity. [91] Therefore, new treatment options to treat dormant liver stages of Plasmodia (i.e., hypnozoites) are urgently needed. [58,59]

2.3. Genetic Diseases

Due to the lack of curative treatments for many inherited liver disorders, gene-replacement therapies using hepatocyte-directed nanomedicines offer interesting therapeutic options. [62] In the

following sections, two exemplary monogenetic liver diseases are described in detail. These examples were chosen because of available animal models which facilitate the development of hepatocyte-directed gene therapy approaches.

- *Bilirubin Metabolism Disorder (e.g., Crigler-Najjar Syndrome)*

Disorders of bilirubin transport and its metabolism result in systemic accumulation of bilirubin. In patients with Rotor syndrome or Dubin-Johnson syndrome, the transport of conjugated bilirubin is impaired due to reduced hepatic uptake or biliary secretion, respectively. [61] Notably, these two bilirubin disorders are asymptomatic. By contrast, the impairment of bilirubin glucuronidation due to defects in a gene encoding for UDP-glucuronosyltransferase 1A1 (UGT1A1, a 59 kDa protein of 533 AA located in the endoplasmic reticulum) results in hyperbilirubinemia and clinical manifestations including jaundice. Gilbert`s syndrome, also called Gilbert-Meulengracht syndrome, is a mild form of unconjugated hyperbilirubinemia. Phenobarbital treatment reduces the bilirubin levels below neurotoxic levels. [93] The complete loss of UGT1A1 function leads to a severe form of jaundice, called hereditary Crigler-Najjar syndrome type 1 (1 case per 1'000'000 births). [62] Without treatment, the excessive unconjugated bilirubin levels cause neurological damages with the final stage of lethal encephalopathy (kernicterus). The only available symptomatic treatment consists of phototherapy for 10 to 12 hours a day to reduce elevated bilirubin levels. At present, liver transplantation is the only curative therapeutic option. [94] To study hepatocyte-directed gene therapy approaches, the Gunn rat is the animal model of choice for Crigler-Najjar syndrome type 1. [95,96]

- *Urea Cycle Disorder (e.g., Ornithine Transcarbamylase Deficiency)*

Urea cycle disorders lead to elevated ammonia levels. Without treatment, the hyperammonia results in severe metabolic encephalopathy. [97] The reasons for this metabolic impairment are

manifold, since many enzymes in the urea cycle can be mutated. In total, urea cycle disorders have an incidence of around 1:20`000. The most common disorder is ornithine transcarbamylase (OTC) deficiency (1 case per 80'000 births). [62]

Other urea cycle disorders are N-acetyl glutamate synthetase (NAGS) deficiency, Carbamoyl phosphate synthetase (CPS) deficiency, Argininosuccinate lyase (ASL) deficiency (Argininosuccinic aciduria), Arginase (ARG) deficiency (Argininemia), or Argininosuccinate synthetase (ASS) deficiency (Citrullinaemia). The most important treatment options are dietary to reduce the protein intake and removal of excessive ammonia from the blood using nitrogen scavenger therapy or hemodialysis. [63] Liver transplantation represents the only curative treatment for urea cycle disorders, especially for neonatal OTC deficiency. The spf/ash mouse model can be used to study gene therapy approaches *in vivo*. [98,99]

II. Nanomedicine – Drug Delivery and Drug Targeting

1. Drug Delivery Technologies

Nanoparticulate drug delivery systems offer a huge potential for the therapy of liver disorders. [100,101] The general concepts and advantages of nanomedicine-based therapeutics are explained in detail in Chapter I of the "Results" section for the treatment of cancer. [102] However, these strategies are also applicable for therapeutic interventions of hepatic diseases in order to enhance efficacy and reduce toxic side effects of administered drugs. [101] The strategy might change depending on the type of disease or drug to be delivered. For example, liver structure, accessibility of target cells, or target receptor expression might change during disease progression. Therefore, the targeting strategy and type of nanomaterial have to be chosen carefully to design a nanocarrier with

an increased therapeutic benefit. Two main groups of nanomaterials were used during this PhD project, namely lipid- or polymer-based materials. [103–105] In the following sections, these drug delivery systems and targeting strategies are described with a focus on hepatocytes and the barriers, which need to be overcome.

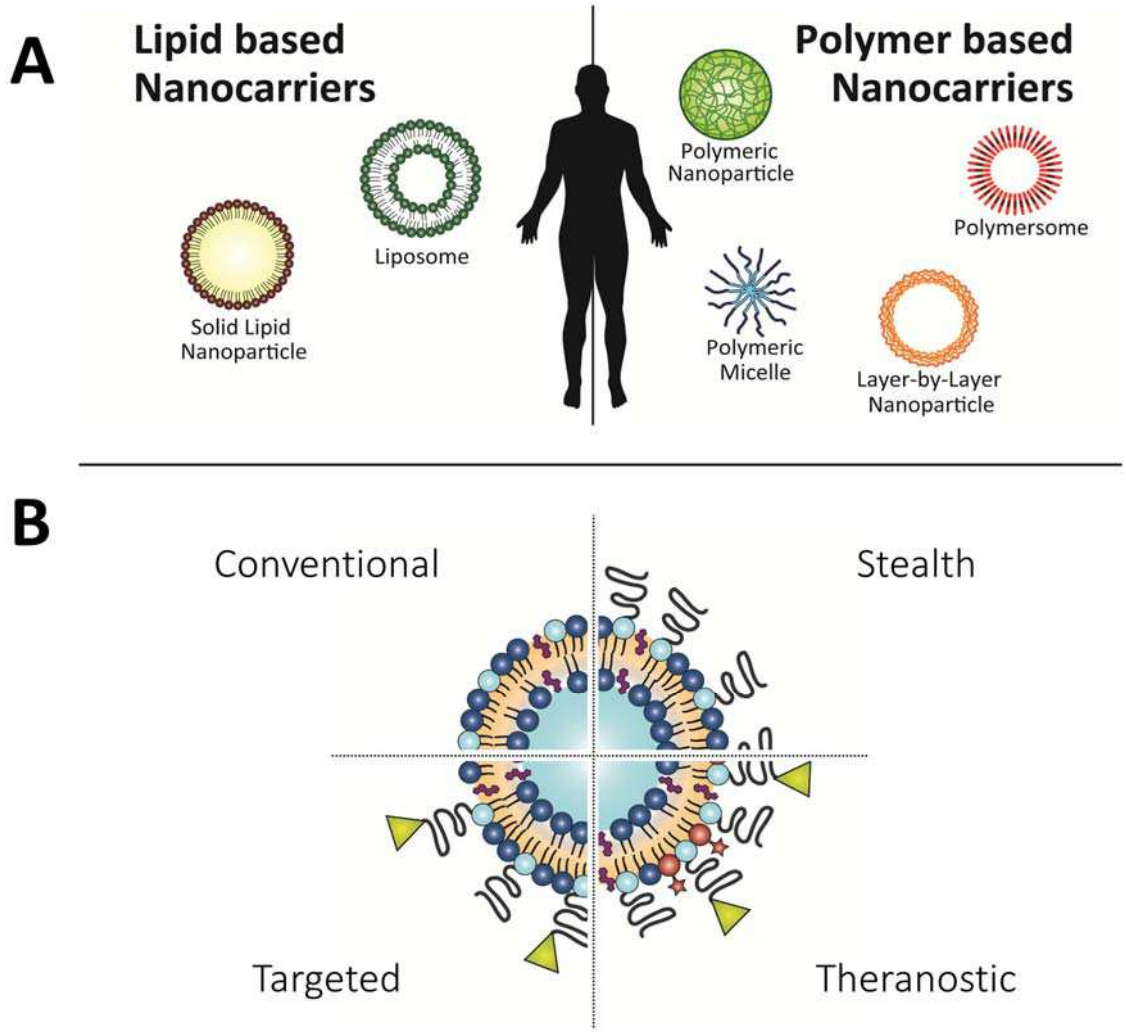

Figure 4: Lipid and polymer-based nanoparticles. (A) Different nanoparticle structures for lipid and polymer-based drug delivery systems are shown. Hydrophilic and/or lipophilic drugs can be encapsulated. (B) Conventional nanoparticles can be functionalized to endow stealth, targeted, or theranostic drug delivery systems. Figure A is adapted from Wicki & Witzigmann *et al.* [102]

1.1. Lipid-based Nanomedicines

The use of lipid-based vesicles as drug delivery system was first described by Gregory Gregoriadis in 1971. [106] He discovered that liposomes, which were initially called "banghasomes" (after their discoverer Alec Bangham) [107,108], change the pharmacokinetic behavior of encapsulated drugs. Based on their structure, lipid-based nanomedicines can be divided into two groups: liposomes and solid lipid nanoparticles (Figure 4). [109] Both lipid systems are multicomponent nanomedicines consisting of various lipids, mainly phospholipids, optionally cholesterol as a stabilizer (i.e., to decrease leakage) and the drug of interest. [110] Liposomes are vesicles with a hydrophilic cavity and a lipophilic membrane, whereas solid lipid nanoparticles are solid spheres, which are surrounded by a lipid monolayer. Depending on the encapsulated drug and formulation method, either hollow or solid lipid-based nanoparticles will be generated. Hydrophilic drugs can be encapsulated inside liposomes, whereas lipophilic drugs can be incorporated in the lipid bilayer. Solid lipid nanoparticles can encapsulate drugs such as nucleic acids inside the nanoparticle core.

Today, lipid-based nanomedicines are the most advanced nanoparticulate drug delivery systems with several formulations in clinical use. [109] Chapter I of the "Results" section describes in detail some of these advances. Several other excellent reviews discuss the field of lipid-based nanomedicines and their advantages for drug delivery in detail. [102,109,111–114] The reader is advised to read these publications for further information.

1.2. Polymer-based Nanomedicines

Polymer-based nanomedicines are another type of nanoparticulate drug delivery system used to modulate the pharmacokinetic and pharmacodynamics profile of drugs. In general, polymer-based nanomedicines consist of natural (e.g., proteins or glycans) or synthetic polymers (especially block copolymers consisting of a stealth, hydrophilic block and a lipophilic block). [102] The huge advantage

of synthetic polymers for therapeutic applications is their great chemical variability. [115] This offers the possibility to influence nanoparticle structure, to modify the surface with targeting ligands or to implement responsiveness to internal or external stimuli. Based on their structure polymer-based nanomedicines can be divided into vesicles (i.e., polymersomes), polymer nanoparticles (i.e., solid spheres), micelles or layer-by-layer capsules (Figure 4). The different forms and their advantages are described in detail in Chapter II of the "Results" section. [115] In addition, several excellent reviews summarize the field of polymer-based nanomedicines. [116–118]

2. Drug Targeting Strategies

The general concepts of passive or active targeting and triggered drug release are described in Chapter I/II of the "Results" section. [102] This paragraph focuses on the various factors, which have to be considered to overcome the different hurdles for successful hepatocyte-specific drug delivery (Figure 5A). In addition, the targeting of the hepatic ASGPR is described in detail. Different targeting ligands are evaluated and recent drug targeting systems from research projects and clinical trials are emphasized.

2.1. Active Targeting of Hepatocytes

The implementation of active drug targeting strategies to parenchymal liver cells offers a huge potential for therapeutic interventions of liver disorders. Importantly, four factors have to be considered for a successful drug delivery to hepatocytes.

First, the general **pharmacokinetic properties** of the nanoparticulate drug delivery systems (NDDS) have to be optimized, i.e., size, surface charge and surface modification (Figure 5). [119]

Nanoparticles for hepatocyte-specific drug delivery have to be small enough to escape from Kupffer cell recognition and pass the fenestrations of liver sinusoids. [17] Nanoparticles with a size below 150 nm are needed in order to pass the fenestrations and gain direct access to the target cell (i.e., hepatocytes). Furthermore, the zeta potential (i.e., surface charge) of nanoparticles has to be controlled. Positively charged nanoparticles have unfavorable pharmacokinetic properties. [120] Upon i.v. injection, these nanoparticles show a high interaction with negatively charged cell surfaces and thus they are quickly sequestered in the lung. [120] By contrast, nanoparticles with a high negative surface charge trigger the recognition by the scavenger receptor on Kupffer cells and resulting in phagocytic clearance. [121] Therefore, ideal hepatocyte-specific nanoparticles should have a slightly negative zeta potential between 0 to -10 mV. [122]

Another important physico-chemical characteristic, which highly influences the pharmacokinetic properties of nanoparticles, is the chemical composition of their surface. Conventional (classical) nanoparticles have no surface modification (Figure 4B). Upon i.v. injection, serum proteins such as complement factors attach to nanoparticles (i.e., opsonization) resulting in a complete change of biodistribution. [123] The reticuloendothelial system (RES, mononuclear phagocyte system) including the hepatic Kupffer cells and macrophages in the spleen recognize these "foreign" particles. [124] As a result, the nanoparticles are rapidly taken up and accumulate in the RES. This fast nanoparticle clearance prevents any pharmacological effect in hepatocytes and in addition enhances extrahepatic side effects. A solution to this problem is the concept of PEGylation (Figure 4B), i.e., grafting of nanoparticles with polyethylene glycol (PEG). PEGylated (stealth, long-circulating, sterically stabilized) nanoparticles have a hydrophilic corona which prevents opsonization. [125] This strategy enhances circulation half-life, and thus increases the chance to deliver drugs to the target cell.

The second factor, which is important for hepatocyte-specific drug delivery, is the **target receptor** (Figure 5A). An ideal target receptor should fulfill following criteria: abundant expression on cell surface (i.e., binding probability and accessibility), predominant/exclusive expression on the target cell type (i.e., selectivity), and efficient internalization properties (i.e., uptake into cells). [126,127] These entire factors are important to increase the therapeutic efficacy in hepatocytes and decrease off-target effects on other organs and other hepatic cell types. One receptor, which fulfills all these criteria for hepatocyte-specific drug delivery, is the asialoglycoprotein receptor. A detailed analysis of the receptor properties can be found in the next section.

Importantly, pathological changes (i.e., tissue alterations) within the liver during disease progression have to be considered. [128] These changes include (i) variations in tissue architecture, which influence the accessibility of the target cell type, and (ii) receptor expression alterations, which influence the targeting specificity. Both pathological changes might have a huge impact on the therapeutic outcome and concomitant side effects. First, liver damage during chronic infections or due to genetic diseases might alter fenestrations of liver sinusoids or change the arrangement of the space of Disse. For instance, elevated production of fibrotic matrix during fibrosis/cirrhosis might limit the extravasation of nanoparticles and therefore the delivery of sufficient concentrations to the side of action, i.e., hepatocytes. [44] Second, target receptor expression might decrease during disease progression as shown for the ASGPR in hepatocellular carcinoma. [128] Both pathological changes influence the targeting strategy significantly and might decrease the therapeutic benefit considerably. To compete with such pathological variations between different patients or within a patient's organ, diagnostic tools to assess the targeting ability of nanoparticulate drug delivery systems are needed (i.e., prognostic factor). [129–131] The combination of therapeutic and diagnostic strategies, i.e., theranostics, is a promising approach to increase the success rate of targeted nanomedicines.

The third important factor for the development of drug targeting strategies is the **targeting ligand** (Figure 5). During the last decades, various ligands have been investigated to recognize and bind to parenchymal liver cells including monovalent and complex carbohydrates, glycomimetics, peptides, proteins or antibodies. In general, the targeting ligand and its surface density on nanocarriers need to be optimized for efficient binding and increased uptake. On one hand, a ligand with a high affinity to its target receptor should be selected resulting in efficient and specific binding to the target cell. On the other hand, it is crucial to optimize the ligand density on the nanoparticle surface. [132,133] If the ligand density is too low, the targeting ability and cell type specificity is decreased. By contrast, an excessive nanocarrier modification with a high ligand density might results in a recruitment of opsonins which could completely change the pharmacokinetic profile in favor of the reticuloendothelial system.

The fourth factor that has to be considered for active targeting of hepatocytes is the availability of suitable ***in vitro* and *in vivo* models** (Figure 5A) to test the developed drug delivery technologies. Successful preclinical tests depend highly on suitable *in vitro* and *in vivo* models (e.g., species independence). Thus this factor might even influence the selection of the target receptor.

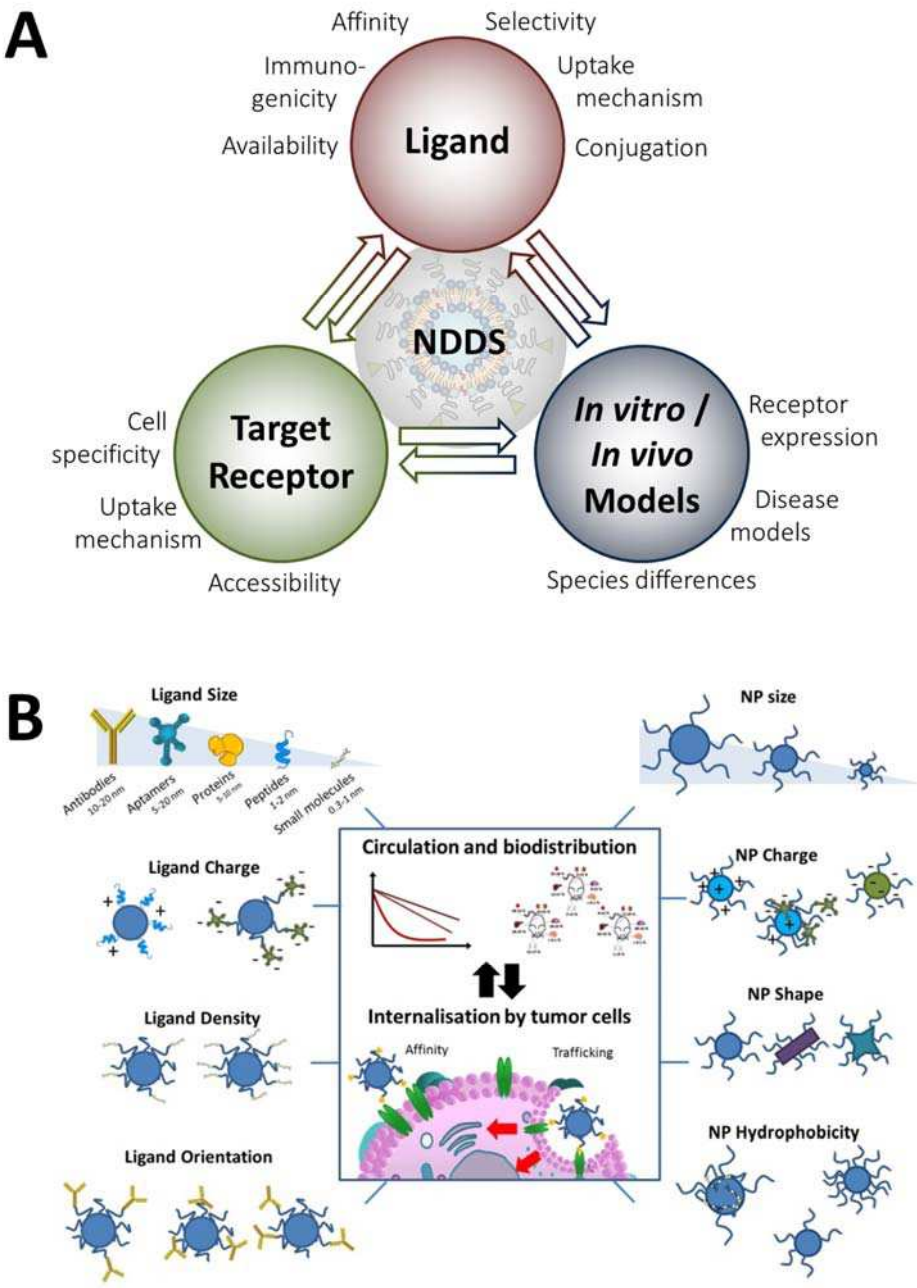

Figure 5: Important factors for active drug targeting using nanoparticles. (A) For active drug targeting using nanoparticulate drug delivery systems (NDDS) four important factors have to be considered: Nanocarrier, Receptor, Ligand, Model System (NRLM). (B) The physico-chemical properties of nanoparticulate drug delivery systems play an important role in the development of targeted nanomedicines. They influence the biodistribution, targeting ability and toxicity profile. Panel B is adapted from Bertrand *et al*. [134]

2.2. ASGPR-specific Targeting

For successful hepatocyte-specific drug delivery, the abundant and exclusive expression of a target receptor on the sinusoidal membrane of parenchymal liver cells is necessary. One receptor, which fulfills this requirement, is the asialoglycoprotein receptor (ASGPR or Ashwell-Morell receptor). [135,136] The following sections explain the structure of the ASGPR and its ligand specificity. In addition, recent approaches for ASGPR-specific drug targeting are described.

ASGPR Structure

The hepatic ASGPR is a C-type ("calcium dependent") lectin receptor, which specifically binds carbohydrates with terminal galactose (Gal) or N-acetylgalactosamine (GalNAc) residues. [137–139] Its physiological function is the clearance of desialylated glycoproteins (i.e., after removal of sialic acid and thus exposure of the terminal key sugars Gal or GalNAc) from circulation. [140]

The ASGPR is a hetero-oligomeric receptor complex consisting of two different subunits, called H1 (hepatic lectin 1, HL1) and H2 (hepatic lectin 2, HL2) (Figure 6A). Both subunits contain an extracellular carbohydrate recognition domain (CRD). A functional receptor is formed by numerous subunits with ratios of 2–5:1 (H1:H2). [141,142] Therefore, several sugars can be recognized at the same time. After ligand binding, the receptor is internalized within minutes by receptor-mediated endocytosis (clathrin-dependent pathway) (Figure 6B/C). [143,144] Approximately 500'000 ASGP receptors per cell are expressed by human or rodent hepatocytes *in vivo*. [145] This receptor density exceeds by orders of magnitude the expression levels in other extrahepatic regions such as the intestine, immune cells or kidney. These extrahepatic tissues account only for 1–5% of the total binding capacity. [146–148] In summary, the ASGPR is an ideal receptor for drug targeting due to its abundant and predominant expression on hepatocytes and the high internalization rate.

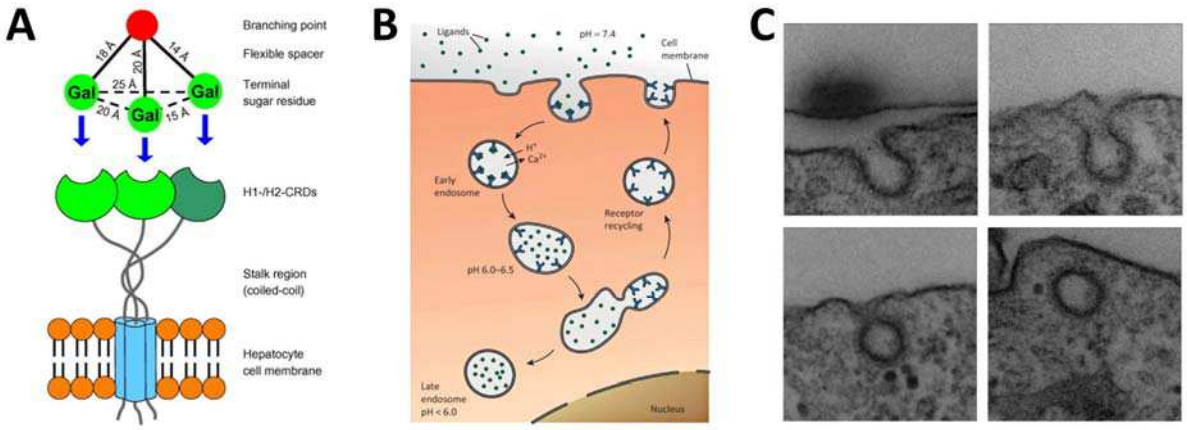

Figure 6: Asialoglycoprotein receptor (ASGPR) structure and endocytosis. (A) Schematic representation of the heterooligomeric ASGPR with carbohydrate recognition domains (CRDs) on each subunit (i.e., H1 and H2). The optimal geometrical conformation of multiantennary carbohydrate ligands is shown. (B) Receptor-mediated endocytosis via clathrin-dependent pathway after ligand binding is represented. Acidification of endosomes leads to separation of the ligand-receptor complex. The receptor recycles back to the membrane, whereas the ligand is further processed (i.e., lysosomal pathway). (C) Transmission electron microscopy analysis of clathrin-dependent uptake. Typical electron dense clathrin pits are visible. Figures are adapted from Khorev *et al.*, Andersen *et al.* and Piccinotti *et al.* [149–151]

- *ASGPR-specific Ligands*

Natural ligands of the ASGPR are glycoproteins from which the terminal sialic acid has been removed. These glycoproteins (e.g., asialofetuin or asialoorosomucoid) have several multiantennary carbohydrates with terminal galactose moieties specifically binding to the ASGPR and thus triggering internalization. In general, these protein-carbohydrate interactions are rather weak, with dissociation constants in the millimolar range. However, with increasing number of sugars binding at the same time to several receptor subunits, the affinity/avidity increases exponentially (tetraantennary > tri- >> bi ->> mono-). This enhancement of affinity due to multivalent binding is called "cluster glycoside effect". [152,153] Dissociation constants of tri- or tetravalent glycans are decreased down to the low nanomolar range. In addition to the multivalent binding, the spatial arrangement of these multiantennary carbohydrates is important for specific binding. Lee *et al.* proposed a model

containing the ideal distances of terminal sugars. This model is optimal for the development of multiantennary ligands with a strong and specific ASGPR binding (Figure 6). [154] Notably, the terminal sugars play an important role for the binding. These influence the affinity significantly, e.g., the ASGPR has a higher affinity for GalNAc as compared to Gal (up to 60-fold). [140,155] The huge advantage of carbohydrate ligands for ASGPR targeting as compared to protein-based ligands is the species independence. The human and rodent ASGPR on hepatocytes exhibit the same carbohydrate recognition pattern. Therefore, *in vitro* results can easily be investigated in first preclinical *in vivo* experiments in rodents.

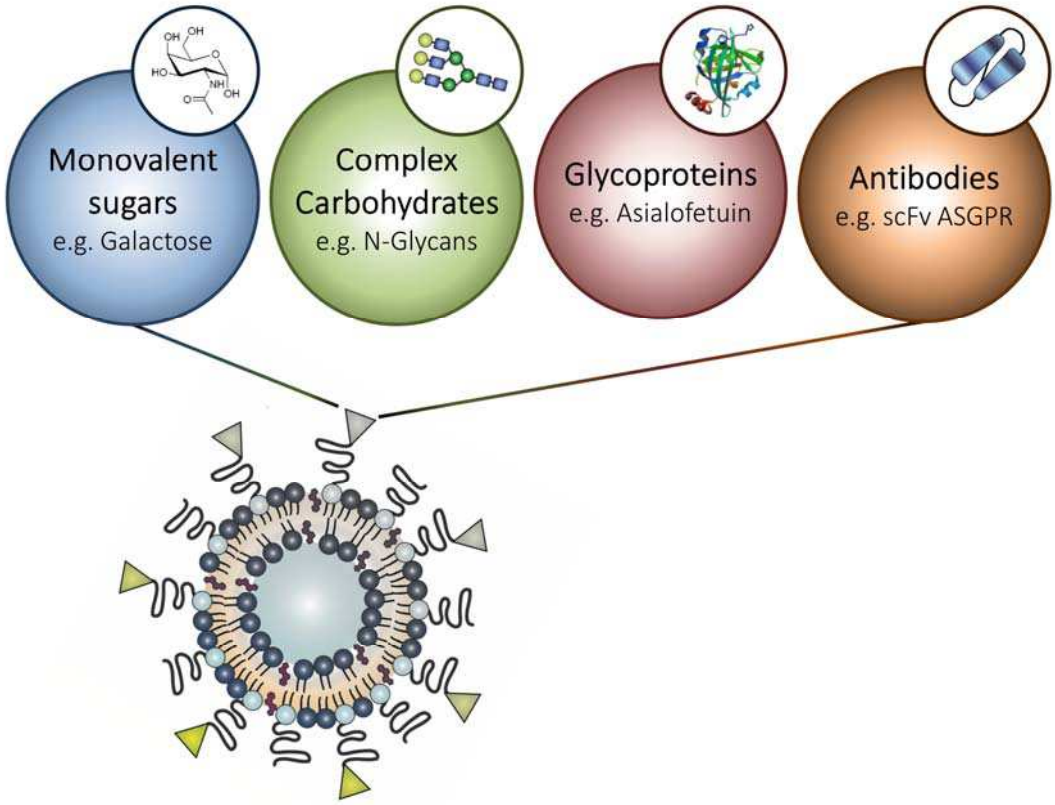

Figure 7: Ligands for Asialoglycoprotein receptor targeting. ASGPR-targeted nanoparticles can be functionalized with different ligands. The targeting ability, conjugation efficiency or immunogenicity of these ligands have to be considered for the selection of an ideal ligand. Carbohydrate ligands are species independent, whereas the amino acid sequence, which is important for recognition by antibodies, might be species dependent.

- *ASGPR-specific drug delivery technologies*

ASGPR-specific drug delivery technologies offer the possibility to specifically target hepatocytes, thereby giving access to a defined cell type within the liver. [156] Several approaches and different ligands for ASGPR-specific targeting have been investigated in research projects as well as in clinical trials (Figure 7). In general, these strategies can be divided into three groups of ligands, i.e., protein-based ligands (e.g., antibodies), natural and synthetic carbohydrates. [155] Antibody-based targeting strategies including antibody-drug conjugates (ADCs) or immunoliposomes are commonly used approaches to target a specific cell type. [102] Therefore, this approach has also been evaluated for ASGPR-specific delivery of an immunotoxin using an anti-ASGPR single-chain antibody. [157]

However, most ASGPR-specific targeting strategies are based on carbohydrate derived ligands. First, naturally occurring glycoproteins bearing multiantennary carbohydrates specifically bind to the ASGPR. Several, research groups have used these hepatotropic glycoproteins to guide nanomedicines specifically to parenchymal liver cells (Figure 7). [158–161] For instance, Dasi and colleagues mediated the gene transfer of human α1-antitrypsin using asialofetuin-modified lipid nanoparticles. [158] In addition, glycoproteins have been enzymatically digested to isolate smaller glycopeptides as ligands. [162] The smallest possible ligands are isolated glycans from glycoproteins, which still have a high binding affinity (Figure 7). The use of such natural, glycoprotein-derived ligands was one part of this PhD project.

The second approach for ASGPR-specific drug targeting is the chemical synthesis of glycomimetics (Figure 7). Monovalent glycomimetics with dissociation constants down to 0.69 μM have been synthetized. [163,164] Furthermore, many attempts have been performed to develop chemical analogues mimicking natural multivalent sugars. [149,165–172] Either the ligand itself was synthetized in a multivalent form or several monovalent sugars have been attached to a nanomaterial backbone to obtain multivalency.

The most successful approaches using this multivalency have been developed in the field of RNA interference therapy (RNAi). Either siRNA is conjugated directly to a trivalent glycan ligand (siRNA-ligand conjugate, Alnylam technology, ALN) or the siRNA is combined with a pegylated polymer backbone (dynamic polyconjugate nanoparticles, Arrowhead Research Corporation technology, ARC). Both technologies are in several clinical trials for the treatment of liver disorders including transthyretin-mediated amyloidosis (NCT02292186, ALN-TTRsc/Revusiran) [64], hypercholesterolemia (NCT02314442, ALN-PCSsc) [173], hemophilia (NCT02554773, ALN-AT3) [174], chronic hepatitis B virus infection (NCT02065336, ARC-520) [175], or α1-antitrypsin deficiency (NCT02363946, ARC-AAT).

In conclusion, ASGPR-targeted nanomedicines, which enhance drug delivery and thereby decrease severe side effects associated with conventional medicines, offer promising therapeutic options and have the potential to overcome the striking limitations of existing, conventional drugs.

III. Gene Delivery

Gene therapy is one of the most important directions for the treatment of genetic liver disorders. [176] However, the translation from bench-to-bedside remains a major hurdle for most nucleic acid delivery systems since there is a lack of efficient and safe carrier systems. So far, only 3.7% of all clinical trials involving gene therapy reached a late clinical phase. [177] These delivery strategies were mostly based on the use of viral vectors. The low success rate of these studies can therefore be attributed to limitations of viral systems with respect to immunogenicity and generalized toxicity. [178] As an alternative, non-viral gene delivery systems are an interesting and safe option, which offer several advantages. [102] Ongoing research projects on RNAi therapeutics using non-viral

carriers are at present one of the most important directions in the treatment of hepatic disorders.

Several companies have initiated research programs and first clinical trials. [179–181] The ligand conjugated and stabilized siRNA constructs used in these studies were designed to efficiently transfer small nucleoside analogues (size of 21–23 bp) into cells to knock down the gene of interest. [182–184] However, the induced pharmacological effects obtained by this siRNA-based strategy are short-lived, i.e., in the range of days in contrast to weeks for gene delivery using a DNA expression plasmid. [185] For example, long-term silencing of Intersectin-1 (a protein regulating the mitochondrial apoptotic pathway in endothelial cells) in the lung necessitated repeated intravenous administration (every 72 hours, for 24 consecutive days) of siRNA/cationic liposome complexes. [186] Therefore, the gene delivery of expression plasmids is the favorable option for long-term therapeutic effects.

1. Plasmid DNA Delivery

Plasmid DNA (pDNA) delivery strategies are based on the use of nanocarriers, which are loaded with a plasmid DNA of interest (e.g., an expression plasmid) (Figure 8). Such delivery systems can accommodate large pDNA polynucleotides with a size of up to 8 kilo bp. It is thus possible to both transfer a gene of interest ("gene delivery" including "knock-in" strategies) leading to the expression of a functional protein or to "knock-down" target genes by gene silencing using DNA-directed RNA interference (ddRNAi). For successful delivery of pDNA and subsequent expression of the encoded, exogenous protein several hurdles have to be overcome: (I) efficient nucleic acid packaging, (II) long plasma circulation, (III) extravasation from sinusoids, (IV) cellular uptake by endocytosis, (V) endosomal escape, (VI) intracellular pDNA release, and (VII) nucleus entry. [104]

To address the major challenge of endosomal escape, specific technologies such as pH responsive systems, pore forming agents, or fusogenic compounds can be used (Figure 8). [187–189] In

the case of the pH buffering effect (i.e., proton sponge effect) ionizable groups of the nanocarrier are protonated during the endo-lysosomal pathway. Thus, the acidification of endosomes is counterbalanced which enhances the action of ATPase enzyme pumps. Finally, the increased intraendosomal ion concentration results in osmotic swelling and endosomal burst.

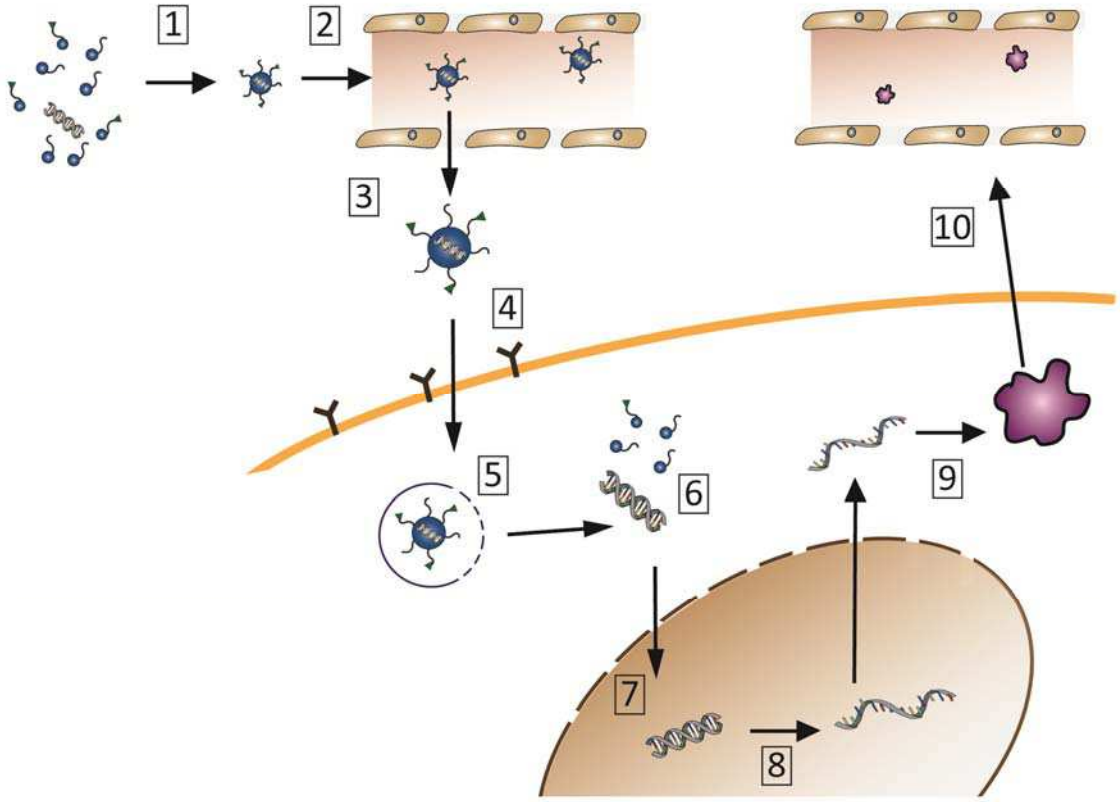

Figure 8: Hurdles for plasmid DNA delivery *in vivo*. (1) Stable plasmid DNA loaded nanoparticles are formed. (2) After injection, the stealth gene delivery system circulates in the blood. (3) After passage of fenestrated sinusoids, (4) the targeted nanoparticles specifically bind to hepatocytes. Subsequently, the cellular uptake of pDNA-nanoparticles is triggered. (5) After endosomal escape, (6) the pDNA is released from the nanocarrier into the cytoplasm. (7) Nuclear trafficking results in (8) transcription of the gene. (9) Finally, the mRNA is transported into the cytoplasm, where the exogenous protein is translated. (10) Further processing results in a mature protein, which performs its function inside the cell or in circulation *in vivo*.

1.1. Targeted Gene Delivery

For the design of targeted nanoparticles, established and safe delivery systems should be used such as sterically stabilized liposomal drug carriers. Thus, a systemic administration of pDNA is possible. Coupled targeting ligands promote tissue-specific nucleic acid delivery. Advantages of such targeted nanoparticulate gene delivery systems can be summarized as follows:

First, the cargo is protected from metabolic degradation since it is enclosed within a nanoparticle. In particular, DNA expression plasmids need to be protected to avoid degradation by plasma derived nucleases. Second, the system is versatile in that different types of molecules can be loaded into nanocarriers, including peptides, polynucleotides, fluorescent markers or small drug molecules. Thus, diagnostic technologies can be combined with therapeutic drug delivery (i.e., theranostics).

Third, the targeting efficiency of the targeting ligand is increased since a limited number of such ligands are needed to direct a nanoparticle loaded with several nucleic acid molecules to a target tissue. This approach is more efficient than direct coupling of a single drug molecule to a single targeting vector. [102] Fourth, the technology can be considered as a modular platform technology where different components can be readily combined and exchanged. Target specificity and pharmacokinetics of the nanocarriers are solely a function of the used targeting vector and the physico-chemical properties. They are not influenced by the transported cargo. Targeting specificity can be adjusted by a simple exchange of the targeting vector or variation of its density. Fifth, the host system is protected from the cargo reducing the risk of unwanted immunological reactions.

In conclusion, the most important key factors for the design of gene delivery systems are the combination of efficient and targeted nucleic acid delivery with low cytotoxicity, cellular uptake, intracellular release and transcription of pDNA (Figure 8).

AIM OF THE THESIS

As outlined above, conventional therapeutics for the treatment of hepatocyte-related diseases are often insufficient. For many incurable or late-stage liver disorders, liver transplantation still is the only available treatment option. Hepatocyte-specific targeting technologies represent a promising therapeutic strategy to overcome the limits of conventional drugs in the treatment of cancer, infections, or genetic diseases. Therefore, the aim of this PhD thesis was the development of drug delivery and targeting strategies for hepatocyte-related disorders and the implementation of imaging and gene delivery technologies. To achieve these objectives several factors had to be explored:

- **Evaluation of nanoparticulate drug delivery technologies**
  - Which nanomaterials are used in clinical applications?
  - Which nanomaterials have stealth properties?
- **Evaluation of hepatocyte-specific targeting strategies**
  - Which receptors are specific for hepatocytes?
  - Which targeting strategies have already been evaluated?
- **Investigation of selected target receptor**
  - What is the receptor expression in health or disease?
  - Are there suitable *in vitro*/*in vivo* models available?
- **Assessment of targeting ligands**
  - Which targeting ligands can be used?
  - What advantages/disadvantages do these ligands have?
- **Development of imaging technologies to analyze uptake mechanisms**
  - Which imaging methods can be used?
  - How can the intracellular fate of nanocarriers be visualized?
- **Exploration of novel nanomaterials for gene delivery**
  - What are important factors for gene delivery?
  - Is it possible to use stealth nanomaterials for gene delivery?

RESULTS

Chapter I: Nanomedicine in Cancer Therapy: Challenges, Opportunities, and Clinical Applications

Chapter II: Polymeric Nanomaterials: Applications in Therapeutics

Chapter III: Variable Asialoglycoprotein Receptor 1 Expression in Liver Disease: Implications for Therapeutic Intervention

Chapter IV: Hepatocyte Targeting Using Pegylated Asialofetuin-Conjugated Liposomes

Chapter V: Isolation of Multiantennary *N*-Glycans from Glycoproteins for Hepatocyte-specific Targeting via Asialoglycoprotein Receptor

Chapter VI: Formation of Lipid and Polymer-based Gold Nanohybrids Using a Nanoreactor Approach

Chapter VII: Biocompatible Polymer-Peptide Hybrid-Based DNA Nanoparticles for Gene Delivery

Chapter I

"Nanomedicine in Cancer Therapy: Challenges, Opportunities, and Clinical Applications"

Witzigmann D, Wicki A*, Balasubramanian V, Huwyler J.*

Journal of Controlled Release. 2015 Feb 28; 200:138-57.

doi: 10.1016/j.jconrel.2014.12.030. (**contributed equally)*

http://www.sciencedirect.com/science/article/pii/S016836591400827X

Highlights: Nanomedicine therapeutics represent an opportunity to achieve sophisticated targeting strategies and multi-functionality. They can improve the pharmacokinetic and pharmacodynamic profiles of conventional therapeutics and thus optimize the efficacy of existing anti-cancer compounds. This review article highlights advances in the field of nano-delivered anti-cancer drugs. In particular, a comprehensive overview of ongoing and completed clinical trials is provided. State-of-the-art drug conjugates and nanocarriers are described. Challenges faced in using nanomedicine products and translating them from experimental conditions to the clinical setting are emphasized, i.e., complex physico-chemical features, safety concerns, and regulatory as well as manufacturing issues. In addition, aspects of nanoparticle engineering that may open up new opportunities for next-generation nanomedicine products in the clinic are covered.

Journal of Controlled Release 200 (2015) 138–157

Contents lists available at ScienceDirect

Journal of Controlled Release

journal homepage: www.elsevier.com/locate/jconrel

Review

Nanomedicine in cancer therapy: Challenges, opportunities, and clinical applications

Andreas Wicki [a,1], Dominik Witzigmann [b,1], Vimalkumar Balasubramanian [c], Jörg Huwyler [b,*]

[a] Division of Oncology, Department of Internal Medicine, University Hospital of Basel, Basel, Switzerland
[b] Division of Pharmaceutical Technology, Department of Pharmaceutical Sciences, University of Basel, Basel, Switzerland
[c] Division of Pharmaceutical Chemistry and Technology, Faculty of Pharmacy, University of Helsinki, Helsinki, Finland

ARTICLE INFO

Article history:
Received 12 November 2014
Accepted 23 December 2014
Available online 26 December 2014

Keywords:
Cancer nanomedicine
Clinical trials
Nanoparticle
Liposome
Drug delivery
Targeting

ABSTRACT

Cancer is a leading cause of death worldwide. Currently available therapies are inadequate and spur demand for improved technologies. Rapid growth in nanotechnology towards the development of nanomedicine products holds great promise to improve therapeutic strategies against cancer. Nanomedicine products represent an opportunity to achieve sophisticated targeting strategies and multi-functionality. They can improve the pharmacokinetic and pharmacodynamic profiles of conventional therapeutics and may thus optimize the efficacy of existing anti-cancer compounds. In this review, we discuss state-of-the-art nanoparticles and targeted systems that have been investigated in clinical studies. We emphasize the challenges faced in using nanomedicine products and translating them from a preclinical level to the clinical setting. Additionally, we cover aspects of nanocarrier engineering that may open up new opportunities for nanomedicine products in the clinic.

Contents

Abbreviations: ADC, antibody drug conjugate; ALL, acute lymphoid leukemia; AML, acute myeloid leukemia; EGF, epidermal growth factor; EGFR, epidermal growth factor receptor; EMA, European Medicines Agency; EPR, enhanced permeability and retention effect; FDA, US Food and Drug Administration; GMP, good manufacturing practice; HPMA, N-(2-hydroxypropyl) methacrylamide; HSA, human serum albumin; IL, immunoliposome; nab, albumin-bound nanoparticle; PD, polydispersity; PEG, polyethylene glycol; PEG-PGA, polyethylene glycol–polyglycolic acid; PLGA-PEG, poly(lactide-co-glycolide acid)–polyethylene glycol; RES, reticulo-endothelial system; sst, somatostatin receptor 2; WHO, World Health Organization.

* Corresponding author at: Division of Pharmaceutical Technology, Department of Pharmaceutical Sciences, University of Basel, Klingelbergstrasse 50, CH-4056 Basel, Switzerland.
E-mail address: joerg.huwyler@unibas.ch (J. Huwyler).
[1] Both authors contributed equally to this work.

http://dx.doi.org/10.1016/j.jconrel.2014.12.030
0168-3659/

1. Introduction

For more than two decades, advances in understanding cancer biology have only slowly been translated into significant improvements in cancer care. The World Health Organization (WHO) attributed 8.2 million deaths to cancer in 2012, which constituted 13% of all deaths. Within the next two decades, new global cancer incidences are expected to increase from 14 million in 2012 to as many as 22 million. One of the main reasons is the lack of selective delivery of anti-cancer compounds to neoplastic tissue. High systemic exposure to anti-neoplastic agents frequently results in dose-limiting toxicity. Therefore, targeted delivery is of utmost importance in order to overcome current limitations in cancer therapy. Recent developments in nanotechnology are expected to improve drug delivery, thereby increasing efficacy while decreasing the side effects of anti-cancer drugs.

Nanocarriers[2] have unique properties such as nanoscale size, high surface-to-volume ratio, and favorable physico-chemical characteristics. They have the potential to modulate both the pharmacokinetic and pharmacodynamic profiles of drugs, thereby enhancing their therapeutic index. Loading of drugs into nanocarriers can increase in vivo stability, extend a compound's blood circulation time, and allow for controlled drug release. Thus, nanomedicine compounds can alter the biodistribution of drugs by allowing them to accumulate preferably at the tumor site. This phenomenon is known as enhanced permeability and retention effect (EPR) (Section 2.2.1).

A wide range of nanomaterials based on organic, inorganic, lipid, protein, or glycan compounds as well as on synthetic polymers have been employed for the development of new cancer therapeutics (Fig. 3). According to the registry maintained by clinicaltrials.gov, a total of 1575 nanomedicine formulations (search terms 'liposome'/'nanoparticle'/'micelle') had been registered for clinical trials by December 2014. As many as 1381 of these are in the field of cancer therapy [1] (Fig. 1B). However, most clinical trials focus on marketed products, such as liposomal doxorubicin or albumin-bound paclitaxel. Either new indications or therapies in combination with other anti-cancer agents are investigated. Our search of the key word 'cancer nanoparticles' in Web of Science® yielded 57,944 publications available in December 2014 (Fig. 1A). This illustrates the huge gap between technical and clinical development. There are concerns that a delay in clinical development of new nanomedicine drugs may be detrimental to cancer patients. With this in mind, we discuss in this review the recent developments of nanomedicine therapeutics in early and late clinical trials. We cover opportunities to develop next-generation clinical nanomedicine therapeutics with advanced functionalities. In addition, we address challenges encountered during drug development and regulatory approval.

2. Key principles of nanomedicine

2.1. Rationale for the development of nanomedicine products for cancer therapy

There are convincing arguments in favor of developing nano-sized therapeutics [2].

[2] The term "nanocarrier" is used in the review article as an umbrella term to describe different types of drug carriers such as micelles, vesicles, and solid nanoparticles.

First, nanoparticles may help to overcome problems of solubility and chemical stability of anti-cancer drugs. Poor water solubility limits the bioavailability of a compound and may hamper the development of anti-cancer agents identified during early drug screens [3]. Uptake and delivery of poorly soluble drugs may be increased by enveloping the compound in a hydrophilic nanocarrier. At the same time, this may increase chemical stability. The PI3K inhibitor and radiosensitizer wortmannin is an example for a drug whose development was stopped because of poor solubility and chemical instability. Using a lipid-based nanocarrier system, the solubility of wortmannin was increased from 4 mg/L to 20 g/L while increasing its stability in vivo [4]. Albumin-bound paclitaxel is another example and will be discussed in detail in Section 3.2.3.

Second, nanocarrier can protect anti-cancer compounds from biodegradation or excretion and thus influence the pharmacokinetic profile of a compound. For example, drugs cleaved enzymatically (e.g., siRNA by RNAses in the plasma, proteins by pepsin or trypsin in the stomach) can be prevented from being degraded by enzymes. Encapsulation of anti-cancer agents into nanocarriers or coupling of biodegradable compounds to synthetic polymers may overcome this problem (Section 3.2).

Third, nanotechnology can help to improve distribution and targeting of anti-tumor medication. Distribution of anti-cancer drugs is defined by their physico-chemical properties and is limited by drug penetration into tumor tissue [5,6] (Fig. 4). Not all nanocarriers intrinsically penetrate tumor tissue [7]. However, nanomedicine compounds can be constructed to improve drug penetration and to redirect chemotherapy or targeted compounds selectively to tumor cells or cells of the stromal compartment. Both passive and active targeting strategies are used to redirect anti-cancer drugs (Sections 2.2 and 3.2).

Fourth, nanocarriers can be designed to release their payload upon a trigger resulting in stimuli-sensitive nanomedicine therapeutics (Section 2.2.3). For example, drugs whose delivery is not primarily pH-dependent, such as doxorubicin, can be conjugated with a pH-sensitive nanoparticle to increase cellular drug uptake and intracellular drug release [8].

Finally, targeted nanomedicine therapeutics may decrease resistance of tumors against anti-cancer drugs. Generally, specific uptake reduces the probability for unspecific, MDR/ATP efflux pump-driven elimination. Therefore, nanomedicine therapeutics may prolong the circulation time of a compound and mediate stimuli-responsive drug release as well as endocytic drug uptake (Section 2.2). This may lead to reduced resistance of tumor cells against targeted nanocarriers [9,10].

2.2. Opportunities: advanced functionalities

In any cancer therapy, there is a balance between potential benefit and potential harm of the treatment. The aim of any nano-application of a drug is to shift this balance in favor of the benefits. General strategies and advanced functionalities of nanomedicine products to improve the drug's therapeutic index are discussed below.

2.2.1. Passive targeting

Most clinically available nanocarrier-based cancer therapeutics are passively targeted first-generation nanomedicine drugs. First generation

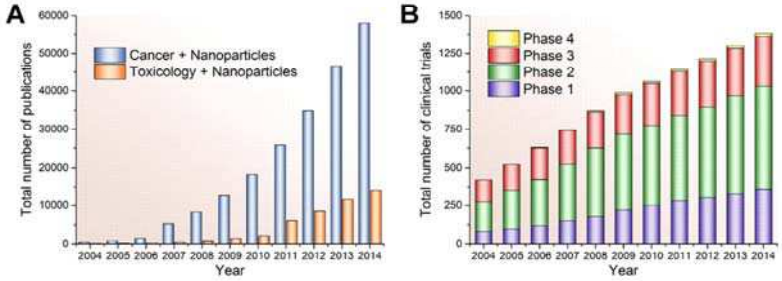

Fig. 1. Total number of publications (Web of Science®) and clinical trials (clinicaltrials.gov) during the last 10 years. (A) The number of publications in the field of nanoparticles for cancer therapy is increasing exponentially. The ratio between new publications in the field of cancer and new publications in the field of toxicology has remained stable over the last 4 years. (B) The number of launched clinical trials (phases 1, 2, 3, and 4) investigating nanomedicine drugs for cancer therapy is increasing constantly over the last 10 years. However, the total number of clinical trials is only about 2% of the total number of publications in the field of cancer nanomedicine.

nanomedicine drugs mainly rely on controlling the pharmacokinetics and biodistribution of a compound by modulating its physicochemical properties [15]. For example, pegylated liposomal doxorubicin (Doxil®/Caelyx®) (Fig. 2D) and nab-paclitaxel (Abraxane®) are first-generation nanomedicine drugs based on passive targeting.

Pathophysiological characteristics of cancers and their environment have been exploited for passive targeting. In particular, the EPR effect promotes the accumulation of nanomedicine drugs in the tumor (Fig. 2A/D). This effect is based on the presence of leaky intratumoral blood vessels, whose endothelium is fenestrated with gaps between 100 nm and 780 nm of size [16]. For example, Kaposi sarcoma is a tumor type with fenestrated vasculature (Fig. 2D) [7]. Thus, by convection and diffusion processes, passive directing of nanomedicine therapeutics into tumors can occur without any specific ligand attached to the surface of the nanocarrier. However, it has been widely accepted that passive targeting based on the EPR effect is not sufficient to control the side effects of cytotoxic drugs and fully exploit the benefits of targeted delivery.

Heterogeneity of the tumor and its stroma, such as a hypoxic gradient, can severely impact on the efficacy of drugs delivered by passive targeting. This can result in reduced or abrogated transport of the compound into the tumor [17]. Recent research has focused on normalization of tumor vasculature before initiating anti-cancer treatment and image-guided analysis of the EPR effect (theranostic approach, see Section 2.2.4) [18,19].

Another factor that limits the access of nanomedicine drugs to the tumor is increased interstitial fluid pressure [20]. Furthermore, the extracellular matrix of certain malignancies, such as pancreatic cancer, limits drug penetration into the tumor [21]. Finally, passive targeting does not prevent accumulation of nanocarriers in other organs with fenestrated endothelium, e.g., the liver and spleen [22].

Therefore, the development of next-generation nanomedicine drugs with advanced functionalities is certainly warranted. Second-generation nanomedicine compounds are based on drug-delivery technologies with an active targeting vector or smart nanocarriers with stimuli-responsive properties. Thus, second-generation nanomedicine compounds hold the promise of improved targeting and increased efficacy [23]. Several next-generation nanomedicine drugs have been developed at a preclinical level, and a few have entered early clinical testing (Tables 3–5). However, none of them has been approved for commercial use as yet.

2.2.2. Active targeting

In the case of active targeting, a high-affinity ligand is attached to the surface of a nanocarrier. The ligand binds selectively to a receptor on the target cell (Fig. 2B). Targeted delivery is ensured by the high specificity of the ligand for its cognate receptor. A wide range of ligands have been used for such purposes including small molecules such as folic acid and carbohydrates, or macromolecules such as peptides, proteins, antibodies, aptamers, and oligonucleotides. One example in clinical trials are doxorubicin-loaded immunoliposomes targeted against the epidermal growth factor receptor (EGFR) (Fig. 2E/F). These active targeted nanocarriers will be further discussed in detail in Section 3.2.2. The ligand must be chosen in a way to allow binding to the target cells while minimizing binding to healthy cells. For efficient targeting, nanocarriers should be stable enough to avoid premature release and degradation of the drug in the circulation.

Similarly, sufficiently prolonged circulation of the drug is vital to avoid unwanted interactions with serum proteins or the immune system (opsonization process), and thus to prevent untimely clearance [24]. Therefore, the density of the targeting ligand needs to be optimized in order to maintain stealth properties and avoid rapid recognition by the reticulo-endothelial system (RES) [25].

As mentioned, active targeting depends on the availability of a target and a specific ligand. However, it is equally important to optimize the density of the targeting ligands per nanocarrier to achieve not only high targeting efficiency but also to ensure an optimal internalization [26]. For instance, gold nanoparticles with different densities of targeting antibodies on the surface exhibit distinct mechanisms of uptake [27,28]. Briefly, gold nanoparticles were targeted with an antibody (C225, cetuximab) to EGFR. Surface-saturated, cetuximab-targeted gold nanoparticles showed dynamin-2 dependent caveolae endocytosis. In contrast, partially cetuximab-covered gold nanoparticles showed Cdc42 dependent phagocytosis involving actin polymerization.

In specific cases, cellular uptake may lead to enhanced pharmacological effects (as demonstrated for immunoliposomes) or may even be a prerequisite when it comes to the implementation of gene therapy approaches (i.e. targeting of nucleic acids). Nevertheless, internalization of nanocarriers is not always needed. For example, small molecules such as doxorubicin can cross the cell membrane by passive diffusion. Creation of a "depot" in the vicinity of the tumor may be sufficient to induce a pharmacological effect. Based on this principle, targeting of the extracellular matrix of tumors by antibody drug conjugates (ADCs) led to curative effects in experimental animals [29,30].

Pitfalls such as anatomical and physiological barriers have to be taken into account for the development of cancer cell targeted nanocarriers (Fig. 2B) [7]. Such barriers may prevent direct interaction between the nanocarrier and its target cell (Fig. 2B, pathway 1) or may hamper deep penetration into neoplastic tissue (binding-site barrier phenomenon) [31]. Active targeting of tumor vasculature can overcome these limitations (Fig. 2B, pathway 2).

In conclusion, nanomedicine aims at achieving an optimal balance between high avidity of the ligand and low opsonization of the nanocarrier. Targeted nanoparticles carry a considerable amount of drug per binding event. This is a further difference between nanocarriers and drug conjugates. Actively targeted nanoparticulate delivery can enhance drug retention in the tumor due to increased cellular binding, minimize non-specific uptake, and circumvent mechanisms of resistance [32].

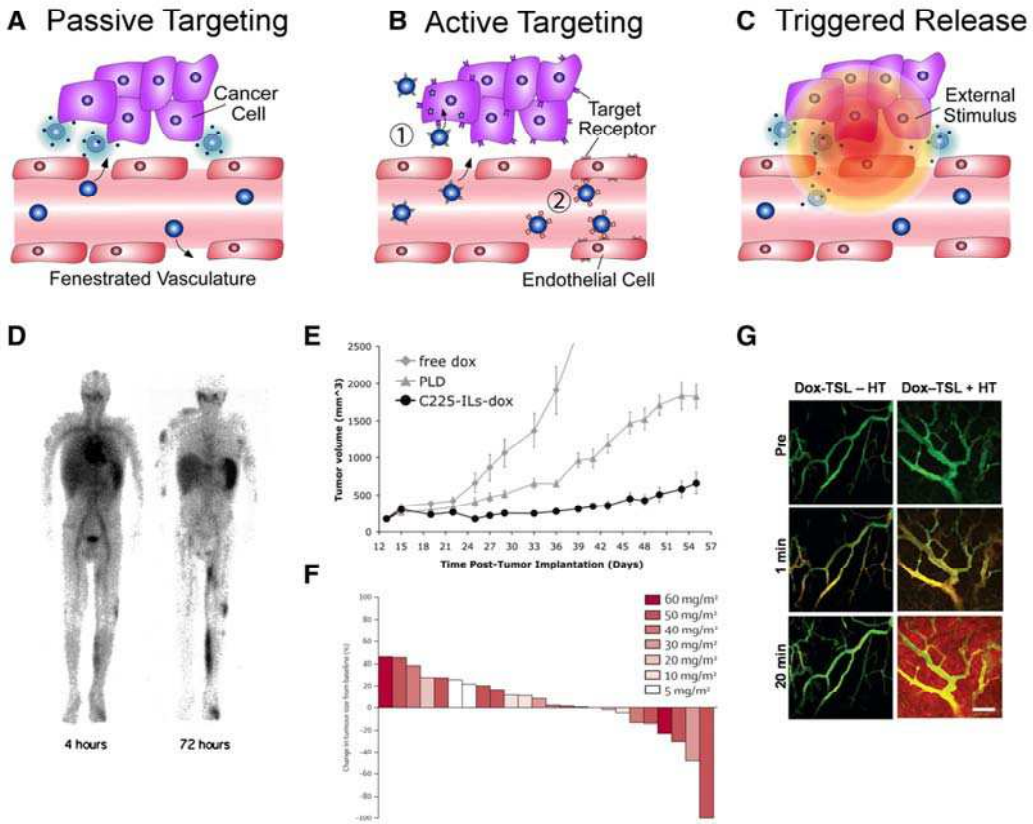

Fig. 2. Schematic illustration of drug targeting strategies (A–C) and examples of nanomedicine therapeutics in clinical cancer care (D–G). (A) Extravasation of nanomedicine therapeutics through fenestrated vasculature leads to passive targeting of tumor tissue. (B) Active targeting of cancer cells (1) or tumor endothelium (2) using ligand-modified nanocarriers. (C) Stimuli-responsive nanocarriers release their payload by internal or external triggers. (D–G) Three different targeting strategies for doxorubicin loaded liposomes are illustrated. (D) Scintigraphy of a patient with Karposi sarcoma (left leg, right arm, and face) after treatment with radiolabeled, pegylated liposomes. Typical accumulation of long-circulating liposomes such as Doxil in neoplastic tissue with leaky vasculature is shown. (E) Active targeting of cancer cells using immunoliposomes against EGFR (anti-EGFR-ILs). Superior therapeutic effect of anti-EGFR-ILs (C225-ILs-dox) in a multidrug-resistant xenograft model compared to free doxorubicin (free dox) or pegylated liposomes (PLD). (F) Waterfall plot representing change in tumor size in patients treated with anti-EGFR-ILs in a phase 1 clinical trial. (G) Intravascular release of doxorubicin (red) from thermosensitive liposomes (TSL) such as thermodox after mild hyperthermia (+HT). Liposomes were injected into nude mice. Drug release was observed using intravital confocal microscopy. Figures are adapted with permission from [11–14].

2.2.3. Stimuli-responsive systems/triggered release

Stimuli-responsive systems act in response to physical, chemical, or biological triggers that promote release of drugs by interfering with the phase, structure, or conformation of the nanocarrier. Stimuli-responsive nanocarriers are similar to the feedback mechanism of biological systems, in which serial biochemical signaling processes are based on the modulation of physico-chemical parameters. The advantage of using stimuli-responsive systems is obvious: the drug is released through a trigger present in the neoplastic tissue, thus minimizing systemic exposure to the compound (Fig. 2C).

Triggers can be divided into internal (patho-physiological/patho-chemical condition) and external (physical stimuli such as temperature, light, ultrasound, magnetic force, and electric fields) stimuli.

Internal stimuli include changes in pH, redox, ionic strength, and shear stress in the target tissues [33,34]. For instance, in solid tumors, the extracellular pH is more acidic than the systemic pH [35]. Similarly, the pH of intracellular organelles (e.g., endosomes and lysosomes) differs from that of the cytoplasm or blood. This condition can be used to enhance intracellular release of drugs from nanocarriers. For example, pH-responsive liposomes were used to trigger the release of the drug and therefore increase the therapeutic efficacy [36].

Furthermore, the overexpression of certain biomolecules and recognition of host-guest interactions within diseased tissues can be used as internal stimuli. Numerous enzyme-based biochemical stimuli, including proteases and glucuronidases that are differentially expressed in normal cells and cancer cells, are useful for responsive systems. For instance, multistage gelatin nanoparticles deeply penetrated into tumor tissue after MMP-2 triggered shrinkage, thereby overcoming anatomical and physiological barriers [37].

Another type of microenvironment that can serve as a trigger for drug release is the hypoxic area of tumors exhibiting low oxygen pressure and poor nutrient levels. Such an environment is rich in reductive agents, which can be used for triggered release from redox-responsive nanocarriers [38]. Disulfide-containing nanocarriers are the most widely studied redox-responsive technology. Increased glutathione levels lead to a cleavage of disulfide bonds and hence trigger the release of drugs in the tumor tissue [39,40].

Physical stimuli are usually applied externally to trigger the release of drugs. Local hyperthermia can induce the release of drugs from thermo-responsive nanocarriers such as ThermoDox (Fig. 2G). In addition, hyperthermia increases vascular permeability thus facilitating delivery of the anti-cancer agents deep into the tumor [41]. The

temperature range for local hyperthermia lies between normal body temperature (37 °C) and a maximum of 42 °C [42].

Using light as an external stimulus is promising due to the simplicity of the application, precise control over spatial exposure, and biocompatibility. Light sources include the ultraviolet or near-infrared ranges [43,44]. With increasing wavelength, the light penetrates deeper into the body. Special devices such as fiberoptic catheters can help to overcome the limitation of light absorption by superficial tissue [7,34].

Moreover, ultrasound has been used to trigger the release of drugs (mainly contrast agents) from responsive systems for cancer diagnosis [45,46]. Release of contrast agents at the tumor site contributes to the specificity of an imaging technique. Magnetic and electric fields are other possible external stimuli. Inorganic and paramagnetic nanoparticles (iron oxide nanoparticles) are responsive to an applied magnetic field. Thus, the nanocarrier can be guided to the tumor with high specificity and release its payload at the target side through a hyperthermic effect. External electric fields can trigger the drug release from conducting polypyrrole nanoparticles [47].

Advances in stimuli-responsive nanocarriers have been discussed in detail in several recent reviews [34,48,49].

2.2.4. Multi-functionality/theranostics

Beyond the first and second generations of nanomedicine drugs that confer single functionality, multifunctional nanocarriers are expected to shortly enter clinical development. Multifunctional nanocarriers have the capability to perform several functions in parallel, such as co-delivery of drugs for combination therapies, multi-targeted delivery, or simultaneous diagnosis and therapy. Recently, numerous types of multifunctional nanocarriers have been developed at the proof-of-concept level and some are described in this section.

Simultaneous delivery of multiple drugs such as doxorubicin and paclitaxel, together with DNA or siRNA, can be an effective strategy against cancer. For instance, multifunctional polymeric nanoparticles loaded with doxorubicin and DNA showed more pronounced suppression of tumor growth than single delivery of either DNA or doxorubicin in both in vitro and in vivo studies [50,51]. In another study, biodegradable polymersomes co-loaded with doxorubicin and paclitaxel were more effective than the free drugs [52]. Likewise, multifunctional pegylated liposomes are able to co-deliver the P-glycoprotein inhibitor tariquidar and paclitaxel to overcome multidrug resistance in tumors [53].

Advanced multifunctional nanomedicine therapeutics have been developed by combining targeted delivery with stimuli-responsive systems. For example, multifunctional polymeric micelles have been used to load drugs into the hydrophobic part and to use the hydrophilic part to attach a targeting ligand (folate-receptor targeting molecules in this case) for enhanced cellular uptake. Additionally, drug release was modulated by a pH-sensitive linker under in vivo conditions [54]. Even more complex multifunctional systems have been developed by combining multiple targeting and delivery of multiple chemotherapeutics [49].

Theranostics are an emerging subset of multifunctional nanomedicine compounds [55]. In general, theranostics provide both the diagnosis and treatment with the same nanoformulation. Theranostic agents can monitor the accumulation of nanomedicine compounds at the target site, visualize biodistribution, quantify triggered drug release, and assess therapeutic efficacy. One of the most important aspects of theranostics is their capability to predict response in individual patients, thus paving the way for personalized medicine. They may also offer a means of dealing with tumor heterogeneity since they do not only indicate the presence of a target but also its exact location in the body. The innovative concepts and strategies of theranostics have not yet been fully evaluated in clinical trials. An exception from this rule is the radiopeptide DOTATOC, which is discussed in Section 3.2.1. However, there are several nanotheranostics in preclinical development [56–58].

3. Nanomedicine in clinical cancer care

Various types of nanomedicine compounds have been used in clinical cancer care, including viral vectors, drug conjugates, lipid-based nanocarriers, polymer-based nanocarriers, and inorganic nanoparticles (Fig. 3) [2]. The different nanomedicine products are discussed below, with special emphasis placed on clinical trials. Most nanomedicine therapeutics are investigated in phase 1 trials in patients with solid tumors. Specific cancer indications are explored in advanced (phases 2 and 3) clinical trials. Nanomedicine products in clinical studies or approved for clinical cancer care are summarized in Tables 1–6. Whenever possible, specific cancer types are indicated.

3.1. Viral nanoparticles for cancer therapy

An elegant way to construct nanoparticles for cancer therapy is the use of tumor-homing viruses engineered to express therapeutic proteins. Pox viruses, such as myxoma or vaccinia strains, preferentially replicate in tumor cells. Specific features of cancer cells, e.g., block of apoptotic pathways, deregulation of cell replication, and immune evasion, are also beneficial for successful pox virus replication [59]. JX-594 is a poxvirus designed to replicate in tumor cells and destroy them via activation of the EGFR-Ras-MAPK signaling pathway. In addition, JX-594 expresses granulocyte colony-stimulating factor (G-CSF) to potentially increase the immunological anti-tumor response. Intratumoral injection of this oncolytic virus in 10 patients with primary or metastatic liver cancer resulted in 3 cases of partial remission and 6 cases of stable disease. Flu-like symptoms and hyperbilirubinemia were the most frequent side effects [60].

In a second phase 1 trial, JX-594 was injected intravenously (i.v.) in 23 patients with advanced solid tumors [61]. The virus homed successfully to the tumor tissue, and dose-related anti-tumor activity of JX-594 was observed. Normal tissue was negative for viral replication. Immediately adjacent epithelium showed uptake, but no replication of the virus. This proof-of-principle study was the first to show dose-related viral replication and tumor response after i.v. injection of an oncolytic virus.

The first successful phase 3 trial with oncolytic viruses was the OPTiM study in patients with advanced (stage IIIB–IV) melanoma [62]. Patients were randomized to receive multiple injections of a Herpes simplex virus (HSV) type 1-derived and GM-CSF-expressing virus (T-Vec) into non-visceral melanoma metastases and a subcutaneous application of GM-CSF. The primary endpoint of the study was durable response (defined as partial or complete remission for 6 or more months). Overall, 16.3% of the patients injected with the virus achieved durable response while only 2.1% did in the control arm [62]. Interestingly, responses were also observed in non-injected metastases, indicating that the virus may also spread to non-injected tumor sites. Cellulitis was the most frequent grade 3/4 toxicity occurring in 2.1% of the study participants. There was a trend towards prolonged survival, which still needs to be confirmed. T-Vec has the potential to become the first oncolytic virus approved for cancer care.

Another phase 3 trial (ASPECT study) investigated sitimagene ceradenovec [63]. This adenoviral vector induces the expression of thymidine kinase in infected cells. Subsequent ganciclovir therapy kills the infected cells because thymidine kinase converts ganciclovir into a cytotoxic nucleoside analog (thymidine kinase/ganciclovir-mediated suicide effect) [64]. Although the trial met the primary endpoint (a composite of time-to-death or reintervention), no convincing improvement of the overall survival was observed.

Several other oncolytic viruses have been tested in clinical trials over the last years, but none of these has reached the market as yet. Their major drawbacks are concerns about biosafety and cytocompatibility [65]. The clinical results and challenges have been discussed in several reviews [66–68].

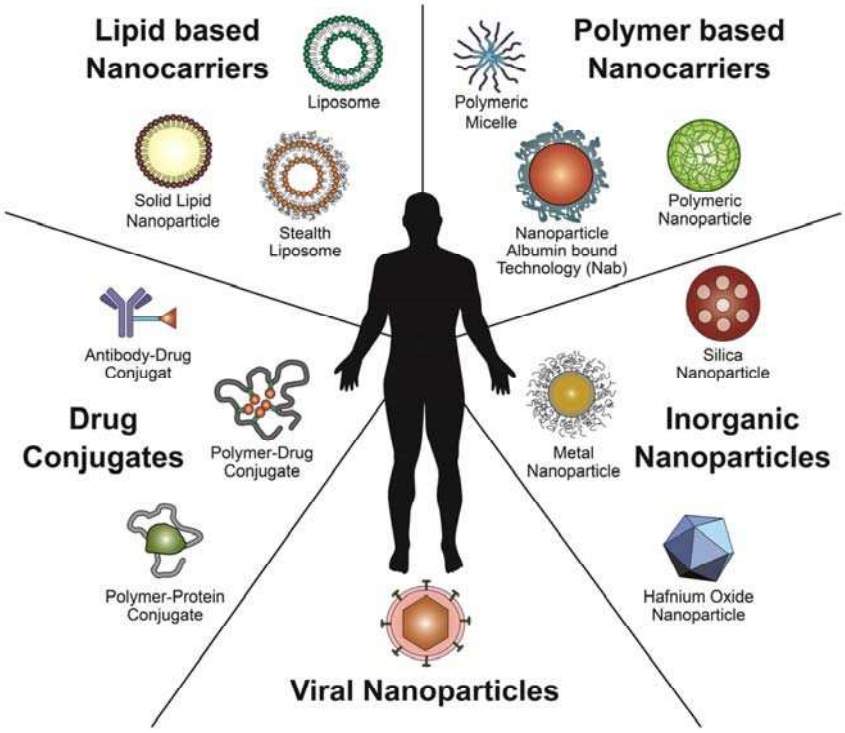

Fig. 3. Schematic illustration of established nanotherapeutic platforms. Different nanomedicine products such as drug conjugates, lipid-based nanocarriers, polymer-based nanocarriers, inorganic nanoparticles, and viral nanoparticles are used in clinical cancer care.

3.2. Organic nanocarriers for cancer therapy

Organic nanocarriers comprise a wide range of natural or synthetic compounds designed for targeted or non-targeted drug delivery. They can roughly be divided into drug conjugates, lipid carriers, protein carriers, glycan carriers, and synthetic polymer carriers. While drug conjugates have made their way well into the clinic, only tentative efforts have been made to introduce nanocarriers based on lipids, proteins, or polymers into clinical practice (Tables 1 and 2).

3.2.1. Drug conjugates

At present, the most successful nanomedicine therapeutics in clinical cancer care are drug conjugates (Tables 1–3). They are defined as nanotherapeutics because of their size scale in the lower nanometer range and their conjugation to active pharmaceutical ingredients [69,70]. The active agents are covalently linked to targeted antibodies and peptides or to polymers. The conjugate is usually mono- or oligomeric, intended to improve targeted delivery of the drug without necessarily impacting on drug solubility, stability, or biodegradability. In contrast, nanocarriers based on lipids, proteins, glycans, or synthetic polymers usually encapsulate the drug, and they obviate the need to link the drug covalently to the carrier.

ADCs approved by regulatory authorities include trastuzumab-emtansine against HER2-overexpressing breast cancer [71] and brentuximab-vedotin against CD30-positive Hodgkin lymphoma and anaplastic large-cell lymphoma [72] (Table 1). Trastuzumab has been in clinical use for some time and is effective in both the adjuvant and palliative settings. Its conjugation to emtansine (DM1), a plant-derived inhibitor of microtubules, significantly increases the ant-tumor activity of trastuzumab. Furthermore, it provides a survival benefit compared to lapatinib and capecitabine in patients with metastasized breast cancer after previous trastuzumab and taxane therapy [71,73].

Vedotin or monomethyl auristatin E is a cytostatic compound with considerable toxicity and is therefore not used in patients in its unconjugated form. However, coupled to an anti-CD30 antibody (brentuximab),

Table 1
Approved antibody drug conjugates (ADCs). Three different ADCs are on the market today (two out of five approved ADCs have been withdrawn from market). They either have a cytotoxic drug payload or a radionuclide payload. More than 30 ADCs are currently undergoing clinical trials. For a detailed list of all ongoing clinical trials see Chari et al., Flygare et al., and Hess et al. [75–77].

Product [company]	ADC	Target	Drug	Indication	Approval	Reference
Cytotoxic drug payload						
Mylotarg® [Pfizer/Wyeth]	Gemtuzumab ozogamicin	CD33	Calicheamicin	Acute myeloid leukemia	2001 (withdrawal 2010)	[166]
Adcetris® [Seattle Genetics]	Brentuximab vedotin	CD30	MMAE	Non-Hodgkin lymphoma	2011	[74]
Kadcyla® [Roche/Genentech/ImmunoGen]	Trastuzumab emtansine	HER2	DM1	Breast cancer	2013	[73]
Radionuclide payload						
Zevalin® [IDEC/Spectrum]	Ibritumomab tiuxetan	CD20	Yttrium-90 or Indium-111	Non-Hodgkin lymphoma	2002	[167]
Bexxar® [Corixa/GlaxoSmithKline]	Tositumomab	CD20	Iodine-131	Non-Hodgkin lymphoma	2003 (withdrawal 2014)	[168]

Table 2
Approved drug conjugates and nanocarriers for cancer therapy. Marketed products are listed alphabetically. Alternative names for the products are given in brackets.

Product [company]	Material	Drug	Indication	Approval	Reference
Abraxane® (ABI-007) [Abraxis/Celgene]	Nanoparticle albumin-bound	Paclitaxel	Breast cancer, pancreatic cancer, non-small-cell lung cancer	2005	[169]
DaunoXome® [Galen]	Liposome	Daunorubicin	Kaposi's sarcoma	1996	[170]
DepoCyt® [Pacira]	Liposome	Cytosine Arabinoside (cytarabine)	Neoplastic meningitis	1999	[171]
Doxil®/Caelyx® [Johnson & Johnson]	Liposome	Doxorubicin	Kaposi's sarcoma Ovarian cancer Breast cancer Multiple myeloma	1995 1999 2003 2007 (Europe, Canada)	[172]
Genexol-PM® (IG-001) [Samyang Biopharm]	PEG-PLA polymeric micelle	Paclitaxel	Breast cancer Lung cancer Ovarian cancer	2007 (South Korea)	[173]
Lipo-Dox® [Taiwan Liposome]	Liposome	Doxorubicin	Kaposi's sarcoma, breast and ovarian cancer	1998 (Taiwan)	[174]
Marqibo® [Talon]	Liposome	Vincristine	Acute lymphoid leukemia	2012 (USA)	[175]
Mepact® [Takeda]	Liposome	Mifamurtide MTP-PE	Osteosarcoma	2009 (EU)	[176]
Myocet® [Cephalon]	Liposome	Doxorubicin	Breast cancer (cyclophosphamide)	2000 (Europe)	[177]
NanoTherm® [Magforce Nanotechnologies]	Iron oxide nanoparticle		Thermal ablation glioblastoma	2010 (Europe)	[135]
Oncaspar® [Enzon/Sigma-tau]	PEG protein conjugate	L-asparaginase	Leukemia	2006	[178]
Zinostatin stimalamer® (Zinostatin) [Yamanouchi]	Polymer protein conjugate	Styrene maleic anhydride neocarzinostatin (SMANCS)	Liver cancer Renal cancer	1994 (Japan)	[179]

thus redirecting it selectively to CD30-expressing cancer cells, vedotin is much less toxic but highly efficacious in patients with Hodgkin's lymphoma [72,74]. Many other ADCs are in clinical trials and further research towards bi- and multispecific hapten binding antibodies will hopefully lead to a next generation of ADCs [75–77].

Polymer-drug conjugates are another interesting group of nano-sized (5–20 nm) drug delivery systems which change the pharmacokinetic profile of a drug [69,78]. More than 15 anti-cancer conjugates are in clinical development (Table 3). All accumulate within tumors via the EPR effect (Section 2.2.1) [79]. The HPMA copolymer-doxorubicin conjugate PK1 is a novel anti-cancer agent with a significantly lower frequency of cardiotoxicity and alopecia than free doxorubicin. A phase 2 study showed promising signs of activity in breast cancer and non-small-cell lung cancer [80]. Additionally, the copolymer backbone of PK1 has been

Table 3
Polymer drug conjugates in clinical trials. Among the available polymer drug conjugates, PK2 is the only one using a conjugated ligand for active targeting. Products are listed alphabetically. Alternative names for the products are given in brackets.

Product [company]	Platform	Ligand (target)	Drug	Indication	Status	Reference
ADI-PEG 20 [Polaris]	PEG protein conjugate		Arginine deaminase	Hepatocellular carcinoma, melanoma	Phase 2/3	[180]
AP5280 [Access Pharmaceuticals]	HPMA drug conjugate		Platinum	Solid tumors	Phase 1/2	[181]
CT-2106 [CTI Biopharma]	Polyglutamic acid drug conjugate		Camptothecin	Colon cancer, ovarian cancer	Phase 1/2	[182]
DE-310 [Daiichi Pharmaceutical]	Carboxymethyldextran polyalcohol drug conjugate		DX-8951 (camptothecin derivate)	Solid tumors	Phase 1	[183]
Delimotecan (Men 4901/T-0128)	Carboxymethyldextran drug conjugate		T-2513 (camptothecin analogue)	Solid tumors	Phase 1	[184]
DOX-OXD (AD-70)	Dextran drug conjugate		Doxorubicin	Solid tumors	Phase 1	[185]
MAG-CPT (PNU166148/Mureletecan) [Pfizer]	HPMA drug conjugate		Camptothecin	Solid tumors	Phase 1	[186]
MTX-HSA	HSA drug conjugate		Methotrexate	Kidney cancer	Phase 2	[187]
NKTR-102 (Etirinotecan pegol) [Nektar]	PEG drug conjugate		Irinotecan	Breast cancer, ovarian cancer, colorectal cancer	Phase 3	[188]
NKTR-105 [Nektar]	PEG drug conjugate		Docetaxel	Solid tumors, ovarian cancer	Phase 1/2	[189]
Pegamotecan (EZ-246) [Enzon]	PEG drug conjugate		Camptothecin	Gastric cancer	Phase 2	[190]
PegAsys [Genentech]/PegIntron [Merck]	PEG protein conjugate		IFNα2a/-IFNα2b	Melanoma, leukemia	Phase 2	[191]
PEG-SN38 (EZN-2208) [Belrose Pharma/Enzon]	PEG drug conjugate		SN38 (irinotecan derivate)	Solid tumors, breast cancer, lymphoma, colorectal cancer	Phase 2	[192]
PK1 (FCE28068) [UK Cancer Research/Pfizer]	HPMA drug conjugate		Doxorubicin	Breast cancer, lung cancer, colorectal	Phase 2	[193]
PK2 (FCE28069) [UK Cancer Research/Pfizer]	HPMA drug conjugate	Galactosamine (lectin)	Doxorubicin	Hepatocellular carcinoma	Phase 2	[81]
PNU166945 [Pfizer]	HPMA drug conjugate		Paclitaxel	Solid tumors	Phase 1	[194]
ProLindac (AP5346)	HPMA drug conjugate		DACH-oxaliplatin	Ovarian cancer	Phase 2	[195]
Taxoprexin [Protarga]	Docosahexaenoic acid drug conjugate		Paclitaxel	Melanoma, liver cancer, adenocarcinoma, kidney cancer, non-small-cell lung cancer	Phase 2/3	[196]
XMT-1001 [Mersana]	Fleximer drug conjugate		Camptothecin	Gastric cancer, lung cancer	Phase 1	[197]
Xyotax, Opaxio (CT-2103) [Cell Therapeutics]	Polyglutamic acid (polyglumex) drug conjugate		Paclitaxel	Lung cancer, ovarian cancer	Phase 3	[198]

Table 4
Lipid-based nanocarriers in clinical trials. Lipid-based nanocarriers are the most widely studied drug delivery systems and several clinical trials are ongoing. Some second-generation drug delivery systems using active targeting or triggered-release mechanisms were evaluated. For active targeting strategies, the targeting ligand and the cognate receptor are indicated. All nanocarriers are intended for parenteral application with the exception of L9NC and SLIT cisplatin (aerosol). Products are listed alphabetically. Alternative names for the products are given in brackets.

Product [company]	Platform	Ligand (target)	Drug	Indication	Status	Reference
2B3-101 [to-BBB]	Liposome	Glutathione	Doxorubicin	Brain metastases of breast cancer	Phase 1/2a	[199]
ALN-VSP [Alnylam]	Lipid nanoparticle	Association with ApoE in vivo (LDLR)	RNAi targeting KSP and VEGF	Liver cancer and liver metastases	Phase 1	[112]
Anti-EGFR Immunoliposomes [University of Basel]	Liposome	Antibody fragment (EGFR)	Doxorubicin	Solid tumors	Phase 1	[13]
Aroplatin (L-NDDP) [Aronex]	Liposome		DACH platin	Colorectal cancer, solid malignancies	Phase 1/2	[200]
ATI-1123 [Azaya Therapeutics]	Liposome		Docetaxel	Solid tumors	Phase 1	[201]
Atu027 [Silence Therapeutics]	Liposome/Lipoplex		siRNA against PKN3	Solid tumors, pancreatic cancer, head and neck cancer	Phase 1/2	[202]
CPX-1 [Celator]	Liposome		Irinotecan HCl/floxuridine	Colorectal cancer	Phase 2	[203]
CPX-351 [Celator]	Liposome		Cytarabine/daunorubicin	Acute myeloid leukemia	Phase 2/3	[204]
C-VISA BikDD [MD Anderson Cancer Center]	Lipid conjugate		Pro-apoptotic Bik gene	Pancreatic cancer	Phase 1	[205]
DCR-MYC (DCR-M1711) [Dicerna Pharmaceuticals]	Lipid nanoparticle		Dicer substrate RNAi (DsiRNA) targeting MYC oncogene	Solid tumors, multiple myeloma, lymphoma	Phase 1	[206]
DPX-0907 (DepoVax) [ImmunoVaccine]	Liposome complex		HLA-A2-restricted peptides, T Helper Peptide, polynucleotide adjuvant	Cancer vaccine for ovarian, breast and prostate cancer	Phase 1	[207]
E7389 Liposome [Eisai]	Liposome		E7389 (Eribulin Mesylate)	Solid tumors	Phase 1	[208]
EGFR antisense DNA Liposomes [University of Pittsburgh]	Liposome		EGFR antisense DNA	Head and neck cancer	Phase 1	[209]
Endo-Tag-1 (MBT-0206) [Medigene]	Liposome		Paclitaxel	Pancreatic cancer, triple negative breast cancer, head and neck cancer	Phase 2 Phase 2 Phase 1/2	[210]
EphA2 Targeting Liposomes [MD Anderson Cancer Center]	Liposome		siRNA targeting the oncoprotein EphA2	Solid tumors	Phase 1	[211]
IHL-305 [Yakult Honsha]	Liposome		Irinotecan (CPT-11)	Solid tumors	Phase 1	[212]
INGN-401 [Introgen/Genprex]	Lipid nanoparticle		FUS1 gene	Lung cancer	Phase 1/2	[213]
Interleukin-2 gene therapy [H. Lee Moffitt Cancer Center]	Liposome		Interleukin-2 Gene	Head and neck cancer	Phase 2	[214]
INX-0076 (Brakiva) [Tekmira]	Liposome		Topotecan	Solid tumors	Phase 1	[215]
INX-0125 (Alocrest) [Tekmira]	Liposome		Vinorelbin	Solid tumors	Phase 1	[216]
L9NC [University of Mexico]	Liposome (aerosol)		9-Nitro-20 (S)-Camptothecin	Non-small-cell lung cancer	Phase 2	[217]
L-Annamycin [Callisto]	Liposome		Annamycin	ALL, AML, doxorubicin-resistant breast cancer	Phase 1 Phase 1 Phase 2	[218]
LE-DT [NeoPharm/Insys]	Liposome		Docetaxel	Solid tumors, pancreas/prostate cancer	Phase 1 Phase 2	[219]
LEM-ETU [NeoPharm/Insys]	Liposome		Mitoxantrone	Solid tumors, lymphoma	Phase 1	[220]
LEP-ETU (PNU-93914) [NeoPharm/Insys]	Liposome		Paclitaxel	Ovarian cancer, breast cancer, lung cancer	Phase 1/2	[221]
LErafAON [INSYS]	Liposome		c-Raf antisense oligonucleotide	Advanced malignancies	Phase 1	[222]
LE-SN38 [NeoPharm/Insys]	Liposome		SN38 (active metabolite of irinotecan)	Colorectal cancer	Phase 2	[223]
LiPlaCis [LiPlasome Pharma]	Liposome		Cisplatin	Solid tumors	Phase 1	[224]
Lipocurc [SignPath Pharma]	Liposome		Curcumin	Advanced cancer	Phase 1b	[225]
Lipoplatin [Regulon]	Liposome		Cisplatin	Non-small-cell lung cancer	Phase 3	[226]
Liposomal Grb-2 [MD Anderson/Bio-Path]	Liposome		Grb2 antisense nucleotide	Leukemia	Phase 1	[227]
Liposomal Tretinoin (ATRA-IV) [MD Anderson/NCI]	Liposome		Tretinoin	Refractory Hodgkin disease, kidney cancer, solid tumors	Phase 1/2	[228]
Lipovaxin-MM [Lipotek]	Lipid based formulation	Single domain antibody fragment (DC-SIGN)	Melanoma antigens and IFN-γ	Melanoma vaccine	Phase 1	[229]
Lipusu [Luye Pharma]	Liposome		Paclitaxel	Solid tumors, gastric cancer, metastatic breast cancer	Phase 2 Approved in China	[230]
MBP-426 [Mebiopharm]	Liposome	Transferrin (transferrin receptor)	Oxaliplatin	Gastric cancer	Phase 2	[231]
MCC-465 [Mitsubishi Pharma]	Liposome	Human Antibody Fragment GAH (tumor antigen)	Doxorubicin	Gastric cancer	Phase 1 (discontinued)	[106]
MM-302 [Merrimack]	Liposome	Antibody (ErbB2/ErbB3)	Doxorubicin	ErbB2-positive breast cancer	Phase 1	[232]
MM-398 (PEP02) [Merrimack]	Liposome		CPT-11 (Irinotecan)	Pancreatic cancer, gastric cancer, glioma	Phase 3 Phase 2 Phase 1	[233]
MRX34 [Mirna Therapeutics]	Liposome		miR-RX34	Liver cancer, solid tumors, lymphoma, myeloma	Phase 1	[234]

(continued on next page)

Table 4 (*continued*)

Product [company]	Platform	Ligand (target)	Drug	Indication	Status	Reference
NanoVNB [Taiwan Liposome]	Liposome		Vinorelbine	Solid tumors	Phase 1	[95]
NL CPT-11 [UCSF]	Liposome		Irinotecan	Recurrent glioma	Phase 1	[235]
Onco-TCS [Inex/Enzon]	Liposome		Vincristin	Non-Hodgkin lymphoma	Phase 2/3	[236]
OSI-211 [OSI Pharmaceuticals]	Liposome		Lurtotecan	small cell lung cancer, ovarian cancer, head and neck cancer	Phase 2	[237]
OSI-7904L [OSI Pharmaceuticals]	Liposome		Thymidylate synthase inhibitor	Colorectal cancer, gastric cancer, head and neck cancer	Phase 2	[238]
PNT2258 [ProNAi Therapeutics]	Liposome		DNAi targeting BCL-2	Non-Hodgkin lymphoma, solid tumors	Phase 1	[239]
Promitil [Lipomedix]	Liposome		Mitomycin-C Prodrug	Solid tumors	Phase 1	[240]
Sarcodoxome [GP Pharma]	Liposome		Doxorubicin	Soft tissue sarcoma	Phase 1/2	[241]
S-CKD602 [Alza]	Liposome		CKD602 (belotecan)	Solid tumors	Phase 1/2	[242]
SGT-53 [SynerGene Therapeutics]	Liposome	scFv Antibody (transferrin receptor)	p53 plasmid DNA	Solid tumors	Phase 1b	[243]
SGT-94 [SynerGene Therapeutics]	Liposome	scFv Antibody (transferrin receptor)	RB94 plasmid DNA	Solid tumors	Phase 1	[244]
SLIT cisplatin [Transave/Insmed]	Lipid product (aerosol)		Cisplatin	Lung cancer (Aerosol)	Phase 2	[245]
SPI-077 [Alza]	Liposome		Cisplatin	Solid tumors, ovarian cancer, head and neck cancer	Phase 2	[246]
Stimuvax (BLP25) [Oncothyreon/Merck]	Liposome		Anti-MUC1 cancer vaccine	Non-small-cell lung cancer	Phase 3	[247]
STMN-1 [Gradalis]	Lipoplex		Pbi-shRNA STMN1	Solid tumors, metastatic cancer	Phase 1	[248]
ThermoDox [Celsion]	Thermo-sensitive liposome		Doxorubicin	Primary hepatocellular carcinoma, refractory chest wall breast cancer, colorectal liver metastases	Phase 3 Phase 2 Phase 2	[249]
TKM-PLK1 (TKM 080301) [Tekmira]	Liposome (SNALP)		RNAi targeting polo-like kinase 1 (POLO)	Liver cancer, neuroendocrine tumors, adrenocortical carcinoma	Phase 1/2	[250]

modified with galactosamine residues for active targeting of the liver. The resulting PK2 was the first drug conjugate with active targeting properties tested in a clinical trial [81] (Table 3).

Radiopeptides represent a specific class of drug conjugates because their size (around 1 nm) is at the limit of the conventional definition of a nanomedicine agent (Section 4.3). The most widely used therapeutic radiopeptides are DOTATOC [82] and DOTATATE. Radiopeptides are built from a peptide component determining the specificity of the compound, and a chelator binding the radioisotope (e.g., ^{90}Y or ^{177}Lu). DOTATOC and DOTATATE bind mainly to the somatostatin receptor 2 (sst2) and thus guide the radioisotope selectively to sst2-overexpressing (usually neuroendocrine) cells. Unfortunately, no phase 3 data are currently available for this treatment modality. A phase 3 trial (NETTER-1, NCT01578239) comparing ^{177}Lu-DOTA0-Tyr3-octreotate with octreotide LAR in patients with advanced sst-expressing neuroendocrine mid-gut tumors is running, with data expected in 2017.

3.2.2. Lipid-based nanocarriers

There are different forms of lipid-based nanocarriers (reviewed by Fang and Al-Suwayeh [83]), the most frequently investigated are liposomes (closed phospholipid bilayers) and micelles (normal phase, oil-in-water micelles). Lipid nanocarriers provide a carrying capacity three to four orders of magnitude greater than ADCs, which typically comprise 1 to 6 drug molecules per monoclonal antibody. Pegylated liposomal doxorubicin (Doxil® or Caelyx®) was the first nanocarrier approved by the US Food and Drug Administration (FDA) in 1995 [84,85]. Today, five more lipid nanocarriers are approved for clinical use: non-pegylated liposomal doxorubicin (Myocet®) [86], non-pegylated liposomal daunorubicin (DaunoXome®) [87], non-pegylated liposomal cytarabine (DepoCyt®) [88], vincristine sulfate liposomes (Marqibo®) [89], and liposomal mifamurtide (Mepact®) [90,91] (Table 2). Of note, none of the six approved lipid nanocarriers is targeted. However, the nano-formulations of doxorubicin, daunorubicin, and vincristine prolong the half-life of the cytotoxic compounds and profoundly improve their toxicity profiles.

As discussed already, lipid nanocarriers, and in particular pegylated liposomes, tend to accumulate in tumor tissue due to the enhanced permeability of intra- and peritumoral vessels and somewhat prolonged retention in cancerous tissue (Section 2.2.1) [92]. Many other non-targeted liposomes are being evaluated in clinical trials (Table 4) [93]. In a recent phase 2 trial, MM-398 (PEP02), a nanocarrier formulation of irinotecan, showed some signs of activity against gastric and gastro-esophageal junction adenocarcinomas in the second line setting [94]. Non-targeted liposomal vinorelbine (NanoVNB®) was tested in a phase 1 trial [95]. With this nano-compound, skin rash was the dose-limiting toxicity.

A well-studied example for altered pharmacokinetics and toxicity of a nano-delivered compound is doxorubicin. The critical cardiotoxicity free (water-dissolved) doxorubicin is markedly reduced with the liposomal formulation. However, liposomal doxorubicin induces more hand-foot syndrome (palmar-plantar erythrodysesthesia) than free doxorubicin. While many would have predicted the lowered cardiotoxicity of pegylated liposomal doxorubicin (it was already known that longer infusion times decreased cardiac side effects of doxorubicin), it is difficult to foresee in silico or in vitro the hand-foot syndrome. This illustrates the difficulty of predicting toxicity profiles of nano-applications of known drugs (Section 4.2). A better understanding of the underlying mechanisms of toxicity is necessary to predict the side effects in humans more accurately.

While liposomal formulations allow for stable encapsulation of a drug, they do not address the issue of targeted delivery. To achieve true targeted delivery, liposomes must be modified on their surface with an agent that confers specificity. One possible approach is the conjugation of antibodies, antibody fragments, or single-chain antibodies to the liposomal surface [96,97]. Coating of liposomes with whole antibodies was reported to reduce the plasma half-life of the resulting immunoliposomes (ILs), probably due to entrapment of Fc-containing ILs in the RES. Therefore, Fc-free antibodies are preferred [98,99]. For example, antibodies such as anti-EGFR (e.g., C225, cetuximab) or anti-VEGFR2 (e.g., DC101) may be cleaved and reduced to produce Fab' fragments. The Fab' fragment is then covalently conjugated to maleimide

groups at the termini of PEG-DSPE chains which reside in the lipid bilayer [100].

In several preclinical experiments, the surface of liposomes was coated with anti-HER2, anti-EGFR, anti-VEGFR2, or other antibodies [101–103]. In mouse models of human cancer, these nanocarriers were shown to deliver cytotoxic compounds specifically to cells expressing the target antigen. Cellular uptake was depended on the interaction of the target antigen on the cell surface and the antibody coating the surface of the liposome. Tumors treated with anti-VEGFR2-targeted and doxorubicin-loaded ILs shrank to 1/6 of the size of those treated with an identical dose of non-targeted liposomal doxorubicin [103]. This illustrates the potency of targeted lipid nanocarriers compared to their non-targeted counterparts. An additional advantage is the capability of targeted ILs, for example anti-EGFR-ILs, to overcome

Table 5
Polymer-based nanocarriers in clinical trials. Polymer-based nanocarriers consist of a natural or synthetic polymer. Most commonly used natural polymers are proteins (e.g., albumin) or glycans (e.g., cyclodextrin). For active targeting strategies, the targeting ligand and cognate receptor are indicated. Products are listed alphabetically. Alternative names for the products are given in brackets.

Product [company]	Polymer	Ligand (target)	Drug	Indication	Status	Reference
ABI-008 [Abraxis/Celgene]	Albumin nanoparticle		Docetaxel	Metastatic breast cancer, prostate cancer	Phase 2	[251]
ABI-009 [Abraxis/Celgene]	Albumin nanoparticle		Rapamycin	Solid tumors, bladder cancer	Phase 1/2	[252]
ABI-011 [Abraxis/Celgene]	Albumin nanoparticle		Thiocolchicine dimer	Solid tumors, lymphoma	Phase 1/2	[253]
BIND-014 [Bind Therapeutics]	PEG-PLGA polymeric nanoparticle	Aptamer (PSMA)	Docetaxel	Non-small-cell lung cancer, prostate cancer	Phase 1/2	[127]
CALAA-01 [Calando Pharmaceuticals]	Cyclodextrin polymeric nanoparticle	Transferrin (transferrin receptor)	siRNA targeting ribonucleotide reductase subunit 2	Solid tumors	Phase 1	[254]
CRLX-101 (IT-101) [Cerulean Pharma]	Cyclodextrin nanoparticle		Camptothecin	Solid tumors, renal cell carcinoma, rectal cancer, non-small-cell lung cancer	Phase 1/2	[255]
DHAD-PBCA-NP	Polymeric nanoparticle		Mitoxantrone	Hepatocellular carcinoma	Phase 2	[130]
Docetaxel-PNP [Samyang Biopharmaceuticals]	Polymeric nanoparticle		Docetaxel	Solid tumors	Phase 1	[256]
Lipotecan (TLC388) [Taiwan Liposome]	Polymeric micelle		TLC388 (Camptothecin derivate)	Liver cancer, renal cancer	Phase 1/2 (orphan drug status)	[257]
Nanotax [CritiTech]	Polymeric nanoparticle		Paclitaxel	Peritoneal neoplasms	Phase 1	[258]
Nanoxel [Fresenius Kabi Oncology]	Polymeric micelle		Paclitaxel	Advanced breast cancer	Phase 1	[259]
NC-4016 [NanoCarrier]	Polymeric micelle		Oxaliplatin	Solid tumors, lymphoma	Phase 1	[260]
NC-6004 (Nanoplatin) [NanoCarrier]	PEG-PGA polymeric micelle		Cisplatin	Pancreas cancer	Phase 2/3	[124]
NC-6300 (K-912) [NanoCarrier]	pH sensitive polymeric micelle		Epirubicin	Solid tumors	Phase 1 (Japan)	[129]
NK-012 [Nippon Kayaku]	PEG-PGA polymeric micelle		SN-38 (active metabolite of irinotecan)	Solid tumors, small cell lung cancer, breast cancer,	Phase 2	[261]
NK-105 [NanoCarrier Nippon Kayaku]	PEG-PAA polymeric micelle		Paclitaxel	Gastric cancer, breast cancer	Phase 2/3	[262]
NK-911 [National Cancer Institute Japan/Nippon Kayaku]	PEG-PAA polymeric micelle		Doxorubicin	Solid tumors	Phase 1	[263]
Paclical [Oasmia Pharmaceutical]	Polymeric micelle		Paclitaxel	Ovarian cancer	Phase 3 (orphan drug status)	[264]
SP1049C [Supratek Pharma]	Polymeric micelle	Pluronic (P-Glycoprotein)	Doxorubicin	Advanced adenocarcinoma	Phase 2/3	[265]
Transdrug BA-003 (Livatag) [BioAlliance Pharma]	Polymeric nanoparticle		Doxorubicin	Hepatocellular carcinoma	Phase 3 (2004 EU orphan drug status)	[266]

Table 6
Inorganic nanoparticles in clinical trials. Inorganic nanomaterials are used for several applications but only Aurimune is designed for drug delivery. Products are listed alphabetically. Alternative names for the products are given in brackets.

Product [company]	Platform	Ligand (target)	Application	Indication	Status	Reference
Aurimune (CYT-6091) CytImmune Sciences]	Colloidal gold		Tumor necrosis factor delivery	Solid tumors	Phase 1/2	[137]
AuroLase [Nanospectra]	Gold-coated silica nanoparticle		Photothermal ablation	Head and neck cancer	Phase 1	[267]
Ferumoxtran-10 (Sinerem/Combidex) [Guerbet/AMAG]	Iron oxide nanoparticle		Magnetic resonance imaging	Prostate cancer	Phase 3	[268]
Ferumoxytol (Feraheme) [MD Anderson/AMAG]	Iron oxide nanoparticle		Magnetic resonance imaging	Head and neck cancer, lymph node cancer	Phase 1	[269]
NanoXray (NBTXR3) [Nanobiotix]	Hafnium oxide nanoparticle		Radiotherapy	Solid tumors	Phase 1	[136]
Targeted SNP [Memorial Sloan Kettering Cancer Center]	Silica nanoparticle	cRGDY (integrin)	Lymph node imaging	Head and neck melanoma	Phase 0	[270]

multidrug resistance in cancer cells (Fig. 2E) [12,104]. In particular, membrane transporters such as P-glycoprotein or MRP-1, which expel anti-cancer agents from cells, are bypassed by targeted ILs [10,105].

The first clinical trial with targeted liposomes involved GAH-coated, doxorubicin-loaded ILs (MCC-465) in patients with metastatic stomach cancer [106]. GAH is a human monoclonal antibody reacting against >90% of human gastric cancers [107,108]. GAH-ILs were given in 3-weekly cycles up to a maximum of 6 cycles. Myelosuppression was the relevant dose-limiting toxicity. Overall, 10 of 18 evaluable patients had stable disease, but no remissions were observed.

The second trial assessing ILs in advanced solid tumors was published recently [13]. In this prospective proof-of-principle study, a fragment of the anti-EGFR antibody cetuximab was conjugated to doxorubicin-loaded pegylated liposomes. Anti-EGFR-ILs were given i.v. every 4 weeks for a total of 6 cycles or until toxicity or progression occurred. Again, myelosuppression was the relevant dose-limiting toxicity. In this heavily pretreated study cohort, some preliminary signs of clinical activity were observed, including one complete remission among 24 evaluable patients (Fig. 2F). With regard to toxicity, anti-EGFR-ILs did not exhibit any cardiac side effects, thus mimicking the favorable cardiotoxicity profile of liposomal doxorubicin. Intriguingly, no case of hand-foot syndrome was observed when treating patients with liposomal doxorubicin labeled with anti-EGFR. In this respect, the toxicity of anti-EGFR-ILs was more similar to free doxorubicin than to liposomal doxorubicin.

Lipid nanocarriers are also being investigated for systemic delivery of nucleic acids and other substances with short plasma half-life (Table 4) [109,110]. Although no such drug has been approved for clinical use as yet, feasibility and efficacy of siRNA delivery (RNAi) with lipid nanocarriers have been demonstrated in first-in-man trials [111,112]. A number of phase 1 trials in solid tumors are ongoing, e.g., NCT01158079 with RNAi directed against kinesin spindle protein (KSP) and vascular endothelial growth factor (VEGF), NCT01262235 with RNAi against polo like kinase 1 (PLK1), and NCT00938574 with RNAi against PKN3, a protein kinase C related molecule in vascular endothelium. More than 15 different lipid-based nanocarriers are currently undergoing clinical trials for the delivery of regulatory nucleic acids in order to silence oncogenes, such as Myc, c-Raf, or Bcl-2, or to express tumor suppressors, such as p53 or Fus1 (Table 4).

Another innovative lipid-based approach in preclinical testing is the squalenoylation technology [113,114]. Anti-cancer drugs, e.g. doxorubicin, are chemically linked to the natural lipid squalene. These conjugates self-organize in water to nanoassemblies with unique characteristics such as high drug payload and prolonged systemic circulation. Squalene–doxorubicin nanoassemblies showed a 95% reduction of pancreatic tumors in xenograft mice models, compared to 29% achieved by free doxorubicin.

3.2.3. Natural polymers: protein and peptide nanocarriers

Only one protein-based nanoparticle has found its way into the clinic so far: albumin-nanoparticle-bound paclitaxel (nab-paclitaxel; Abraxane®) is used for the therapy of breast cancer, non-small-cell lung cancer, and pancreatic cancer (Table 2). Paclitaxel is a cytotoxic compound isolated from the bark of the pacific yew tree (*Taxus brevifolia*). Since paclitaxel itself is poorly water soluble, it is dissolved in Cremophor EL, a polyethoxylated castor oil. However, this solvent is the reason for the frequent allergic reactions to the drug. Therefore, alternative formulations were investigated. By incorporating paclitaxel into an albumin-nanoparticle, drug solubility is improved and the use of castor oil can be avoided.

At the same time, the pharmacokinetic profile of paclitaxel is altered, which may account for the increase in neurological side effects observed with nab-paclitaxel compared to solvent-based paclitaxel. Nab-paclitaxel is not an active targeted nanoparticle in the strict sense of the term. However, albumin may mediate transcytosis of the compound via the gp60 receptor on the endothelium and thus enhance its delivery to the tumor [115]. In clinical trials, nab-paclitaxel improved response rates compared to conventional paclitaxel in breast cancer patients [116]. In combination with gemcitabine, nab-paclitaxel increased survival compared to gemcitabine monotherapy in patients with pancreatic cancer [117]. In a phase 3 study, the combination of nab-paclitaxel with carboplatin was tested in patients with advanced non-small-cell lung cancer (CA031 study, NCT00540514). Patients in the nab-paclitaxel/carboplatin arm had longer progression-free survival than those in the solvent-based paclitaxel/carboplatin arm, but overall survival was not significantly different [118].

The success of nab-paclitaxel has paved the way for the development of other albumin stabilized nanoparticles undergoing clinical trials such as ABI-008, ABI-009, and ABI-011 (Table 5). Other peptide-based nanocarriers such as self-assembling avidin-biotin-based nanocomplexes are being evaluated in preclinical models and may hopefully undergo clinical trials in the near future [119].

3.2.4. Natural polymers: glycan nanocarriers

Currently, there are no approved glycan nanocarriers for systemic cancer therapy. However, glycan nanoparticles have been tested in proof-of-concept phase 1 and in phase 2 trials (Table 5). In a phase 2 clinical trial, cyclodextrin nanoparticles were used as carriers for camptothecin in patients with advanced solid tumors. CRLX-101 (formerly IT-101) showed fewer side effects than free camptothecin and the overall response rate was 64% [120].

CALAA-01 is another polymer nanoparticle (50–70 nm) based on cyclodextrin and PEG in clinical development for siRNA delivery. It is targeted to human transferrin receptors overexpressed on cancer cells to silence the expression of the M2 subunit of ribonucleotide reductase. Intracellular release of siRNA is triggered by an acidic endosomal pH [121].

Preclinically, chitosan-based glycan nanoparticles have been used to develop an oral formulation of the cytotoxic compound gemcitabine [122]. Gemcitabine-loaded chitosan nanoparticles were about 95 nm in diameter. Intestinal uptake increased 3–5 fold compared to free oral gemcitabine.

3.2.5. Synthetic polymer-based nanocarriers

Because of their chemical versatility, synthetic polymer nanocarriers are a promising tool for nanomedicine therapeutics [123]. Table 5 summarizes all synthetic polymer nanocarriers in clinical trials.

As an example, the PEG–PGA polymeric micelle NC-6004 (Nanoplatin®) for the delivery of cisplatin was tested in a phase 1 trial. Compared to the free drug, NC-6004 was associated with less oto- and neurotoxicity as well as nausea, and the disease control rate was encouraging [124]. A phase 3 clinical trial in patients with pancreatic cancer is underway. In addition, several other polymeric micelles such as NK-012 or NK-105 are investigated in advanced clinical trials (Table 5) [125].

The first targeted polymeric nanoparticle in clinical trials is BIND-014. It is made up of docetaxel-encapsulated PLGA–PEG nanoparticles targeted to prostate-specific membrane antigen (PSMA). In various animal models, BIND-014 has delivered up to 10 times more docetaxel to tumors than free docetaxel. The nanoparticle system exhibited prolonged residence time in circulation, and more extensive retention in the tumor. In addition, tumor shrinkage in animal models was the same at a fifth of the dose of free docetaxel. There are also some preliminary signs of activity in phase 1 studies [126,127]. The same nanoparticle platform technology is in preclinical evaluation for the delivery of cisplatin [128].

A variety of other synthetic polymer nanocarriers have been evaluated in phase 1 trials, including epirubicin-loaded polymeric micelles [129] and mitoxantrone-loaded polybutylcyanoacrylate nanoparticles [130] (Table 5).

Furthermore, phase 1 clinical trials for other polymeric nanocarriers are expected in 2015. The Cristal therapeutics polymeric technologies (CriPec®) approach is used to formulate transiently stable polymeric micelles with biodegradable crosslinking for tunable drug release [131]. Through cleavage of the linker, the drug is released at a constant rate from its polymeric, micellar form. First preclinical studies have shown that accumulation of CriPec docetaxel at the tumor site is much higher than free docetaxel.

An innovative approach to improve liver function and reduce tumor burden in hepatocellular cancer (HCC) is the delivery of short-activating RNA (saRNA) with poly(amidoamine) dendrimers (PAMAM). This approach was successfully tested preclinically in a rat model of HCC and will hopefully enter clinical trials soon [132].

3.3. Inorganic nanoparticles for cancer therapy

Inorganic nanoparticles are used for a variety of applications, including tumor imaging, enhancement of radiotherapy, or drug delivery [133]. Iron oxide nanoparticles are mainly used for diagnostic purposes [134] and some are tested in clinical studies for magnetic resonance imaging of tumors. NanoTherm® is an aqueous colloidal dispersion of iron oxide nanoparticles. Upon instillation in the tumor, thermal ablation is performed with an alternating magnetic field applicator (magnetic hyperthermia). The most robust data are available for glioblastoma [135]. NanoTherm® has gained marketing approval in several European countries.

Recently, the first clinical trial with hafnium oxide nanoparticles has started. The nanoparticles are investigated in patients with soft tissue sarcoma as a radiosensitizer [136]. A phase 2 clinical trial is expected to start at the end of 2014.

No inorganic nanoparticle for drug delivery has reached marketing approval as yet (Table 2). Some of them are in early clinical testing (Table 6), for example pegylated colloidal gold-TNFα particles for cancer therapy [137] and silicon nanocarriers for parenteral peptide delivery [138].

4. Challenges and current limitations

Nanomedicine is as one of the most promising and advanced approaches in the development of frontier cancer treatment. Thousands of publications suggest that nanomedicine therapeutics are effective in cancer treatment, both in vitro and in vivo (Fig. 1A). However, only very few nanocarrier-based cancer therapeutics have successfully entered clinical trials (Fig. 1B). Thus, it is important to address the challenges in developing optimized nanomedicine products for clinical use [139].

4.1. Physico-chemical characterization of nanomaterials

In general, the main physico-chemical features of nanocarriers are structure, composition, size, surface properties, porosity, charge, and aggregation behavior [140,141]. Variability within these properties makes it difficult to characterize nanomedicine products before and after administration. Quantitative analytical methods have to be able to monitor all necessary quality aspects of the nano-sized compounds.

Polydispersity (PD) is a measure of heterogeneity of particles with regard to size, shape, or mass. It plays a major role in characterizing nanocarriers because even small variations in PD and physico-chemical characteristics can cause dramatic changes in secondary properties such as biocompatibility, toxicity, and in vivo outcomes (Fig. 4) [142–145].

Therefore, nanomedicine products should be characterized on a batch-to-batch basis, using multiple methods. The majority of nanomedicine drugs are formulated in aqueous buffers representing the ionic strength of physiological pH. However, nanocarriers may interact with other biological fluids (e.g. blood serum) or biomolecules (e.g. proteins), which may lead to aggregation or agglomeration of particles [146]. Such interactions can significantly alter the function of nanomedicine compounds in biological systems. As discussed earlier, the final form of nanomedicine products should be fully characterized under clinically relevant conditions.

Characterization of stability and storage aspects (shelf-life) of nanomedicine products is also challenging. Biodegradable nanomaterials such as polymers have been increasingly used in the development of nanomedicine products [147]. After polymer degradation and when reaching biological fluids such as blood serum, nanocarriers can again change their physico-chemical properties such as size, drug loading, and release profile. This may have an impact on their performance in vivo. Similarly, storage in aqueous solutions including buffers and even in a lyophilized powder form can alter the properties of nanocarriers [148].

There is a substantial need to improve quality assessment of nanomaterials by developing well-defined and reproducible standards. Moreover, in vitro and in vivo models accurately representing the clinical setting must be developed.

4.2. Safety concerns

Wide-spread use of nanoparticles makes it necessary to address toxicity issues for the human health and environment. The nano-scale dimension of nanomedicine products is similar to that of intracellular organelles or biomolecules involved in cell signaling. Several studies have demonstrated that nanoparticles may be associated with detrimental biological interactions. This has led to the emergence of nanotoxicology as an independent field of research [143,149]. An increasing amount of data is becoming available regarding the toxicity of nanoparticles (Fig. 1A).

Nonetheless, it remains difficult to compare the toxicity of nanomaterials with that of macromaterials. Currently used toxicity assays for nanomaterials are the same as those used for classical drugs. Thus, assessment of nanoparticle toxicity may be inadequate at present and the development of complementary toxicity assays for nanomedicine compounds should be encouraged [150,151]. Multiple factors modulate the toxicity of nanomaterials. Properties such as size, shape, surface area, surface charge, porosity, or hydrophobicity affect the behavior and performance of nanomedicine drugs at the nano-bio interface (Fig. 4). The many variables involved hamper the full toxicological characterization of nanomedicine products. Acute toxicity of nanomedicine compounds usually comprises complement activation, hemolysis, inflammation, oxidative stress, or impaired mitochondrial function (Fig. 4) [152,153]. Analyzing chronic toxicity is more demanding, and data are largely missing.

In clinical development, risks may be minimized by combining more advanced or even predictive diagnostic tools with novel targeting strategies. Thus, "safe-responders" may be identified, and individualized cancer therapy can be realized [154]. Theranostic approaches offer a huge potential in this direction (Section 2.2.4).

Apart from medical issues, environmental concerns have also been expressed. The biomedical, chemical, and cosmetic industry is increasingly using nanomaterials in large-scale production. This renders the monitoring of environmental or occupational exposure to nanoparticles and its consequences more challenging but also more important [155].

4.3. Regulatory issues

A number of nanomedicine products for cancer therapy have been approved by the FDA and European Medicines Agency (EMA) (Tables 1 and 2). They fulfill the current safety requirements set forth by these agencies. However, FDA, EMA, and other regulatory bodies have not yet implemented specific guidelines for drug products containing nanomaterials. The FDA approach to regulate products of nanotechnology has been outlined in a recent article [156]. In June 2014, the FDA released a guidance for industry entitled "Considering Whether an FDA-Regulated Product Involves the Application of

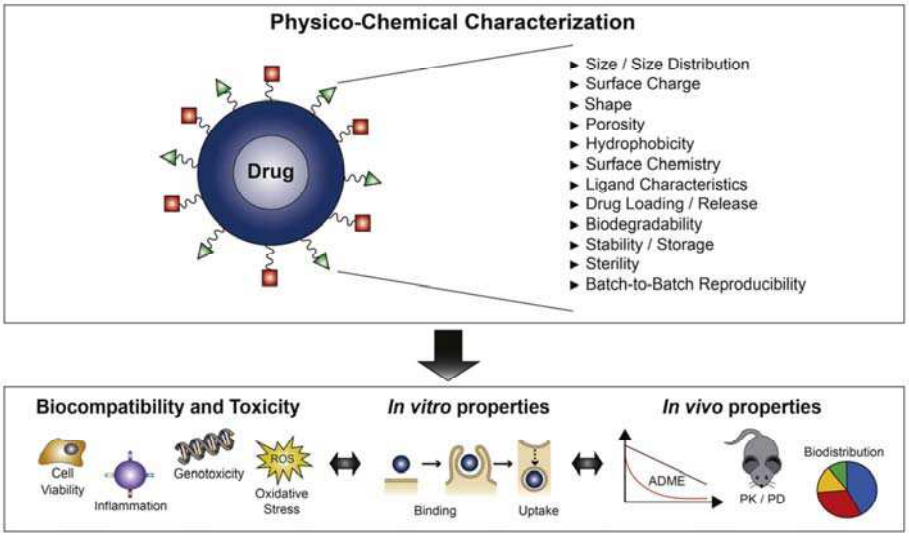

Fig. 4. Cascade for nanomaterial characterization. The physico-chemical properties of nanocarriers affect their pharmacokinetic and pharmacodynamic profiles (Sections 2 and 4.1). Detailed characterization of nanomedicine products is necessary to predict their performance in the clinical setting.

Nanotechnology" [157]. There, nanomaterials are defined as engineered materials with at least one dimension between 1-100 nm. Materials with dimensions up to 1 μm are also included if they exhibit nano-properties, i.e., if quantum effects can be observed. An update of the EMA definition is expected in 2015.

In the absence of evidence and guidance, regulatory decisions on nanomedicine therapeutics are based on individual assessment of benefits and risks [158]. However, this process is time-consuming and may result in regulatory delays for nanomedicine products. Effective regulation requires maintaining high-level expertise in innovative technologies. For example, the FDA collaborates with the Nanotechnology Characterization Laboratory (NCL) to facilitate the regulatory review and in-depth characterization of nanomedicine products. As a part of the Horizon 2020 project, the European Technology Platform on Nanomedicine (ETPN) intends to set up a European Nano-Characterisation Laboratory (EU-NCL) [159].

Regulatory issues are not only relevant for clinical trials and the approval process, but also for the development of cutting-edge technologies to characterize nanomedicine products and monitor their quality. In particular, there is an urgent need for clear guidelines for characterization and quality control of nano-similars, i.e. generic derivatives of nanomedicine products [160]. Lipodox, the first generic liposomal product was approved by the FDA in 2013.

In conclusion, regulatory approval of nanomedicine therapeutics remains challenging. Emergence of nanocarriers developed with more advanced and multifunctional tools is expected to even increase the complexity of the approval process. It will be critical for regulatory agencies to refine and standardize requirements for the approval of nanomedicine products to provide patients with timely access to innovative treatments.

4.4. Manufacturing issues

Manufacturing of nanomedicine products for commercialization is technically challenging and Good Manufacturing Practice (GMP)-compliant production is a major hurdle. Usually, preclinical and early clinical studies have been carried out with a small amount of nanomaterial. In large-scale production, batch-to-batch variations of physical and chemical properties may occur due to the polydispersity of the nanomaterial [161]. Therefore, manufacturing of nanoparticle-based cancer therapeutics at an industrial level requires tight control of physico-chemical properties on a batch-to-batch basis [162]. This makes the chemistry, manufacturing, and control (CMC) process more demanding. An example for the challenges encountered in the production of nanomedicine therapeutics is the Doxil® shortage [163,164]. The production of Doxil® had to be suspended in November 2011 due to manufacturing and sterility issues. The ensuing shortage of Doxil® lasted until 2014 and resulted in delayed therapies for patients, increased medication costs, and the adoption of an alternate manufacturing approach for Doxil®.

Thus, reproducibility and product analysis are critical parameters for a GMP-compliant, large-scale production of nanomedicine products. For instance, common bioconjugation methods such as maleimide or succinimide reactions occur at a very narrow pH interval in order to prevent hydrolysis. When advanced, pH-responsive nanomedicine compounds are produced, the pH interval must be maintained during the whole manufacturing process. Thus, well-defined production steps are required [158].

The high costs of the raw materials and the need for a tedious multi-step production process make the production of nanomedicine therapeutics expensive. For example, manufacturing of commercially available nano-sized drugs such as Abraxane® and Doxil® is far more expensive than the production of their free-drug counterparts (paclitaxel and doxorubicin) [165]. This may dissuade pharmaceutical companies from taking up large-scale production of nanocarriers. Therefore, the clinical benefit of nanomedicine drugs has to be large in order to offset the development and manufacturing costs and to justify higher prices compared to conventional therapeutics [93].

5. Conclusions

Nanomedicine represents one of the fastest growing research areas and is regarded as one of the most promising tools for frontier cancer treatment. Several nanomedicine platforms have been developed and many are used in clinical cancer care. The most important advantages and disadvantages of the different strategies are summarized in Table 7. This table provides an expert opinion on clinical opportunities and summarizes preferred applications for the discussed technologies. Several phase 3 trials have already proven clear benefit of nano-delivered anti-cancer drugs. Nevertheless, nanomaterial

Table 7
Opportunities and challenges of nanomedicine anticancer therapeutics. Expert opinion on most important advantages and disadvantages of different therapeutic strategies.

Nanotherapeutic strategy	Pros	Cons
Targeting principle		
Passive targeting	Ample clinical experience Prolonged circulation time	Unspecific drug delivery Anatomical and physiological barriers
Active targeting	Increased uptake in target cells Less off-target effects Overcoming drug resistance	Large scale production not yet attempted Specific targeting necessary Binding-site barrier (cancer cell targeting)
Stimuli-responsive systems	High specificity Increased drug release	Highly sophisticated manufacturing Specific targeting necessary
Theranostics	Combination of therapy and imaging (personalized medicine) Prediction of therapeutic response	Regulatory/manufacturing challenges Additional equipment necessary Predicitve value of molecular target needs to be assessed in a biomarker trial
Platform		
Viral nanoparticles	Gene therapy approach	Immunogenic Viral spread to unaffected organs
Drug conjugates	Clinically used Small size (deeper penetration)	Limited carrying capacity
• Antibody drug conjugates	Active targeting	Coupling strategies Specific target necessary
• Polymer drug conjugates	Tailored biodistribution of drug	Mostly passive targeting
Lipid-based nanocarriers	Clinically used Biocompatible/biodegradable	
• Conventional liposomes	Reduced adverse drug effects	Rapid clearance via RES
• Pegylated liposomes	Passive targeting Reduced toxicity	Dependent on EPR effect Mostly no improved efficacy
Protein-based nanocarriers	Clinically used	Immunogenic Poor metabolic stabilty
Polymer-based nanocarriers	Chemical versatility	No approved product yet Degradation products of the nanocarrier
Inorganic nanoparticles	May improve imaging	No drug delivery Degradation products of the nanoparticle

characterization, safety concerns, and regulatory as well as manufacturing issues hamper the widespread application of cancer nanomedicine therapeutics. Comprehensive and reproducible characterization of nanomedicine products to predict their efficacy and safety in humans is warranted. Standards for in vitro and in vivo models are required to predict the performance of nanomedicine therapeutics in the clinic. Moreover, well-defined criteria and comprehensive guidelines for both regulatory approval and large-scale industrial production are urgently needed. Timely contact with regulators is recommended to discuss new nanotechnology platforms at an early stage and to expedite evaluation and approval processes. In this promising area of cancer nanomedicine, the cooperation of all parties involved (i.e., research laboratories, regulatory agencies, and industry) is necessary to afford patients rapid access to innovative, safe, and efficacious treatment options.

Acknowledgment

The authors thank Dr. Silvia Rogers for editorial assistance and Andrea Fehrenbach for graphic support. Financial support was provided by the Swiss Centre of Applied Human Toxicology (SCAHT).

References

[1] A service of the U.S. National Institutes of HealthRetrieved Dec. 2014 http://clinicaltrials.gov2014.
[2] R. Duncan, R. Gaspar, Nanomedicine(s) under the microscope, Mol. Pharm. 8 (2011) 2101–2141. http://dx.doi.org/10.1021/mp200394t.
[3] H.D. Williams, N.L. Trevaskis, S.A. Charman, R.M. Shanker, W.N. Charman, C.W. Pouton, et al., Strategies to address low drug solubility in discovery and development, Pharmacol. Rev. 65 (2013) 315–499.
[4] S. Karve, M.E. Werner, R. Sukumar, N.D. Cummings, J.A. Copp, E.C. Wang, et al., Revival of the abandoned therapeutic wortmannin by nanoparticle drug delivery, Proc. Natl. Acad. Sci. U. S. A. 109 (2012) 8230–8235. http://dx.doi.org/10.1073/pnas.1120508109.
[5] A.I. Minchinton, I.F. Tannock, Drug penetration in solid tumours, Nat. Rev. Cancer 6 (2006) 583–592. http://dx.doi.org/10.1038/nrc1893.
[6] X.-Q. Zhang, X. Xu, N. Bertrand, E. Pridgen, A. Swami, O.C. Farokhzad, Interactions of nanomaterials and biological systems: implications to personalized nanomedicine, Adv. Drug Deliv. Rev. 64 (2012) 1363–1384. http://dx.doi.org/10.1016/j.addr.2012.08.005.
[7] T. Lammers, F. Kiessling, W.E. Hennink, G. Storm, Drug targeting to tumors: principles, pitfalls and (pre-) clinical progress, J. Control. Release 161 (2012) 175–187. http://dx.doi.org/10.1016/j.jconrel.2011.09.063.
[8] J.-Z. Du, X.-J. Du, C.-Q. Mao, J. Wang, Tailor-made dual pH-sensitive polymer-doxorubicin nanoparticles for efficient anticancer drug delivery, J. Am. Chem. Soc. 133 (2011) 17560–17563. http://dx.doi.org/10.1021/ja207150n.
[9] C.-M.J. Hu, L. Zhang, Therapeutic nanoparticles to combat cancer drug resistance, Curr. Drug Metab. 10 (2009) 836–841.
[10] J. Huwyler, A. Cerletti, G. Fricker, A.N. Eberle, J. Drewe, By-passing of P-glycoprotein using immunoliposomes, J. Drug Target. 10 (2002) 73–79. http://dx.doi.org/10.1080/10611860290007559.
[11] K.J. Harrington, S. Mohammadtaghi, P.S. Uster, D. Glass, A.M. Peters, R.G. Vile, et al., Effective targeting of solid tumors in patients with locally advanced cancers by radiolabeled pegylated liposomes, Clin. Cancer Res. 7 (2001) 243–254.
[12] C. Mamot, R. Ritschard, A. Wicki, W. Küng, J. Schuller, R. Herrmann, et al., Immunoliposomal delivery of doxorubicin can overcome multidrug resistance mechanisms in EGFR-overexpressing tumor cells, J. Drug Target. 20 (2012) 422–432. http://dx.doi.org/10.3109/1061186X.2012.680960.
[13] C. Mamot, R. Ritschard, A. Wicki, G. Stehle, T. Dieterle, L. Bubendorf, et al., Tolerability, safety, pharmacokinetics, and efficacy of doxorubicin-loaded anti-EGFR immunoliposomes in advanced solid tumours: a phase 1 dose-escalation study, Lancet Oncol. 13 (2012) 1234–1241. http://dx.doi.org/10.1016/S1470-2045(12)70476-X.
[14] A.A. Manzoor, L.H. Lindner, C.D. Landon, J.-Y. Park, A.J. Simnick, M.R. Dreher, et al., Overcoming limitations in nanoparticle drug delivery: triggered, intravascular release to improve drug penetration into tumors, Cancer Res. 72 (2012) 5566–5575. http://dx.doi.org/10.1158/0008-5472.CAN-12-1683.
[15] P.L. Golden, J. Huwyler, W.M. Pardridge, Treatment of large solid tumors in mice with daunomycin-loaded sterically stabilized liposomes, Drug Deliv. 5 (1998) 207–212. http://dx.doi.org/10.3109/10717549809052036.
[16] S.K. Hobbs, W.L. Monsky, F. Yuan, W.G. Roberts, L. Griffith, V.P. Torchilin, et al., Regulation of transport pathways in tumor vessels: role of tumor type and microenvironment, Proc. Natl. Acad. Sci. U. S. A. 95 (1998) 4607–4612.
[17] U. Prabhakar, H. Maeda, R.K. Jain, E.M. Sevick-Muraca, W. Zamboni, O.C. Farokhzad, et al., Challenges and key considerations of the enhanced permeability and retention effect for nanomedicine drug delivery in oncology, Cancer Res. 73 (2013) 2412–2417. http://dx.doi.org/10.1158/0008-5472.CAN-12-4561.
[18] T. Stylianopoulos, R.K. Jain, Combining two strategies to improve perfusion and drug delivery in solid tumors. Proc. Natl. Acad. Sci. U. S. A. 110 (2013) 18632–18637. http://dx.doi.org/10.1073/pnas.1318415110.
[19] B. Theek, L.Y. Rizzo, J. Ehling, F. Kiessling, T. Lammers, The theranostic path to personalized nanomedicine, Clin. Transl. Imaging Rev. Nucl. Med. Mol. Imaging 2 (2014) 66–76. http://dx.doi.org/10.1007/s40336-014-0051-5.
[20] R.K. Jain, T. Stylianopoulos, Delivering nanomedicine to solid tumors, Nat. Rev. Clin. Oncol. 7 (2010) 653–664. http://dx.doi.org/10.1038/nrclinonc.2010.139.
[21] P.P. Provenzano, C. Cuevas, A.E. Chang, V.K. Goel, D.D. Von Hoff, S.R. Hingorani, Enzymatic targeting of the stroma ablates physical barriers to treatment of pancreatic ductal adenocarcinoma, Cancer Cell 21 (2012) 418–429. http://dx.doi.org/10.1016/j.ccr.2012.01.007.
[22] M. Gaumet, A. Vargas, R. Gurny, F. Delie, Nanoparticles for drug delivery: the need for precision in reporting particle size parameters, Eur. J. Pharm. Biopharm. 69 (2008) 1–9. http://dx.doi.org/10.1016/j.ejpb.2007.08.001.
[23] O.C. Farokhzad, R. Langer, Nanomedicine: developing smarter therapeutic and diagnostic modalities, Adv. Drug Deliv. Rev. 58 (2006) 1456–1459. http://dx.doi.org/10.1016/j.addr.2006.09.011.
[24] P. Detampel, D. Witzigmann, S. Krähenbühl, J. Huwyler, Hepatocyte targeting using pegylated asialofetuin-conjugated liposomes, J. Drug Target. (2013). http://dx.doi.org/10.3109/1061186X.2013.860982.
[25] R. van Furth, Z.A. Cohn, J.G. Hirsch, J.H. Humphrey, W.G. Spector, H.L. Langevoort, The mononuclear phagocyte system: a new classification of macrophages, monocytes, and their precursor cells, Bull. World Health Organ. 46 (1972) 845–852.
[26] L.M. Bareford, P.W. Swaan, Endocytic mechanisms for targeted drug delivery, Adv. Drug Deliv. Rev. 59 (2007) 748–758. http://dx.doi.org/10.1016/j.addr.2007.06.008.
[27] S. Bhattacharyya, R. Bhattacharya, S. Curley, M.A. McNiven, P. Mukherjee, Nanoconjugation modulates the trafficking and mechanism of antibody induced receptor endocytosis, Proc. Natl. Acad. Sci. U. S. A. 107 (2010) 14541–14546. http://dx.doi.org/10.1073/pnas.1006507107.

[28] S. Bhattacharyya, R.D. Singh, R. Pagano, J.D. Robertson, R. Bhattacharya, P. Mukherjee, Switching the targeting pathways of a therapeutic antibody by nanodesign, Angew. Chem. Int. Ed. Engl. 51 (2012) 1563–1567. http://dx.doi.org/10.1002/anie.201105432.

[29] E. Perrino, M. Steiner, N. Krall, G.J.L. Bernardes, F. Pretto, G. Casi, et al., Curative properties of noninternalizing antibody-drug conjugates based on maytansinoids, Cancer Res. 74 (2014) 2569–2578. http://dx.doi.org/10.1158/0008-5472.CAN-13-2990.

[30] R. Danielli, R. Patuzzo, P.A. Ruffini, A. Maurichi, L. Giovannoni, G. Elia, et al., Armed antibodies for cancer treatment: a promising tool in a changing era, Cancer Immunol. Immunother. (2014). http://dx.doi.org/10.1007/s00262-014-1621-0.

[31] M. Juweid, R. Neumann, C. Paik, M.J. Perez-Bacete, J. Sato, W. van Osdol, et al., Microparmacology of monoclonal antibodies in solid tumors: direct experimental evidence for a binding site barrier, Cancer Res. 52 (1992) 5144–5153.

[32] R. van der Meel, L.J.C. Vehmeijer, R.J. Kok, G. Storm, E.V.B. van Gaal, Ligand-targeted particulate nanomedicines undergoing clinical evaluation: current status, Adv. Drug Deliv. Rev. 65 (2013) 1284–1298. http://dx.doi.org/10.1016/j.addr.2013.08.012.

[33] M.N. Holme, I.A. Fedotenko, D. Abegg, J. Althaus, L. Babel, F. Favarger, et al., Shear-stress sensitive lenticular vesicles for targeted drug delivery, Nat. Nanotechnol. 7 (2012) 536–543. http://dx.doi.org/10.1038/nnano.2012.84.

[34] A. Jhaveri, P. Deshpande, V. Torchilin, Stimuli-sensitive nanopreparations for combination cancer therapy, J. Control. Release (2014). http://dx.doi.org/10.1016/j.jconrel.2014.05.002.

[35] I.F. Tannock, D. Rotin, Acid pH in tumors and its potential for therapeutic exploitation, Cancer Res. 49 (1989) 4373–4384.

[36] Y. Obata, S. Tajima, S. Takeoka, Evaluation of pH-responsive liposomes containing amino acid-based zwitterionic lipids for improving intracellular drug delivery in vitro and in vivo, J. Control. Release 142 (2010) 267–276. http://dx.doi.org/10.1016/j.jconrel.2009.10.023.

[37] C. Wong, T. Stylianopoulos, J. Cui, J. Martin, V.P. Chauhan, W. Jiang, et al., Multistage nanoparticle delivery system for deep penetration into tumor tissue, Proc. Natl. Acad. Sci. U. S. A. 108 (2011) 2426–2431. http://dx.doi.org/10.1073/pnas.1018382108.

[38] E. Fleige, M.A. Quadir, R. Haag, Stimuli-responsive polymeric nanocarriers for the controlled transport of active compounds: concepts and applications, Adv. Drug Deliv. Rev. 64 (2012) 866–884. http://dx.doi.org/10.1016/j.addr.2012.01.020.

[39] Y.-C. Wang, F. Wang, T.-M. Sun, J. Wang, Redox-responsive nanoparticles from the single disulfide bond-bridged block copolymer as drug carriers for overcoming multidrug resistance in cancer cells, Bioconjug. Chem. 22 (2011) 1939–1945. http://dx.doi.org/10.1021/bc200139n.

[40] D. Kirpotin, K. Hong, N. Mullah, D. Papahadjopoulos, S. Zalipsky, Liposomes with detachable polymer coating: destabilization and fusion of dioleoylphosphatidylethanolamine vesicles triggered by cleavage of surface-grafted poly(ethylene glycol), FEBS Lett. 388 (1996) 115–118.

[41] D. Needham, G. Anyarambhatla, G. Kong, M.W. Dewhirst, A new temperature-sensitive liposome for use with mild hyperthermia: characterization and testing in a human tumor xenograft model, Cancer Res. 60 (2000) 1197–1201.

[42] B.M. Dicheva, G.A. Koning, Targeted thermosensitive liposomes: an attractive novel approach for increased drug delivery to solid tumors, Expert Opin. Drug Deliv. 11 (2014) 83–100. http://dx.doi.org/10.1517/17425247.2014.866650.

[43] N. Fomina, C. McFearin, M. Sermsakdi, O. Edigin, A. Almutairi, UV and near-IR triggered release from polymeric nanoparticles, J. Am. Chem. Soc. 132 (2010) 9540–9542. http://dx.doi.org/10.1021/ja102595j.

[44] R. Bardhan, S. Lal, A. Joshi, N.J. Halas, Theranostic nanoshells: from probe design to imaging and treatment of cancer, Acc. Chem. Res. 44 (2011) 936–946. http://dx.doi.org/10.1021/ar200023x.

[45] N. Rapoport, K.-H. Nam, R. Gupta, Z. Gao, P. Mohan, A. Payne, et al., Ultrasound-mediated tumor imaging and nanotherapy using drug loaded, block copolymer stabilized perfluorocarbon nanoemulsions, J. Control. Release 153 (2011) 4–15. http://dx.doi.org/10.1016/j.jconrel.2011.01.022.

[46] A. Schroeder, R. Honen, K. Turjeman, A. Gabizon, J. Kost, Y. Barenholz, Ultrasound triggered release of cisplatin from liposomes in murine tumors, J. Control. Release 137 (2009) 63–68. http://dx.doi.org/10.1016/j.jconrel.2009.03.007.

[47] J. Ge, E. Neofytou, T.J. Cahill, R.E. Beygui, R.N. Zare, Drug release from electric-field-responsive nanoparticles, ACS Nano 6 (2012) 227–233. http://dx.doi.org/10.1021/nn203430m.

[48] M.S. Shim, Y.J. Kwon, Stimuli-responsive polymers and nanomaterials for gene delivery and imaging applications, Adv. Drug Deliv. Rev. 64 (2012) 1046–1059. http://dx.doi.org/10.1016/j.addr.2012.01.018.

[49] V. Torchilin, Multifunctional and stimuli-sensitive pharmaceutical nanocarriers, Eur. J. Pharm. Biopharm. 71 (2009) 431–444. http://dx.doi.org/10.1016/j.ejpb.2008.09.026.

[50] C. Liu, F. Liu, L. Feng, M. Li, J. Zhang, N. Zhang, The targeted co-delivery of DNA and doxorubicin to tumor cells via multifunctional PEI-PEG based nanoparticles, Biomaterials 34 (2013) 2547–2564. http://dx.doi.org/10.1016/j.biomaterials.2012.12.038.

[51] H. Fan, Q.-D. Hu, F.-J. Xu, W.-Q. Liang, G.-P. Tang, W.-T. Yang, In vivo treatment of tumors using host-guest conjugated nanoparticles functionalized with doxorubicin and therapeutic gene pTRAIL, Biomaterials 33 (2012) 1428–1436. http://dx.doi.org/10.1016/j.biomaterials.2011.10.043.

[52] F. Ahmed, R.I. Pakunlu, A. Brannan, F. Bates, T. Minko, D.E. Discher, Biodegradable polymersomes loaded with both paclitaxel and doxorubicin permeate and shrink tumors, inducing apoptosis in proportion to accumulated drug, J. Control. Release 116 (2006) 150–158. http://dx.doi.org/10.1016/j.jconrel.2006.07.012.

[53] N.R. Patel, A. Rathi, D. Mongayt, V.P. Torchilin, Reversal of multidrug resistance by co-delivery of tariquidar (XR9576) and paclitaxel using long-circulating liposomes, Int. J. Pharm. 416 (2011) 296–299. http://dx.doi.org/10.1016/j.ijpharm.2011.05.082.

[54] X. Guo, C. Shi, J. Wang, S. Di, S. Zhou, pH-triggered intracellular release from actively targeting polymer micelles, Biomaterials 34 (2013) 4544–4554. http://dx.doi.org/10.1016/j.biomaterials.2013.02.071.

[55] M. Liong, J. Lu, M. Kovochich, T. Xia, S.G. Ruehm, A.E. Nel, et al., Multifunctional inorganic nanoparticles for imaging, targeting, and drug delivery, ACS Nano 2 (2008) 889–896. http://dx.doi.org/10.1021/nn800072t.

[56] L.Y. Rizzo, B. Theek, G. Storm, F. Kiessling, T. Lammers, Recent progress in nanomedicine: therapeutic, diagnostic and theranostic applications, Curr. Opin. Biotechnol. 24 (2013) 1159–1166. http://dx.doi.org/10.1016/j.copbio.2013.02.020.

[57] E. Blanco, C.W. Kessinger, B.D. Sumer, J. Gao, Multifunctional micellar nanomedicine for cancer therapy, Exp. Biol. Med. 234 (2009) 123–131. http://dx.doi.org/10.3181/0808-MR-250.

[58] S. Mura, P. Couvreur, Nanotheranostics for personalized medicine, Adv. Drug Deliv. Rev. 64 (2012) 1394–1416. http://dx.doi.org/10.1016/j.addr.2012.06.006.

[59] D.H. Kirn, S.H. Thorne, Targeted and armed oncolytic poxviruses: a novel multi-mechanistic therapeutic class for cancer, Nat. Rev. Cancer 9 (2009) 64–71. http://dx.doi.org/10.1038/nrc2545.

[60] B.-H. Park, T. Hwang, T.-C. Liu, D.Y. Sze, J.-S. Kim, H.-C. Kwon, et al., Use of a targeted oncolytic poxvirus, JX-594, in patients with refractory primary or metastatic liver cancer: a phase I trial, Lancet Oncol. 9 (2008) 533–542. http://dx.doi.org/10.1016/S1470-2045(08)70107-4.

[61] C.J. Breitbach, J. Burke, D. Jonker, J. Stephenson, A.R. Haas, L.Q.M. Chow, et al., Intravenous delivery of a multi-mechanistic cancer-targeted oncolytic poxvirus in humans, Nature 477 (2011) 99–102. http://dx.doi.org/10.1038/nature10358.

[62] R.H.I. Andtbacka, F.A. Collichio, T. Amatruda, N.N. Senzer, J. Chesney, K.A. Delman, et al., OPTiM: a randomized phase III trial of talimogene laherparepvec (T-VEC) versus subcutaneous (SC) granulocyte-macrophage colony-stimulating factor (GM-CSF) for the treatment (tx) of unresected stage IIIB/C and IV melanoma, J. Clin. Oncol. 31 (2013) (http://meetinglibrary.asco.org/content/117592-132, (accessed July 3, 2014)).

[63] M. Westphal, S. Ylä-Herttuala, J. Martin, P. Warnke, P. Menei, D. Eckland, et al., Adenovirus-mediated gene therapy with sitimagene ceradenovec followed by intravenous ganciclovir for patients with operable high-grade glioma (ASPECT): a randomised, open-label, phase 3 trial, Lancet Oncol. 14 (2013) 823–833. http://dx.doi.org/10.1016/S1470-2045(13)70274-2.

[64] C. Beck, S. Cayeux, S.D. Lupton, B. Dörken, T. Blankenstein, The thymidine kinase/ganciclovir-mediated "suicide" effect is variable in different tumor cells, Hum. Gene Ther. 6 (1995) 1525–1530. http://dx.doi.org/10.1089/hum.1995.6.12-1525.

[65] R. Vile, D. Ando, D. Kirn, The oncolytic virotherapy treatment platform for cancer: Unique biological and biosafety points to consider, Cancer Gene Ther. 9 (2002) 1062–1067. http://dx.doi.org/10.1038/sj.cgt.7700548.

[66] M. Aghi, R.L. Martuza, Oncolytic viral therapies – the clinical experience, Oncogene 24 (2005) 7802–7816. http://dx.doi.org/10.1038/sj.onc.1209037.

[67] T.-C. Liu, E. Galanis, D. Kirn, Clinical trial results with oncolytic virotherapy: a century of promise, a decade of progress, Nat. Clin. Pract. Oncol. 4 (2007) 101–117. http://dx.doi.org/10.1038/ncponc0736.

[68] M.J.V. Vähä-Koskela, J.E. Heikkilä, A.E. Hinkkanen, Oncolytic viruses in cancer therapy, Cancer Lett. 254 (2007) 178–216. http://dx.doi.org/10.1016/j.canlet.2007.02.002.

[69] R. Duncan, Polymer conjugates as anticancer nanomedicines, Nat. Rev. Cancer 6 (2006) 688–701. http://dx.doi.org/10.1038/nrc1958.

[70] A. Hawe, W.L. Hulse, W. Jiskoot, R.T. Forbes, Taylor dispersion analysis compared to dynamic light scattering for the size analysis of therapeutic peptides and proteins and their aggregates, Pharm. Res. 28 (2011) 2302–2310. http://dx.doi.org/10.1007/s11095-011-0460-3.

[71] S. Verma, D. Miles, L. Gianni, I.E. Krop, M. Welslau, J. Baselga, et al., Trastuzumab emtansine for HER2-positive advanced breast cancer, N. Engl. J. Med. 367 (2012) 1783–1791. http://dx.doi.org/10.1056/NEJMoa1209124.

[72] A. Younes, N.L. Bartlett, J.P. Leonard, D.A. Kennedy, C.M. Lynch, E.L. Sievers, et al., Brentuximab vedotin (SGN-35) for relapsed CD30-positive lymphomas, N. Engl. J. Med. 363 (2010) 1812–1821. http://dx.doi.org/10.1056/NEJMoa1002965.

[73] H.A. Burris, H.S. Rugo, S.J. Vukelja, C.L. Vogel, R.A. Borson, S. Limentani, et al., Phase II study of the antibody drug conjugate trastuzumab-DM1 for the treatment of human epidermal growth factor receptor 2 (HER2)-positive breast cancer after prior HER2-directed therapy, J. Clin. Oncol. 29 (2011) 398–405. http://dx.doi.org/10.1200/JCO.2010.29.5865.

[74] A. Younes, A.K. Gopal, S.E. Smith, S.M. Ansell, J.D. Rosenblatt, K.J. Savage, et al., Results of a pivotal phase II study of brentuximab vedotin for patients with relapsed or refractory Hodgkin's lymphoma, J. Clin. Oncol. 30 (2012) 2183–2189. http://dx.doi.org/10.1200/JCO.2011.38.0410.

[75] R.V.J. Chari, M.L. Miller, W.C. Widdison, Antibody-drug conjugates: an emerging concept in cancer therapy, Angew. Chem. Int. Ed. Engl. 53 (2014) 3796–3827. http://dx.doi.org/10.1002/anie.201307628.

[76] J.A. Flygare, T.H. Pillow, P. Aristoff, Antibody-drug conjugates for the treatment of cancer, Chem. Biol. Drug Des. 81 (2013) 113–121. http://dx.doi.org/10.1111/cbdd.12085.

[77] C. Hess, D. Venetz, D. Neri, Emerging classes of armed antibody therapeutics against cancer, MedChemComm 5 (2014) 408–431. http://dx.doi.org/10.1039/C3MD00360D.

[78] R. Duncan, M.J. Vicent, F. Greco, R.I. Nicholson, Polymer-drug conjugates: towards a novel approach for the treatment of endocrine-related cancer, Endocr. Relat. Cancer 12 (Suppl. 1) (2005) S189–S199. http://dx.doi.org/10.1677/erc.1.01045.

[79] Y. Takakura, R.I. Mahato, M. Hashida, Extravasation of macromolecules, Adv. Drug Deliv. Rev. 34 (1998) 93–108. http://dx.doi.org/10.1016/S0169-409X(98)00006-4.

[80] L.W. Seymour, D.R. Ferry, D.J. Kerr, D. Rea, M. Whitlock, R. Poyner, et al., Phase II studies of polymer-doxorubicin (PK1, FCE28068) in the treatment of breast, lung and colorectal cancer, Int. J. Oncol. 34 (2009) 1629–1636.

[81] L.W. Seymour, D.R. Ferry, D. Anderson, S. Hesslewood, P.J. Julyan, R. Poyner, et al., Hepatic drug targeting: phase I evaluation of polymer-bound doxorubicin, J. Clin. Oncol. 20 (2002) 1668–1676.

[82] L. Villard, A. Romer, N. Marincek, P. Brunner, M.T. Koller, C. Schindler, et al., Cohort study of somatostatin-based radiopeptide therapy with [(90)Y-DOTA]-TOC versus [(90)Y-DOTA]-TOC plus [(177)Lu-DOTA]-TOC in neuroendocrine cancers, J. Clin. Oncol. 30 (2012) 1100–1106. http://dx.doi.org/10.1200/JCO.2011.37.2151.

[83] J.-Y. Fang, S.A. Al-Suwayeh, Nanoparticles as delivery carriers for anticancer prodrugs, Expert Opin. Drug Deliv. 9 (2012) 657–669. http://dx.doi.org/10.1517/17425247.2012.679927.

[84] Y. Barenholz, Doxil®—the first FDA-approved nano-drug: lessons learned, J. Control. Release 160 (2012) 117–134. http://dx.doi.org/10.1016/j.jconrel.2012.03.020.

[85] M. Harrison, D. Tomlinson, S. Stewart, Liposomal-entrapped doxorubicin: an active agent in AIDS-related Kaposi's sarcoma, J. Clin. Oncol. 13 (1995) 914–920.

[86] S. Chan, N. Davidson, E. Juozaityte, F. Erdkamp, A. Pluzanska, N. Azarnia, et al., Phase III trial of liposomal doxorubicin and cyclophosphamide compared with epirubicin and cyclophosphamide as first-line therapy for metastatic breast cancer, Ann. Oncol. 15 (2004) 1527–1534. http://dx.doi.org/10.1093/annonc/mdh393.

[87] P.S. Gill, J. Wernz, D.T. Scadden, P. Cohen, G.M. Mukwaya, J.H. von Roenn, et al., Randomized phase III trial of liposomal daunorubicin versus doxorubicin, bleomycin, and vincristine in AIDS-related Kaposi's sarcoma, J. Clin. Oncol. 14 (1996) 2353–2364.

[88] N. Gökbuget, C.-M. Hartog, R. Bassan, H.-G. Derigs, H. Dombret, R. Greil, et al., Liposomal cytarabine is effective and tolerable in the treatment of central nervous system relapse of acute lymphoblastic leukemia and very aggressive lymphoma, Haematologica 96 (2011) 238–244. http://dx.doi.org/10.3324/haematol.2010.028092.

[89] S. O'Brien, G. Schiller, J. Lister, L. Damon, S. Goldberg, W. Aulitzky, et al., High-dose vincristine sulfate liposome injection for advanced, relapsed, and refractory adult Philadelphia chromosome-negative acute lymphoblastic leukemia, J. Clin. Oncol. 31 (2013) 676–683. http://dx.doi.org/10.1200/JCO.2012.46.2309.

[90] J.E. Frampton, Mifamurtide: a review of its use in the treatment of osteosarcoma, Paediatr. Drugs 12 (2010) 141–153. http://dx.doi.org/10.2165/11204910-000000000-00000.

[91] P.A. Meyers, C.L. Schwartz, M.D. Krailo, J.H. Healey, M.L. Bernstein, D. Betcher, et al., Osteosarcoma: the addition of muramyl tripeptide to chemotherapy improves overall survival—a report from the Children's Oncology Group, J. Clin. Oncol. 26 (2008) 633–638. http://dx.doi.org/10.1200/JCO.2008.14.0095.

[92] Y. Matsumura, H. Maeda, A new concept for macromolecular therapeutics in cancer chemotherapy: mechanism of tumoritropic accumulation of proteins and the antitumor agent smancs, Cancer Res. 46 (1986) 6387–6392.

[93] T.M. Allen, P.R. Cullis, Liposomal drug delivery systems: from concept to clinical applications, Adv. Drug Deliv. Rev. 65 (2013) 36–48. http://dx.doi.org/10.1016/j.addr.2012.09.037.

[94] A.C. Roy, S.R. Park, D. Cunningham, Y.K. Kang, Y. Chao, L.T. Chen, et al., A randomized phase II study of PEP02 (MM-398), irinotecan or docetaxel as a second-line therapy in patients with locally advanced or metastatic gastric or gastro-oesophageal junction adenocarcinoma, Ann. Oncol. 24 (2013) 1567–1573. http://dx.doi.org/10.1093/annonc/mdt002.

[95] S.-H. Yang, C.-C. Lin, Z.-Z. Lin, Y.-L. Tseng, R.-L. Hong, A phase I and pharmacokinetic study of liposomal vinorelbine in patients with advanced solid tumor, Invest. New Drugs 30 (2012) 282–289. http://dx.doi.org/10.1007/s10637-010-9522-3.

[96] J. Huwyler, D. Wu, W.M. Pardridge, Brain drug delivery of small molecules using immunoliposomes, Proc. Natl. Acad. Sci. U. S. A. 93 (1996) 14164–14169.

[97] A. Koshkaryev, R. Sawant, M. Deshpande, V. Torchilin, Immunoconjugates and long circulating systems: origins, current state of the art and future directions, Adv. Drug Deliv. Rev. 65 (2013) 24–35. http://dx.doi.org/10.1016/j.addr.2012.08.009.

[98] J.D. Byrne, T. Betancourt, L. Brannon-Peppas, Active targeting schemes for nanoparticle systems in cancer therapeutics. Adv. Drug Deliv. Rev. 60 (2008) 1615–1626. http://dx.doi.org/10.1016/j.addr.2008.08.005.

[99] K. Maruyama, N. Takahashi, T. Tagawa, K. Nagaike, M. Iwatsuru, Immunoliposomes bearing polyethyleneglycol-coupled Fab' fragment show prolonged circulation time and high extravasation into targeted solid tumors in vivo, FEBS Lett. 413 (1997) 177–180.

[100] C. Mamot, D.C. Drummond, U. Greiser, K. Hong, D.B. Kirpotin, J.D. Marks, et al., Epidermal growth factor receptor (EGFR)-targeted immunoliposomes mediate specific and efficient drug delivery to EGFR- and EGFRvIII-overexpressing tumor cells, Cancer Res. 63 (2003) 3154–3161.

[101] C. Mamot, D.C. Drummond, C.O. Noble, V. Kallab, Z. Guo, K. Hong, et al., Epidermal growth factor receptor-targeted immunoliposomes significantly enhance the efficacy of multiple anticancer drugs in vivo, Cancer Res. 65 (2005) 11631–11638. http://dx.doi.org/10.1158/0008-5472.CAN-05-1093.

[102] J.W. Park, K. Hong, D.B. Kirpotin, G. Colbern, R. Shalaby, J. Baselga, et al., Anti-HER2 immunoliposomes: enhanced efficacy attributable to targeted delivery, Clin. Cancer Res. 8 (2002) 1172–1181.

[103] A. Wicki, C. Rochlitz, A. Orleth, R. Ritschard, I. Albrecht, R. Herrmann, et al., Targeting tumor-associated endothelial cells: anti-VEGFR2 immunoliposomes mediate tumor vessel disruption and inhibit tumor growth, Clin. Cancer Res. 18 (2012) 454–464. http://dx.doi.org/10.1158/1078-0432.CCR-11-1102.

[104] J. Huwyler, J. Drewe, S. Krähenbuhl, Tumor targeting using liposomal antineoplastic drugs, Int. J. Nanomedicine 3 (2008) 21–29.

[105] A. Schnyder, S. Krähenbühl, J. Drewe, J. Huwyler, Targeting of daunomycin using biotinylated immunoliposomes: pharmacokinetics, tissue distribution and in vitro pharmacological effects, J. Drug Target. 13 (2005) 325–335. http://dx.doi.org/10.1080/10611860500206674.

[106] Y. Matsumura, M. Gotoh, K. Muro, Y. Yamada, K. Shirao, Y. Shimada, et al., Phase I and pharmacokinetic study of MCC-465, a doxorubicin (DXR) encapsulated in PEG immunoliposome, in patients with metastatic stomach cancer, Ann. Oncol. 15 (2004) 517–525.

[107] T. Hamaguchi, Y. Matsumura, Y. Nakanishi, K. Muro, Y. Yamada, Y. Shimada, et al., Antitumor effect of MCC-465, pegylated liposomal doxorubicin tagged with newly developed monoclonal antibody GAH, in colorectal cancer xenografts, Cancer Sci. 95 (2004) 608–613.

[108] S. Hosokawa, T. Tagawa, H. Niki, Y. Hirakawa, K. Nohga, K. Nagaike, Efficacy of immunoliposomes on cancer models in a cell-surface-antigen-density-dependent manner, Br. J. Cancer 89 (2003) 1545–1551. http://dx.doi.org/10.1038/sj.bjc.6601341.

[109] Z. Li, T.M. Rana, Therapeutic targeting of microRNAs: current status and future challenges, Nat. Rev. Drug Discov. (2014). http://dx.doi.org/10.1038/nrd4359 (advance online, publication).

[110] C.V. Pecot, G.A. Calin, R.L. Coleman, G. Lopez-Berestein, A.K. Sood, RNA interference in the clinic: challenges and future directions, Nat. Rev. Cancer 11 (2011) 59–67. http://dx.doi.org/10.1038/nrc2966.

[111] T. Coelho, D. Adams, A. Silva, P. Lozeron, P.N. Hawkins, T. Mant, et al., Safety and efficacy of RNAi therapy for transthyretin amyloidosis, N. Engl. J. Med. 369 (2013) 819–829. http://dx.doi.org/10.1056/NEJMoa1208760.

[112] J. Tabernero, G.I. Shapiro, P.M. LoRusso, A. Cervantes, G.K. Schwartz, G.J. Weiss, et al., First-in-humans trial of an RNA interference therapeutic targeting VEGF and KSP in cancer patients with liver involvement, Cancer Discov. 3 (2013) 406–417. http://dx.doi.org/10.1158/2159-8290.CD-12-0429.

[113] P. Couvreur, B. Stella, L.H. Reddy, H. Hillaireau, C. Dubernet, D. Desmaële, et al., Squalenoyl nanomedicines as potential therapeutics, Nano Lett. 6 (2006) 2544–2548. http://dx.doi.org/10.1021/nl061942q.

[114] A. Maksimenko, F. Dosio, J. Mougin, A. Ferrero, S. Wack, L.H. Reddy, et al., A unique squalenoylated and nonpegylated doxorubicin nanomedicine with systemic long-circulating properties and anticancer activity, Proc. Natl. Acad. Sci. U. S. A. 111 (2014) E217–E226. http://dx.doi.org/10.1073/pnas.1313459110.

[115] D. Predescu, S.M. Vogel, A.B. Malik, Functional and morphological studies of protein transcytosis in continuous endothelia, Am. J. Physiol. Lung Cell. Mol. Physiol. 287 (2004) L895–L901. http://dx.doi.org/10.1152/ajplung.00075.2004.

[116] W.J. Gradishar, S. Tjulandin, N. Davidson, H. Shaw, N. Desai, P. Bhar, et al., Phase III trial of nanoparticle albumin-bound paclitaxel compared with polyethylated castor oil-based paclitaxel in women with breast cancer, J. Clin. Oncol. 23 (2005) 7794–7803. http://dx.doi.org/10.1200/JCO.2005.04.937.

[117] D.D.V. Hoff, T.J. Ervin, F.P. Arena, E.G. Chiorean, J.R. Infante, M.J. Moore, et al., Results of a randomized phase III trial (MPACT) of weekly nab-paclitaxel plus gemcitabine versus gemcitabine alone for patients with metastatic adenocarcinoma of the pancreas with PET and CA19-9 correlates, J. Clin. Oncol. 31 (2013) (http://meetinglibrary.asco.org/content/116827-132, (accessed July 10, 2014)).

[118] M.A. Socinski, I. Bondarenko, N.A. Karaseva, A.M. Makhson, I. Vynnychenko, I. Okamoto, et al., Weekly nab-paclitaxel in combination with carboplatin versus solvent-based paclitaxel plus carboplatin as first-line therapy in patients with advanced non-small-cell lung cancer: final results of a phase III trial, J. Clin. Oncol. 30 (2012) 2055–2062. http://dx.doi.org/10.1200/JCO.2011.39.5848.

[119] W. Qu, W.-H. Chen, Y. Kuang, X. Zeng, S.-X. Cheng, X. Zhou, et al., Avidin–biotin interaction mediated peptide assemblies as efficient gene delivery vectors for cancer therapy, Mol. Pharm. 10 (2013) 261–269. http://dx.doi.org/10.1021/mp300392z.

[120] G.J. Weiss, J. Chao, J.D. Neidhart, R.K. Ramanathan, D. Bassett, J.A. Neidhart, et al., First-in-human phase 1/2a trial of CRLX101, a cyclodextrin-containing polymer-camptothecin nanopharmaceutical in patients with advanced solid tumor malignancies, Invest. New Drugs 31 (2013) 986–1000. http://dx.doi.org/10.1007/s10637-012-9921-8.

[121] M.E. Davis, The first targeted delivery of siRNA in humans via a self-assembling, cyclodextrin polymer-based nanoparticle: from concept to clinic. Mol. Pharm. 6 (2009) 659–668. http://dx.doi.org/10.1021/mp900015y.

[122] K. Derakhshandeh, S. Fathi, Role of chitosan nanoparticles in the oral absorption of gemcitabine, Int. J. Pharm. 437 (2012) 172–177. http://dx.doi.org/10.1016/j.ijpharm.2012.08.008.

[123] N. Kamaly, Z. Xiao, P.M. Valencia, A.F. Radovic-Moreno, O.C. Farokhzad, Targeted polymeric therapeutic nanoparticles: design, development and clinical translation, Chem. Soc. Rev. 41 (2012) 2971–3010. http://dx.doi.org/10.1039/c2cs15344k.

[124] R. Plummer, R.H. Wilson, H. Calvert, A.V. Boddy, M. Griffin, J. Sludden, et al., A Phase I clinical study of cisplatin-incorporated polymeric micelles (NC-6004) in patients with solid tumours, Br. J. Cancer 104 (2011) 593–598. http://dx.doi.org/10.1038/bjc.2011.6.

[125] H. Cabral, K. Kataoka, Progress of drug-loaded polymeric micelles into clinical studies, J. Control. Release 190 (2014) 465–476. http://dx.doi.org/10.1016/j.jconrel.2014.06.042.

[126] O.C. Farokhzad, J. Cheng, B.A. Teply, I. Sherifi, S. Jon, P.W. Kantoff, et al., Targeted nanoparticle-aptamer bioconjugates for cancer chemotherapy in vivo, Proc. Natl. Acad. Sci. U. S. A. 103 (2006) 6315–6320. http://dx.doi.org/10.1073/pnas.0601755103.

[127] J. Hrkach, D. Von Hoff, M. Mukkaram Ali, E. Andrianova, J. Auer, T. Campbell, et al., Preclinical development and clinical translation of a PSMA-targeted docetaxel nanoparticle with a differentiated pharmacological profile, Sci. Transl. Med. 4 (2012) 128–139. http://dx.doi.org/10.1126/scitranslmed.3003651.

[128] S. Dhar, N. Kolishetti, S.J. Lippard, O.C. Farokhzad, Targeted delivery of a cisplatin prodrug for safer and more effective prostate cancer therapy in vivo, Proc.

Natl. Acad. Sci. U. S. A. 108 (2011) 1850–1855. http://dx.doi.org/10.1073/pnas.1011379108.
[129] M. Harada, I. Bobe, H. Saito, N. Shibata, R. Tanaka, T. Hayashi, et al., Improved anti-tumor activity of stabilized anthracycline polymeric micelle formulation, NC-6300, Cancer Sci. 102 (2011) 192–199. http://dx.doi.org/10.1111/j.1349-7006.2010.01745.x.
[130] Q. Zhou, X. Sun, L. Zeng, J. Liu, Z. Zhang, A randomized multicenter phase II clinical trial of mitoxantrone-loaded nanoparticles in the treatment of 108 patients with unresected hepatocellular carcinoma, Nanomed. Nanotechnol. Biol. Med. 5 (2009) 419–423. http://dx.doi.org/10.1016/j.nano.2009.01.009.
[131] C.J. Rijcken, C.J. Snel, R.M. Schiffelers, C.F. van Nostrum, W.E. Hennink, Hydrolysable core-crosslinked thermosensitive polymeric micelles: synthesis, characterisation and in vivo studies, Biomaterials 28 (2007) 5581–5593. http://dx.doi.org/10.1016/j.biomaterials.2007.08.047.
[132] V. Reebye, P. Sætrom, P.J. Mintz, K.-W. Huang, P. Swiderski, L. Peng, et al., Novel RNA oligonucleotide improves liver function and inhibits liver carcinogenesis in vivo, Hepatology 59 (2014) 216–227. http://dx.doi.org/10.1002/hep.26669.
[133] H.-C. Huang, S. Barua, G. Sharma, S.K. Dey, K. Rege, Inorganic nanoparticles for cancer imaging and therapy, J. Control. Release 155 (2011) 344–357. http://dx.doi.org/10.1016/j.jconrel.2011.06.004.
[134] R.W. Ross, A.L. Zietman, W. Xie, J.J. Coen, D.M. Dahl, W.U. Shipley, et al., Lymphotropic nanoparticle-enhanced magnetic resonance imaging (LNMRI) identifies occult lymph node metastases in prostate cancer patients prior to salvage radiation therapy, Clin. Imaging 33 (2009) 301–305. http://dx.doi.org/10.1016/j.clinimag.2009.01.013.
[135] P. Rivera Gil, D. Hühn, L.L. del Mercato, D. Sasse, W.J. Parak, Nanopharmacy: inorganic nanoscale devices as vectors and active compounds, Pharmacol. Res. 62 (2010) 115–125. http://dx.doi.org/10.1016/j.phrs.2010.01.009.
[136] L. Maggiorella, G. Barouch, C. Devaux, A. Pottier, E. Deutsch, J. Bourhis, et al., Nanoscale radiotherapy with hafnium oxide nanoparticles, Future Oncol. 8 (2012) 1167–1181. http://dx.doi.org/10.2217/fon.12.96.
[137] S.K. Libutti, G.F. Paciotti, A.A. Byrnes, H.R. Alexander, W.E. Gannon, M. Walker, et al., Phase I and pharmacokinetic studies of CYT-6091, a novel PEGylated colloidal gold-rhTNF nanomedicine, Clin. Cancer Res. 16 (2010) 6139–6149. http://dx.doi.org/10.1158/1078-0432.CCR-10-0978.
[138] M. Kovalainen, J. Mönkäre, M. Kaasalainen, J. Riikonen, V.-P. Lehto, J. Salonen, et al., Development of porous silicon nanocarriers for parenteral peptide delivery, Mol. Pharm. 10 (2013) 353–359. http://dx.doi.org/10.1021/mp300494p.
[139] R. Gaspar, R. Duncan, Polymeric carriers: preclinical safety and the regulatory implications for design and development of polymer therapeutics, Adv. Drug Deliv. Rev. 61 (2009) 1220–1231. http://dx.doi.org/10.1016/j.addr.2009.06.003.
[140] B. Fubini, M. Ghiazza, I. Fenoglio, Physico-chemical features of engineered nanoparticles relevant to their toxicity, Nanotoxicology 4 (2010) 347–363. http://dx.doi.org/10.3109/17435390.2010.509519.
[141] H. Kettiger, A. Schipanski, P. Wick, J. Huwyler, Engineered nanomaterial uptake and tissue distribution: from cell to organism, Int. J. Nanomedicine 8 (2013) 3255–3269. http://dx.doi.org/10.2147/IJN.S49770.
[142] K.L. Aillon, Y. Xie, N. El-Gendy, C.J. Berkland, M.L. Forrest, Effects of nanomaterial physicochemical properties on in vivo toxicity, Adv. Drug Deliv. Rev. 61 (2009) 457–466. http://dx.doi.org/10.1016/j.addr.2009.03.010.
[143] M.A. Dobrovolskaia, S.E. McNeil, Immunological properties of engineered nanomaterials, Nat. Nanotechnol. 2 (2007) 469–478. http://dx.doi.org/10.1038/nnano.2007.223.
[144] A.E. Nel, L. Mädler, D. Velegol, T. Xia, E.M.V. Hoek, P. Somasundaran, et al., Understanding biophysicochemical interactions at the nano-bio interface, Nat. Mater. 8 (2009) 543–557. http://dx.doi.org/10.1038/nmat2442.
[145] G.F. Paciotti, L. Myer, D. Weinreich, D. Goia, N. Pavel, R.E. McLaughlin, et al., Colloidal gold: a novel nanoparticle vector for tumor directed drug delivery, Drug Deliv. 11 (2004) 169–183. http://dx.doi.org/10.1080/10717540490433895.
[146] N. Bertrand, J.-C. Leroux, The journey of a drug-carrier in the body: an anatomo-physiological perspective, J. Control. Release 161 (2012) 152–163. http://dx.doi.org/10.1016/j.jconrel.2011.09.098.
[147] J.K. Vasir, V. Labhasetwar, Biodegradable nanoparticles for cytosolic delivery of therapeutics, Adv. Drug Deliv. Rev. 59 (2007) 718–728. http://dx.doi.org/10.1016/j.addr.2007.06.003.
[148] D.C. Drummond, O. Meyer, K. Hong, D.B. Kirpotin, D. Papahadjopoulos, Optimizing liposomes for delivery of chemotherapeutic agents to solid tumors, Pharmacol. Rev. 51 (1999) 691–744.
[149] N. Lewinski, V. Colvin, R. Drezek, Cytotoxicity of nanoparticles, Small 4 (2008) 26–49. http://dx.doi.org/10.1002/smll.200700595.
[150] V. Stone, H. Johnston, R.P.F. Schins, Development of in vitro systems for nanotoxicology: methodological considerations, Crit. Rev. Toxicol. 39 (2009) 613–626. http://dx.doi.org/10.1080/10408440903120975.
[151] C.M. Sayes, K.L. Reed, D.B. Warheit, Assessing toxicity of fine and nanoparticles: Comparing in vitro measurements to in vivo pulmonary toxicity profiles, Toxicol. Sci. 97 (2007) 163–180. http://dx.doi.org/10.1093/toxsci/kfm018.
[152] A. Mayer, M. Vadon, B. Rinner, A. Novak, R. Wintersteiger, E. Froehlich, The role of nanoparticle size in hemocompatibility, Toxicology 258 (2009) 139–147. http://dx.doi.org/10.1016/j.tox.2009.01.015.
[153] J. Szebeni, F. Muggia, A. Gabizon, Y. Barenholz, Activation of complement by therapeutic liposomes and other lipid excipient-based therapeutic products: prediction and prevention, Adv. Drug Deliv. Rev. 63 (2011) 1020–1030. http://dx.doi.org/10.1016/j.addr.2011.06.017.
[154] S. Nie, Y. Xing, G.J. Kim, J.W. Simons, Nanotechnology applications in cancer, Annu. Rev. Biomed. Eng. 9 (2007) 257–288. http://dx.doi.org/10.1146/annurev.bioeng.9.060906.152025.
[155] K. Tiede, A.B.A. Boxall, S.P. Tear, J. Lewis, H. David, M. Hassellov, Detection and characterization of engineered nanoparticles in food and the environment, Food Addit. Contam. Part A: Chem. Anal. Control Expo. Risk Assess. 25 (2008) 795–821. http://dx.doi.org/10.1080/02652030802007553.
[156] M.A. Hamburg, Science and regulation. FDA's approach to regulation of products of nanotechnology, Science 336 (2012) 299–300. http://dx.doi.org/10.1126/science.1205441.
[157] U.S. Food and Drug Administration, Guidance for Industry - Considering Whether an FDA-Regulated Product Involves the Application of Nanotechnology, http://www.fda.gov/regulatoryinformation/guidances/ucm257698.htm2014.
[158] N. Desai, Challenges in development of nanoparticle-based therapeutics, AAPS J. 14 (2012) 282–295. http://dx.doi.org/10.1208/s12248-012-9339-4.
[159] European Technology Platform Nanomedicine, White Paper on Contribution of Nanomedicine to Horizon 2020, http://www.etp-nanomedicine.eu/public/news-events/news/etpn-white-paper-contribution-of-nanomedicine-to-horizon-2020-available 2013.
[160] S. Tinkle, S.E. McNeil, S. Mühlebach, R. Bawa, G. Borchard, Y.C. Barenholz, et al., Nanomedicines: addressing the scientific and regulatory gap, Ann. N. Y. Acad. Sci. 1313 (2014) 35–56. http://dx.doi.org/10.1111/nyas.12403.
[161] W.C. Zamboni, V. Torchilin, A.K. Patri, J. Hrkach, S. Stern, R. Lee, et al., Best practices in cancer nanotechnology: perspective from NCI nanotechnology alliance, Clin. Cancer Res. 18 (2012) 3229–3241. http://dx.doi.org/10.1158/1078-0432.CCR-11-2938.
[162] K. Langer, M.G. Anhorn, I. Steinhauser, S. Dreis, D. Celebi, N. Schrickel, et al., Human serum albumin (HSA) nanoparticles: reproducibility of preparation process and kinetics of enzymatic degradation, Int. J. Pharm. 347 (2008) 109–117. http://dx.doi.org/10.1016/j.ijpharm.2007.06.028.
[163] A. McBride, L.M. Holle, C. Westendorf, M. Sidebottom, N. Griffith, R.J. Muller, et al., National survey on the effect of oncology drug shortages on cancer care, Am. J. Health Syst. Pharm. 70 (2013) 609–617. http://dx.doi.org/10.2146/ajhp120563.
[164] J.L. Berger, A. Smith, K.K. Zorn, P. Sukumvanich, A.B. Olawaiye, J. Kelley, et al., Outcomes analysis of an alternative formulation of PEGylated liposomal doxorubicin in recurrent epithelial ovarian carcinoma during the drug shortage era, OncoTargets Ther. 7 (2014) 1409–1413. http://dx.doi.org/10.2147/OTT.S62881.
[165] D.B. Resnik, S.S. Tinkle, Ethics in nanomedicine, Nanomedicine 2 (2007) 345–350. http://dx.doi.org/10.2217/17435889.2.3.345.
[166] P.F. Bross, J. Beitz, G. Chen, X.H. Chen, E. Duffy, L. Kieffer, et al., Approval summary: gemtuzumab ozogamicin in relapsed acute myeloid leukemia, Clin. Cancer Res. 7 (2001) 1490–1496.
[167] F. Morschhauser, J. Radford, A. Van Hoof, U. Vitolo, P. Soubeyran, H. Tilly, et al., Phase III trial of consolidation therapy with yttrium-90-ibritumomab tiuxetan compared with no additional therapy after first remission in advanced follicular lymphoma, J. Clin. Oncol. 26 (2008) 5156–5164. http://dx.doi.org/10.1200/JCO.2008.17.2015.
[168] S.J. Horning, A. Younes, V. Jain, S. Kroll, J. Lucas, D. Podoloff, et al., Efficacy and safety of tositumomab and iodine-131 tositumomab (Bexxar) in B-cell lymphoma, progressive after rituximab, J. Clin. Oncol. 23 (2005) 712–719. http://dx.doi.org/10.1200/JCO.2005.07.040.
[169] N. Desai, V. Trieu, Z. Yao, L. Louie, S. Ci, A. Yang, et al., Increased antitumor activity, intratumor paclitaxel concentrations, and endothelial cell transport of cremophor-free, albumin-bound paclitaxel, ABI-007, compared with cremophor-based paclitaxel, Clin. Cancer Res. 12 (2006) 1317–1324. http://dx.doi.org/10.1158/1078-0432.CCR-05-1634.
[170] E. Rivera, Liposomal anthracyclines in metastatic breast cancer: clinical update, Oncologist 8 (Suppl. 2) (2003) 3–9.
[171] M.J. Glantz, K.A. Jaeckle, M.C. Chamberlain, S. Phuphanich, L. Recht, L.J. Swinnen, et al., A randomized controlled trial comparing intrathecal sustained-release cytarabine (DepoCyt) to intrathecal methotrexate in patients with neoplastic meningitis from solid tumors, Clin. Cancer Res. 5 (1999) 3394–3402.
[172] F.M. Muggia, J.D. Hainsworth, S. Jeffers, P. Miller, S. Groshen, M. Tan, et al., Phase II study of liposomal doxorubicin in refractory ovarian cancer: antitumor activity and toxicity modification by liposomal encapsulation, J. Clin. Oncol. 15 (1997) 987–993.
[173] K.S. Lee, H.C. Chung, S.A. Im, Y.H. Park, C.S. Kim, S.-B. Kim, et al., Multicenter phase II trial of Genexol-PM, a Cremophor-free, polymeric micelle formulation of paclitaxel, in patients with metastatic breast cancer, Breast Cancer Res. Treat. 108 (2008) 241–250. http://dx.doi.org/10.1007/s10549-007-9591-y.
[174] N. Khemapech, S. Oranratanaphan, W. Termrungruanglert, R. Lertkhachonsuk, A. Vasurattana, Salvage chemotherapy in recurrent platinum-resistant or refractory epithelial ovarian cancer with Carboplatin and distearoylphosphatidylcholine pegylated liposomal Doxorubicin (lipo-dox®), Asian Pac. J. Cancer Prev. 14 (2013) 2131–2135.
[175] M.A. Rodriguez, R. Pytlik, T. Kozak, M. Chhanabhai, R. Gascoyne, B. Lu, et al., Vincristine sulfate liposomes injection (Marqibo) in heavily pretreated patients with refractory aggressive non-Hodgkin lymphoma: report of the pivotal phase 2 study, Cancer 115 (2009) 3475–3482. http://dx.doi.org/10.1002/cncr.24359.
[176] K. Venkatakrishnan, Y. Liu, D. Noe, J. Mertz, M. Bargfrede, T. Marbury, et al., Pharmacokinetics and pharmacodynamics of liposomal mifamurtide in adult volunteers with mild or moderate hepatic impairment, Br. J. Clin. Pharmacol. 77 (2014) 998–1010. http://dx.doi.org/10.1111/bcp.12261.
[177] G. Batist, G. Ramakrishnan, C.S. Rao, A. Chandrasekharan, J. Gutheil, T. Guthrie, et al., Reduced cardiotoxicity and preserved antitumor efficacy of liposome-

encapsulated doxorubicin and cyclophosphamide compared with conventional doxorubicin and cyclophosphamide in a randomized, multicenter trial of metastatic breast cancer, J. Clin. Oncol. 19 (2001) 1444–1454.
[178] P.A. Dinndorf, J. Gootenberg, M.H. Cohen, P. Keegan, R. Pazdur, FDA drug approval summary: pegaspargase (oncaspar) for the first-line treatment of children with acute lymphoblastic leukemia (ALL), Oncologist 12 (2007) 991–998. http://dx.doi.org/10.1634/theoncologist.12-8-991.
[179] H. Maeda, SMANCS and polymer-conjugated macromolecular drugs: advantages in cancer chemotherapy, Adv. Drug Deliv. Rev. 46 (2001) 169–185. http://dx.doi.org/10.1016/S0169-409X(00)00134-4.
[180] P.A. Ott, R.D. Carvajal, N. Pandit-Taskar, A.A. Jungbluth, E.W. Hoffman, B.-W. Wu, et al., Phase I/II study of pegylated arginine deiminase (ADI-PEG 20) in patients with advanced melanoma, Invest. New Drugs 31 (2013) 425–434. http://dx.doi.org/10.1007/s10637-012-9862-2.
[181] J.M. Rademaker-Lakhai, C. Terret, S.B. Howell, C.M. Baud, R.F. De Boer, D. Pluim, et al., A Phase I and pharmacological study of the platinum polymer AP5280 given as an intravenous infusion once every 3 weeks in patients with solid tumors, Clin. Cancer Res. 10 (2004) 3386–3395. http://dx.doi.org/10.1158/1078-0432.CCR-03-0315.
[182] J. Homsi, G.R. Simon, C.R. Garrett, G. Springett, R. De Conti, A.A. Chiappori, et al., Phase I trial of poly-L-glutamate camptothecin (CT-2106) administered weekly in patients with advanced solid malignancies, Clin. Cancer Res. 13 (2007) 5855–5861. http://dx.doi.org/10.1158/1078-0432.CCR-06-2821.
[183] O. Soepenberg, M.J.A. de Jonge, A. Sparreboom, P. de Bruin, F.A.L.M. Eskens, G. de Heus, et al., Phase I and pharmacokinetic study of DE-310 in patients with advanced solid tumors, Clin. Cancer Res. 11 (2005) 703–711.
[184] S.A. Veltkamp, E.O. Witteveen, A. Capriati, A. Crea, F. Animati, M. Voogel-Fuchs, et al., Clinical and pharmacologic study of the novel prodrug delimotecan (MEN 4901/T-0128) in patients with solid tumors, Clin. Cancer Res. 14 (2008) 7535–7544. http://dx.doi.org/10.1158/1078-0432.CCR-08-0438.
[185] S. Danhauser-Riedl, E. Hausmann, H.D. Schick, R. Bender, H. Dietzfelbinger, J. Rastetter, et al., Phase I clinical and pharmacokinetic trial of dextran conjugated doxorubicin (AD-70, DOX-OXD), Invest. New Drugs 11 (1993) 187–195.
[186] D. Bissett, J. Cassidy, J.S. de Bono, F. Muirhead, M. Main, L. Robson, et al., Phase I and pharmacokinetic (PK) study of MAG-CPT (PNU 166148): a polymeric derivative of camptothecin (CPT), Br. J. Cancer 91 (2004) 50–55. http://dx.doi.org/10.1038/sj.bjc.6601922.
[187] C. Bolling, T. Graefe, C. Lübbing, F. Jankevicius, S. Uktveris, A. Cesas, et al., Phase II study of MTX-HSA in combination with cisplatin as first line treatment in patients with advanced or metastatic transitional cell carcinoma, Invest. New Drugs 24 (2006) 521–527. http://dx.doi.org/10.1007/s10637-006-8221-6.
[188] A. Awada, A.A. Garcia, S. Chan, G.H.M. Jerusalem, R.E. Coleman, M.T. Huizing, et al., Two schedules of etirinotecan pegol (NKTR-102) in patients with previously treated metastatic breast cancer: a randomised phase 2 study, Lancet Oncol. 14 (2013) 1216–1225. http://dx.doi.org/10.1016/S1470-2045(13)70429-7.
[189] E. Calvo, U. Hoch, D.J. Maslyar, A.W. Tolcher, Dose-escalation phase I study of NKTR-105, a novel pegylated form of docetaxel, J. Clin. Oncol. 28 (15 s) (2010) (http://meetinglibrary.asco.org/content/51700-74, (accessed July 23, 2014).
[190] L.C. Scott, J.C. Yao, A.B. Benson, A.L. Thomas, S. Falk, R.R. Mena, et al., A phase II study of pegylated-camptothecin (pegamotecan) in the treatment of locally advanced and metastatic gastric and gastro-oesophageal junction adenocarcinoma, Cancer Chemother. Pharmacol. 63 (2009) 363–370. http://dx.doi.org/10.1007/s00280-008-0746-2.
[191] S.P. Egusquiaguirre, M. Igartua, R.M. Hernández, J.L. Pedraz, Nanoparticle delivery systems for cancer therapy: advances in clinical and preclinical research, Clin. Transl. Oncol. 14 (2012) 83–93. http://dx.doi.org/10.1007/s12094-012-0766-6.
[192] A. Patnaik, K.P. Papadopoulos, A.W. Tolcher, M. Beeram, S. Urien, L.J. Schaaf, et al., Phase I dose-escalation study of EZN-2208 (PEG-SN38), a novel conjugate of poly(ethylene) glycol and SN38, administered weekly in patients with advanced cancer, Cancer Chemother. Pharmacol. 71 (2013) 1499–1506. http://dx.doi.org/10.1007/s00280-013-2149-2.
[193] P.A. Vasey, S.B. Kaye, R. Morrison, C. Twelves, P. Wilson, R. Duncan, et al., Phase I clinical and pharmacokinetic study of PK1 [N-(2-hydroxypropyl)methacrylamide copolymer doxorubicin]: first member of a new class of chemotherapeutic agents-drug-polymer conjugates. Cancer Research Campaign Phase I/II Committee, Clin. Cancer Res. 5 (1999) 83–94.
[194] J.M. Meerum Terwogt, W.W. ten Bokkel Huinink, J.H. Schellens, M. Schot, I.A. Mandjes, M.G. Zurlo, et al., Phase I clinical and pharmacokinetic study of PNU166945, a novel water-soluble polymer-conjugated prodrug of paclitaxel, Anticancer Drugs 12 (2001) 315–323.
[195] D.P. Nowotnik, E. Cvitkovic, ProLindac (AP5346): a review of the development of an HPMA DACH platinum polymer therapeutic, Adv. Drug Deliv. Rev. 61 (2009) 1214–1219. http://dx.doi.org/10.1016/j.addr.2009.06.004.
[196] A.Y. Bedikian, R.C. DeConti, R. Conry, S. Agarwala, N. Papadopoulos, K.B. Kim, et al., Phase 3 study of docosahexaenoic acid-paclitaxel versus dacarbazine in patients with metastatic malignant melanoma, Ann. Oncol. 22 (2011) 787–793. http://dx.doi.org/10.1093/annonc/mdq438.
[197] A.V. Yurkovetskiy, R.J. Fram, XMT-1001, a novel polymeric camptothecin pro-drug in clinical development for patients with advanced cancer, Adv. Drug Deliv. Rev. 61 (2009) 1193–1202. http://dx.doi.org/10.1016/j.addr.2009.01.007.
[198] P. Sabbatini, C. Aghajanian, D. Dizon, S. Anderson, J. Dupont, J.V. Brown, et al., Phase II study of CT-2103 in patients with recurrent epithelial ovarian, fallopian tube, or primary peritoneal carcinoma, J. Clin. Oncol. 22 (2004) 4523–4531. http://dx.doi.org/10.1200/JCO.2004.12.043.
[199] P.J. Gaillard, C.C.M. Appeldoorn, R. Dorland, J. van Kregten, F. Manca, D.J. Vugts, et al., Pharmacokinetics, brain delivery, and efficacy in brain tumor-bearing mice of glutathione pegylated liposomal doxorubicin (2B3-101), PLoS One 9 (2014) e82331. http://dx.doi.org/10.1371/journal.pone.0082331.
[200] T. Dragovich, D. Mendelson, S. Kurtin, K. Richardson, D. Von Hoff, A. Hoos, A phase 2 trial of the liposomal DACH platinum L-NDDP in patients with therapy-refractory advanced colorectal cancer, Cancer Chemother. Pharmacol. 58 (2006) 759–764. http://dx.doi.org/10.1007/s00280-006-0235-4.
[201] Azaya Therapeutics, Inc., Safety Study of a Liposomal Docetaxel Formulation in Patients With Solid Tumors Who Have Failed Previous TherapiesRetrieved July 2014 clinicaltrials.gov/ct2/show/NCT01041235 2009.
[202] D. Strumberg, B. Schultheis, U. Traugott, C. Vank, A. Santel, O. Keil, et al., Phase I clinical development of Atu027, a siRNA formulation targeting PKN3 in patients with advanced solid tumors, Int. J. Clin. Pharmacol. Ther. 50 (2012) 76–78.
[203] G. Batist, K.A. Gelmon, K.N. Chi, W.H. Miller, S.K.L. Chia, L.D. Mayer, et al., Safety, pharmacokinetics, and efficacy of CPX-1 liposome injection in patients with advanced solid tumors, Clin. Cancer Res. 15 (2009) 692–700. http://dx.doi.org/10.1158/1078-0432.CCR-08-0515.
[204] E.J. Feldman, J.E. Lancet, J.E. Kolitz, E.K. Ritchie, G.J. Roboz, A.F. List, et al., First-in-man study of CPX-351: a liposomal carrier containing cytarabine and daunorubicin in a fixed 5:1 molar ratio for the treatment of relapsed and refractory acute myeloid leukemia, J. Clin. Oncol. 29 (2011) 979–985. http://dx.doi.org/10.1200/JCO.2010.30.5961.
[205] X. Xie, W. Xia, Z. Li, H.-P. Kuo, Y. Liu, Z. Li, et al., Targeted expression of BikDD eradicates pancreatic tumors in noninvasive imaging models, Cancer Cell 12 (2007) 52–65. http://dx.doi.org/10.1016/j.ccr.2007.05.009.
[206] H. Dudek, D.H. Wong, R. Arvan, A. Shah, K. Wortham, B. Ying, et al., Knockdown of β-catenin with dicer-substrate siRNAs reduces liver tumor burden in vivo, Mol. Ther. J. Am. Soc. Gene Ther. 22 (2014) 92–101. http://dx.doi.org/10.1038/mt.2013.233.
[207] A. Penwell, K. Sharp, M. Mansour, L. Sammatur, Development and validation of an HPLC/UV assay for separation and quantification of peptide antigens from a liposomal vaccine delivery platform, J. Pharm. Biomed. Anal. 66 (2012) 176–182. http://dx.doi.org/10.1016/j.jpba.2012.03.046.
[208] Y. Yu, C. Desjardins, P. Saxton, G. Lai, E. Schuck, Y.N. Wong, Characterization of the pharmacokinetics of a liposomal formulation of eribulin mesylate (E7389) in mice, Int. J. Pharm. 443 (2013) 9–16. http://dx.doi.org/10.1016/j.ijpharm.2013.01.010.
[209] Y. He, Q. Zeng, S.D. Drenning, M.F. Melhem, D.J. Tweardy, L. Huang, et al., Inhibition of human squamous cell carcinoma growth in vivo by epidermal growth factor receptor antisense RNA transcribed from the U6 promoter, J. Natl. Cancer Inst. 90 (1998) 1080–1087. http://dx.doi.org/10.1093/jnci/90.14.1080.
[210] A. Awada, I.N. Bondarenko, J. Bonneterre, E. Nowara, J.M. Ferrero, A.V. Bakshi, et al., A randomized controlled phase II trial of a novel composition of paclitaxel embedded into neutral and cationic lipids targeting tumor endothelial cells in advanced triple-negative breast cancer (TNBC), Ann. Oncol. 25 (2014) 824–831. http://dx.doi.org/10.1093/annonc/mdu025.
[211] C.N. Landen, A. Chavez-Reyes, C. Bucana, R. Schmandt, M.T. Deavers, G. Lopez-Berestein, et al., Therapeutic EphA2 gene targeting in vivo using neutral liposomal small interfering RNA delivery, Cancer Res. 65 (2005) 6910–6918. http://dx.doi.org/10.1158/0008-5472.CAN-05-0530.
[212] J.R. Infante, V.L. Keedy, S.F. Jones, W.C. Zamboni, E. Chan, J.C. Bendell, et al., Phase I and pharmacokinetic study of IHL-305 (PEGylated liposomal irinotecan) in patients with advanced solid tumors, Cancer Chemother. Pharmacol. 70 (2012) 699–705. http://dx.doi.org/10.1007/s00280-012-1960-5.
[213] C. Lu, D.J. Stewart, J.J. Lee, L. Ji, R. Ramesh, G. Jayachandran, et al., Phase I clinical trial of systemically administered TUSC2(FUS1)-nanoparticles mediating functional gene transfer in humans, PLoS One 7 (2012) e34833. http://dx.doi.org/10.1371/journal.pone.0034833.
[214] H. Lee Moffitt Cancer Center and Research Institute, Interleukin-2 Gene or Methotrexate in Treating Patients With Recurrent or Refractory Stage III or Stage IV Head and Neck CancerRetrieved July 2014 http://clinicaltrials.gov/ct2/show/NCT00006033 2000.
[215] P. Tardi, E. Choice, D. Masin, T. Redelmeier, M. Bally, T.D. Madden, Liposomal encapsulation of topotecan enhances anticancer efficacy in murine and human xenograft models, Cancer Res. 60 (2000) 3389–3393.
[216] S.C. Semple, R. Leone, J. Wang, E.C. Leng, S.K. Klimuk, M.L. Eisenhardt, et al., Optimization and characterization of a sphingomyelin/cholesterol liposome formulation of vinorelbine with promising antitumor activity, J. Pharm. Sci. 94 (2005) 1024–1038. http://dx.doi.org/10.1002/jps.20332.
[217] C.F. Verschraegen, B.E. Gilbert, A.J. Huaringa, R. Newman, N. Harris, F.J. Leyva, et al., Feasibility, phase I, and pharmacological study of aerosolized liposomal 9-nitro-20(S)-camptothecin in patients with advanced malignancies in the lungs, Ann. N. Y. Acad. Sci. 922 (2000) 352–354.
[218] D.J. Booser, F.J. Esteva, E. Rivera, V. Valero, L. Esparza-Guerra, W. Priebe, et al., Phase II study of liposomal annamycin in the treatment of doxorubicin-resistant breast cancer, Cancer Chemother. Pharmacol. 50 (2002) 6–8. http://dx.doi.org/10.1007/s00280-002-0464-0.
[219] J.F. Deeken, R. Slack, G.J. Weiss, R.K. Ramanathan, M.J. Pishvaian, J. Hwang, et al., A phase I study of liposomal-encapsulated docetaxel (LE-DT) in patients with advanced solid tumor malignancies, Cancer Chemother. Pharmacol. 71 (2013) 627–633. http://dx.doi.org/10.1007/s00280-012-2048-y.
[220] S. Ugwu, A. Zhang, M. Parmar, B. Miller, T. Sardone, V. Peikov, et al., Preparation, characterization, and stability of liposome-based formulations of mitoxantrone, Drug Dev. Ind. Pharm. 31 (2005) 223–229. http://dx.doi.org/10.1081/DDC-200047850.
[221] M. Slingerland, H.-J. Guchelaar, H. Rosing, M.E. Scheulen, L.J.C. van Warmerdam, J.H. Beijnen, et al., Bioequivalence of liposome-entrapped paclitaxel easy-to-use

(LEP-ETU) formulation and paclitaxel in polyethoxylated castor oil: a randomized, two-period crossover study in patients with advanced cancer, Clin. Ther. 35 (2013) 1946–1954. http://dx.doi.org/10.1016/j.clinthera.2013.10.009.
[222] A. Dritschilo, C.H. Huang, C.M. Rudin, J. Marshall, B. Collins, J.L. Dul, et al., Phase I study of liposome-encapsulated c-raf antisense oligodeoxyribonucleotide infusion in combination with radiation therapy in patients with advanced malignancies, Clin. Cancer Res. 12 (2006) 1251–1259. http://dx.doi.org/10.1158/1078-0432.CCR-05-1260.
[223] A. Pal, S. Khan, Y.-F. Wang, N. Kamath, A.K. Sarkar, A. Ahmad, et al., Preclinical safety, pharmacokinetics and antitumor efficacy profile of liposome-entrapped SN-38 formulation, Anticancer Res 25 (2005) 331–341.
[224] M.J.A. de Jonge, M. Slingerland, W.J. Loos, E.A.C. Wiemer, H. Burger, R.H.J. Mathijssen, et al., Early cessation of the clinical development of LiPlaCis, a liposomal cisplatin formulation, Eur. J. Cancer 1990 (46) (2010) 3016–3021. http://dx.doi.org/10.1016/j.ejca.2010.07.015.
[225] D. Matabudul, K. Pucaj, G. Bolger, B. Vcelar, M. Majeed, L. Helson, Tissue distribution of (Lipocurc™) liposomal curcumin and tetrahydrocurcumin following two- and eight-hour infusions in Beagle dogs, Anticancer Res 32 (2012) 4359–4364.
[226] G.P. Stathopoulos, D. Antoniou, J. Dimitroulis, J. Stathopoulos, K. Marosis, P. Michalopoulou, Comparison of liposomal cisplatin versus cisplatin in non-squamous cell non-small-cell lung cancer, Cancer Chemother. Pharmacol. 68 (2011) 945–950. http://dx.doi.org/10.1007/s00280-011-1572-5.
[227] A.M. Tari, Y. Gutiérrez-Puente, G. Monaco, C. Stephens, T. Sun, M. Rosenblum, et al., Liposome-incorporated Grb2 antisense oligodeoxynucleotide increases the survival of mice bearing bcr-abl-positive leukemia xenografts, Int. J. Oncol. 31 (2007) 1243–1250.
[228] S.A. Boorjian, M.I. Milowsky, J. Kaplan, M. Albert, M.V. Cobham, D.M. Coll, et al., Phase 1/2 clinical trial of interferon alpha2b and weekly liposome-encapsulated all-trans retinoic acid in patients with advanced renal cell carcinoma, J. Immunother. 1997 (30) (2007) 655–662. http://dx.doi.org/10.1097/CJI.0b013e31805449a8.
[229] C.L. van Broekhoven, C.R. Parish, C. Demangel, W.J. Britton, J.G. Altin, Targeting dendritic cells with antigen-containing liposomes: a highly effective procedure for induction of antitumor immunity and for tumor immunotherapy, Cancer Res. 64 (2004) 4357–4365. http://dx.doi.org/10.1158/0008-5472.CAN-04-0138.
[230] X. Xu, L. Wang, H.-Q. Xu, X.-E. Huang, Y.-D. Qian, J. Xiang, Clinical comparison between paclitaxel liposome (Lipusu®) and paclitaxel for treatment of patients with metastatic gastric cancer, Asian Pac. J. Cancer Prev. 14 (2013) 2591–2594.
[231] R. Suzuki, T. Takizawa, Y. Kuwata, M. Mutoh, N. Ishiguro, N. Utoguchi, et al., Effective anti-tumor activity of oxaliplatin encapsulated in transferrin-PEG-liposome, Int. J. Pharm. 346 (2008) 143–150. http://dx.doi.org/10.1016/j.ijpharm.2007.06.010.
[232] C.F. McDonagh, A. Huhalov, B.D. Harms, S. Adams, V. Paragas, S. Oyama, et al., Antitumor activity of a novel bispecific antibody that targets the ErbB2/ErbB3 oncogenic unit and inhibits heregulin-induced activation of ErbB3, Mol. Cancer Ther. 11 (2012) 582–593. http://dx.doi.org/10.1158/1535-7163.MCT-11-0820.
[233] A.H. Ko, M.A. Tempero, Y.-S. Shan, W.-C. Su, Y.-L. Lin, E. Dito, et al., A multinational phase 2 study of nanoliposomal irinotecan sucrosofate (PEP02, MM-398) for patients with gemcitabine-refractory metastatic pancreatic cancer, Br. J. Cancer 109 (2013) 920–925. http://dx.doi.org/10.1038/bjc.2013.408.
[234] A. Bouchie, First microRNA mimic enters clinic, Nat. Biotechnol. 31 (2013) 577. http://dx.doi.org/10.1038/nbt0713-577.
[235] University of California, San Francisco, A Phase I Trial of Nanoliposomal CPT-11 (NL CPT-11) in Patients With Recurrent High-Grade GliomasRetrieved July 2014 http://clinicaltrials.gov/ct2/show/NCT00734682 2008.
[236] A.H. Sarris, F. Hagemeister, J. Romaguera, M.A. Rodriguez, P. McLaughlin, A.M. Tsimberidou, et al., Liposomal vincristine in relapsed non-Hodgkin's lymphomas: early results of an ongoing phase II trial, Ann. Oncol. 11 (2000) 69–72.
[237] F. Duffaud, M. Borner, P. Chollet, J.B. Vermorken, J. Bloch, M. Degardin, et al., Phase II study of OSI-211 (liposomal lurtotecan) in patients with metastatic or locoregional recurrent squamous cell carcinoma of the head and neck. An EORTC New Drug Development Group study, Eur. J. Cancer 40 (2004) 2748–2752.
[238] G. Beutel, H. Glen, P. Schöffski, J. Chick, S. Gill, J. Cassidy, et al., Phase I study of OSI-7904 L, a novel liposomal thymidylate synthase inhibitor in patients with refractory solid tumors, Clin. Cancer Res. 11 (2005) 5487–5495. http://dx.doi.org/10.1158/1078-0432.CCR-05-0104.
[239] A.W. Tolcher, W.V. Rodrigueza, D.W. Rasco, A. Patnaik, K.P. Papadopoulos, A. Amaya, et al., A phase 1 study of the BCL2-targeted deoxyribonucleic acid inhibitor (DNAi) PNT2258 in patients with advanced solid tumors, Cancer Chemother. Pharmacol. 73 (2014) 363–371. http://dx.doi.org/10.1007/s00280-013-2361-0.
[240] A.A. Gabizon, D. Tzemach, A.T. Horowitz, H. Shmeeda, J. Yeh, S. Zalipsky, Reduced toxicity and superior therapeutic activity of a mitomycin C lipid-based prodrug incorporated in pegylated liposomes, Clin. Cancer Res. 12 (2006) 1913–1920. http://dx.doi.org/10.1158/1078-0432.CCR-05-1547.
[241] S. Mitragotri, Nanoparticulate drug delivery perspectives on the transition from laboratory to market Foreword, Nanoparticulate Drug Deliv. Perspect. Transit. Lab. Mark, Woodhead Publ Ltd, Cambridge, 2012, pp. XIII–XIV.
[242] J.H. Hwang, M.C. Lim, S.-S. Seo, S.-Y. Park, S. Kang, Phase II study of belotecan (CKD 602) as a single agent in patients with recurrent or progressive carcinoma of uterine cervix, Jpn. J. Clin. Oncol. 41 (2011) 624–629. http://dx.doi.org/10.1093/jjco/hyr017.
[243] N. Senzer, J. Nemunaitis, D. Nemunaitis, C. Bedell, G. Edelman, M. Barve, et al., Phase I study of a systemically delivered p53 nanoparticle in advanced solid tumors, Mol. Ther. J. Am. Soc. Gene Ther. 21 (2013) 1096–1103. http://dx.doi.org/10.1038/mt.2013.32.
[244] K.F. Pirollo, A. Rait, Q. Zhou, X. Zhang, J. Zhou, C.-S. Kim, et al., Tumor-targeting nanocomplex delivery of novel tumor suppressor RB94 chemosensitizes bladder carcinoma cells in vitro and in vivo, Clin. Cancer Res. 14 (2008) 2190–2198. http://dx.doi.org/10.1158/1078-0432.CCR-07-1951.
[245] B.P.H. Wittgen, P.W.A. Kunst, K. van der Born, A.W. van Wijk, W. Perkins, F.G. Pilkiewicz, et al., Phase I study of aerosolized SLIT cisplatin in the treatment of patients with carcinoma of the lung, Clin. Cancer Res. 13 (2007) 2414–2421. http://dx.doi.org/10.1158/1078-0432.CCR-06-1480.
[246] N. Seetharamu, E. Kim, H. Hochster, F. Martin, F. Muggia, Phase II study of liposomal cisplatin (SPI-77) in platinum-sensitive recurrences of ovarian cancer, Anticancer Res 30 (2010) 541–545.
[247] G. Kroemer, L. Zitvogel, L. Galluzzi, Victories and deceptions in tumor immunology: Stimuvax(®), Oncoimmunology 2 (2013) e23687. http://dx.doi.org/10.4161/onci.23687.
[248] Gradalis, Inc., Phase I Intratumoral Pbi-shRNA STMN1 LP in Advanced and/or Metastatic Cancer (STMN1-LP)Retrieved July 2014 http://clinicaltrials.gov/ct2/show/NCT01505153 2012.
[249] R.T. Poon, N. Borys, Lyso-thermosensitive liposomal doxorubicin: an adjuvant to increase the cure rate of radiofrequency ablation in liver cancer, Future Oncol. 7 (2011) 937–945. http://dx.doi.org/10.2217/fon.11.73.
[250] A.D. Judge, M. Robbins, I. Tavakoli, J. Levi, L. Hu, A. Fronda, et al., Confirming the RNAi-mediated mechanism of action of siRNA-based cancer therapeutics in mice, J. Clin. Invest. 119 (2009) 661–673. http://dx.doi.org/10.1172/JCI37515.
[251] M.J. Hawkins, P. Soon-Shiong, N. Desai, Protein nanoparticles as drug carriers in clinical medicine, Adv. Drug Deliv. Rev. 60 (2008) 876–885. http://dx.doi.org/10.1016/j.addr.2007.08.044.
[252] A.M. Gonzalez-Angulo, F. Meric-Bernstam, S. Chawla, G. Falchook, D. Hong, A. Akcakanat, et al., Weekly nab-Rapamycin in patients with advanced nonhematologic malignancies: final results of a phase I trial, Clin. Cancer Res. 19 (2013) 5474–5484. http://dx.doi.org/10.1158/1078-0432.CCR-12-3110.
[253] Celgene Corporation, A Phase 1 Trial of ABI-011 in Patients With Advanced Solid Tumors or LymphomasRetrieved July 2014 http://clinicaltrials.gov/ct2/show/NCT01163071 2010.
[254] M.E. Davis, J.E. Zuckerman, C.H.J. Choi, D. Seligson, A. Tolcher, C.A. Alabi, et al., Evidence of RNAi in humans from systemically administered siRNA via targeted nanoparticles, Nature 464 (2010) 1067–1070. http://dx.doi.org/10.1038/nature08956.
[255] S. Gaur, Y. Wang, L. Kretzner, L. Chen, T. Yen, X. Wu, et al., Pharmacodynamic and pharmacogenomic study of the nanoparticle conjugate of camptothecin CRLX101 for the treatment of cancer, Nanomed. Nanotechnol. Biol. Med. (2014). http://dx.doi.org/10.1016/j.nano.2014.04.003.
[256] J. Jung, S.-J. Park, H.K. Chung, H.-W. Kang, S.-W. Lee, M.H. Seo, et al., Polymeric nanoparticles containing taxanes enhance chemoradiotherapeutic efficacy in non-small cell lung cancer, Int. J. Radiat. Oncol. Biol. Phys. 84 (2012) e77–e83. http://dx.doi.org/10.1016/j.ijrobp.2012.02.030.
[257] S. Ghamande, C.-C. Lin, D.C. Cho, G.I. Shapiro, E.L. Kwak, M.H. Silverman, et al., A phase 1 open-label, sequential dose-escalation study investigating the safety, tolerability, and pharmacokinetics of intravenous TLC388 administered to patients with advanced solid tumors, Invest. New Drugs 32 (2014) 445–451. http://dx.doi.org/10.1007/s10637-013-0044-7.
[258] K.F. Roby, F. Niu, R.A. Rajewski, C. Decedue, B. Subramaniam, P.F. Terranova, Syngeneic mouse model of epithelial ovarian cancer: effects of nanoparticulate paclitaxel, Nanotax, Adv. Exp. Med. Biol. 622 (2008) 169–181.
[259] A. Madaan, P. Singh, A. Awasthi, R. Verma, A.T. Singh, M. Jaggi, et al., Efficiency and mechanism of intracellular paclitaxel delivery by novel nanopolymer-based tumor-targeted delivery system, Nanoxel(TM), Clin. Transl. Oncol. 15 (2013) 26–32. http://dx.doi.org/10.1007/s12094-012-0883-2.
[260] T. Ueno, K. Endo, K. Hori, N. Ozaki, A. Tsuji, S. Kondo, et al., Assessment of antitumor activity and acute peripheral neuropathy of 1,2-diaminocyclohexane platinum (II)-incorporating micelles (NC-4016), Int. J. Nanomedicine 9 (2014) 3005–3012. http://dx.doi.org/10.2147/IJN.S60564.
[261] T. Hamaguchi, T. Doi, T. Eguchi-Nakajima, K. Kato, Y. Yamada, Y. Shimada, et al., Phase I study of NK012, a novel SN-38-incorporating micellar nanoparticle, in adult patients with solid tumors, Clin. Cancer Res. 16 (2010) 5058–5066. http://dx.doi.org/10.1158/1078-0432.CCR-10-0387.
[262] K. Kato, K. Chin, T. Yoshikawa, K. Yamaguchi, Y. Tsuji, T. Esaki, et al., Phase II study of NK105, a paclitaxel-incorporating micellar nanoparticle, for previously treated advanced or recurrent gastric cancer, Invest. New Drugs 30 (2012) 1621–1627. http://dx.doi.org/10.1007/s10637-011-9709-2.
[263] Y. Matsumura, T. Hamaguchi, T. Ura, K. Muro, Y. Yamada, Y. Shimada, et al., Phase I clinical trial and pharmacokinetic evaluation of NK911, a micelle-encapsulated doxorubicin, Br. J. Cancer 91 (2004) 1775–1781. http://dx.doi.org/10.1038/sj.bjc.6602204.
[264] Oasmia Pharmaceutical AB, Study of Paclitaxel in Patients With Ovarian CancerRetrieved July 2014 http://clinicaltrials.gov/ct2/show/NCT00989131 2009.
[265] J.W. Valle, A. Armstrong, C. Newman, V. Alakhov, G. Pietrzynski, J. Brewer, et al., A phase 2 study of SP1049C, doxorubicin in P-glycoprotein-targeting pluronics, in patients with advanced adenocarcinoma of the esophagus and gastroesophageal junction, Invest. New Drugs 29 (2011) 1029–1037. http://dx.doi.org/10.1007/s10637-010-9399-1.
[266] L. Barraud, P. Merle, E. Soma, L. Lefrançois, S. Guerret, M. Chevallier, et al., Increase of doxorubicin sensitivity by doxorubicin-loading into nanoparticles for hepatocellular carcinoma cells in vitro and in vivo, J. Hepatol. 42 (2005) 736–743. http://dx.doi.org/10.1016/j.jhep.2004.12.035.
[267] J. Li, S. Gupta, C. Li, Research perspectives: gold nanoparticles in cancer theranostics, Quant. Imaging Med. Surg. 3 (2013) 284–291. http://dx.doi.org/10.3978/j.issn.2223-4292.2013.12.02.
[268] A.S. Fortuin, H. Meijer, L.C. Thompson, J.A. Witjes, J.O. Barentsz, Ferumoxtran-10 ultrasmall superparamagnetic iron oxide-enhanced diffusion-weighted imaging magnetic resonance imaging for detection of metastases in normal-sized lymph nodes in patients with bladder and prostate cancer: do we enter the era after

extended pelvic lymph node dissection? Eur. Urol. 64 (2013) 961–963. http://dx.doi.org/10.1016/j.eururo.2013.08.017 (discussion 963).
[269] S.S. Hedgire, M. Mino-Kenudson, A. Elmi, S. Thayer, C. Fernandez-del Castillo, M.G. Harisinghani, Enhanced primary tumor delineation in pancreatic adenocarcinoma using ultrasmall super paramagnetic iron oxide nanoparticle-ferumoxytol: an initial experience with histopathologic correlation, Int. J. Nanomedicine 9 (2014) 1891–1896. http://dx.doi.org/10.2147/IJN.S59788.
[270] M. Benezra, O. Penate-Medina, P.B. Zanzonico, D. Schaer, H. Ow, A. Burns, et al., Multimodal silica nanoparticles are effective cancer-targeted probes in a model of human melanoma, J. Clin. Invest. 121 (2011) 2768–2780. http://dx.doi.org/10.1172/JCI45600.

Chapter II

"Polymeric Nanomaterials: Applications in Therapeutics"

Witzigmann D, Camblin M, Huwyler J, Balasubramanian V.

Encyclopedia of Biomedical Polymers and Polymeric Biomaterials, 1st Ed.; Mishra, M. 2015; Vol. 8, p. 5364-78.

Highlights: During the last decades, intensive efforts have been made to develop new types of nanomaterials for biomedical applications. Polymers that spontaneously self-assemble in aqueous solution into various nanoscale structures such as micelles, nanoparticles, and vesicles have a huge potential to serve as nanocarriers for various therapeutic applications. This review article highlights the fundamental and physicochemical properties of self-assembled morphologies like micelles, polymeric nanoparticles, vesicles (polymersomes), and layer-by-layer capsules. Formulation characteristics such as loading efficiency, stability, and release properties of polymeric nanocarrier systems are covered. Biological properties of the polymeric nanomaterials and their therapeutic applications from the delivery of small drug molecules to proteins and gene delivery are emphasized.

Nanomaterials: Therapeutic Applications

Dominik Witzigmann
Marine Camblin
Jörg Huwyler
Vimalkumar Balasubramanian
Division of Pharmaceutical Technology, University of Basel, Basel, Switzerland

Abstract
In recent years, uses of engineered nanomaterials have increased in day-to-day life, especially in biomedical applications. In this direction, advances in polymer science have significantly contributed to the development of polymeric nanomaterials for drug delivery applications. Particularly, intensive efforts have been made to develop new types of nanomaterials through self-assembly techniques. Polymers that can spontaneously self-assemble in aqueous solution into various nanoscale structures such as micelles, nanoparticles, and vesicles have huge potential to serve as nanocarriers for various therapeutic applications. By controlling the number of physicochemical parameters that can influence the self-assembly process, it is possible to tailor the desired morphology of the nanostructures and to engineer different properties of the nanostructures. This entry reviews the fundamental and physicochemical properties of self-assembled morphologies like micelles, nanoparticles, vesicles (polymersomes), and layer-by-layer capsules that are driven by template-directed assembly. We cover formulation characteristics such as loading efficiency, stability, and release properties of polymeric nanocarrier systems with recent examples. We emphasize the biological properties of the polymeric nanomaterials and their therapeutic applications from the delivery of small drug molecules to proteins and gene delivery.

INTRODUCTION

Drug molecules have often unfavorable pharmacokinetic properties. Encountered problems may include low bioavailability, poor distribution to target tissues, accumulation in non-target tissues and low metabolic stability. Consequently, their therapeutic efficiency is decreased and off target toxicity is more pronounced in conventional approaches. Those issues raise the pressing need of more sophisticated and smart drug delivery systems (DDSs) to improve the performance of classical therapeutics. Nanomaterial-based formulations offer the possibility to modulate pharmacokinetic properties of delivered drugs. Unique nanoscale properties of nanomaterials such as high surface-to-volume ratio due to their nanoscale size (20–200 nm) and enhanced physicochemical properties make them an ideal candidate for nanocarriers. They can, for example, be loaded with a drug of interest. As a result, increase in the apparent solubility of the administered drug and change in the pharmacokinetic properties has the potential to improve the therapeutic efficiency and efficacy.

The main aim of the present review is to discuss the therapeutic use of nanocarriers as DDSs. A wide range of nanomaterials made of organic, inorganic, lipid, polymer, and peptide-based compounds have been proposed as nanocarriers for such therapeutic applications. As compared to clinically established nanocarriers such as liposomal DDSs, polymeric nanomaterials have recently gained attention due to their unique properties. First, physicochemical properties and chemical versatility nature of polymers can be used to combine polymers with drugs (covalent and noncovalent approach) that can dramatically improve the drug characteristics in terms of solubility, stability, and permeability. Second, polymers can be chemically modified to conjugate with targeting vectors such as antibodies, peptides, and aptamers to guide them to specific tissue or cells in the body. Third, environmental responsiveness such as pH and temperature of polymers can be used to control the release profile of the drug in a specified area of interest. It has to be emphasized that polymers can offer the biological properties to be nontoxic, biodegradable, and biocompatible. These are essential requirements for therapeutic applications. In this entry, we discuss recent developments of polymeric nanomaterials forming self-assembled nanostructures such as micelles, nanoparticles, polymersomes, and template-directed assembly-forming layer-by-layer (LbL) capsules for various therapeutic applications (Fig. 1).

POLYMERIC MICELLES

General Characteristics

Polymeric micelles are self-assembled nanostructures consisting of a compact hydrophobic core surrounded by a hydrophilic corona. Micelles are dynamic structures

Encyclopedia of Biomedical Polymers and Polymeric Biomaterials DOI: 10.1081/E-EBPP-120050055

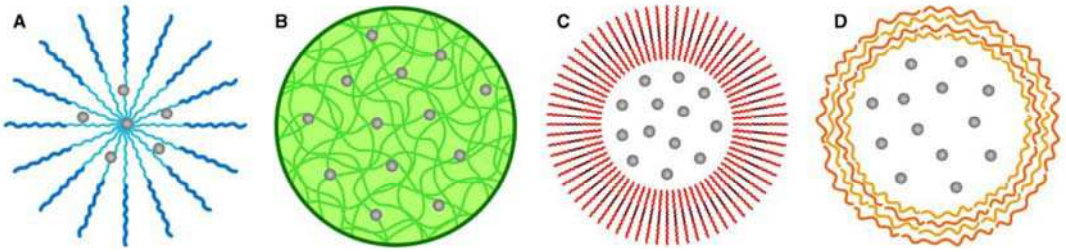

Fig. 1 Schematic illustration of different types of polymeric nanomaterial based nanocarriers (**A**) polymeric micelle, (**B**) polymeric NP, (**C**) polymersome, and (**D**) LbL capsule. Gray dots represent the transported drug.

composed of amphiphilic block copolymers possessing both hydrophilic and hydrophobic blocks. Amphiphilic copolymers begin to self-assemble in solution into micelles at a specific and narrow concentration range, which is known as critical micelle concentration (CMC). One of the main reasons why amphiphilic copolymers self-assemble themselves in aqueous solution is their tendency to isolate the hydrophobic blocks from the aqueous environment and to reach a state of minimum energy. This process is driven by an increase in entropy of water molecules interacting with hydrophobic molecules.[1] Above the CMC, micelle structures are thermodynamically stable and below the CMC, micelles are unstable. The relative size of the hydrophobic block of the copolymer is the most important factor that affects the process of micelle formation.

Amphiphilic block copolymers can form a variety of self-assembled structures in solutions where the solvent preferentially solvates one of the blocks. The most common structures formed by these amphiphilic copolymers are spherical micelles, cylindrical micelles, and vesicles. Depending on the length of the hydrophobic block, spherical micelles can be classified as star-like or crew-cut micelles. When the length of the hydrophilic block is longer than the hydrophobic block, it forms the star-like micelles. Crew-cut micelles are formed when the hydrophilic block is shorter than the hydrophobic block. As the hydrophilic block length decreases, the morphology of the micelles change from spherical to cylindrical (also called worm-like or rod micelles). Recent approaches showed that by controlling the self-assembly of the amphiphilic block copolymers different types of micellar morphologies can be obtained. These types of micellar morphologies include disk-like, toroidal, bi-continuous, cross-linked, and Janus micelles.[2,3] In most cases, polymeric micelles are prepared by two different methods. In the first method, amphiphilic copolymers are directly dissolved in water. During spontaneous self-assembly, drugs can be loaded simply by adding them to the polymers. In the second method, copolymers are dissolved in organic solvent. The solvent is removed by evaporation resulting in a thin film of copolymers. Drugs can then be loaded during the rehydration and self-assembly process of the film exposed to an aqueous solution. These techniques are referred to as direct dissolution and film rehydration method, respectively.[4]

Formulation Characteristics

Classically, polymeric micelles have been utilized to improve the solubilization and loading of hydrophobic drug molecules. When maximum solubilization capacity of the micelles is achieved, drugs cannot be loaded further into the micelles. Thus, solubilization and drug loading efficiency are directly linked parameters.[1] To improve drug solubilization, hydrotropic polymers can be used instead of conventional amphiphilic copolymers.[5,6] Furthermore, solubilization and loading efficiency can also be dependent on the hydrophobicity level of the drugs. For instance, conventional poly(ethylene glycol)–polylactide acid (PEG–PLA) micelles improved the solubilization of paclitaxel (PTX) by a factor of 50, compared to the less hydrophobic nifedipine (factor of 20), due to a higher hydrophobicity level. Similarly, hydrotropic polymer based poly(ethylene glycol)–poly(2-amino-2-methyl-butyl)acrylamide (PEG-PDMBA) micelles showed the dramatic solubility enhancement for PTX (6000-fold increased solubility) compared with nifedipine (60-fold increased solubility). Interestingly, poly(ethylene glycol)–poly [2-(4-vinylbenzyloxy)-*N*,*N*-diethylnicotinamide] (PEG-PDENA) micelles showed high specificity toward the solubilizing properties for PTX (about 9000-fold increased loading) than for the other drugs.[6]

Compatibility between drug molecules and the micelle core is the major determinant of drug solubility and loading efficiency.[5] In one study, the influence of copolymer was investigated on the solubilization of PTX. In this study, PEG-PDENA (hydrotropic polymer) micelles showed the highest loading capacity of PTX (37.4%) compared to the conventional poly(ethylene glycol)–polyphosphoramidate (PEG-PPA) and PEG-PLA micelles that showed 14.7% and 27.6% of PTX loading due to the compatibility between PTX and PDENA.[5] In addition to the single drug loading, micelles offer the possibility to load multiple drugs into single micelles at clinically relevant doses. PTX, etoposide (ETO), docetaxel (DTXL), and 17-allylamino-17-demethyoxygeldanamycin (17-AAG) were solubilized in PEG-PLA micelles within the combinations PTX/17-AAG, ETO/17-AAG, DTXL/17-AAG, and PTX/ETO/17-AAG. Two-drug and three-drug combinations in micelles

retained the 94% and 97% of loaded drugs, respectively, compared to the single drug micelles that retained 16% to 32% of the loaded drugs. The presence of 17-AAG in those micelles helped to stabilize the formulation and to offer greater stability of the drugs at the same level of solubilization as single drug micelles.[7]

Stability of micelles is crucial for drug delivery applications. To improve the stability of drug loaded micelles, several strategies have been explored such as enhancing the compatibility between the drug and the block copolymer, cross-linking of the micelle core/corona, and lowering the CMC by altering the polymer.[4] Classical PEG-PLA micelles loaded with PTX showed stability over a period of 4–5 days. To overcome this limitation, hydrotropic polymers have been linked to PEG to develop PEG-PDENA micelles that increase the micellar stability for a period of 25 days due to the compatibility of PDENA and PTX.[5] Polymeric micelles cross-linked with ionic cores by using block ionomer complexes of poly(ethylene oxide)–poly(methacrylic acid) (PEO-PMA) and divalent metal cations showed colloidal stability for a prolonged period of time.[8] Moreover, cross-linking of micelles increased the stability without affecting the drug loading capacity.[4]

Therapeutic Applications

Polymeric micelles are one of the widely used nano-carrier systems due to their unique properties, usually ranging from 20 to 200 nm in size for drug delivery application.[1] High colloidal stability of polymeric micelles is mainly due to the low CMC of the polymers that prevents the dissociation of micelles and offers high stability in biological systems, where it is diluted after intravenous injection. Polymeric micelles have better rigidity and stability than phospholipid micelles due to the covalent link between the polymeric blocks.[4] The hydrophobicity of the micellar core permits the incorporation and stabilization of wide range of small drug molecules, such as doxorubicin (DOX), PTX, amphothericin B, cisplatin, cyclosporine, and hydroxyl camptothecin.[9] Hydrophilic corona of the micelle offers the stealth properties to escape the reticuloendothelial system (RES). These properties lead to a significant increase in the blood residence time of micelles, allow them to permeate the blood vessels, and to accumulate efficiently at the tumor site.[10] The nano-size of polymeric micelles may also facilitate the deep penetration of carrier to tumor tissue and ease of their uptake by tumor cells.[9]

Anticancer drugs such as DOX and PTX are commonly used cancer therapeutics. However, low water solubility, acute toxicity to normal cells, and multidrug resistance are the major issues that can be surmounted by using polymeric micelles. For instance, poloxamer micelles [poly(ethylene oxide–poly(propylene oxide)] loaded with DOX entered clinical trials in Canada in 1999 and completed phase II in esophageal adenocarcinoma.[11] Pharmacokinetic and biodistribution of these micelles in healthy mice showed a 2.1-fold increase of area under the curve (AUC), 2.1-fold decrease in clearance, and 1.5-fold decrease in volume of distribution compared to the free DOX. In-vivo (in mice) and at equal dose, poloxamer micelles showed to be more effective than free DOX in solid tumor models. In another approach, use of polymeric micelles made of PEO–poly(D,L-lactic acid) [PDLLA] hamper the unwanted toxic side effects associated with solubilizing agent, Cremophor EL®, which is present in the commercial PTX formulations (Taxol®). Intravenous administration of PTX micelles in nude mice caused 91% decrease in the tumor volume that showed high therapeutic efficiency. Additionally, polymeric micelles offer the possibility of introducing high dose of PTX without any potential side effects.[12] In another study, PEO-poly(4-phenyl-L-butanoate)-L-aspartamide) (PPBA) micelles loaded with PTX (NK-105) showed 87-fold increase in AUC, 86-fold decrease in clearance, and 15-fold decrease in volume of distribution compared with marketed product Taxol® after intravenous injection. Micelles had a long circulation time in blood and were able to evade serum protein binding. Enhanced accumulation in the tumor (25-fold) and stronger antitumor activity in C-26 tumor bearing mice model at a single administration of NK-105 leads to the efficient tumor regression.[13]

In addition to the delivery of small hydrophobic molecules, micelles can serve to deliver large therapeutic proteins. Different PEG-PLA diblock copolymer-based micelles have been investigated for the delivery of recombinant human erythropoietin (rhEPO) in Sprague-Dawley rats.[14] This study showed a twofold increase of AUC with the micelles (from 23 μg/L·hr to 33 μg/L·hr) compared to the native rhEPO (16 μg/L·hr). Plasma concentration of rhEPO was twofold higher with the micelles (i.e., 39.88 ng/mL) than with the native rhEPO. Micelles increased the half-life of rhEPO in blood circulation from 2.0 hr (native rhEPO) to 4.4 hr due to the stealth property of the PEG.[14] Micellar formulation of rhEPO enhanced the pharmacological effect of the drug (i.e., increased level of hemoglobin by 48.72%) demonstrating that micellar delivery of the protein did not affect protein functionality. In an alternative approach, human serum albumin (HSA) was loaded into poly(ethylene glycol)–poly(amino ester) (PEG-PAE) micelles and the delivery was enhanced by a pH-dependent stimulus at reduced pH in ischemic tissue. Accumulation of labeled albumin in ischemic brain areas of rats after IV injection indicated that this type of formulation can be used for targeted protein delivery in experimental models of cerebral ischemia (Fig. 2).[15]

Polycationic-based polymeric micelles have an ability to form complexes with negatively charged plasmid DNA (pDNA). Thus, DNA can be packed into micelles for gene delivery. DNA is thereby protected from enzymatic and hydrolytic degradation. Intravenous injection of pDNA/PEG–poly-L-lysine (PLL) micelles showed circulation of intact pDNA in the blood circulation for 3 hr when compared to naked pDNA that is eliminated from the

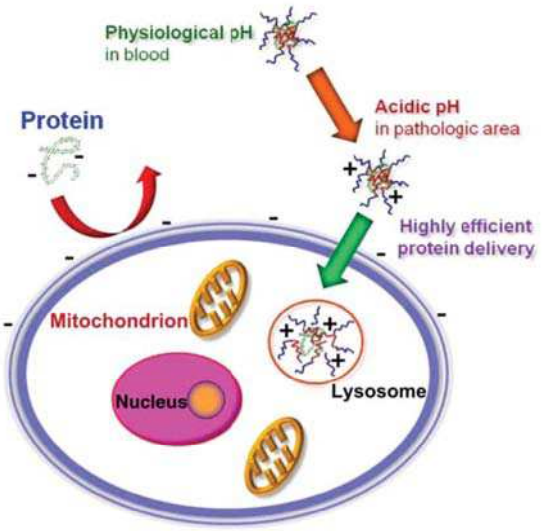

Fig. 2 Schematic representation of pH-tunable micelles loaded with a therapeutic protein to implement a drug targeting strategy. At appropriate pH for noninvasive administration (pH 7 or over), the protein-loaded micelles are stable. If the pH turns acidic (pH < 7), the ionized amino groups of the PAE block forming the micelles are positively charged. This promotes uptake into a diseased tissue, which is characterized by a low pH (e.g., ischemic tissue). At low pH, block copolymers from micelles dissolve and release the transported protein.
Source: From Gao et al.[15] © 2012, with permission from Elsevier.

circulation within 5 min.[16] Micelles are also capable of co-delivering DNA and other drugs. Micelles composed of copolymer poly(*N*-methyldietheneamine sebacate)-[(cholesteryl oxocarbonylamido ethyl) methyl bis(ethylene) ammonium bromide] sebacate (PMDS-CES) were shown to transport PTX within the hydrophobic core and pDNA within the corona. Combined delivery of PTX and pDNA suppressed the tumor growth in a 4T1 mouse breast cancer model three times more efficiently than the single delivery of drug and pDNA in micelles.[17] Furthermore, a combination of small interfering ribonucleic acid (siRNA) and PTX demonstrated synergistic effects. MDA-MB-231 human breast carcinoma cells were incubated with micelles containing drug and siRNA. After 4 hr, cell viability decreased from 78% to 58%. As the siRNA cytotoxicity was only about 8%, there was a clear synergistic effect associated with the co-delivery of PTX and siRNA.[17]

POLYMERIC NANOPARTICLES

General Characteristics

Polymeric nanoparticles (NPs) are spherical, colloidal particles consisting of macromolecular materials, in which the active pharmaceutical ingredient (API) is dissolved, entrapped, encapsulated, and/or adsorbed or attached.[18] Although NP size ranges from 10 to 1000 nm, the optimal requirement for drug delivery applications is <200 nm. Three approaches are used to prepare polymeric NPs: (i) dispersion of preformed polymers; (ii) polymerization of monomers for synthetic polymers; and (iii) ionic gelation or coazervation for hydrophilic polymers. Depending on the method of preparation, nanospheres or nanocapsules are designed to tune the release profile (Fig. 3). In general, the process of drug release from NPs is mediated by (i) drug solubility; (ii) diffusion through the NP matrix/polymer wall; (iii) NP matrix erosion; (iv) desorption of adsorbed drug; or (v) a combination of all these factors.[20]

Nanospheres are matrix systems, in which the drug is physically and uniformly dispersed and released by diffusion and erosion.[21] If the erosion of the matrix is faster than the diffusion process, the release mainly depends on the degradation kinetics of the material and results typically in a first order kinetics. Biodegradable polymers have the advantage that they degrade in vivo either enzymatically or nonenzymatically to nontoxic, biocompatible products. One of the disadvantages of nanospheres is the direct contact of the API to the environment at the surface, which can lead to degradation of the compound and burst release. From a drug delivery point of view, nanocapsules can overcome these negative characteristics. Nanocapsules are vesicular systems, in which the drug is encapsulated in a cavity surrounded by a polymer membrane.[22] Depending on the inner core liquid, aqueous or lipophilic, variations of drug solubility are possible. As compared to nanospheres, nanocapsules have the advantage of (i) increased drug protection; (ii) advanced controlled release; and (iii) higher drug loading capacity. Nanocapsules release drugs by a zero order diffusion driven process, which is influenced by the preparation method for these nanocarriers.[23]

Formulation Characteristics

Two different types of polymers have been employed for the development of NPs, namely natural and synthetic materials. The most commonly used natural polymers are gelatin, alginate, albumin, and chitosan, which are considered to be biodegradable and nontoxic.[24] To prepare albumin-bound nanoparticles (NAB), the API is mixed with HSA in a solvent and pressed through a jet to form NPs in the size range of 50–200 nm. The first polymeric NP product, which is used clinically, is the NAB-formulation Abraxane® (ABI-007) containing the mitotic inhibitor PTX. This technology is approved for the treatment of breast cancer and non-small cell lung cancer (NSCLC). Additional clinical trials are ongoing.[25,26]

Another commonly used natural polymer is chitosan, which offers additional advantages like increased paracellular permeability and excellent mucoadhesive properties.[27,28] pDNA-loaded chitosan NPs demonstrated nasal

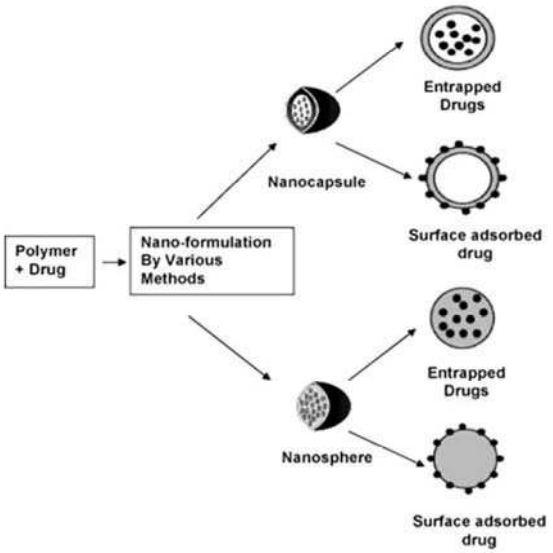

Fig. 3 Schematic representation of methods used to prepare different types of NPs (e.g., nanocapsules and nanospheres). Drug is entrapped within particles or absorbed to the surface. Black dots represent the transported drug.
Source: From Kumari et al.[19] © 2010, with permission from Elsevier.

mucosal immunization against hepatitis B at low pH.[29] However, at physiological pH, the permeation effect by interactions with components of the tight junctions is limited due to the decreased charge (pK_a of amine groups is 6.2). Therefore, quaternary chitosan derivatives such as *N*-trimethyl chitosan (TMC) have been evaluated to overcome this limitation. This derivative has a positive charge independent of the pH and is soluble over a wide pH range, which affects the mucoadhesive and penetration-enhancing properties.[30] Nasal administration of mucoadhesive and rapid antigen-releasing TMC NPs demonstrated the promise of noninvasive vaccination.[31] Furthermore, chitosan has a high loading capacity for nucleic acids with an encapsulation efficiency of 96.2%, owing to ionic interactions.[29]

The use of synthetic polymers in place of natural polymers can offer a wide range of chemical versatility. This includes improved loading efficiency, functionalization properties, and pharmacokinetic profiles. Synthetic polymers like PLA, polyglycolide acid (PGA), polylactide-*co*-glycolide acid (PLGA), poly(ε-caprolactone) (PCL), polyalkylcyanoacrylate (PACA), polyanhydrides, or polymethacrylates have been prepared from a great pool of synthetic and readily available monomers. Depending on the material, different release characteristics from hours up to weeks could be achieved.[19] The polyester PLGA/PLA and PCL are the most commonly used synthetic materials since they are biocompatible, biodegradable, and nontoxic. They are approved for clinical use by the Food and Drug Administration (FDA) and European Medicines Agency (EMA).[32,33] In presence of water, the ester linkages of PLGA and PLA are hydrolyzed and the drug is released. The metabolites (monomers), lactide acid and glycolide acid, are not toxic and are removed by endogenous metabolic pathways such as the citric acid or cori cycle.[34] An interesting property of PLGA is its degradation kinetic, which is a function of the copolymer ratio. Higher glycolide content lowers the time required for its degradation.[35] A significant decrease in the release rate and enhanced entrapment efficiency of estradiol in PLGA NPs were observed with increase in lactide content and molecular weight.[36] However, an acidic microenvironment is generated during degradation that may negatively affect the stability of the loaded API.[37] Common PLGA copolymer ratios (lactide/glycolide molar ratio) are 50:50 and 75:25.[38] To overcome the limitation of hydrolytic stability of polylactides, PCL is often preferred for long-lasting DDSs. A drug release of up to 20 days was achieved with vinblastin loaded PCL-NPs.[39]

Therapeutic Applications

During the last decades, polymeric NPs were used to deliver small molecules, larger peptides and proteins, and expression plasmids.[40] For instance, the natural compound curcumin has chemotherapeutic activity in cancer but a poor bioavailability and suboptimal pharmacokinetic characteristics are limiting factors. However, the encapsulation into PLGA-NPs enhanced the therapeutic efficacy in-vitro compared to free curcumin.[41] The IC50 of curcumin-NPs was 9.1 μM in MDA-MB-231 cells compared to 16.4 μM for the free curcumin. In another study, coencapsulation of the anticancer drug vincristine and chemosensitizer verapamil into PLGA-NPs showed moderate reversion of multidrug resistance in breast cancer cells in vitro.[42] In an alternative approach, DOX combined with the thermal-optical agent indocyanine green (ICG) allows dual application of chemotherapy and hyperthermia for improved cytotoxicity. The DOX-ICG-PLGA-NPs resulted in enhanced cytotoxicity in Dx5 human uterine cancer cells in vitro.[43]

NPs have to be sterically protected in order to prolong their half-life in the circulation. Using PEG, a hydrophilic protective layer can be created to block and delay the opsonization process.[44] To further increase the therapeutic efficacy, targeted delivery of the NPs to specific cells is performed. A aptamer-funtionalized polymeric NP (BIND-014), which is a PEG-PLGA formulation of DTXL, currently completed a phase I clinical study (Fig. 4).[45] In another study, stealth PEG-PLGA-NPs were used as a delivery vehicle for cisplatin,[46] resulting in an 80 times increased toxicity of the cytotoxic agent. Another aptamer-funtionalized PEG-PLGA-NP containing PTX showed a significant decrease in tumor growth and an increase in survival in a glioma xenograft model compared to the

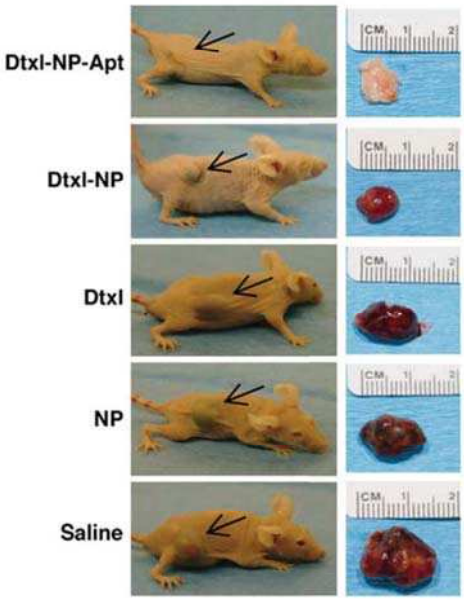

Fig. 4 Comparative prostate tumor regression study in a xenograft mouse model. The left panel shows mice of each treatment group. Black arrows indicate the position of the prostate cancer cell tumor. The right side indicates the tumor size at the endpoint. In the DTXL-NP-Apt group (i.e., mice treated with DTXL loaded PEG-NPs with prostate specific membrane antigen (PSMA) targeting aptamers) the tumor was completely regressed compared with the control treated mice, which received placebo (Saline), empty nanoparticles (NP), DTXL, or nontargeting DTXL-NPs.
Source: From Farokhzad et al.[45] © 2006, with permission from National Academy of Sciences.

unmodified counterparts.[47] Therapeutic proteins and peptides have very limited gastrointestinal bioavailability. They are sensitive to proteolytic enzymes and do not cross passively the biological barriers. NPs can be used to overcome issues associated with peptide and protein delivery. Oral administered insulin-Eudragit-PCL-NPs showed a 52% reduction in blood glucose level in diabetic rats. Their mucoadhesive properties were proposed to enhance gastrointestinal bioavailability.[48] In another study, erythropoietin loaded into oligochitosan NPs was investigated in rats for neuroprotection.[49,50]

Polymeric NPs also have a great potential for the application of nucleic acid gene delivery, because they can overcome the major drawbacks of their viral counterparts like immunogenicity and toxicity. Additionally, they offer the possibility of cheaper large-scale production. The natural polysaccharide chitosan and the noncationic polymer PLGA are the most commonly used nonviral gene vectors for siRNA and pDNA. The inhibition of tumor angiogenesis and growth by PLGA-NP-mediated p53 gene therapy in mice was evaluated recently.[51] In this study, xenografts of p53 mutant tumors were treated with a single intratumoral injection of p53-gene-loaded NPs. Greater levels of apoptosis, antiproliferative activity, decreased angiogenic activity, and finally improved survival indicate that PLGA has potential for sustained gene delivery. The effectiveness of gene silencing with siRNA loaded PLGA-NPs have been evaluated to overcome tumor drug resistance.[52] Silencing of the multidrug resistance protein 1 (MDR1) gene sensitized resistant tumor cells to chemotherapy, as demonstrated by increased PTX accumulation. In a recent study, RGD (Arg-Gly-Asp) peptide-labeled chitosan NPs loaded with siRNA were used for targeted silencing of multiple growth-promoting genes.[53] An inhibition of tumor growth (87% reduction, $P < 0.001$) in an $\alpha v\beta 3$-integrin tumor mouse model was shown with siRNA targeting plexin domain-containing protein 1 (PLXDC-1) that is upregulated in ovarian cancer vasculature. A promising approach for the treatment of NSCLC based on the inhibition of telomerase in cancer cells was carried out with chitosan-coated PLGA-NPs. These NPs with a mean size of 160 nm enhanced the delivery of the antisense oligonucleotide 2′-*O*-methyl-RNA to human lung cancer cells. Telomerase inhibition (80%) and telomere shortening (from 5.8 kb to 4 kb) in A549 indicated the potential for in-vivo applications. The cationic NPs showed no cytotoxicity and could be easily modified for active tumor-cell targeting.[54]

POLYMERSOMES

General Characteristics

Polymersomes are artificial vesicles made of synthetic amphiphilic block copolymers and form via a self-assembly process. Generally speaking, polymersomes are hollow spheres, containing an aqueous core that is surrounded by a bilayer membrane. This membrane is composed of a hydrophobic layer sandwiched between internal and external hydrophilic layer forming coronas.[55] Polymersomes were developed as DDS for the transport of either hydrophilic and/or hydrophobic molecules. Compared with liposomes that are lipid analogs, polymersomes have a thick and strong synthetic membrane, conferring a better physicochemical stability as well as lower elasticity and permeability.[2] Polymersomes can be prepared from various types of block copolymers such as nonbiodegradable polymers, degradable polymers, and biocompatible polymers.[56] Depending on the type of polymerization used for synthesis, di-block copolymers (AB), tri-block copolymers (ABA, BAB, or ABC), or even multiblock copolymers can be designed, allowing to tune different properties of the polymersomes.[2] Many factors influence the formation of polymersomes including hydrophilic/hydrophobic block lengths of the copolymer, solvent ratios, concentration of the polymer, and method of preparation. More importantly, volume ratio of hydrophilic to hydrophobic block copolymer fraction influences the formation of polymersomes.

It has been reported that hydrophilic to hydrophobic ratio of less than 1:2 highly favors the formation of polymersomes followed by the ratio of less than 1:3 and ratio more than 1:1 favor the micelle formation.[55] However, the hydrophilic to hydrophobic ratio is not the only determining parameter for polymersome formation.

Although several techniques have been employed to prepare polymersomes, solvent switch and film rehydration techniques are the commonly used methods. In solvent switch amphiphilic block copolymer is dissolved in a suitable organic solvent that is slowly exchanged by an aqueous solution either by adding water to organic polymer solution or vice versa. This technique makes the hydrophobic blocks insoluble, generating copolymer self-assembly into polymersomes as a result of increasing interfacial tension between the hydrophobic blocks and water. In film rehydration, amphiphilic copolymers are dissolved in an organic solvent that is removed by evaporation to form a thin film. An aqueous solution is used to rehydrate the film. Upon mixing, the aqueous phase permeates through defects in the film layers that inflate and finally form vesicles upon separation from the surface.[55,57] Different mechanisms have been reported and proposed for the formation of polymersomes.[58,59] Conventionally, copolymers form a bilayer and close-up to form a vesicular structure. In another mechanism, spherical micelles are formed and then changed into rods, which become flattened and form paddle shape structures. Then these structures transform to circular lamellae that finally close-up to form polymersomes.[60]

Formulation Characteristics

High loading efficiency is a prerequisite for polymersome-based formulation in drug delivery. Loading efficiency can be dependent on preparation method, formation mechanism, and molecular composition of the copolymers. In one study, PEO-poly(benzyl-L-aspartate) (PEO-PBLA) and PEO-poly(2,4,6-trimethoxybenzylidene pentaerythritol carbonate) (PEO-PTMBPEC) based polymersomes were loaded with DOX and showed loading efficiencies of 12% and 8%, respectively.[61] Loading efficiency can be improved using poly(trimethylene carbonate) if the pH of the loading solution is raised to a pH above the pK_a of DOX during the loading process.[62] Using direct dissolution of PEG-polypropylene sulfide (PPS) copolymers, polymersomes achieved higher encapsulation efficiencies for larger protein molecules such as ovalbumin (37%), bovine serum albumin (19%), and bovine gamma-globulin (15%). This method requires a short time for encapsulation, is solvent-free, and simple as compared to methods used for loading of liposomes and other polymersomes.[63] It should be noted that the hollow core of the polymersomes encapsulate the surrounding environment during the self-assembly. Therefore, encapsulation efficiency can also be dependent on the formation mechanism of the polymersomes.

Polymersomes usually exhibit higher stability than polymeric micelles and liposomes due to their thicker membrane. For example, polymersomes made of poly(γ-benzyl L-glutamate)-hyaluronan (PBLG-HYA) loaded with DTXL have shown excellent colloidal stability both at room temperature and at 4°C for one month. More than 90% of DTXL was recovered after storage of DTXL-loaded polymersomes and can be readily lyophilized without alternation in loading content of DTXL for a period of six months storage at 4°C. However, redispersion of lyophilized polymersomes needed a sonication step to accelerate the dispersion time and eliminate the few aggregates still present in solution.[64]

Polymersomes release the loaded drugs through various mechanisms. Furthermore, recently third generation smart systems were designed, where release of drugs from polymersomes can be controlled with external environmental stimuli such as UV light, temperature, and oxidation-reduction.[65] The widely used mechanism for release is degradation of hydrophobic blocks of the polymersomes mediated by simple hydrolysis. This type of degradation is accelerated at acidic pH as found within the endolysosomal compartments of cells.[65] Another possible release mechanism involves the diffusion based permeation of the loaded drug through the polymersome membrane. PEO-PCL polymersomes loaded with DOX showed immediate burst release of 20% of DOX (from 0 hr to 8 hr) by diffusion, followed by a sustained release (up to 14 days) facilitated by pH-driven hydrolysis of the polymersome membrane.[66] The advantages of using stimuli-responsive polymersomes for DDSs have been reviewed extensively elsewhere.[67]

Therapeutic Applications

Polymersomes can readily accommodate a number of drug molecules in the aqueous compartment as well as in their hydrophobic membrane. For instance, to overcome the limitations of DTXL such as low solubility and side effects, this chemotherapeutic drug was incorporated in PBLG-HYA polymersomes. New Zealand rabbits received an IV injection of either polymersome-encapsulated DTXL or free drug. Comparing the plasma profiles, the DTXL-loaded PBLG-HYA polymersomes exhibited a higher maximal concentration (17.97 μg/mL) than the DTXL solution (11.72 μg/mL). The polymersome formulation significantly improved half-life and AUC of DTXL ($t_{1/2}$ = 19.90 hr and AUC = 209.32 μg/mL) compared to the DTXL solution ($t_{1/2}$ = 4.79 hr and AUC = 60.6 μg/mL). Hemolysis tests were performed on human blood and about 30% red blood cell hemolysis (DTXL side-effect) was observed with DTXL solution while less than 5% hemolysis occurred with DTXL-loaded PBLG-HYA polymersomes. Biodistribution studies showed an accumulation of the polymersome formulation at the tumor site in BalB/c mice, and a significantly higher uptake by tumor cells with the polymersomes than with the free drug.[64]

In another series of experiments, biodegradable polymersomes based on PEO-PLA block copolymers were prepared. A hydrophobic drug (PTX) was incorporated into the vesicle membrane. Alternatively, a hydrophilic drug (DOX) was encapsulated within the vesicle core. DOX-PTX loaded into polymersomes showed higher maximum tolerated doses (MDT) of 3 mg/kg for DOX and 7.5 mg/kg for PTX, which is increased by the factor of two compared to free DOX and PTX. In-vitro studies in MDA-MB231 human breast cancer cells with DOX-PTX polymersomes showed a potent antitumor activity without any other toxic side-effects. Polymersomes loaded with DOX-PTX showed 16-fold increased toxicity in tumor cells as compared to both free drugs, leading to a high tumor apoptosis and ultimately increased therapeutic efficacy (Fig. 5).[68]

Therapeutic applications of proteins are challenging due to poor tissue distribution, rapid elimination by renal clearance, and enzymatic degradation. Polymersomes may be promising candidate for delivering a wide range of proteins without affecting their functionality. Polymersomes formed by film rehydration are able to incorporate transmembrane proteins in the bilayer as well as encapsulate proteins in the aqueous core without loss of their functional conformation.[65,69]

Recently, polymersomes were utilized to encapsulate DNA for delivering into cells. Biomimetic, pH-sensitive polymersomes were prepared using poly[2-(methacryloyloxy) ethyl-phosphorylcholine]-*co*-poly[2-(diisopropylamino) ethyl methcrylate] (PMPC-PDPA) diblock copolymers.[70] Under mild acidic condition, pDNA formed a complex with PMPC-PDPA copolymer by electrostatic interaction and the pDNA was encapsulated into the polymersomes at pH 7.5.[70] The pDNA-encapsulated polymersomes used the endocytic pathway to enter the cells and the pDNA escaped to the cytosol due to low pH in the endosomal environment. Experiments with DNA-encapsulated polymersomes clearly showed that the pH-dependent release of plasmid and the transfection efficiency was comparable with the commercially available transfection agent Lipofectamine® (Fig. 6).[70] In addition, the polymeric vesicles exhibited less toxicity and no proinflammatory response with less leakage. The biomimetic surface reduces nonspecific interactions with blood plasma proteins and thereby increases the half-life in the circulation of the polymersomes.[70] In another approach, polymersomes forming diblock copolymer poly(oligoethylene glycol methacrylate)–poly(2-(diisopropylamino)ethyl methacrylate) (POEGMA–PDPA) were used to incorporate pDNA into multicompartment capsules via a LbL technique. By this method, very high loading (60% efficiency) was achieved due to cationic amine groups on the PDPA block, which are protonated at low pH.[71] In another experiment, siRNA was encapsulated into PEO-b-PLA and antisense oligonucleotides (AON) were encapsulated into PEG-b-PCL by a co-solvent method. Loaded oligos were released and escaped from the endosomes by hydrolytic degradation of the polymersomes.[72] In gene silencing experiments, siRNA-(PEO-b-PLA) based polymersomes showed a knockdown efficiency of 40% and

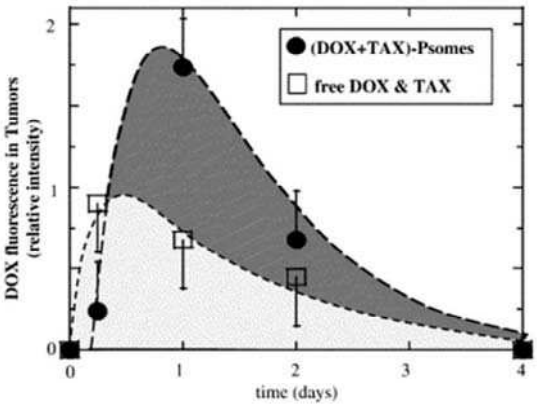

Fig. 5 Tissue accumulation profile of DOX loaded polymersomes in breast cancer tumors. Fluorescence intensity analysis of DOX reveals that accumulation of polymersomes in tumors regions was higher (dark grey) compared to the free drugs (DOX & PTX). Maximal release and tumor tissue accumulation of DOX + PTX loaded polymersomes occur within one day.
Source: From Ahmed et al.[68] © 2006, with permission from Elsevier.

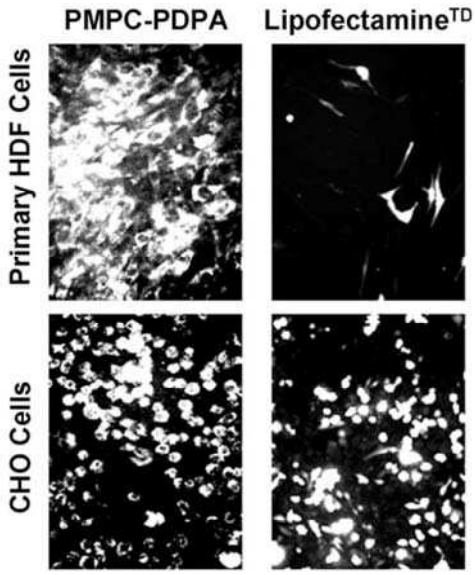

Fig. 6 Delivery of pDNA using pH-dependent polymersomes made of PMPC-PDPA. Polymersomes showed the efficient expression of green fluorescent protein in primary HDF cells and CHO cells and compared with the commercially available LipofectamineTD.
Source: From Lomas et al.[70] © 2007, with permission from WILEY-VCH.

the result was similar to that of Lipofectamine 2000. AON polymeric vesicles were successfully delivered in-vivo to dystrophin-deficient mice with delivery efficiency above 50% and significantly expressed the dystrophin.[72] It was also reported that PMPC-PDPA polymersomes loaded with enhanced green fluorescent protein (EGFP) siRNA showed significant decrease in the EGFP production in cells. After 48 hr, a 70% EGFP expression silencing was observed without affecting the proliferation of the cells.[73]

LAYER-BY-LAYER CAPSULES

General Characteristics

LbL capsules are polymeric multilayer capsules (PMLC) prepared by alternate adsorption of polymers onto a template via complementary interactions such as electrostatic interactions, hydrogen bonding, and covalent linkage.[74–77] In brief, the colloidal template is immersed into an aqueous solution of polymers to build the first surrounding layer. Subsequently, the excess polymer is removed and a second layer of an interacting polymer is absorbed.[78] These two steps are repeated alternately, resulting in a core–shell particle. By altering the number of layer depositions, the film thickness can be easily regulated. The template is finally dissolved to form a multilayered hollow capsule.[79] Dissolution of organic templates like polystyrene or melamine formaldehyde requires strong acids or organic solvents that can hamper the applicability for therapeutics and particularly biomolecules. Moreover, organic solvents can influence the carrier stability by destroying the capsule shell.[80] To overcome these problems, inorganic templates like silica (0.5–5 μm), calcium carbonate (3–5 μm), manganese carbonate, or metal particles are preferred. Inorganic templates are easily dissolved under mild conditions that do not affect the encapsulated drug.[81,82] The initial template strongly influences size distribution and shape of the PMLC.

The constituents of the capsule shell can tailor the chemical and mechanical properties of the PMLCs. For polyelectrolyte capsules, a large variety of charged compounds like synthetic polymers, polypeptides, polysaccharides, nucleic acids, or NPs are used.[83–85] The negative charge of the polyanions is often achieved by sulfonate or carbonate groups whereas polycations mostly have amino or imino groups.[86] Thus, the selected buffer for the synthesis should maintain a high degree of ionization. Phosphate-buffered saline at pH 7.4 offers the maintenance of the charge as well as the physiological condition for many biotherapeutics. Well-studied polyanion/polycation systems for multilayer assembly are polystyrene sulfonate (PSS)/poly allylamine (PAH), PSS/chitosan, heparin/albumin, heparin/poly(ethylene imine) (PEI), dextran sulfate (DS)/chitosan, DS/poly (L-arginine), DS/PEI, and alginate/PLL. To avoid cytotoxic effects of some polycations, hydrogen bonding offers an alternative interaction for LbL assembly. PEI and PLL showed mitochondrial-mediated cell death in a range of human cell lines in-vitro.[87–89] Therefore, poly(*N*-vinylpyrrolidone (PVPON) as hydrogen-bond acceptor and PMA as hydrogen-bond donor have been successfully used. At the end of the production process, it is necessary to cross-link the capsule shell to prevent its destruction at physiological pH and to entrap the drug inside the NP cavity. Carbodiimide chemistry and thiol oxidation are commonly used methods for cross-linking.[90,91]

Formulation Characteristics

Drugs are encapsulated into the carrier mainly by two procedures: (i) postloading or (ii) preloading (Fig. 7). Capsules can be prepared without a compound and the capsule shell can be permeabilized for a postloading process.[93] The capsule wall can be opened by changing pH, ionic strength, solvent polarity, or temperature to allow the diffusion of therapeutics into the capsule interior.[94–97] Returning to the original medium conditions can entrap the drugs inside the capsules. For example, the permeability of biodegradable dextran/chitosan capsules for protein encapsulation can be regulated by variations in pH. At pH values >8, electrostatic repulsion of the polymers leads to an opening of the capsule wall. However, in acidic conditions, the membrane tightens and drugs of interest are entrapped inside the micron-sized hollow capsules.[98] In general, the encapsulation efficiency of the postloading procedure is low. Additionally, the conditions for inducing pores may not be suitable for many biomolecules. An improved variation of this technique is the preloading of the capsule with a sequestering agent, which has a high affinity to the drug. Therefore, the loading process during the diffusion can be increased. Examples include the use of dextran sulfate to increase the encapsulation of DOX.[99]

In contrast to the postloading procedure, porous inorganic templates like mesoporous silica particles offer the possibility of drug preloading due to their large surface area. The polymeric layers adsorb onto the preloaded template.[100,101] Drug crystals as initial template have attracted attention owing to their high encapsulation efficiency.[102–106] For instance, proteins can be directly encapsulated by LbL assembly onto protein crystals.[107] Moreover, other techniques are reported for the drug incorporation. Hydrophobic association is an encapsulation strategy, which was successfully used for natural polyphenols. The anticancer compounds were incorporated into gelatin-based 200 nm NPs surrounded by a 5–20 nm thick LbL shell of polyelectrolytes. The polyphenol loading varied from 20% to 70%.[108] Apart from single drug delivery, polymeric capsules offer the possibility to formulate a DDS, which can release two or more incorporated drugs gradually from a single carrier.[109] Encapsulation of two proteins in separate positions of the capsule showed a time-modulated release. One protein was

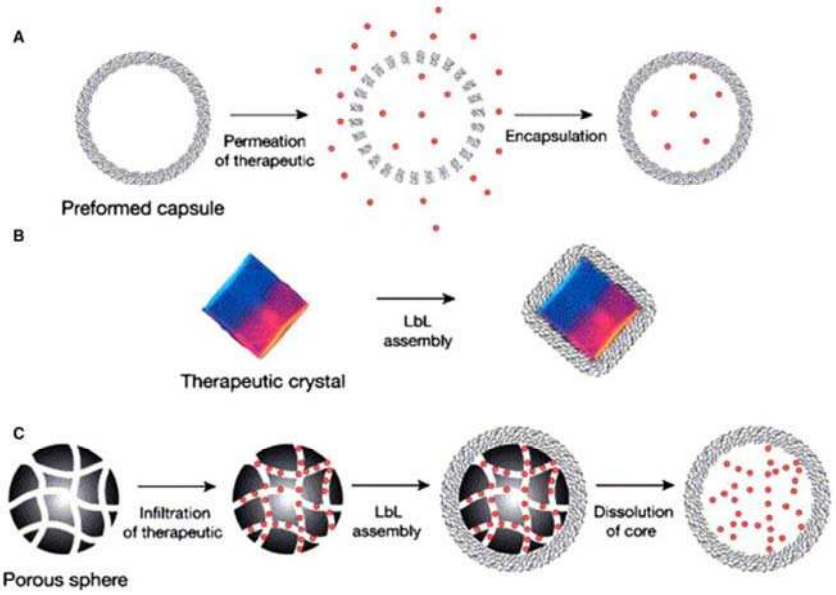

Fig. 7 Different encapsulation methods for loading drugs into LbL capsules: (**A**) postloading procedure of a preformed capsule, (**B**) encapsulation of drug crystals, and (**C**) preloading of porous templates. Gray dots represent loaded drug.
Source: From Johnston et al.[92] © 2006, with permission from Elsevier.

incorporated inside the cavity and the second one between the layers of the shell.[110]

Therapeutic Applications

A versatile spectrum of therapeutics can be incorporated into LbL capsules. Recently, the effect of anticancer drug-loaded capsules has been investigated. Gold NPs coated with a PAH/PSS multilayer were modified with *N*-(2-hydroxypropyl)methacrylamide (HPMA) and a pro-drug of DOX was linked onto the surface.[111] Specific cleavage of the peptide linker by cathepsin B could release DOX from the stealth core-shell-particle after endocytosis in-vitro. Another successfully used encapsulation strategy for DOX is emulsion templating.[112] DOX/oleic acid–loaded PMA capsules (500 nm) demonstrated an enhanced toxicity in a human colorectal cancer cell line in vitro as compared to the free drug. A further improvement of LbL capsules is the smart system that releases the payload by environmental stimuli.[113] Different formulation techniques and polymer combinations can trigger drug release depending on pH or reducing conditions. Redox-responsive capsules demonstrated a novel release method for DOX PMLCs. The disulfide cross-linked shell was stabilized in an oxidizing environment but disrupted under reducing conditions releasing an anticancer drug into the cytoplasm. By this technique, the cytotoxicity of the drug was increased 5000 times compared with the free drug.[114] In a pH-triggered release study LbL-containing quantum dots with a pH-responsible layer were passively navigated to hypoxic regions of solid tumors in vivo and showed a pH-triggered response.[115] PEG was linked to the PLL layer using an iminobiotin-neutravidin interaction, which can be destablized at low pH.[116]

Macromolecules like proteins can also be loaded into PMLCs. Biodegradable multilayered capsules loaded with the cytokine bFGF prolonged the proliferation of L929 fibroblast cells due to sustained release.[98] In general, the LbL technique used for proteins results in micrometer-sized particles. This size is big compared to other nanoparticulate technologies and therefore not suitable for intravenous application.[117] The delivery of nucleic acids like pDNA and siRNA with multilayered capsules is a promising research area. The first successful gene transfection using functional DNA-loaded PMLCs was demonstrated with silica-assisted LbL assembly of dextran and protamine.[118] Recently, single-polyelectrolyte capsules were investigated for the transfection of melanoma cells with pDNA in vitro.[119] Cross-linked PLL particles were co-loaded with pDNA of a nuclear transcription factor and alpha-melanocyte-stimulating hormone as a reporter hormone. The gene expression was significantly increased (70%). In another study, RNA interference was studied by incorporating siRNA into PEI layers on gold NPs.[120] The production of EGFP in CHO-K1 cells was knocked down to about 28%. The versatility and modularity of LbL assembly can be used to introduce multiple functionalities. Drug encapsulation, triggered release, active targeting, and imaging could be achieved with one

single carrier.[121] Furthermore, polymer capsules containing liposomal subcompartments, so-called capsosomes, can co-encapsulate different drugs and trigger the release by encapsulated enzymatic catalysis.[122,123] Nevertheless, the production of capsules <1 μm without aggregation is quite challenging and would be not acceptable for various applications.[124] Further improvements are necessary to produce capsules less than 200 nm in diameter, which is a common size used in DDSs.

CONCLUSION

Over the last two decades, considerable efforts were paid to the development of self-assembling and template-directed copolymer-based nanostructures. These new and innovative nanomaterials can be used for different types of therapeutic drug delivery applications. Polymeric nanomaterial-based DDSs including micelles, NPs, polymersomes and LbL capsules have been extensively studied. Mechanistic studies of the self-assembly process of different types of copolymers have demonstrated the possibility to modulate the physicochemical properties and morphology of resultant nanostructures. Numerous strategies have been explored to improve drug loading, to control drug release, and to improve the stability of nanocarriers in biological systems. Advanced technologies include the design of polymeric nanomaterials with the possibility to introduce multifunctionalities, responsiveness to environmental stimuli, active targeting, biocompatible, and biodegradable properties. Although numerous studies have been reported using polymeric nanomaterials, the clinical realization of drug targeting strategies remains a challenge.

ACKNOWLEDGMENTS

Financial support of the Swiss Centre of Applied Human Toxicology (SCAHT) and the "Freie Akademische Gesellschaft Basel (FAG)" is acknowledged. We thank Annette Roulier for graphical assistance with the figures.

REFERENCES

1. Letchford, K.; Burt, H. A review of the formation and classification of amphiphilic block copolymer nanoparticulate structures: Micelles, nanospheres, nanocapsules and polymersomes. Eur. J. Pharm. Biopharm. **2007**, *65* (3), 259–269.
2. Blanazs, A.; Armes, S.P.; Ryan, A.J. Self-assembled block copolymer aggregates: From micelles to vesicles and their biological applications. Macromol. Rapid Commun. **2009**, *30* (4–5), 267–277.
3. Holder, S.J.; Sommerdijk, N.A.J.M. New micellar morphologies from amphiphilic block copolymers: Disks, toroids and bicontinuous micelles. Polym. Chem. **2011**, *2* (5), 1018–1028.
4. Kulthe, S.S.; Choudhari, Y.M.; Inamdar, N.N.; Mourya, V. Polymeric micelles: Authoritative aspects for drug delivery. Des. Monomers Polym. **2012**, *15* (5), 465–521.
5. Huh, K.M.; Lee, S.C.; Cho, Y.W.; Lee, J.; Jeong, J.H.; Park, K. Hydrotropic polymer micelle system for delivery of paclitaxel. J Control. Release **2005**, *101* (1–3), 59–68.
6. Kim, J.Y.; Kim, S.; Pinal, R.; Park, K. Hydrotropic polymer micelles as versatile vehicles for delivery of poorly water-soluble drugs. J. Control. Release **2011**, *152* (1), 13–20.
7. Shin, H.-C.; Alani, A.W.; Rao, D.A.; Rockich, N.C.; Kwon, G.S. Multi-drug loaded polymeric micelles for simultaneous delivery of poorly soluble anticancer drugs. J. Control. Release **2009**, *140* (3), 294–300.
8. Bronich, T.K.; Keifer, P.A.; Shlyakhtenko, L.S.; Kabanov, A.V. Polymer micelle with cross-linked ionic core. J. Am. Chem. Soc. **2005**, *127* (23), 8236–8237.
9. Aliabadi, H.M.; Lavasanifar, A. Polymeric micelles for drug delivery. Expert Opin. Drug Deliv. **2006**, *3* (1), 139–162.
10. Kim, S.; Shi, Y.; Kim, J.Y.; Park, K.; Cheng, J.X. Overcoming the barriers in micellar drug delivery: Loading efficiency, in vivo stability, and micelle-cell interaction. Expert Opin collaborators have studied Drug Deliv. **2010**, *7* (1), 49–62.
11. Batrakova, E.V.; Kabanov, A.V. Pluronic block copolymers: Evolution of drug delivery concept from inert nanocarriers to biological response modifiers. J. Control. Release **2008**, *130* (2), 98–106.
12. Leung, S.Y.L.; Jackson, J.; Miyake, H.; Burt, H.; Gleave, M.E. Polymeric micellar paclitaxel phosphorylates Bcl-2 and induces apoptotic regression of androgen-independent LNCaP prostate tumors. Prostate **2000**, *44* (2), 156–163.
13. Hamaguchi, T.; Matsumura, Y.; Suzuki, M.; Shimizu, K.; Goda, R.; Nakamura, I.; Nakatomi, I.; Yokoyama, M.; Kataoka, K.; Kakizoe, T. NK105, a paclitaxel-incorporating micellar nanoparticle formulation, can extend in vivo antitumour activity and reduce the neurotoxicity of paclitaxel. Br. J. Cancer **2005**, *92* (7), 1240–1246.
14. Shi, Y.; Huang, W.; Liang, R.; Sun, K.; Zhang, F.; Liu, W.; Li, Y. Improvement of in vivo efficacy of recombinant human erythropoietin by encapsulation in PEG-PLA micelle. Int. J. Nanomed. **2013**, *8* (1), 1–11.
15. Gao, G.H.; Park, M.J.; Li, Y.; Im, G.H.; Kim, J.H.; Kim, H.N.; Lee, J.W.; Jeon, P.; Bang, O.Y.; Lee, J.H.; Lee, D.S. The use of pH-sensitive positively charged polymeric micelles for protein delivery. Biomaterials **2012**, *33* (35), 9157–9164.
16. Nishiyama, N.; Jang, W.D.; Date, K.; Miyata, K.; Kataoka, K. Photochemical enhancement of transgene expression by polymeric micelles incorporating plasmid DNA and dendrimer-based photosensitizer. J. Drug Target. **2006**, *14* (6), 413–424.
17. Wang, L.; Chierico, L.; Little, D.; Patikarnmonthon, N.; Yang, Z.; Azzouz, M.; Madsen, J.; Armes, S.P.; Battaglia, G. Encapsulation of biomacromolecules within polymersomes by electroporation. Angew. Chem. Int. Ed. **2012**, *51* (44), 11122–11125.
18. Kreuter, J. Nanoparticles—a historical perspective. Int. J. Pharm. **2007**, *331* (1), 1–10.

19. Kumari, A.; Yadav, S.K.; Yadav, S.C. Biodegradable polymeric nanoparticles based drug delivery systems. Colloids Surf. B Biointerfaces **2010**, *75* (1), 1–18.
20. Singh, R.; Lillard, J.W., Jr. Nanoparticle-based targeted drug delivery. Exp. Mol. Pathol. **2009**, *86* (3), 215–223.
21. Soppimath, K.S.; Aminabhavi, T.M.; Kulkarni, A.R.; Rudzinski, W.E. Biodegradable polymeric nanoparticles as drug delivery devices. J. Control. Release **2001**, *70* (1–2), 1–20.
22. Brigger, I.; Dubernet, C.; Couvreur, P. Nanoparticles in cancer therapy and diagnosis. Adv. Drug Deliv. Rev. **2002**, *54* (5), 631–651.
23. Mora-Huertas, C.E.; Fessi, H.; Elaissari, A. Polymer-based nanocapsules for drug delivery. Int. J. Pharm. **2010**, *385* (1–2), 113–142.
24. Kratz, F. Albumin as a drug carrier: Design of prodrugs, drug conjugates and nanoparticles. J. Control. Release **2008**, *132* (3), 171–183.
25. Kratz, F.; Elsadek, B. Clinical impact of serum proteins on drug delivery. J. Control. Release **2012**, *161* (2), 429–445.
26. Uchegbu, I.F.; Siew, A. Nanomedicines and nanodiagnostics come of age. J. Pharm. Sci. **2013**, *102* (2), 305–310.
27. Takeuchi, H.; Yamamoto, H.; Kawashima, Y. Mucoadhesive nanoparticulate systems for peptide drug delivery. Adv. Drug Deliv. Rev. **2001**, *47* (1), 39–54.
28. Thanou, M.; Verhoef, J.C.; Junginger, H.E. Oral drug absorption enhancement by chitosan and its derivatives. Adv. Drug Deliv. Rev. **2001**, *52* (2), 117–126.
29. Khatri, K.; Goyal, A.K.; Gupta, P.N.; Mishra, N.; Vyas, S.P. Plasmid DNA Loaded chitosan nanoparticles for nasal mucosal immunization against hepatitis B. Int. J. Pharm. **2008**, *354* (1–2), 235–241.
30. Amidi, M.; Mastrobattista, E.; Jiskoot, W.; Hennink, W.E. Chitosan-based delivery systems for protein therapeutics and antigens. Adv. Drug Deliv. Rev. **2010**, *62* (1), 59–82.
31. Slutter, B.; Bal, S.; Keijzer, C.; Mallants, R.; Hagenaars, N.; Que, I.; Kaijzel, E.; van Eden, W.; Augustijns, P.; Löwik, C.; Bouwstra, J.; Broere, F.; Jiskoot, W. Nasal vaccination with *N*-trimethyl chitosan and PLGA based nanoparticles: Nanoparticle characteristics determine quality and strength of the antibody response in mice against the encapsulated antigen. Vaccine **2010**, *28* (38), 6282–6291.
32. Chawla, J.S.; Amiji, M.M. Biodegradable poly(ε-caprolactone) nanoparticles for tumor-targeted delivery of tamoxifen. Int. J. Pharm. **2002**, *249* (1–2), 127–138.
33. Irache, J.M.; Esparza, I.; Gamazo, C.; Agüeros, M.; Espuelas, S. Nanomedicine: Novel approaches in human and veterinary therapeutics. Vet. Parasitol. **2011**, *180* (1–2), 47–71.
34. Athanasiou, K.A.; Niederauer, G.G.; Agrawal, C.M. Sterilization, toxicity, biocompatibility and clinical applications of polylactic acid/polyglycolic acid copolymers. Biomaterials **1996**, *17* (2), 93–102.
35. Shive, M.S.; Anderson, J.M. Biodegradation and biocompatibility of PLA and PLGA microspheres. Adv. Drug Deliv. Rev. **1997**, *28* (1), 5–24.
36. Mittal, G.; Sahana, D.K.; Bhardwaj, V.; Ravi Kumar, M.N. Estradiol loaded PLGA nanoparticles for oral administration: Effect of polymer molecular weight and copolymer composition on release behavior in vitro and in vivo. J. Control. Release **2007**, *119* (1), 77–85.
37. Estey, T.; Kang, J.; Schwendeman, S.P.; Carpenter, J.F. BSA degradation under acidic conditions: A model for protein instability during release from PLGA delivery systems. J. Pharm. Sci. **2006**, *95* (7), 1626–1639.
38. Astete, C.E.; Sabliov, C.M. Synthesis and characterization of PLGA nanoparticles. J. Biomater. Sci. Polym. Ed. **2006**, *17* (3), 247–289.
39. Prabu, P.; Chaudhari, A.A.; Dharmaraj, N.; Khil, M.S.; Park, S.Y.; Kim, H.Y. Preparation, characterization, in-vitro drug release and cellular uptake of poly(caprolactone) grafted dextran copolymeric nanoparticles loaded with anticancer drug. J. Biomed. Mater. Res. A **2009**, *90A* (4), 1128–1136.
40. Couvreur, P.; Vauthier, C. Nanotechnology: Intelligent design to treat complex disease. Pharm. Res. **2006**, *23* (7), 1417–1450.
41. Yallapu, M.M.; Gupta, B.K.; Jaggi, M.; Chauhan, S.C. Fabrication of curcumin encapsulated PLGA nanoparticles for improved therapeutic effects in metastatic cancer cells. J. Colloid. Interface Sci. **2010**, *351* (1), 19–29.
42. Song, X.R.; Cai, Z.; Zheng, Y.; He, G.; Cui, F.Y.; Gong, D.Q.; Hou, S.X.; Xiong, S.J.; Lei, X.J.; Wei, Y.Q. Reversion of multidrug resistance by co-encapsulation of vincristine and verapamil in PLGA nanoparticles. Eur. J. Pharm. Sci. **2009**, *37* (3–4), 300–305.
43. Tang, Y.; Lei, T.; Manchanda, R.; Nagesetti, A.; Fernandez-Fernandez, A.; Srinivasan, S.; McGoron, A.J. Simultaneous delivery of chemotherapeutic and thermal-optical agents to cancer cells by a polymeric (PLGA) nanocarrier: An in vitro study. Pharm. Res. **2010**, *27* (10), 2242–2253.
44. Owens, D.E.; Peppas, N.A. Opsonization, biodistribution, and pharmacokinetics of polymeric nanoparticles. Int. J. Pharm. **2006**, *307* (1), 93–102.
45. Farokhzad, O.C.; Cheng, J.; Teply, B.A.; Sherifi, I.; Jon, S.; Kantoff, P.W.; Richie, J.P.; Langer, R. Targeted nanoparticle-aptamer bioconjugates for cancer chemotherapy in vivo. Proc. Natl. Acad. Sci. U.S.A. **2006**, *103* (16), 6315–6320.
46. Dhar, S.; Gu, F.X.; Langer, R.; Farokhzad, O.C.; Lippard, S.J. Targeted delivery of cisplatin to prostate cancer cells by aptamer functionalized Pt(IV) prodrug-PLGA-PEG nanoparticles. Proc. Natl. Acad. Sci. U.S.A. **2008**, *105* (45), 17356–17361.
47. Guo, J.; Gao, X.; Su, L.; Xia, H.; Gu, G.; Pang, Z.; Jiang, X.; Yao, L.; Chen, J.; Chen, H. Aptamer-functionalized PEG-PLGA nanoparticles for enhanced anti-glioma drug delivery. Biomaterials **2011**, *32* (31), 8010–8020.
48. Damge, C.; Socha, M.; Ubrich, N.; Maincent, P. Poly(epsilon-caprolactone)/eudragit nanoparticles for oral delivery of aspart-insulin in the treatment of diabetes. J. Pharm. Sci. **2010**, *99* (2), 879–889.
49. Wang, T.; Hu, Y.; Leach, M.K.; Zhang, L.; Yang, W.; Jiang, L.; Feng, Z.Q.; He, N. Erythropoietin-loaded oligochitosan nanoparticles for treatment of periventricular leukomalacia. Int. J. Pharm. **2012**, *422* (1–2), 462–471.
50. Liu, W.; Shen, Y.; Plane, J.M.; Pleasure, D.E.; Deng, W. Neuroprotective potential of erythropoietin and its derivative carbamylated erythropoietin in periventricular leukomalacia. Exp. Neurol. **2011**, *230* (2), 227–239.

51. Prabha, S.; Sharma, B.; Labhasetwar, V. Inhibition of tumor angiogenesis and growth by nanoparticle-mediated p53 gene therapy in mice. Cancer Gene Ther. **2012**, *19* (8), 530–537.
52. Patil, Y.B.; Swaminathan, S.K.; Sadhukha, T.; Ma, L.; Panyam, J. The use of nanoparticle-mediated targeted gene silencing and drug delivery to overcome tumor drug resistance. Biomaterials **2010**, *31* (2), 358–365.
53. Han, H.D.; Mangala, L.S.; Lee, J.W.; Shahzad, M.M.; Kim, H.S.; Shen, D.; Nam, E.J.; Mora, E.M.; Stone, R.L.; Lu, C.; Lee, S.J.; Roh, J.W.; Nick, A.M.; Lopez-Berestein, G.; Sood, A.K. Targeted gene silencing using RGD-labeled chitosan nanoparticles. Clin. Cancer Res. **2010**, *16* (15), 3910–3922.
54. Beisner, J.; Dong, M.; Taetz, S.; Nafee, N.; Griese, E.U.; Schaefer, U.; Lehr, C.M.; Klotz, U.; Mürdter, T.E. Nanoparticle mediated delivery of 2'-O-methyl-RNA leads to efficient telomerase inhibition and telomere shortening in human lung cancer cells. Lung Cancer **2010**, *68* (3), 346–354.
55. Lee, J.S.; Feijen, J. Polymersomes for drug delivery: Design, formation and characterization. J. Control. Release **2012**, *161* (2), 473–483.
56. Jain, J.P.; Ayen, W.Y.; Kumar, N. Self assembling polymers as polymersomes for drug delivery. Curr. Pharm. Des. **2011**, *17* (1), 65–79.
57. Howse, J.R.; Jones, R.A.; Battaglia, G.; Ducker, R.E.; Leggett, G.J.; Ryan, A.J. Templated formation of giant polymer vesicles with controlled size distributions. Nat. Mater. **2009**, *8* (6), 507–511.
58. Uneyama, T. Density functional simulation of spontaneous formation of vesicle in block copolymer solutions. J. Chem. Phys. **2007**, *126* (11), 114902.
59. He, X.; Schmid, F. Dynamics of spontaneous vesicle formation in dilute solutions of amphiphilic diblock copolymers. Macromolecules **2006**, *39* (7), 2654–2662.
60. Chen, L.; Shen, H.; Eisenberg, A. Kinetics and mechanism of the rod-to-vesicle transition of block copolymer aggregates in dilute solution. J. Phys. Chem. B **1999**, *103* (44), 9488–9497.
61. Kataoka, K.; Matsumoto, T.; Yokoyama, M.; Okano, T.; Sakurai, Y.; Fukushima, S.; Okamoto, K.; Kwon, G.S. Doxorubicin-loaded poly(ethylene glycol)–poly(β-benzyl-l-aspartate) copolymer micelles: Their pharmaceutical characteristics and biological significance. J. Control. Release **2000**, *64* (1–3), 143–153.
62. Sanson, C.; Schatz, C.; Le Meins, J.F.; Soum, A.; Thévenot, J.; Garanger, E.; Lecommandoux, S. A simple method to achieve high doxorubicin loading in biodegradable polymersomes. J. Control. Release **2010**, *147* (3), 428–435.
63. O'Neil, C.P.; Suzuki, T.; Demurtas, D.; Finka, A.; Hubbell, J.A. A novel method for the encapsulation of biomolecules into polymersomes via direct hydration. Langmuir **2009**, *25* (16), 9025–9029.
64. Upadhyay, K.K.; Bhatt, A.N.; Castro, E.; Mishra, A.K.; Chuttani, K.; Dwarakanath, B.S.; Schatz, C.; Le Meins, J.F.; Misra, A.; Lecommandoux, S. In vitro and in vivo evaluation of docetaxel loaded biodegradable polymersomes. Macromol. Biosci. **2010**, *10* (5), 503–512.
65. Christian, D.A.; Cai, S.; Bowen, D.M.; Kim, Y.; Pajerowski, J.D.; Discher, D.E. Polymersome carriers: From self-assembly to siRNA and protein therapeutics. Eur. J. Pharm. Biopharm. **2009**, *71* (3), 463–474.
66. Ghoroghchian, P.P.; Li, G.; Levine, D.H.; Davis, K.P.; Bates, F.S.; Hammer, D.A.; Therien, M.J. Bioresorbable vesicles formed through spontaneous self-assembly of amphiphilic poly(ethylene oxide)-block-polycaprolactone. Macromolecules **2006**, *39* (5), 1673–1675.
67. Onaca, O.; Enea, R.; Hughes, D.W.; Meier, W. Stimuli-responsive polymersomes as nanocarriers for drug and gene delivery. Macromol. Biosci. **2009**, *9* (2), 129–139.
68. Ahmed, F.; Pakunlu, R.I.; Brannan, A.; Bates, F.; Minko, T.; Discher, D.E. Biodegradable polymersomes loaded with both paclitaxel and doxorubicin permeate and shrink tumors, inducing apoptosis in proportion to accumulated drug. J. Control. Release **2006**, *116* (2), 150–158.
69. Tanner, P.; Baumann, P.; Enea, R.; Onaca, O.; Palivan, C.; Meier, W. Polymeric vesicles: From drug carriers to nanoreactors and artificial organelles. Acc. Chem. Res. **2011**, *44* (10), 1039–1049.
70. Lomas, H.; Canton, I.; MacNeil, S.; Du, J.; Armes, S.P.; Ryan, A.J.; Lewis, A.L.; Battaglia, G. Biomimetic pH sensitive polymersomes for efficient DNA encapsulation and delivery. Adv. Mater. **2007**, *19* (23), 4238–4243.
71. Lomas, H.; Johnston, A.P.; Such, G.K.; Zhu, Z.; Liang, K.; Van Koeverden, M.P.; Alongkornchotikul, S.; Caruso, F. Polymersome-loaded capsules for controlled release of DNA. Small **2011**, *7* (14), 2109–2119.
72. Kim, Y.; Tewari, M.; Pajerowski, J.D.; Cai, S.; Sen, S.; Williams, J.H.; Sirsi, S.R.; Lutz, G.J.; Discher, D.E. Polymersome delivery of siRNA and antisense oligonucleotides. J. Control. Release **2009**, *134* (2), 132–140.
73. Lewis, A.L.; Battaglia, G.; Canton, I.; Stratford, P.W. Amphiphilic Block Copolymers For Nucleic Acid Delivery, http://patent.ipexl.com/U2S/20110151013.html (accessed Mar 27, 2013).
74. Quinn, J.F.; Johnston, A.P.; Such, G.K.; Zelikin, A.N.; Caruso, F. Next generation, sequentially assembled ultrathin films: Beyond electrostatics. Chem. Soc. Rev. **2007**, *36* (5), 707–718.
75. Zhang, Y.J.; Guan, Y.I.N.G.; Yang, S.; Xu, J.; Han, C.C. Fabrication of hollow capsules based on hydrogen bonding. Adv. Mater. **2003**, *15* (10), 832–835.
76. Kozlovskaya, V.; Ok, S.; Sousa, A.; Libera, M.; Sukhishvili, S.A. Hydrogen-bonded polymer capsules formed by layer-by-layer self-assembly. Macromolecules **2003**, *36* (23), 8590–8592.
77. Such, G.K.; Tjipto, E.; Postma, A.; Johnston, A.P.; Caruso, F. Ultrathin, responsive polymer click capsules. Nano Lett. **2007**, *7* (6), 1706–1710.
78. Decher, G.; Hong, J. Buildup of ultrathin multilayer films by a self-assembly process .1. Consecutive adsorption of anionic and cationic bipolar amphiphiles on charged surfaces. Makromol. Chem. Macromol. Symp. **1991**, *46* (1) 321–327.
79. Caruso, F.; Caruso, R.A.; Möhwald, H. Nanoengineering of inorganic and hybrid hollow spheres by colloidal templating. Science **1998**, *282* (5391), 1111–1114.
80. Dejugnat, C.; Sukhorukov, G.B. pH-responsive properties of hollow polyelectrolyte microcapsules templated on various cores. Langmuir **2004**, *20* (17), 7265–7269.

81. Volodkin, D.V.; Larionova, N.I.; Sukhorukov, G.B. Protein encapsulation via porous CaCO3 microparticles templating. Biomacromolecules **2004**, *5* (5), 1962–1972.
82. Itoh, Y.; Matsusaki, M.; Kida, T.; Akashi, M. Enzyme-responsive release of encapsulated proteins from biodegradable hollow capsules. Biomacromolecules **2006**, *7* (10), 2715–2718.
83. Peyratout, C.S.; Dahne, L. Tailor-made polyelectrolyte microcapsules: From multilayers to smart containers. Angew. Chem. Int. Ed. **2004**, *43* (29), 3762–3783.
84. De Geest, B.G.; Sanders, N.N., Sukhorukov, G.B.; Demeester, J.; De Smedt, S.C. Release mechanisms for polyelectrolyte capsules. Chem. Soc. Rev. **2007**, *36* (4), 636–649.
85. De Cock, L.J.; De Koker, S.; De Geest, B.G.; Grooten, J.; Vervaet. C.; Remon, J.P.; Sukhorukov. G.B.; Antipina, M.N. Polymeric multilayer capsules in drug delivery. Angew. Chem. Int. Ed. **2010**, *49* (39), 6954–6973.
86. Ai, H.; Jones, S.A.; Lvov, Y.M. Biomedical applications of electrostatic layer-by-layer nano-assembly of polymers, enzymes, and nanoparticles. Cell Biochem. Biophys. **2003**, *39* (1), 23–43.
87. Fischer, D.; Li, Y.; Ahlemeyer, B.; Krieglstein, J.; Kissel, T. In vitro cytotoxicity testing of polycations: Influence of polymer structure on cell viability and hemolysis. Biomaterials **2003**, *24* (7), 1121–1131.
88. Moghimi, S.M.; Symonds, P.; Murray, J.C.; Hunter, A.C.; Debska, G.; Szewczyk, A. A two-stage poly(ethylenimine)-mediated cytotoxicity: Implications for gene transfer/therapy. Mol. Ther. **2005**, *11* (6), 990–995.
89. Symonds, P.; Murray, J.C.; Hunter, A.C.; Debska, G.; Szewczyk, A.; Moghimi, S.M. Low and high molecular weight poly(L-lysine)s/poly(L-lysine)-DNA complexes initiate mitochondrial-mediated apoptosis differently. FEBS Lett. **2005**, *579* (27), 6191–6198.
90. Kozlovskaya, V.; Kharlampieva, E.; Mansfield, M.L.; Sukhishvili, S.A. Poly(methacrylic acid) hydrogel films and capsules: Response to pH and ionic strength, and encapsulation of macromolecules. Chem. Mater. **2006**, *18* (2), 328–336.
91. Zelikin, A.N.; Li, Q.; Caruso, F. Disulfide-stabilized poly(methacrylic acid) capsules: Formation, cross-linking, and degradation behavior. Chem. Mat. **2008**, *20* (8), 2655–2661.
92. Johnston, A.P.R.; Cortez, C.; Angelatos, A.S.; Caruso, F. Layer-by-layer engineered capsules and their applications. Curr. Opin. Colloid Interface Sci. **2006**, *11* (4), 203–209.
93. De Koker, S.; Hoogenboom, R.; De Geest, B.G. Polymeric multilayer capsules for drug delivery. Chem. Soc. Rev **2012**, *41* (7), 2867–2884.
94. Shutava, T.; Prouty, M.; Kommireddy, D.; Lvov, Y. pH responsive decomposable layer-by-layer nanofilms and capsules on the basis of tannic acid. Macromolecules **2005**, *38* (7), 2850–2858.
95. Ibarz, G.; Dähne, L.; Donath, E.; Moehwald, H. Smart micro- and nanocontainers for storage, transport, and release. Adv. Mater. **2001**, *13* (17), 1324–1327.
96. Lvov, Y.; Antipov, A.A.; Mamedov, A.; Möhwald, H.; Sukhorukov, G.B. Urease encapsulation in nanoorganized microshells. Nano Lett. **2001**, *1* (3), 125–128.
97. Koehler, K.; Sukhorukov, G.B. Heat treatment of polyelectrolyte multilayer capsules: A versatile method for encapsulation. Adv. Funct. Mater. **2007**, *17* (13), 2053–2061.
98. Itoh, Y.; Matsusaki, M.; Kida, T.; Akashi, M. Locally controlled release of basic fibroblast growth factor from multilayered capsules. Biomacromolecules **2008**, *9* (8), 2202–2206.
99. Khopade, A.J.; Caruso, F. Stepwise self-assembled poly(amidoamine) dendrimer and poly(styrenesulfonate) microcapsules as sustained delivery vehicles. Biomacromolecules **2002**, *3* (6), 1154–1162.
100. Wang, Y.; Yu, A.; Caruso, F. Nanoporous polyelectrolyte spheres prepared by sequentially coating sacrificial mesoporous silica spheres. Angew. Chem. Int. Ed. **2005**, *44* (19), 2888–2892.
101. Yu, A.; Wang, Y.; Barlow, E.; Caruso, F. Mesoporous silica particles as templates for preparing enzyme-loaded biocompatible microcapsules. Adv. Mater. **2005**, *17* (14), 1737–1741.
102. Zheng, Z.; Zhang, X.; Carbo, D.; Clark, C.; Nathan, C.; Lvov, Y. Sonication-assisted synthesis of polyelectrolyte-coated curcumin nanoparticles. Langmuir **2010**, *26* (11), 7679–7681.
103. Chen, Y.; Lin, X.; Park, H.; Greever, R. Study of artemisinin nanocapsules as anticancer drug delivery systems. Nanomed. Nanotechnol. Biol. Med. **2009**, *5* (3), 316–322.
104. Zhang, F.; Wu, Q.; Chen, Z.C.; Zhang, M.; Lin, X.F. Hepatic-targeting microcapsules construction by self-assembly of bioactive galactose-branched polyelectrolyte for controlled drug release system. J. Colloid Interface Sci. **2008**, *317* (2), 477–484.
105. Pargaonkar, N.; Lvov, Y.M.; Li, N.; Steenekamp, J.H.; de Villiers, M.M. Controlled release of dexamethasone from microcapsules produced by polyelectrolyte layer-by-layer nanoassembly. Pharm. Res. **2005**, *22* (5), 826–835.
106. Caruso, F.; Trau, D.; Möhwald, H.; Renneberg, R. Enzyme encapsulation in layer-by-layer engineered polymer multilayer capsules. Langmuir **2000**, *16* (4), 1485–1488.
107. Balabushevitch, N.G.; Sukhorukov, G.B.; Moroz, N.A.; Volodkin, D.V.; Larionova, N.I.; Donath, E.; Mohwald, H. Encapsulation of proteins by layer-by-layer adsorption of polyelectrolytes onto protein aggregates: Factors regulating the protein release. Biotechnol. Bioeng. **2001**, *76* (3), 207–213.
108. Shutava, T.G.; Balkundi, S.S.; Vangala, P.; Steffan, J.J.; Bigelow, R.L.; Cardelli, J.A.; O'Neal, D.P.; Lvov, Y.M. Layer-by-layer-coated gelatin nanoparticles as a vehicle for delivery of natural polyphenols. ACS Nano **2009**, *3* (7), 1877–1885.
109. Matsusaki, M.; Akashi, M. Functional multilayered capsules for targeting and local drug delivery. Expert Opin. Drug Deliv. **2009**, *6* (11), 1207–1217.
110. Itoh, Y.; Matsusaki, M.; Kida, T.; Akashi, M. Time-modulated release of multiple proteins from enzyme-responsive multilayered capsules. Chem. Lett. **2008**, *37* (3), 238–239.
111. Schneider, G.F.; Subr, V.; Ulbrich, K.; Decher, G. Multifunctional cytotoxic stealth nanoparticles. A model approach with potential for cancer therapy. Nano Lett. **2009**, *9* (2), 636–642.

112. Sivakumar, S.; Bansal, V.; Cortez, C.; Chong, S.F.; Zelikin, A.N.; Caruso, F. Degradable, surfactant-free, monodisperse polymer-encapsulated emulsions as anticancer drug carriers. Adv. Mater. **2009**, *21* (18), 1820–1824.
113. Sukhishvili, S.A. Responsive polymer films and capsules via layer-by-layer assembly. Curr. Opin. Colloid Interface Sci. **2005**, *10* (1–2), 37–44.
114. Yan, Y.; Johnston, A.P.; Dodds, S.J.; Kamphuis, M.M.; Ferguson, C.; Parton, R.G.; Nice, E.C.; Heath, J.K.; Caruso, F. Uptake and intracellular fate of disulfide-bonded polymer hydrogel capsules for doxorubicin delivery to colorectal cancer cells. ACS Nano **2010**, *4* (5), 2928–2936.
115. Poon, Z.; Chang, D.; Zhao, X.; Hammond, P.T. Layer-by-layer nanoparticles with a ph-sheddable layer for in vivo targeting of tumor hypoxia. ACS Nano **2011**, *5* (6), 4284–4292.
116. Wohl, B.M.; Engbersen, J.F.J. Responsive layer-by-layer materials for drug delivery. J. Control. Release **2012**, *158* (1), 2–14.
117. Staedler, B.; Price, A.D.; Zelikin, A.N. A critical look at multilayered polymer capsules in biomedicine: Drug carriers, artificial organelles, and cell mimics. Adv. Funct. Mater. **2011**, *21* (1), 14–28.
118. Reibetanz, U.; Claus, C.; Typlt, E.; Hofmann, J.; Donath, E. Defoliation and plasmid delivery with layer-by-layer coated colloids. Macromol. Biosci. **2006**, *6* (2), 153–160.
119. Zhang, X.; Oulad-Abdelghani, M.; Zelkin, A.N.; Wang, Y.; Haîkel, Y.; Mainard, D.; Voegel, J.C.; Caruso, F.; Benkirane-Jessel, N. Poly(L-lysine) nanostructured particles for gene delivery and hormone stimulation. Biomaterials **2010**, *31* (7), 1699–1706.
120. Elbakry, A.; Zaky, A.; Liebl, R.; Rachel, R.; Goepferich, A.; Breunig, M. Layer-by-layer assembled gold nanoparticles for siRNA delivery. Nano Lett. **2009**, *9* (5), 2059–2064.
121. del Mercato, L.L.; Rivera-Gil, P.; Abbasi, A.Z.; Ochs, M.; Ganas, C.; Zins, I.; Sönnichsen, C.; Parak, W.J. LbL multilayer capsules: Recent progress and future outlook for their use in life sciences. Nanoscale **2010**, *2* (4), 458–467.
122. Staedler, B.; Chandrawati, R.; Price, A.D.; Chong, S.F.; Breheney, K.; Postma, A.; Connal, L.A.; Zelikin, A.N.; Caruso, F. A microreactor with thousands of subcompartments: Enzyme-loaded liposomes within polymer capsules. Angew. Chem. Int. Ed. **2009**, *48* (24), 4359–4362.
123. Chandrawati, R.; Odermatt, P.D.; Chong, S.F.; Price, A.D; Städler, B.; Caruso, F. Triggered cargo release by encapsulated enzymatic catalysis in capsosomes. Nano Lett. **2011**, *11* (11), 4958–4963.
124. De Geest, B.G.; Sukhorukov, G.B.; Möhwald, H. The pros and cons of polyelectrolyte capsules in drug delivery. Expert Opin. Drug Deliv. **2009**, *6* (6), 613–624.

Chapter III

"Variable Asialoglycoprotein Receptor 1 Expression in Liver Disease: Implications for Therapeutic Intervention"

Witzigmann D, Quagliata L, Schenk SH, Quintavalle C, Terracciano LM, Huwyler J.

Hepatology Research. 2015 Sep 30. doi: 10.1111/hepr.12599.

http://onlinelibrary.wiley.com/doi/10.1111/hepr.12599/abstract

Highlights: For a successful clinical outcome of hepatocyte-targeted drug delivery systems it is important to carefully consider the asialoglycoprotein receptor 1 (ASGR1) expression level and expression pattern. In this study, the ASGR1 expression was analyzed at the mRNA and protein level using various liver cancer-derived cell lines as well as human tissue specimens, from both normal and pathological liver. Several analytical techniques including RT-PCR, flow cytometry, confocal microscopy, RNA microarray, and immunohistochemistry were used. The analysis revealed an altered ASGR1 expression level in cirrhotic specimens or hepatocellular carcinoma. In the future, this study will be instrumental for the development of ASGPR-targeted nanomedicines and companion diagnostics in order to translate targeted nanomedicines from basic research to the clinic.

Hepatology Research 2015 doi: 10.1111/hepr.12599

Original Article

Variable asialoglycoprotein receptor 1 expression in liver disease: Implications for therapeutic intervention

Dominik Witzigmann,[1] Luca Quagliata,[2] Susanne H. Schenk,[1] Cristina Quintavalle,[2] Luigi M. Terracciano[2] and Jörg Huwyler[1]

[1]*Division of Pharmaceutical Technology, Department of Pharmaceutical Sciences; and* [2]*Institute of Pathology, Molecular Pathology Division, University Hospital of Basel, Basel, Switzerland*

Aim: One of the most promising strategies for the treatment of liver diseases is targeted drug delivery via the asialoglycoprotein receptor (ASGPR). The success of this approach heavily depends on the ASGPR expression level on parenchymal liver cells. In this study, we assessed the mRNA and protein expression levels of the major receptor subunit, ASGR1, in hepatocytes both *in vitro* and *in vivo*.

Methods: *In vitro*, various liver cancer-derived cell lines were evaluated. *In vivo*, we screened the *ASGR1* mRNA on 59 hepatocellular carcinoma and matched non-neoplastic tissue using RNA microarray. In addition, 350 human liver specimens of patients with hepatocellular carcinoma or non-neoplastic liver diseases were screened for ASGR1 protein level using tissue microarray analysis.

Results: Our data reveal that the ASGR1 mRNA expression directly correlates with the protein level. We demonstrate that the ASGR1 expression is upregulated in cirrhotic specimens and is significantly decreased with increasing hepatocellular carcinoma grade.

Conclusion: Because the ASGR1 expression levels are variable between patients, our findings suggest that ASGPR-based targeting strategies should be combined with ASGPR-companion diagnostics to maximize clinical benefit.

Key words: asialoglycoprotein receptor, drug delivery, hepatocyte, liver disease, nanomedicine

INTRODUCTION

LIVER DISEASES ARE a leading cause of death worldwide with increasing incidence rates.[1] The hepatocytes within the liver have been implicated in many hepatic diseases including hepatocellular carcinoma (HCC), viral hepatitis, or genetic and metabolic disorders.[2] Conventional pharmacotherapies for these diseases encounter significant drawbacks including dose-limiting off-target effects. Thus, improved tissue- and cellular-specific targeted therapies are desperately needed.[3] Recently, active targeted drug delivery systems such as nanomedicines or RNA interference (RNAi) therapeutics have attracted much attention for their ability to treat hepatic diseases more efficiently and with reduced side-effects.[4–6] Such approaches imply that the drug delivery system is modified with a ligand, which binds with high specificity to hepatocytes. Thus, the pharmacokinetic and pharmacodynamic profile of the active compound is altered and its therapeutic index is potentially improved.[7]

Currently, the most promising receptor studied for hepatocyte-specific drug targeting is the asialoglycoprotein receptor (ASGPR or Ashwell–Morell receptor),[2,8] a C-type lectin, which mediates the endocytosis of serum glycoproteins.[9,10] The ASGPR is predominantly expressed on the sinusoidal, basolateral membrane of hepatocytes and has a high affinity for galactose (Gal) or N-acetylgalactosamine (GalNAc) containing ligands.[11,12] Its localization, high expression and efficient internalization rate make the ASGPR an ideal target for cell type-specific drug delivery systems.[13]

Over the last decades, many therapeutics have been developed to target the ASGPR for hepatocyte specific delivery of small molecules, proteins or nucleic acids.[14–19] The most promising technologies are in the field of RNAi. Revusiran (ALN-TTRSc), a ligand modified siRNA therapeutic, is currently in a phase 2 clinical study for the treatment of transthyretin-mediated amyloidosis (NCT02292186).[6,20] Another RNAi phase 2 clinical trial

Correspondence: Professor Jörg Huwyler, Division of Pharmaceutical Technology, Department of Pharmaceutical Sciences, University of Basel, Klingelbergstrasse 50, CH-4056 Basel, Switzerland. Email: joerg.huwyler@unibas.ch

Conflict of interest: The authors declare that they have no conflict of interests.

Received 30 July 2015; revision 7 September 2015; accepted 19 September 2015.

is underway with a GalNAc modified dynamic polyconjugate (ARC-520) to treat chronic hepatitis B virus infections (NCT02065336).[21,5] Several other preclinical studies for hepatocyte-specific diseases are ongoing using these two RNAi platform technologies.[4,22,23]

Asialoglycoprotein receptor-targeted therapies may also offer an alternative pharmacotherapy[24] for HCC, which is the second leading cause of cancer-related deaths worldwide.[25] The initiation and development of hepatocarcinogenesis is a multistep process occurring over years, with underlying liver cirrhosis in most of the cases. Only patients diagnosed at early stage of the disease are eligible for curative treatments such as systemic chemotherapy or chemoembolization, which have striking disadvantages[26,27] and low success rates.[28] Targeted nanomedicines can be used to deliver small molecules or nucleic acids with antineoplastic effects[2] to the target cell and additionally overcome P-glycoprotein-dependent anticancer drug efflux.[29] Apoptin-induced apoptosis or downregulation of oncogenic miRNA are two preclinical gene therapeutic approaches to selectively kill malignant liver cells[30,31] which would benefit from enhanced therapeutic strategies using targeted nanomedicines. Furthermore, the treatment of genetic disorders such as α1-antitrypsin deficiency[32] or hemochromatosis[33] which are associated with an increased risk for cirrhosis and HCC would highly benefit from targeted gene delivery systems.

There are three major factors important for successful active targeting. First, therapeutics need to be able to access the target cell type. The liver sinusoids have fenestrations up to 150 nm allowing the blood direct contact to the basolateral membrane of hepatocytes.[34] Thus, nanomedicine therapeutics, usually below 120 nm in size, have the correct size to access the hepatocytes.[35] Second, the targeting ligand and its density need to be optimized for efficient binding and increased uptake. The balance between targeting ability and recruitment of opsonins is a critical factor for an optimized pharmacokinetic profile.[36] Finally, it is crucial to study the precise tissue distribution and expression of the target receptor. To increase specificity and to trigger the uptake of targeted therapeutics, ideally, the receptor should be highly and exclusively expressed by the target cell.

In contrast to the numerous research articles on highly sophisticated nanomedicines and RNAi therapeutics, there are only a few studies which address the endogenous expression of the target receptor in health and disease. The ASGPR is a heterooligomeric membrane receptor with two homologous subunits, ASGR1 (H1/HL1) and ASGR2 (H2/HL2). The stoichiometry of the ASGPR is still disputed with an ASGR1 : ASGR2 ratio of between 2 and 5:1.[37] Although both subunits contain a carbohydrate recognition domain, the major subunit ASGR1 plays the central biological role.[38]

Because expression of the ASGR1 is one of the three major success factors for targeted drug delivery, patients with low ASGR1 expression levels would not be perfectly suitable for ASGPR-targeted nanomedicines. Therefore, informative studies exploring levels of ASGR1 in health and disease would be of clinical benefit, because it would allow the clinician to personalize the medicine in a case-by-case manner. Here, we investigate the ASGR1 expression both at the mRNA and protein level using liver-derived cell lines as well as human tissue specimens, from both normal and pathological liver. A special focus is given to samples from patients suffering from HCC and its major risk factor, cirrhosis.

METHODS

ASGR1 expression in hepatic cell lines, *in vitro*

DETAILED PROCEDURES FOR the analysis of ASGR1 mRNA (i.e. quantitative real-time polymerase chain reaction [qRT–PCR]) and protein (i.e. flow cytometry and confocal laser scanning microscopy) expression in different hepatic cell lines (i.e. HepG2, PLC/PRF/5, Hep3B, Sk-Hep1, SNU449, HuH6, HuH7, HLE, Mahlavu, HepT1, cryopreserved human hepatocytes, and the ASGPR-expressing model cell line 1–7-1) are provided in the Supplementary Information. In brief, qRT–PCR was performed using predeveloped TaqManAssays (Invitrogen [San Diego, CA, USA], Life Technologies [Carlsbad, CA, USA]). C_t values of *ASGR1* mRNA (Hs01005019_m1) were normalized to four different housekeeping genes (β-actin, glyceraldehyde 3-phosphate dehydrogenase [GAPDH], prolylpeptidyl isomerase A [PPIA] and ribosomal protein large P0 [RPLP0]). For analysis of ASGR1 protein expression, cells were incubated with the primary anti-ASGR1 antibody (HPA011954; Prestige Antibodies®, Sigma-Aldrich, St Louis, MO, USA), followed by incubation with a fluorescent-labeled secondary antibody. Flow cytometry analysis of 20,000 cells was performed using a FACS CantoII SOP (Special Order Product; Becton Dickinson, Franklin Lakes, NJ, USA). Confocal laser scanning microscopy was performed using an Olympus FV-1000 inverted confocal fluorescence microscope (Olympus, Tokyo, Japan) and a 60× objective (numerical aperture, 1.40).

Patient samples for RNA and tissue microarray (TMA)

Patients' specimens with comprehensive clinicopathological and follow-up data were obtained from the Institute of

Pathology, University Hospital of Basel, Switzerland. The ethics committee of the Institute of Pathology, University Hospital of Basel, approved the study. HCC diagnosis was verified by pathological examination, no anticancer treatments were given before biopsy collection. Tumor differentiation was defined according to Edmondson's grading system. Only biopsies containing at least 50% of tumor cells and no necrotic area have been used in this study. Roughly, 60% of patients whose specimens were used for TMA construction underwent surgical resection without prior treatment for HCC, and the remaining were collected from autopsy cases.

Analysis of human liver specimens

Transcriptomic analysis of *ASGR1* mRNA and tissue microarray analysis of ASGR1 and CD3 protein staining are described in detail in the Supplementary Information. *ASGR1* mRNA expression was assessed in 64 liver specimens including patient samples of different etiology such as alcohol-related HCC ($n = 30$), no virus/no alcohol-related HCC ($n = 5$), hepatitis B virus (HBV)/hepatitis C virus (HCV)-related HCC ($n = 24$) and normal healthy liver specimens ($n = 5$) using the GeneChip®Human Gene 1.0ST arrays (Affymetrix, Santa Clara, CA, USA). None of the patients received any therapeutic treatment before the biopsy. The TMA was constructed as previously described by Baumhoer *et al.*[39] using a total of 446 tissue specimens from both HCC and non-neoplastic liver tissue samples. ASGR1 and CD3 protein levels were investigated by immunohistochemistry using a liver tissue microarray. For further evaluations of ASGR1 protein expression, 350 specimens were suitable for analysis including 76 normal liver, 73 HCC grade I, 82 HCC grade II, 25 HCC grade III and 84 cirrhotic tissue specimens. For the evaluation of CD3 protein expression, 328 specimens were suitable for analysis including 69 normal liver, 173 HCC and 81 cirrhotic tissue specimens. Causes of exclusion were either the absence of tissue punch or poor staining quality. All tissue samples were retrieved from the Institute of Pathology, University Hospital of Basel, Switzerland.

Statistical analysis

The statistical analysis was performed as described previously.[40] In brief, the χ^2-test and Fisher's exact test for non-parametric variables were used. All tests were two-sided and $P < 0.05$ was considered to be statistically significant. Analysis was performed using GraphPad Prism software version 6 (GraphPad Software, La Jolla, CA, USA).

RESULTS

Variable expression of ASGR1 in hepatic cells, *in vitro*

HEPG2 CELLS ARE almost the only hepatic cell line used to study ASGPR targeting strategies. Therefore, the aim of the present study was to evaluate alternative cell models for ASGPR-targeted nanomedicines. In a first set of experiments, we evaluated the *ASGR1* mRNA expression in 10 different hepatic cells lines and a pool of mixed sex primary human hepatocytes (PHH) using qRT–PCR analysis (Fig. 1a). To compensate for variations such as sample-to-sample deviations, we used four different housekeeping genes, namely, β-actin, GAPDH, PPIA and RPLP0. The expression of *ASGR1* mRNA is significantly different between

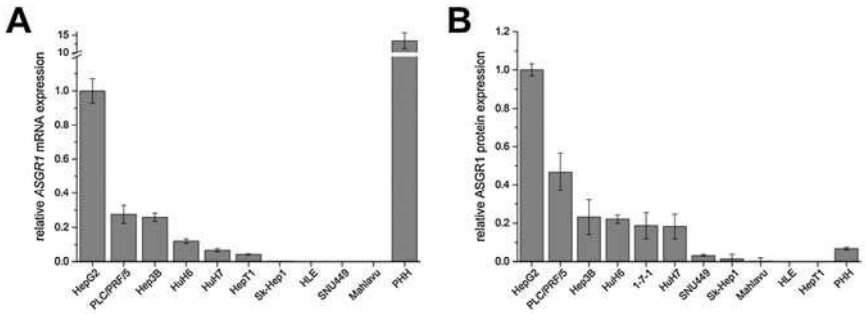

Figure 1 Asialoglycoprotein receptor 1 (*ASGR1*) mRNA expression and ASGPR1 protein level in different cell lines. (a) Quantitative reverse transcription polymerase chain reaction analysis of *ASGR1* mRNA expression in different liver cancer-derived cell lines and primary human hepatocytes (PHH). Glyceraldehyde 3-phosphate dehydrogenase (GAPDH), β-actin, prolylpeptidyl isomerase A (PPIA) and ribosomal protein large P0 (RPLP0) were used as housekeeping genes. Mean values are given as ±standard deviation (SD) relative to the expression in HepG2 ($n = 3$). (b) Quantitative analysis of ASGR1 protein expression in different cell lines using flow cytometry. Mean values are given as ±SD relative to the expression in HepG2 ($n = 3$).

the liver-derived cell lines (Fig. 1a). The cells are classified into four distinct groups: negative, low, intermediate and high depending on their *ASGR1* mRNA expression level. SK-Hep1, HLE, SNU 449 and Mahlavu are negative for *ASGR1* mRNA. HepT1, HuH7 and HuH6 show a low *ASGR1* mRNA expression. An intermediate expression level is found in PLC/PRF/5 and Hep3B cells. Of the 10 different cell lines, HepG2 is the only cell line with high *ASGR1* mRNA expression, being fourfold higher than the intermediate expression group. PHH show an *ASGR1* mRNA expression approximately 14-fold higher than HepG2 cells.

To examine the correlation between the ASGR1 mRNA abundance and the protein expression level, flow cytometry analysis was used to quantify the protein level of ASGR1 in all the hepatic cell lines, in PHH and in the ASGPR-expressing model cell line 1–7-1 (Fig. 1b). The relative mean fluorescence intensity of the ASGR1 protein staining normalized to HepG2 cells indicates a correlation with the mRNA level in most of the cell lines. HepG2 cells show the highest ASGR1 protein expression, followed by PLC/PRF/5 with approximately twofold decrease. Hep3B, HuH6 and HuH7 cells show an intermediate ASGR1 protein expression. The remaining cell lines show a low or negative expression for ASGR1 protein. PHH express a low amount of ASGR1 protein which does not correlate with the mRNA levels (see DISCUSSION).[41,42] The murine model cell line 1–7-1 exhibits an intermediate ASGR1 protein expression (Fig. 1b).

To further evaluate the qualitative ASGR1 protein expression on a cellular level, all cell lines were analyzed using confocal laser scanning microscopy (Fig. S1). The results from flow cytometry analysis were confirmed. A strong positive ASGR1 staining, which was evenly distributed throughout the cells, was observed for HepG2 cells. Cell lines with an intermediate ASGR1 protein staining exhibit a heterogeneous staining distribution. PHH which are much bigger in size compared with the hepatic cell lines showed only a slight staining. 1–7-1 cells resulted in a staining comparable to the intermediate expression group.

ASGR1 mRNA expression in human liver specimens

BECAUSE THE EXPRESSION of the ASGPR is a prerequisite for successful active targeting of hepatocytes *in vivo*, we screened human liver specimens of patients with HCC and non-neoplastic liver diseases for the ASGR1 expression. To evaluate the *ASGR1* expression in human liver tissue at the mRNA level, we performed a global transcriptomic analysis using the GeneChip®Human Gene 1.0ST array, as previously described.[40] *ASGR1* mRNA is significantly reduced in HCC tumor samples compared with healthy liver specimens (Fig. 2a). In addition, paired biopsies show a slight decrease of *ASGR1* mRNA in HCC specimens compared with their non-tumoral counterparts (Fig. 2a). Of note, with increasing HCC grade (Edmondson grade III–IV vs I–II), *ASGR1* mRNA is more markedly decreased (Fig. 2b). Although no significant changes are observed for *ASGR1* mRNA levels in tumor samples of non-metastatic versus metastatic status or high versus low proliferation index specimens (as defined by Ki67 positivity) (Fig. 2c,d), a clear trend in the direction of decreased *ASGR1* mRNA expression in metastatic or high proliferative tumor samples is noticeable. Patients' stratification according to etiology revealed no significant correlation with *ASGR1* mRNA levels (Fig. 2e).

ASGR1 protein expression in human liver specimens

To validate the results obtained by transcriptome profiling of liver biopsies, we performed an immunohistochemistry staining for ASGR1 protein in a large cohort of liver specimens using a liver-specific TMA. The TMA comprised a total of 446 liver samples with 350 specimens suitable for further analysis as described in METHODS. Figure 3 (a–d) shows representative images of different ASGR1 protein staining intensities from 0 up to +3, indicating negative, weak, moderate and strong ASGR1 expression, respectively.

The TMA data analysis revealed that ASGR1 protein expression is reduced in HCC samples ($P = 0.057$). Both the HCC and non-neoplastic samples showed marked variability regarding ASGR1 protein staining (Table 1), further corroborating our mRNA profiling. Interestingly, 58.2% of the analyzed HCC cases were negative for ASGR1 staining, versus normal liver, in which only 40.8% were ASGR1 negative (Table 1). It is noteworthy that with increasing HCC Edmondson grade, the ASGR1 protein level decreases (Fig. 4a, Table S1). Grade I HCC samples showed 21.9% ASGR1 positive (+2) samples compared with 11.0% and 8.0% in grade II and III HCC specimens, respectively (Fig. 4a, Table S1). The analysis of tumor–node–metastasis stage of HCC specimens revealed a clear decrease of ASGR1 protein with increasing stage of HCC (Fig. 4b–d, Table S1). Stratification of the TMA samples based on their etiology revealed a decreased ASGR1 protein expression for alcohol-related HCC compared with HBV/HCV-related HCC. Less than 10% of the alcohol-related HCC showed a +2/+3 ASGR1 protein staining compared with 23.3% for virus-related HCC samples (Fig. 4e, Table S1).

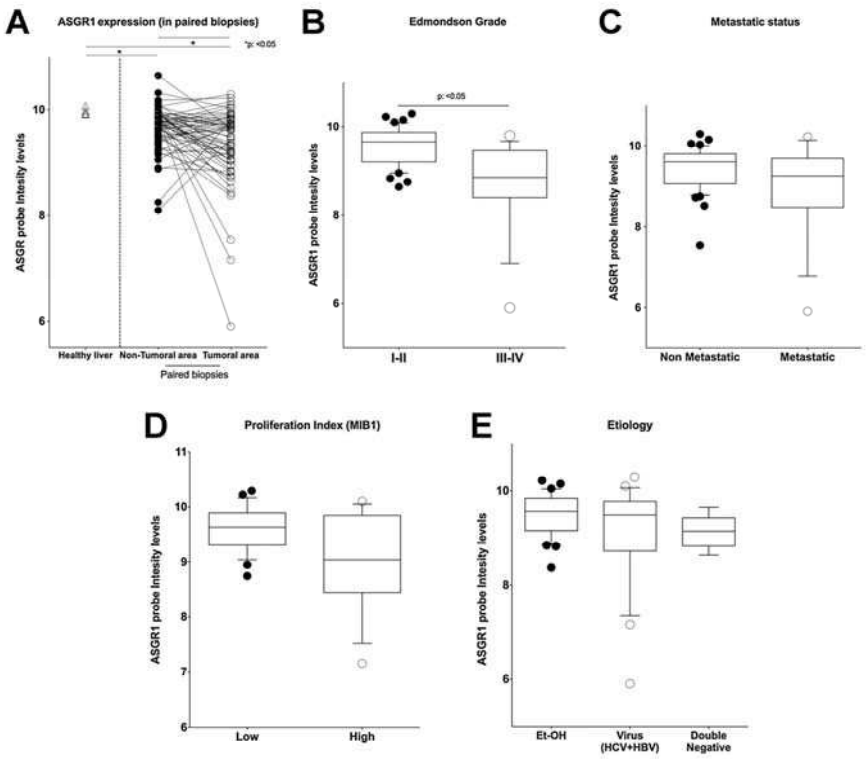

Figure 2 Asialoglycoprotein receptor 1 (*ASGR1*) mRNA expression levels in human liver tissue. Analysis of *ASGR1* mRNA expression using Huge 1.0 RNA-microarray data. (a) Correlation of *ASGR1* mRNA expression in hepatocellular carcinoma (HCC) samples and matched non-tumoral liver tissue. *ASGR1* expression of HCC specimens in correlation with (b) Edmondson grade, (c) metastatic status, (d) proliferation index and (e) etiology. Et-OH, ethyl alcohol; HBV, hepatitis B virus; HCV, hepatitis C virus.

To further explore the observed decrease of ASGR1 protein staining in the HCC specimens, we focused our analysis on a subset of 59 HCC samples (comprised from the original cohort used for the TMA construction) matched with adjacent non-tumoral liver tissue. Figure 5 shows representative images of TMA punches from HCC liver tissue (Fig. 5b) and matched, adjacent non-tumoral liver (Fig. 5a). We observed decreased ASGR1 protein expression in HCC samples versus matched non-neoplastic tissue in 25 out of 59 paired samples (Fig. 5c). In the remaining matched samples, with the exception of one case, there was no change in ASGR1 protein staining (33/59 paired samples). Overall, HCC specimens are twice as often ASGR1 protein negative (67.8%) compared with matched non-tumoral liver samples (33.9%). Interestingly, the TMA analysis showed that some specimens expressed a strong basolateral, sinusoidal ASGR1 membrane staining. Representative images of liver tissue samples, exhibiting a preferred membrane (membrane score 1) versus homogenously distributed (membrane score 0) ASGR1 protein staining, are shown in Figure 3(e,f), respectively. The membrane staining analysis reveals significantly higher membrane staining ($P = 0.0003$) in normal liver specimens (68.9%) comparative to HCC samples (35.1%) (Table S2).

Because cirrhosis is a major underlying cause of HCC, we wanted to test if ASGR1 levels differed between the two patient groups. Interestingly, ASGR1 protein expression is increased in cirrhotic tissue specimens compared with normal liver or HCC samples (Table 1, Fig. 6a–c inserts). More than 75% of the cirrhotic tissue specimens were ASGR1 positive, whereas only 42% showed ASGR1 protein expression in HCC samples ($P < 0.0001$) (Table 1).

Recently, it has been shown that cytokines involved in inflammatory processes increase ASGPR levels.[43] To assess if immune-mediated stimulation of ASGR1 protein expression plays a role in cirrhosis, we performed a CD3

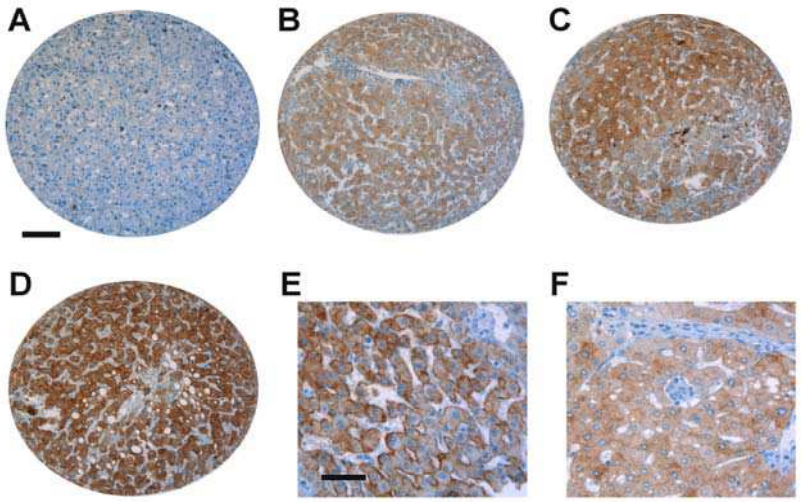

Figure 3 Immunohistochemical staining of asialoglycoprotein receptor 1 (ASGR1) protein in tissue microarray punches. Representative images of ASGR1 immunostaining with staining score (a) 0, (b) +1, (c) +2 and (d) +3. (e) Images of samples with preferential ASGR1 membrane staining or (f) distributed ASGR1 staining are shown (scale bars, 100 μm).

Table 1 Summary of asialoglycoprotein receptor (ASGPR)1 protein levels in tissue samples from normal liver, hepatocellular carcinoma (HCC) and cirrhotic nodules

Tissue Type	ASGR1 Staining Score n (%)		2	3	χ^2	*P*
	0	1				
Normal liver	31 (40.8)	26 (34.2)	17 (22.4)	2 (2.6)	7.523	0.0570
HCC	107 (58.2)	42 (22.8)	28 (15.2)	7 (3.8)		
Normal liver	31 (40.8)	26 (34.2)	17 (22.4)	2 (2.6)	6.269	0.0992
Cirrhotic nodules	19 (22.6)	38 (45.2)	25 (29.8)	2 (2.4)		
Cirrhotic nodules	19 (22.6)	38 (45.2)	25 (29.8)	2 (2.4)	31.710	<0.0001
HCC	107 (58.2)	42 (22.8)	28 (15.2)	7 (3.8)		

Semiquantitative evaluation of staining intensity in normal liver ($n = 76$), HCC ($n = 184$) and cirrhotic nodules ($n = 84$) was performed using tissue microarray (TMA). Results were analyzed using the χ^2-test. Corresponding *P*-values are given.

immunostaining to evaluate the rate of liver-infiltrating T lymphocytes using the identical TMA (Fig. 6, Table 2). Of the 446 liver samples, 320 tissue specimens were suitable for further analysis as described in METHODS. We observed a significant increase in CD3 protein staining in cirrhotic specimens (91.4%) compared with normal liver (53.6%) and HCC (54.3%) ($P < 0.0001$) (Fig. 6, Table 2). Moreover, of the CD3 positive cirrhotic specimens, 63.5% had greater than 10% liver-infiltrating T cells (Fig. 6b) (data not shown). In sharp contrast, of the CD3 positive normal liver (Fig. 6a) and HCC (Fig. 6c) specimens, only 27.0% and 43.6% had more than 10% infiltrating T cells, respectively (data not shown). Low but consistent levels of CD3 protein staining in normal liver (>85% of all specimens had only ≤5% infiltrating T cells) represent the normal physiological number of T cells in human liver.

DISCUSSION

THE ASGPR IS abundantly and predominantly expressed on parenchymal liver cells with up to 500,000 receptors/cell.[44,45] Upon ligand binding, the ligand-receptor complex gets internalized into the hepatocyte by clathrin-mediated endocytosis.[21] Therefore, the ASGPR is a promising receptor for targeted drug delivery systems, especially for therapeutics which depend on internalization such as nucleic acids.[7]

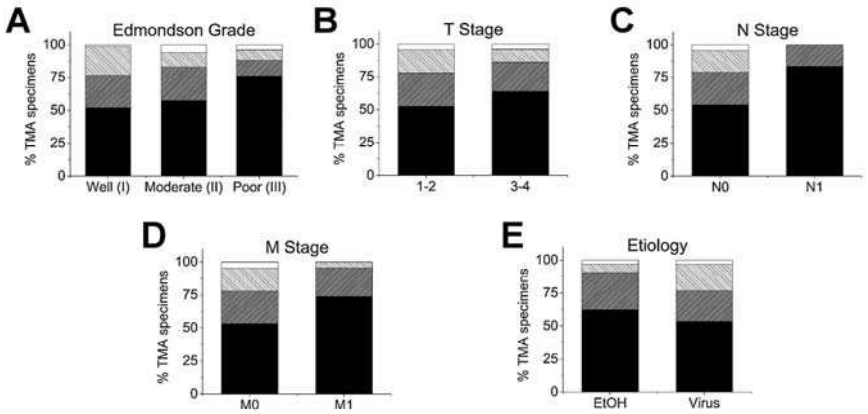

Figure 4 Asialoglycoprotein receptor 1 (ASGR1) protein expression levels in hepatocellular carcinoma (HCC) specimens. Analysis of ASGR1 protein expression using tissue microarray. ASGR1 expression of HCC specimens in correlation with (a) Edmondson grade, (b) tumor (T) stage, (c) node (N) stage, (d) metastasis (M) stage and (e) etiology.

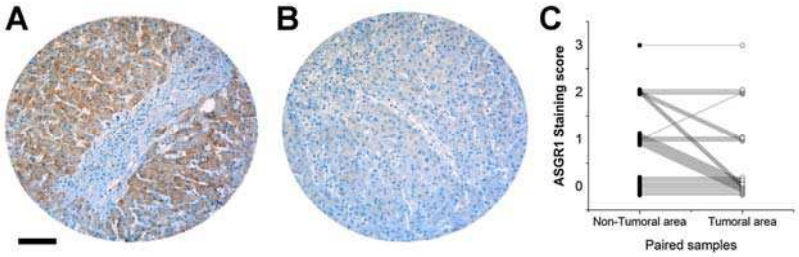

Figure 5 Tissue microarray samples of hepatocellular carcinoma (HCC) and matched adjacent non-tumoral liver tissue samples. Representative images of asialoglycoprotein receptor 1 (ASGR1) immunostaining in (a) matched adjacent non-tumoral liver tissue sample and (b) HCC tissue area (scale bars, 100 μm). (c) Comparison of ASGR1 expression in non-tumoral liver areas and corresponding HCC tumoral areas.

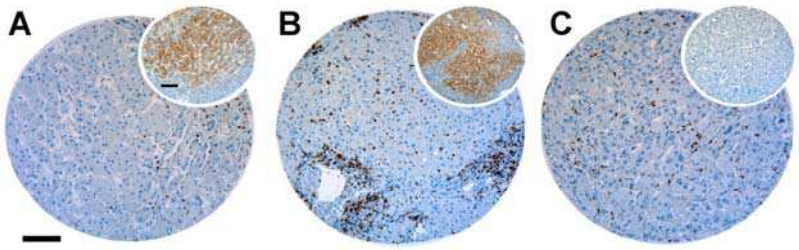

Figure 6 Immunohistochemical staining of CD3 protein in tissue microarray punches. Representative images of CD3 immunostaining in (a) non-tumoral liver tissue, (b) cirrhotic specimen and (c) hepatocellular carcinoma (scale bars, 100 μm). Inserts show asialoglycoprotein receptor 1 immunostaining of identical tissue cores (scale bars, 50 μm).

Several *in vitro* and *in vivo* models are available to study ASGPR-targeted nanomedicines. Primary hepatocytes or the large number of HCC-derived immortalized cell lines are used for drug screening. 3-D hepatospheres reproduce essential aspects of the *in vivo* situation and thus may be more suitable for the translation of targeting strategies to the *in vivo* situation.[46] To study the effect of drugs on HCC *in vivo*, there are many different animal models

Table 2 Summary of CD3 protein levels in tissue samples from normal liver, hepatocellular carcinoma (HCC) and cirrhotic specimens

Tissue type	CD3 staining, *n* (%)		χ^2	*P*
	Negative	Positive		
Normal liver	32 (46.4)	37 (53.6)	0.010	0.9201
HCC	79 (45.7)	94 (54.3)		
Normal liver	32 (46.4)	37 (53.6)	27.580	<0.0001
Cirrhotic nodules	7 (8.6)	74 (91.4)		
Cirrhotic nodules	7 (8.6)	74 (91.4)	33.770	<0.0001
HCC	79 (45.7)	94 (54.3)		

Evaluation of CD3 staining in normal liver ($n = 69$), HCC ($n = 173$) and cirrhotic nodules ($n = 81$) was performed using tissue microarray (TMA). Results were analyzed using the χ^2-test. Corresponding *P*-values are given

available including chemical-induced HCC, xenograft models (ectopic, orthotopic, hollow fiber model) or genetically modified animals. All of the different *in vivo* models have specific advantages and limitations. A careful selection of the correct model is important for successful translation into the clinic. Several excellent reviews summarize the various animal models.[47–50]

In vitro, hepatocyte targeting has mainly been studied using HepG2 cells.[51–53] Some studies have been performed with other cells lines such as HuH7 or Sk-Hep1.[54–56] However, a systematic study directly comparing ASGPR expression in several different hepatic cell lines was so far missing. Here, we performed a comprehensive analysis of ASGR1 expression both on mRNA and on protein level in 10 liver cancer-derived cell lines and in PHH. Interestingly, liver-derived cell lines display a wide spectrum of variability from negative to intermediate/high ASGR1 expression. We observed a clear correlation between ASGR1 mRNA and protein level. The only exception is freshly isolated PHH which show a high ASGR1 mRNA level but a low protein expression. However, the PHH were prepared by enzymatic digestion of liver tissue, a procedure which has been shown previously to degrade the ASGPR.[41,42]

Liver cancer-derived cell lines are generally poorly differentiated. However, after classification of the hepatic cell lines into "poorly" and "well" differentiated cell lines based on the expression of hepatic markers such as α-fetoprotein and hepatocyte nuclear factor 4α,[57] we observed a clear correlation between differentiation status and ASGR1 protein expression. "Poorly" differentiated cell lines such as Mahlavu or SNU449 are ASGR1 negative whereas "well" differentiated cell lines such as HepG2 or Hep3B show an intermediate/high ASGR1 protein expression. The correlation of ASGR1 protein expression levels with mRNA and with differentiation status *in vitro* was confirmed by subsequent microarray studies using human liver-derived samples (see below).

Notably, only HepG2 exhibited a high and homogeneous ASGR1 protein expression pattern. The other ASGR1-expressing cell lines examined had a more heterogenous distribution among the cell population. Such results further highlight the importance to carefully consider the ASGR1 expression level and expression pattern for preclinical research on active targeted drug delivery systems *in vitro*. The murine fibroblast cell line 1–7-1 showed intermediate ASGR1 protein staining, which is comparable to some human cell lines such as Hep3B or HuH7. Therefore, our work confirms the value of this established model cell line to study endocytotic processes[58,59] and intracellular pathways upon ASGPR-targeted drug delivery.

In addition to the *in vitro* experiments, the major objective of our present study was to analyze ASGR1 expression in human-derived liver tissue using a combination of RNA microarray analysis and TMA evaluation. Our RNA microarray data were obtained from snap-frozen needle biopsies of patients who did not receive any pharmacotherapy prior biopsy collection, and not from resected liver specimens that are often exposed to ischemic or therapy-induced damage. This greatly increases the integrity of our study because the quality of the tissue is optimally preserved.

Our study reveals that ASGR1 mRNA and protein expression is reduced in HCC compared with normal, non-tumoral liver. The reduction in ASGR1 is more prominent in poorly differentiated (grade III/IV) HCC specimens. It is important to mention that we obtained the same trends for both mRNA and protein levels with two independent patient cohorts (liver biopsies and liver resected samples). Our results are consistent with other studies which assessed only the ASGR1 protein levels in smaller sample cohorts.[60–62]

Our observations regarding the ASGR1 protein expression pattern underscores the need for a careful evaluation of targeted drug delivery approaches. Our study shows that normal liver specimens have significantly higher levels of membrane-associated ASGR1 compared with HCC samples. ASGR1 membrane expression is closely associated with targeting efficiency, uptake efficacy and thus therapeutic benefit. The knowledge of ASGR1 expression and cellular localization in liver tissue may have a significant impact on the outcome of a targeted therapy. This information is important, because clinicians can tailor their patients' therapy on an individual basis. The knowledge of molecular mechanisms influencing ASGR1 expression may be of additional benefit. Thus, further studies are warranted.

A surprising finding in our study was the increased ASGR1 protein expression in cirrhotic specimens. This may be attributed to a stimulation of the immune system. Our study shows that cirrhotic specimens have significantly higher levels of liver-infiltrating T lymphocytes compared with HCC samples or normal liver specimens ($P < 0.0001$). Therefore, it is tempting to speculate that the activation of the immune system and increase in liver-infiltrating T cells leads to an increased ASGR1 protein expression in patients suffering from cirrhosis. Most probably an early immune response increases the ASGPR expression in hepatocytes due to cytokine stimulation.[43] Because cirrhosis is a major risk factor for HCC, our findings are interesting for the development of new therapeutic strategies. Further studies focusing on the interplay of the immunobiology and the ASGPR expression in patients with cirrhosis are warranted.[63] In addition, future studies should address the correlation of ASGR1 expression levels and other clinicopathological factors (e.g. serum alanine aminotransferase levels).

The ASGPR has been proposed as a promising hepatocyte-specific drug target. However, we found a wide spectrum of ASGR1 mRNA and protein expression in different patient liver samples. In contrast to the claims of several previous studies on ASGPR-targeted nanomedicines, here we show that this targeting approach may not be suited to the treatment of all HCC cases. Indeed, our results clearly suggest that only a subset of patients would benefit from such an ASGPR-targeted approach. Nonetheless, our study highlights that ASGPR assessment could be used in HCC patients to allow for careful preselection of patients[64] and to evaluate the possibility for an ASGPR-based therapeutic intervention in early stages of the disease.

Receptor-specific radiopharmaceuticals such as the technetium-99*m*-labeled asialoglycoprotein analog TcGSA offer the possibility of liver imaging and thus assessment of ASGPR receptor status.[65,66] This imaging agent is already approved in Japan. Other ASGPR-imaging approaches are in preclinical development such as targeted superparamagnetic iron oxide nanoparticles for magnetic resonance imaging.[67] The need for ASGPR-companion diagnostics can be demonstrated in a recent phase 1 clinical trial in HCC patients. The HPMA copolymer-doxorubicin conjugate PK2 (FCE28069) was developed to specifically target parenchymal liver cells via the ASGPR in patients with HCC.[68,69] The success rate was variable and only some patients showed a response.[68] This may be attributed to variable ASGPR expression levels in different patients, which would be consistent with our study, where we show lower and variable ASGR1 expression in HCC patients.

In the future, trace-labeled analogs of the nanomedicine product should be used in clinical trials to image the receptor status.[69] These theranostic strategies for combined therapy and imaging offer huge potential benefits.[70] The individual nanomedicine distribution in patients can be assessed to predict treatment outcomes and therefore pave the way for personalized medicine. Targeted nanomedicines may improve the intratumoral drug concentration and in addition trigger the uptake into hepatic cells. For example, in the case of PK2, the targeting ligand increased the intratumoral drug concentration in patients with ASGPR positive HCC up to 50-fold compared with the non-targeted polymer. However, further investigations are necessary to address possible side-effects on healthy hepatocytes that may express more ASGPR.

In summary, using a combination of *in vitro* and human-derived data, we highlight the importance of a detailed receptor expression assessment before using ASGPR-targeted therapeutics. Our *in vitro* results give important information as to the correct model cell lines to use to study ASGPR-targeted nanomedicines in the preclinical setting. Our human liver tissue-derived data shows the necessity to couple the development of ASGPR-targeted nanomedicines with companion diagnostics in order to achieve successful clinical outcomes. Increased ASGPR expression levels in patients with cirrhosis (and thus at higher risk of liver complications or HCC development) offer promising therapeutic options. Further studies to elucidate the ASGPR expression in patients with hepatitis or genetic diseases are needed to significantly increase the success rate of pharmacotherapies against hepatocyte-specific diseases.

ACKNOWLEDGMENTS

THE FINANCIAL SUPPORT Of the Swiss Centre of Applied Human Toxicology (SCAHT) is acknowledged. The authors thank Dr Adam Lister for editorial assistance. We thank the group of Professor Meyer zu Schwabedissen for support with qRT–PCR experiments. In addition, we thank Dr Birk Poller from Novartis (Basel, Switzerland) for providing PHH.

REFERENCES

1 Williams R. Global challenges in liver disease. *Hepatology* 2006; **44**: 521–6.
2 Poelstra K, Prakash J, Beljaars L. Drug targeting to the diseased liver. *J Control Release* 2012; **161**: 188–97.
3 Reddy LH, Couvreur P. Nanotechnology for therapy and imaging of liver diseases. *J Hepatol* 2011; **55**: 1461–6.

4 Rozema DB, Lewis DL, Wakefield DH, *et al.* Dynamic PolyConjugates for targeted in vivo delivery of siRNA to hepatocytes. *Proc Natl Acad Sci U S A* 2007; **104**: 12982–7.
5 Sebestyén MG, Wong SC, Trubetskoy V, *et al.* Targeted In Vivo Delivery of siRNA and an Endosome-Releasing Agent to Hepatocytes. *Methods Mol Biol* 2015; **1218**: 163–86.
6 Kanasty R, Dorkin JR, Vegas A, *et al.* Delivery materials for siRNA therapeutics. *Nat Mater* 2013; **12**: 967–77.
7 Wicki A, Witzigmann D, Balasubramanian V, *et al.* Nanomedicine in cancer therapy: Challenges, opportunities, and clinical applications. *J Control Release* 2015; **200**: 138–57.
8 Wu J, Nantz MH, Zern MA. Targeting hepatocytes for drug and gene delivery: emerging novel approaches and applications. *Front Biosci* 2002; **7**: d717–25.
9 Steirer LM, Park EI, Townsend RR, *et al.* The asialoglycoprotein receptor regulates levels of plasma glycoproteins terminating with sialic acid alpha2,6-galactose. *J Biol Chem* 2009; **284**: 3777–83.
10 Park EI, Mi Y, Unverzagt C, *et al.* The asialoglycoprotein receptor clears glycoconjugates terminating with sialic acid alpha 2,6GalNAc. *Proc Natl Acad Sci U S A* 2005; **102**: 17125–9.
11 Stockert RJ. The asialoglycoprotein receptor: relationships between structure, function, and expression. *Physiol Rev* 1995; **75**: 591–609.
12 Ashwell G, Harford J. Carbohydrate-Specific Receptors of the Liver. *Annu Rev Biochem* 1982; **51**: 531–54.
13 Rensen PC, Sliedregt LA, Ferns M, *et al.* Determination of the upper size limit for uptake and processing of ligands by the asialoglycoprotein receptor on hepatocytes in vitro and in vivo. *J Biol Chem* 2001; **276**: 37577–84.
14 Zhou X, Zhang M, Yung B, *et al.* Lactosylated liposomes for targeted delivery of doxorubicin to hepatocellular carcinoma. *Int J Nanomedicine* 2012; **7**: 5465–74.
15 Xiao Y, Zhang H, Zhang Z, *et al.* Synthesis of novel tetravalent galactosylated DTPA-DSPE and study on hepatocyte-targeting efficiency in vitro and in vivo. *Int J Nanomedicine* 2013; **8**: 3033–50.
16 Wang X, Sun H, Meng F, *et al.* Galactose-decorated reduction-sensitive degradable chimaeric polymersomes as a multifunctional nanocarrier to efficiently chaperone apoptotic proteins into hepatoma cells. *Biomacromolecules* 2013; **14**: 2873–82.
17 Barrett SE, Burke RS, Abrams MT, *et al.* Development of a liver-targeted siRNA delivery platform with a broad therapeutic window utilizing biodegradable polypeptide-based polymer conjugates. *J Control Release* 2014; **183**: 124–37.
18 Nair JK, Willoughby JLS, Chan A, *et al.* Multivalent N-acetylgalactosamine-conjugated siRNA localizes in hepatocytes and elicits robust RNAi-mediated gene silencing. *J Am Chem Soc* 2014; **136**: 16958–61.
19 Prakash TP, Graham MJ, Yu J, *et al.* Targeted delivery of antisense oligonucleotides to hepatocytes using triantennary N-acetyl galactosamine improves potency 10-fold in mice. *Nucleic Acids Res* 2014; **42**: 8796–807.
20 Castaño A, Drachman BM, Judge D, *et al.* Natural history and therapy of TTR-cardiac amyloidosis: emerging disease-modifying therapies from organ transplantation to stabilizer and silencer drugs. *Heart Fail Rev* 2014; **20**: 163–78.
21 Wooddell CI, Rozema DB, Hossbach M, *et al.* Hepatocyte-targeted RNAi Therapeutics for the Treatment of Chronic Hepatitis B Virus Infection. *Mol Ther* 2013; **21**: 973–85.
22 Sehgal A, Vaishnaw A, Fitzgerald K. Liver as a target for oligonucleotide therapeutics. *J Hepatol* 2013; **59**: 1354–9.
23 Lorenzer C, Dirin M, Winkler A-M, *et al.* Going beyond the liver: Progress and challenges of targeted delivery of siRNA therapeutics. *J Control Release* 2015; **203C**: 1–15.
24 Yan J-J, Liao J-Z, Lin J-S, *et al.* Active radar guides missile to its target: receptor-based targeted treatment of hepatocellular carcinoma by nanoparticulate systems. *Tumour Biol* 2014; **36**: 55–67.
25 Yang JD, Roberts LR. Hepatocellular carcinoma: A global view. *Nat Rev Gastroenterol Hepatol* 2010; **7**: 448–58.
26 Keating GM, Santoro A. Sorafenib: a review of its use in advanced hepatocellular carcinoma. *Drugs* 2009; **69**: 223–40.
27 Bruix J. Treatment of hepatocellular carcinoma. *Hepatology* 1997; **25**: 259–62.
28 Llovet JM, Ricci S, Mazzaferro V, *et al.* Sorafenib in advanced hepatocellular carcinoma. *N Engl J Med* 2008; **359**: 378–90.
29 Huwyler J, Cerletti A, Fricker G, *et al.* By-passing of P-glycoprotein using immunoliposomes. *J Drug Target* 2002; **10**: 73–9.
30 Peng D-J, Sun J, Wang Y-Z, *et al.* Inhibition of hepatocarcinoma by systemic delivery of Apoptin gene via the hepatic asialoglycoprotein receptor. *Cancer Gene Ther* 2007; **14**: 66–73.
31 Zhang M, Zhou X, Wang B, *et al.* Lactosylated gramicidin-based lipid nanoparticles (Lac-GLN) for targeted delivery of anti-miR-155 to hepatocellular carcinoma. *J Control Release* 2013; **168**: 251–61.
32 Stoller JK, Aboussouan LS. alpha 1-antitrypsin deficiency. *Lancet* 2005; **365**: 2225–36.
33 Ganz T. Hepcidin, a key regulator of iron metabolism and mediator of anemia of inflammation. *Blood* 2003; **102**: 783–8.
34 Gaumet M, Vargas A, Gurny R, *et al.* Nanoparticles for drug delivery: the need for precision in reporting particle size parameters. *Eur J Pharm Biopharm* 2008; **69**: 1–9.
35 Maeda H, Wu J, Sawa T, *et al.* Tumor vascular permeability and the EPR effect in macromolecular therapeutics: a review. *J Control Release* 2000; **65**: 271–84.
36 van Furth R, Cohn ZA, Hirsch JG, *et al.* The mononuclear phagocyte system: a new classification of macrophages, monocytes, and their precursor cells. *Bull World Health Organ* 1972; **46**: 845–52.
37 Bider MD, Cescato R, Jenö P, *et al.* High-affinity ligand binding to subunit H1 of the asialoglycoprotein receptor in the absence of subunit H2. *Eur J Biochem* 1995; **230**: 207–12.
38 Fuhrer C, Geffen I, Huggel K, *et al.* The two subunits of the asialoglycoprotein receptor contain different sorting information. *J Biol Chem* 1994; **269**: 3277–82.
39 Baumhoer D, Tornillo L, Stadlmann S, *et al.* Glypican 3 expression in human nonneoplastic, preneoplastic, and

neoplastic tissues: a tissue microarray analysis of 4,387 tissue samples. *Am J Clin Pathol* 2008; **129**: 899–906.
40 Quagliata L, Matter MS, Piscuoglio S, *et al.* Long noncoding RNA HOTTIP/HOXA13 expression is associated with disease progression and predicts outcome in hepatocellular carcinoma patients. *Hepatology* 2014; **59**: 911–23.
41 Lundquist P, Englund G, Skogastierna C, *et al.* Functional ATP-binding cassette drug efflux transporters in isolated human and rat hepatocytes significantly affect assessment of drug disposition. *Drug Metab Dispos* 2014; **42**: 448–58.
42 Weigel PH, Oka JA. The surface content of asialoglycoprotein receptors on isolated hepatocytes is reversibly modulated by changes in temperature. *J Biol Chem* 1983; **258**: 5089–94.
43 Kato J, Mogi Y, Kohgo Y, *et al.* Suppressive effect of ethanol on the expression of hepatic asialoglycoprotein receptors augmented by interleukin-1beta, interleukin-6, and tumor necrosis factor-alpha. *J Gastroenterol* 1998; **33**: 855–9.
44 Schwartz AL, Geuze HJ, Lodish HF. Recycling of the asialoglycoprotein receptor: biochemical and immunocytochemical evidence. *Philos Trans R Soc Lond B Biol Sci* 1982; **300**: 229–35.
45 Eto T, Takahashi H. Enhanced inhibition of hepatitis B virus production by asialoglycoprotein receptor-directed interferon. *Nat Med* 1999; **5**: 577–81.
46 van Zijl F, Mikulits W. Hepatospheres: Three dimensional cell cultures resemble physiological conditions of the liver. *World J Hepatol* 2010; **2**: 1–7.
47 Li Y, Tang Z-Y, Hou J-X. Hepatocellular carcinoma: insight from animal models. *Nat Rev Gastroenterol Hepatol* 2012; **9**: 32–43.
48 Heindryckx F, Colle I, Van Vlierberghe H. Experimental mouse models for hepatocellular carcinoma research. *Int J Exp Pathol* 2009; **90**: 367–86.
49 Bakiri L, Wagner EF. Mouse models for liver cancer. *Mol Oncol* 2013; **7**: 206–23.
50 Bagi CM, Andresen CJ. Models of hepatocellular carcinoma and biomarker strategy. *Cancers (Basel)* 2010; **2**: 1441–52.
51 Detampel P, Witzigmann D, Krähenbühl S, *et al.* Hepatocyte targeting using pegylated asialofetuin-conjugated liposomes. *J Drug Target* 2013; **22**: 232–41.
52 Kim TH, Park IK, Nah JW, *et al.* Galactosylated chitosan/DNA nanoparticles prepared using water-soluble chitosan as a gene carrier. *Biomaterials* 2004; **25**: 3783–92.
53 Ma J, Huang C, Yao X, *et al.* Inhibition of hepatitis B virus and induction of hepatoma cell apoptosis by ASGPR-directed delivery of shRNAs. *PLoS One* 2012; **7**: e46096.
54 Trahtenherts A, Benhar I. An Internalizing Antibody Specific for the Human Asialoglycoprotein Receptor. *Hybridoma* 2009; **28**: 225–33.
55 Khorev O, Stokmaier D, Schwardt O, *et al.* Trivalent, Gal/GalNAc-containing ligands designed for the asialoglycoprotein receptor. *Bioorg Med Chem* 2008; **16**: 5216–31.
56 Li J, Chen L, Zhang X, *et al.* Detection of circulating tumor cells in hepatocellular carcinoma using antibodies against asialoglycoprotein receptor, carbamoyl phosphate synthetase 1 and pan-cytokeratin. *PLoS One* 2014; **9**: e96185.
57 Yuzugullu H, Benhaj K, Ozturk N, *et al.* Canonical Wnt signaling is antagonized by noncanonical Wnt5a in hepatocellular carcinoma cells. *Mol Cancer* 2009; **8**: 90.
58 Shia MA, Lodish HF. The two subunits of the human asialoglycoprotein receptor have different fates when expressed alone in fibroblasts. *Proc Natl Acad Sci U S A* 1989; **86**: 1158–62.
59 Spiess M. The asialoglycoprotein receptor: a model for endocytic transport receptors. *Biochemistry* 1990; **29**: 10009–18.
60 Hyodo I, Mizuno M, Yamada G, *et al.* Distribution of asialoglycoprotein receptor in human hepatocellular carcinoma. *Liver* 1993; **13**: 80–5.
61 Trerè D, Fiume L, De Giorgi LB, *et al.* The asialoglycoprotein receptor in human hepatocellular carcinomas: its expression on proliferating cells. *Br J Cancer* 1999; **81**: 404–8.
62 Shi B, Abrams M, Sepp-Lorenzino L. Expression of asialoglycoprotein receptor 1 in human hepatocellular carcinoma. *J Histochem Cytochem* 2013; **61**: 901–9.
63 Rigopoulou EI, Roggenbuck D, Smyk DS, *et al.* Asialoglycoprotein receptor (ASGPR) as target autoantigen in liver autoimmunity: lost and found. *Autoimmun Rev* 2012; **12**: 260–9.
64 Ojha T, Rizzo L, Storm G, *et al.* Image-guided drug delivery: preclinical applications and clinical translation. *Expert Opin Drug Deliv* 2015; **12**: 1203–7.
65 Kokudo N, Vera DR, Makuuchi M. Clinical application of TcGSA. *Nucl Med Biol* 2003; **30**: 845–9.
66 Kobayashi K, Hattori N, Manabe O, *et al.* Postoperative Assessment of Hepatic Asialoglycoprotein Receptor Function with Tc-99 m GSA: The Safety Margin of Resection Size in Living Donor Liver Transplantation. *Ann Transplant* 2015; **20**: 51–8.
67 Huang G, Diakur J, Xu Z, *et al.* Asialoglycoprotein receptor-targeted superparamagnetic iron oxide nanoparticles. *Int J Pharm* 2008; **360**: 197–203.
68 Seymour LW, Ferry DR, Anderson D, *et al.* Hepatic Drug Targeting: Phase I Evaluation of Polymer-Bound Doxorubicin. *J Clin Oncol* 2002; **20**: 1668–76.
69 Julyan PJ, Seymour LW, Ferry DR, *et al.* Preliminary clinical study of the distribution of HPMA copolymers bearing doxorubicin and galactosamine. *J Control Release* 1999; **57**: 281–90.
70 Theek B, Rizzo LY, Ehling J, *et al.* The Theranostic Path to Personalized Nanomedicine. *Clin Transl Imaging* 2014; **2**: 66–76.

Supporting Information

Additional supporting information may be found in the online version of this article at the publisher's web site.

Hepatology Research

SUPPLEMENTARY INFORMATION

Variable asialoglycoprotein receptor 1 expression in liver disease: Implications for therapeutic intervention

Dominik Witzigmann,[1] Luca Quagliata,[2] Susanne H. Schenk,[1] Cristina Quintavalle,[2] Luigi M. Terracciano[2] and Jörg Huwyler[1]

[1]*Division of Pharmaceutical Technology, Department of Pharmaceutical Sciences; and* [2]*Institute of Pathology, Molecular Pathology Division, University Hospital of Basel, Basel, Switzerland*

*** Author for correspondence:**
Prof. Dr. Jörg Huwyler
phone: +41 (0)61 267 15 13
e-mail: joerg.huwyler@unibas.ch

Supplementary Methods

Cell Lines

Liver cancer-derived lines HepG2, PLC/PRF/5, Hep3B, Sk-Hep1, and SNU449 were obtained from the cell depository of the Institute of Pathology, University Hospital of Basel, Switzerland. HuH6 and HuH7 were obtained from RIKEN Cell Bank (Ibaraki, Japan). HLE was obtained from the Health Science Research Resources Bank (Osaka, Japan). Mahlavu was kindly provided by Sanofi Aventis. Prof. Dr. Dietrich von Schweinitz (University Hospital Basel, Switzerland) kindly provided the HepT1 cell line [1]. The stable mouse NIH/3T3 fibroblast cell line 1-7-1, which expresses both ASGPR subunits, was provided by Prof. Dr. Martin Spiess [2]. LiverPool 20-Donor Mixed Gender Pooled Cryopreserved Human Hepatocytes were obtained from BioreclamationIVT. All cell lines were cultured as recommended by the provider.

Relative mRNA expression analysis of *ASGR1 in vitro* using qRT-PCR

Total RNA for the quantitative real-time polymerase chain reaction (qRT-PCR) was isolated from cell lines at 80% confluence using TRI Reagent (Sigma Aldrich) according to the manufacturer's recommendation. Total RNA from Cryopreserved Human Hepatocytes was extracted directly after thawing using TRI reagent. After a DNAse digest, cDNA was synthesized using the ProtoScript M-MuLV Kit (New England BioLabs) with random hexamer primers. qRT-PCR for the quantification of *ASGR1* mRNA expression was performed using predeveloped TaqManAssays (Invitrogen, Life Technologies) as described elsewhere [3]. The measurements of *ASGR1* mRNA (Hs01005019_m1) were normalized to four different housekeeping genes, namely beta-actin (Hs99999903_m1), GAPDH (4310884E), PPIA (Hs99999904_m1), and RPLP0 (Hs99999902_m1). Relative mRNA expression in different cell lines was calculated using the standard $\Delta\Delta C_t$ method [4].

Flow Cytometry and Immunofluorescence

Quantitative analysis of ASGR1 protein expression in the different cell lines was performed using flow cytometry analysis. The cells were incubated with the primary anti-ASGR1 antibody (HPA011954; Prestige Antibodies®, dilution 1:25) at RT for 45 min, followed by incubation at 4°C with secondary R-PE GαR antibody (Invitrogen, Life Technologies, dilution 1:200) for 60 min. Cells were excited at 561 nm and doublets were excluded. The fluorescence signal of R-PE was detected in FL5 (586/15). To analyze the relative ASGR1 protein expression FlowJo VX software (TreeStar) was used.

Immunofluorescence analysis for qualitative assessment of ASGR1 protein expression was performed using confocal laser scanning microscopy (CLSM). Cell lines were seeded on poly-D-lysin coated coverslips and allowed to adhere for 24 hours. Cells were fixed with 4% paraformaldehyde for 15 min and incubated with the primary anti-ASGR1 antibody (HPA011954; Prestige Antibodies®, dilution 1:25) one hour at RT. After three washing steps the secondary Alexa Fluor® 488 GαR antibody (Invitrogen, Life Technologies, dilution 1:400) was added and cells were incubated overnight at 4°C. After additional washing steps the nuclei were counterstained using Hoechst 33342 (1 μg/mL). Finally, the cover slips were embedded in Prolong Gold antifade reagent (Invitrogen, Life Technologies). The cells were excited at 488 nm and the fluorescence was measured above 516 nm. Background fluorescence was assessed using unstained cells.

Relative mRNA expression of *ASGR1* in human liver tissue samples

RNA for the microarray was isolated and handled as previously described [5]. Briefly, extracted RNA quality and quantity were analysed with the Bioanalyzer 2100 using the RNA6000 Chip (Agilent). DNAse-treated total RNA (270 ng) was subjected to target synthesis using the WT Expression kit (Ambion) following standard recommendations. Then the array was hybridised. The GeneChips were scanned with an Affymetrix GeneChip Scanner 3000. DAT images and CEL files of the microarrays were generated using Affymetrix GeneChip Command Control (v4.0). CEL files were imported into Qlucore software and Robust Multichip Average (RMA), normalized, and principal component analysed. Quantile normalization and data processing were performed using the GeneSpringGXv11.5.1 software package (Agilent). The gene signature value was

assessed using the BRB-ArrayTool (v4.3.2, NIH). Ingenuity software (Qiagen) was used to perform pathway analysis.

Tissue Microarray (TMA) and Immunohistochemistry

TMA sections (4 μm thick) were immuno-stained with an anti-ASGR1 primary antibody (Prestige Antibodies®, dilution 1:50) or an anti-CD3 primary antibody (Dako, dilution 1:1600), followed by a HRP-conjugated secondary antibody using a ventana system (Roche Diagnostics). Finally, the slides were stained with hematoxylin and eosin. ASGR1 protein immunoreactivity was scored semi-quantitatively by evaluating the staining intensity as described by Allred *et al.* [6] (0=negative for ASGR1 and 3=highest intensity of ASGR1). Clinico-pathological data of the different HCC subsets are summarized in Supplementary Table 1. CD3 protein staining was scored as % of infiltrating inflammatory cells.

Supplementary Figures

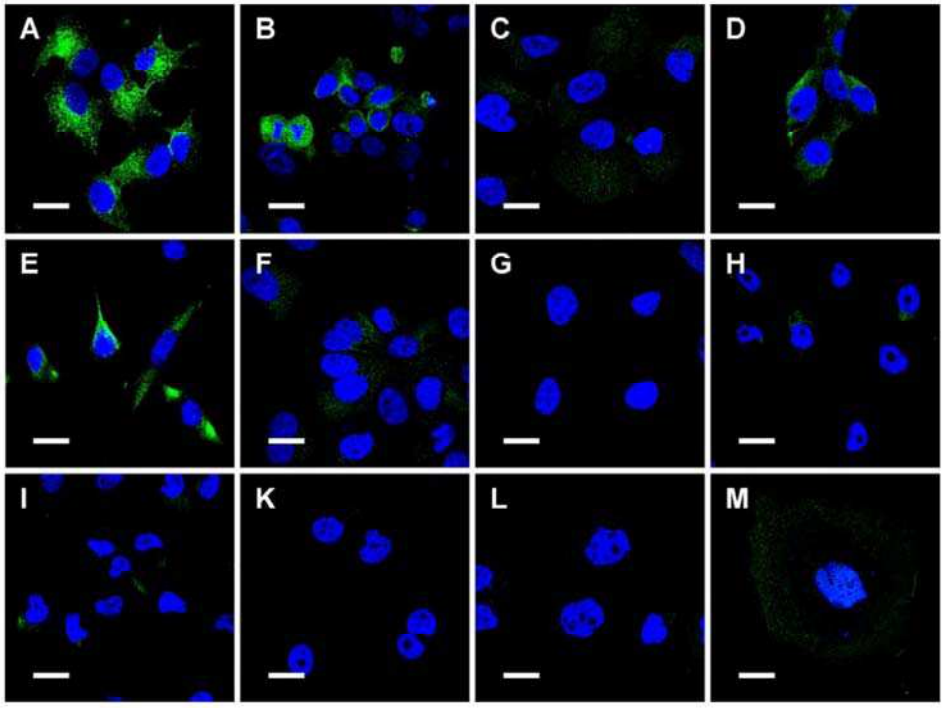

Figure S1. Qualitative evaluation of ASGR1 protein expression in different cell lines by confocal laser scanning microscopy analysis. Representative immunofluorescence images of ASGR1 protein (green) expression in different liver cancer-derived cell lines such as (a) HepG2, (b) PLC/PRF/5, (c) Hep3B, (d) HuH6, (f) HuH7, (g) SNU449, (h) Sk-Hep1, (i) Mahlavu, (k) HLE, and (l) HepT1. Panel (m) shows primary human hepatocytes (PHH), and panel (e) the human ASGPR-expressing mouse fibroblast cell line 1-7-1. Scale bars represent 20 μm.

Supplementary Tables

Supplementary Table 1: Summary of ASGR1 protein levels in correlation with clinico-pathological factors. Semi-quantitative evaluation of staining intensity in hepatocellular carcinoma (n = 184) tissue specimens by tissue microarray (TMA) analysis. Results were analyzed using the Chi-square test (χ^2 test). Corresponding *p* values are given.

Factors		ASGR1 Staining Score n (%)					
		0	1	2	3	$\chi 2$	*p*
Age	</=65	27 (57.4)	8 (17.0)	9 (19.1)	3 (6.4)	2.682	0.4433
	>65	80 (58.4)	34 (24.8)	19 (13.9)	4 (2.9)		
Gender	Female	22 (56.4)	9 (23.1)	6 (15.4)	2 (5.1)	0.02821	0.9988
	Male	85 (58.6)	33 (22.8)	22 (15.2)	5 (3.4)		
Nstage (11 missing values)	0	87 (54.0)	40 (24.8)	27 (16.8)	7 (4.3)	4.551	0.2078
	1	10 (83.3)	2 (16.7)	0 (0.0)	0 (0.0)		
Tstage (18 missing values)	1-2	61 (52.6)	29 (25.0)	21 (18.1)	5 (4.3)	2.416	0.4907
	3-4	32 (64.0)	11 (22.0)	5 (10.0)	2 (4.0)		
Mstage (11 missing values)	0	80 (53.3)	37 (24.7)	26 (17.3)	7 (4.7)	4.805	0.1867
	1	17 (73.9)	5 (21.7)	1 (4.3)	0 (0.0)		
Edmondson stage (4 missing values)	Well (I)	38 (52.1)	18 (24.7)	16 (21.9)	1 (1.4)	9.718	0.1370
	Moderate (II)	47 (57.3)	21 (25.6)	9 (11.0)	5 (6.1)		
	Poor (III)	19 (76.0)	3 (12.0)	2 (8.0)	1 (4.0)		
Multifocality (9 missing valucs)	No	38 (49.4)	22 (28.6)	14 (18.2)	3 (3.9)	3.693	0.2966
	Yes	62 (63.3)	19 (19.4)	13 (13.3)	4 (4.1)		
Vascular Invasion (25 missing values)	No	53 (54.6)	27 (27.8)	13 (13.4)	4 (4.1)	4.152	0.2455
	Yes	38 (61.3)	9 (14.5)	12 (19.4)	3 (4.8)		
Etiology (62 missing values)	Alcohol	20 (62.5)	9 (28.1)	2 (6.3)	1 (3.1)	3.302	0.3474
	Viral Infection	48 (53.3)	21 (23.3)	18 (20.0)	3 (3.3)		

Supplementary Table 2: Summary of ASGR1 protein expression on cell membrane in tissue samples from normal liver, hepatocellular carcinoma (HCC), and cirrhotic nodules. Qualitative evaluation of ASGR1 membrane expression in ASGR1 protein positive samples from normal liver (n = 45), HCC (n = 77), and cirrhotic nodules (n = 65) was performed using tissue microarray (TMA). Results were analyzed using the Chi-square test (χ^2 test). Corresponding *p* values are given.

Tissue Type	ASGR1 Membrane Score n (%)			
	0	1	$\chi 2$	*p*
Normal liver	14 (31.1)	31 (68.9)	13.030	0.0003
HCC	50 (64.9)	27 (35.1)		
Normal liver	14 (31.1)	31 (68.9)	28.400	< 0.0001
Cirrhotic nodules	53 (81.5)	12 (18.5)		
Cirrhotic nodules	53 (81.5)	12 (18.5)	4.887	0.0272
HCC	50 (64.9)	27 (35.1)		

Supplementary References

1 Pietsch T, Fonatsch C, Albrecht S, et al. Characterization of the continuous cell line HepT1 derived from a human hepatoblastoma. *Lab Invest* 1996;74:809-818.

2 Bider MD, Cescato R, Jenö P, et al. High-affinity ligand binding to subunit H1 of the asialoglycoprotein receptor in the absence of subunit H2. *Eur J Biochem* 1995;230:207-212.

3 Meyer Zu Schwabedissen HE, Begunk R, Hussner J, et al. Cell-specific expression of uptake transporters--a potential approach for cardiovascular drug delivery devices. *Mol Pharm* 2014;11:665-672.

4 Schmittgen TD, Livak KJ. Analyzing real-time PCR data by the comparative C(T) method. *Nat Protoc* 2008;3:1101-1108.

5 Quagliata L, Matter MS, Piscuoglio S, et al. Long noncoding RNA HOTTIP/HOXA13 expression is associated with disease progression and predicts outcome in hepatocellular carcinoma patients. *Hepatology* 2014;59:911-923.

6 Allred DC, Harvey JM, Berardo M, et al. Prognostic and predictive factors in breast cancer by immunohistochemical analysis. *Mod Pathol* 1998;11:155-168.

Chapter IV

"Hepatocyte Targeting Using Pegylated Asialofetuin-Conjugated Liposomes"

Detampel P, Witzigmann D, Krähenbühl S, Huwyler J.

Journal of Drug Targeting. 2013 Dec 13; 22(3):232-41.

doi: 10.3109/1061186X.2013.860982

http://www.tandfonline.com/doi/abs/10.3109/1061186X.2013.860982?journalCode=idrt20

Highlights: Active drug targeting to parenchymal liver cells improves therapeutic efficacy in the liver and reduces side effects in non-diseased tissues such as the spleen. This study aimed to develop a hepatocyte-specific drug delivery strategy using pegylated liposomes modified with asialofetuin. Active targeting of the hepatic asialoglycoprotein receptor (ASGPR) and internalization via receptor-mediated endocytosis was studied *in vitro* and confirmed *in vivo* in the rat. Different types of encapsulated model compounds, including membrane-linked fluorochromes and quantum dots, were used to demonstrate the feasibility of the targeting strategy. This study is the first successful attempt to target the hepatic ASGPR with ligand-conjugated, pegylated liposomes. This approach might be instrumental to implement novel drug targeting strategies for the treatment of hepatic diseases.

Journal of Drug Targeting

http://informahealthcare.com/drt
ISSN: 1061-186X (print), 1029-2330 (electronic)

J Drug Target, 2014; 22(3): 232–241
 DOI: 10.3109/1061186X.2013.860982

informa healthcare

Hepatocyte targeting using pegylated asialofetuin-conjugated liposomes

Pascal Detampel[1], Dominik Witzigmann[1], Stephan Krähenbühl[2], and Jörg Huwyler[1]

[1]Department of Pharmaceutical Sciences, Division of Pharmaceutical Technology, University of Basel, Basel, Switzerland, and [2]Division of Clinical Pharmacology and Toxicology, University Hospital, Basel, Switzerland

Abstract

Background and purpose: The hepatocyte asialoglycoprotein receptor mediates uptake of desiaylated glycoproteins by receptor-mediated endocytosis. This work explores a hepatocyte-specific targeting strategy using asialofetuin (AF) covalently coupled to pegylated liposomes. *Methods*: AF was conjugated to the distal end of polyethylene glycol–functionalized phospholipids. Chemical modification of AF did not interfere with its receptor interaction. AF-liposomes had a size of less than 130 nm, were judged to be monodisperse and were labelled with fluorescent organic dyes or loaded with quantum dots.
Results: *In vitro*, binding and cellular uptake of fluorescent AF-liposomes by HepG2 hepatocellular carcinoma cells were reduced at low temperature and could be competitively inhibited by an excess of unbound AF. Hepatocyte-specific targeting and internalization of AF-liposomes *in vivo* was confirmed in the rat and could be competitively inhibited by co-injection of unbound AF. In contrast, non-pegylated liposomes accumulated in cells of the reticulo-endothelial system such as hepatic Kupffer cells and spleen after intravenous administration.
Conclusion: We conclude that the use of AF-conjugated, pegylated liposomes is a promising strategy to avoid the reticuloendothelial system and specifically target hepatocytes via the asialoglycoprotein receptor *in vitro* as well as *in vivo*.

Keywords

Asialofetuin, asialoglycoprotein receptor, hepatocyte, HepG2, liver targeting, quantum dots

History

Received 2 September 2013
Revised 18 October 2013
Accepted 28 October 2013
Published online 12 December 2013

Introduction

Incidence rates of hepatic diseases have steadily increased over the past decades, but available pharmacotherapies are often not optimal [1]. Delivery of compounds specifically to hepatocytes (i.e. the liver parenchymal cells accounting for approximately 80% of liver cell mass) would be desirable, for instance, in chronic hepatitis caused by hepatitis B virus (HBV) and hepatitis C virus (HCV) [2,3], non-alcoholic steatohepatitis [4] and hepatocellular carcinoma (HCC) [5]. Moreover, delivery of genes would offer interesting therapeutic opportunities in genetic disorders such as Wilson's disease, α1-antitrypsin deficiency, hereditary hemochromatosis and certain coagulopathies.

Specific targeting of drugs to the liver can be achieved using particulate drug carriers such as liposomes [6]. However, a major problem associated with this approach is the unspecific phagocytic uptake of nanoparticles and conventional, non-pegylated liposomes by cells of the immune system. This leads to a very short half-life of these particles in the circulation and their accumulation in cells of the reticuloendothelial system (RES), such as hepatic Kupffer cells [6]. To overcome this limitation, the surface of particles can be modified by covalent attachment of polyethylene glycol (PEG) [7]. The hydrophilic PEG corona increases the colloidal stability of particles, hinders the adsorption of plasma proteins, minimizes nonspecific accumulation in liver and spleen, and reduces systemic particle clearance.

Passive targeting of solid tumours with pegylated liposomes has become an established therapy in various oncological indications. However, some malignancies cannot be treated effectively in this way. In particular, pegylated liposomes with doxorubicin are not effective against HCC [8]. Moreover, treatment of HCV infection necessitates drug delivery to hepatocytes [9]. Virus latency in these cells may lead to a phenotype, which is identical to one of the healthy cells. Therefore, alternative strategies to target hepatocytes are needed.

The most promising strategy to target hepatocytes is via the asialoglycoprotein receptor (ASGPR), which is predominantly expressed on liver parenchymal cells [10] where it exhibits a high affinity for terminal D-galactose (Gal) and N-acetyl-D-galactosamine (GalNAc) residues of glycans from glycoproteins [11,12]. In addition, similar binding affinities between various mammalian species make this receptor an ideal target to develop active drug delivery strategies for hepatocytes. Gal attached to the surface of liposomes was used in several studies, albeit with variable success [13–15]). The binding affinity of bi- and tri-antennary glycan residues towards the ASGPR is two to four orders of magnitude stronger than that of isolated Gal or mono-antennary glycans [10,16]. The naturally occurring glycoprotein AF, for example, carries multiple Gal-terminated bi- and

Author for correspondence: Prof. Dr. Jörg Huwyler, Department of Pharmaceutical Sciences, Division of Pharmaceutical Technology, University of Basel, Klingelbergstrasse 50, CH-4056 Basel, Switzerland. Tel: +41 (0)61 267 15 13. E-mail: joerg.huwyler@unibas.ch

DOI: 10.3109/1061186X.2013.860982

tri-antennary glycans [17]. AF was previously used as a targeting vector for liposomes and showed a predominant uptake by hepatocytes *in vitro* and *in vivo* [18–22]. However, studies performed with Gal- or AF-conjugated liposomes exhibited marked variability with respect to the extent and specificity of the uptake by hepatocytes, probably because all of them employed conventional, non-pegylated liposomal formulations.

This study aimed to develop and validate a drug targeting strategy for hepatocytes *in vitro* and *in vivo*. AF was attached to pegylated liposomes using PEG as a linker, allowing AF to be flexibly tethered to the liposome surface. Cellular binding and intracellular accumulation of AF-PEG-liposomes were studied *in vitro* using the hepatocellular carcinoma cell line HepG2. Specific targeting of hepatocytes and avoidance of the RES *in vivo* were demonstrated in the rat. Different types of encapsulated model compounds, including membrane-linked fluorochromes and quantum dots (QDs), were used to demonstrate the feasibility of the targeting strategy.

Materials and methods

Materials

Asiaolofetuin (AF, Lot. 069K7425V), 5(6)-carboxyfluorescein (CF), 5(6)-carboxyfluorescein N-hydroxysuccinimide ester (CF-NHS), cholesterol, 2-iminothiolane (Traut's reagent), 5,5-dithiobis(2-nitrobenzoic acid) [Ellman's reagent], poly-D-lysine hydrobromide (mol wt 70 000–150 000), Hoechst 33342, 7-amino-actinomycin D (7-AAD), Mowiol 4-88 and all other reagents were of analytical grade and were obtained from Sigma-Aldrich (Buchs, Switzerland). The lipids 1,2-distearoyl-sn-glycero-3-phosphocholine (DSPC), 1,2-distearoyl-sn-glycero-3-phosphoethanolamine (DSPE), DOPE-N-(carboxyfluorescein) [PE-CF], DSPE-N-(polyethyleneglycol-2000) [DSPE-PEG(2000)], DSPE-N-(maleimide polyethyleneglycol-2000) [DSPE-PEG(2000)-Mal] and DOPE-N-(lissamine rhodamine B sulfonyl) [PE-Rho] were purchased from Avanti Polar-Lipids (Alabaster, AL). QDot 625 ITK was obtained from Invitrogen, Life Technologies (Zug, Switzerland). The modified Lowry protein assay kit and CBQCA protein quantification kit were obtained from Pierce (Rockford, IL) and Molecular Probes (Eugene, OR), respectively, and were used with bovine serum albumin (BSA) or AF as a standard.

Fluorescent labelling of asialofetuin

AF was labelled with CF-NHS by cross-linking the N-terminus of the protein backbone or the ε-amines of lysine side chains. In brief, AF was incubated together with a 10-fold excess of CF-NHS in a $NaHCO_3$ buffer (50 mM, pH 8.5) for 2 h on ice. Excess of CF-NHS was removed by FPLC size exclusion chromatography using a Sephadex G-50 fine column (1.6 cm × 20 cm, GE Healthcare) eluting with 0.01 M phosphate-buffered saline (PBS; 0.01 M phosphate and 150 mM sodium chloride), pH 7.2. Eluates were stored at –20 °C. Final protein concentration was determined using a modified Lowry protein assay. The degree of fluorescent labelling was calculated based on absorbance measurements at 280 nm using different molar extinction coefficients for protein and fluorescent dye.

Preparation and characterization of liposomes

Thiolation of proteins and coupling to pegylated liposomes through maleimide-functionalized lipids were done as described previously [23]. In brief, AF (2.7 mg, 60 nmol) was dissolved in a buffer containing 0.1 M phosphate and 1 mM ethylenediaminetetraacetic acid (EDTA), pH 8. All experiments were carried out with the same batch of AF. The solution was thiolated with a 200-fold molar excess of Traut's (2-iminothiolane) reagent for 1 h at room temperature. Thiolated AF was purified and concentrated in Amicon Ultra-4 centrifugal filter units, 10 kDa cut-off (Millipore, Zug, Switzerland), with 0.1 M PBS containing 1 mM EDTA, pH 7.2. The amount of attached sulfhydryl groups was determined by Ellman's reaction [23], using a freshly prepared cysteine solution as a standard. In parallel, DSPC (5.5 μmol), cholesterol (4.5 μmol), DSPE-PEG(2000) (0.27 μmol), DSPE-PEG(2000)-Mal (0.06 μmol) and PE-Rho (0.04 μmol) or PE-CF (0.04 μmol) were dissolved in chloroform/methanol (2:1, v/v). For conventional, non-pegylated liposomes, DSPE-PEG(2000) and DSPE-PEG(2000)-Mal were replaced by DSPE (0.33 μmol). Solvent was removed at 60 °C using a Rotavapor A-134 (Büchi, Switzerland). After 1 h, a homogenous dry lipid film was formed, which was hydrated for 10 min at 60 °C by agitation after addition of 3 g glass beats (diameter 5 mm) and 1 ml of 0.1 M PBS containing 1 mM EDTA, pH 7.2. For passive loading of carboxyfluorescein, the hydration buffer was supplemented with 5(6)-carboxyfluorescein (60 mM). The resulting multilaminar vesicles were subjected to five freeze-thaw cycles. Liposomes were extruded at 60 °C five times through a polycarbonate membrane with a pore size of 100 nm (Avanti Polar-Lipids, Alabaster, AL) and nine times through a membrane with a pore size of 50 nm. For AF conjugation, the thiolated protein was mixed with liposomes and incubated overnight at room temperature. Conjugated liposomes were purified by size exclusion chromatography using a Superose 6 prep column (1.6 cm × 20 cm, GE Healthcare) eluting with 0.01 M PBS, pH 7.2. Average liposomal sizes and zeta potential were measured by dynamic and electrophoretic light scattering, respectively, using a Delsa Nano C (Beckman Coulter, Nyon, Switzerland). Liposomes loaded with QDs were prepared with the following modifications: Lipids were hydrated in a 100-nM solution of QDs 625 ITK in 0.1 M PBS containing 1 mM EDTA, pH 7.2, and extrusion was performed five times through a 200-nm filter, followed by nine extrusions through an 80 nm filter. The amount of AF coupled to liposomes was measured by the CBQCA protein quantification kit (Molecular Probes, Life Technologies, Grand Island, NY). Lipid content was either calculated based on peak areas from size exclusion chromatography or determined by a modified Stewart assay [24], using DSPC as a standard. In brief, samples were incubated with chloroform:aqueous 0.1 M ammonium ferrothiocyanate (1:1; v/v), vortexed and centrifuged at 300 *g* for 5 min at room temperature. Absorbance of the chloroform layer was measured at a wavelength of 485 nm.

Cell culture

HepG2 cells were kindly provided by Prof. Dr. Dietrich von Schweinitz (University Hospital Basel, Switzerland). The

cells were cultured at 37 °C under 5% CO_2 and saturated humidity in DMEM low glucose (1 g/l) containing 10% foetal bovine serum (FBS), 0.1 mM non-essential amino acids (NEAA), 2 mM Glutamax and 10 mM Hepes (all obtained from Gibco, Life Technologies). Cells were confirmed to be free of mycoplasma (MycoAlert, Lonza, Rockland, ME).

In vitro uptake assay and confocal fluorescence microscopy

HepG2 cells were cultured on poly-D-lysine-coated glass cover slips (#1.5, Menzel, Braunschweig, Germany). Cells were washed with warm D-PBS (Gibco) and pre-incubated for 1 h in DMEM low glucose without phenol red. For competition experiments, free AF was added to the medium during the pre-incubation period. Cells were incubated for the indicated period with AF-CF or liposomes conjugated with AF-PEG at 4 °C or 37 °C. Nucleus counterstaining was performed by adding Hoechst 33342 (1 μg/ml) during the last 5 min of the uptake experiment. Cells were washed three times with cold D-PBS and fixed for 15 min with 2% paraformaldehyde at 4 °C. After an additional washing step, slides were embedded in Prolong Gold antifade reagent (Gibco) and sealed with nail polisher after drying. Samples were analysed with an Olympus FV-1000 inverted confocal fluorescence microscopy (Olympus Ltd., Tokyo, Japan), using a 60x PlanApo N oil-immersion objective (numerical aperture 1.40). Images were processed using either Imaris software (version 7.4, Bitplane, Zürich, Switzerland) or Gimp 2.8 software (GNU image manipulation programme, http://www.gimp.org). Liposomes containing QDs were activated by illumination at 400 nm (210 mW/cm^2) or 490 nm (190 mW/cm^2), using a pE-2 LED (CoolLED, Andover, UK) excitation system. Lambda scans of images containing QDs were done with a fixed excitation wavelength of 488 nm and variable emission between 550 nm and 700 nm, with a bandwidth of 10 nm and step size of 2 nm. Defined regions of interest (ROIs) were analysed using the Olympus Fluoview software (version 3.1, Olympus).

Flow cytometry

Uptake experiments and competition studies were performed as described above. Cells were washed three times with cold D-PBS and detached using Accutase (Sigma-Aldrich), followed by centrifugation at 200 *g* for 5 min at 4 °C and resuspended in staining buffer containing D-PBS, 2% FCS and 0.1% NaN_3. To exclude fluorescence signal of surface bound carboxyfluorescein-conjugates, trypan blue (0.2%) was added as a quenching agent [25]. For analysing extracellular ASGPR, cells were incubated in staining buffer with mouse anti-human ASGPR-1/2 IgG (diluted 1:40) for 30 min at 20 °C. After washing and centrifugation (200 *g* for 5 min at 4 °C), the cells were incubated with goat anti-mouse-RPE (diluted 1:200) in staining buffer (30 min at 20 °C). To exclude apoptotic cells, 7-AAD (2 μg/ml) was added to the cell suspension at least 20 min prior to analysis. Flow cytometry analysis of 10 000 to 20 000 cells was carried out using a FACS Canto II flow cytometer (Becton Dickinson, San Jose, CA) and FlowJo VX software (TreeStar, Ashland, OR). The cells were excited at 488 nm and apoptotic cells were excluded using FL2 (685LP – 695/40). The fluorescence signal of CF was detected in fluorescence channel FL1 (505LP – 530/30).

Animal experiments

All animal experiments were carried out in accordance with the Swiss legislation on animal welfare. Male CD rats (300 g body weight, $n = 3$ animals for each experiment) with catheterized jugular vein were obtained from Charles River Laboratories (L'Arbresle Cedex, France). Non-pegylated liposomes (nominal 3 μmol phospholipids per animal), AF-PEG-liposomes (nominal 3 μmol phospholipids per animal), free AF in 0.9% NaCl (7 mg per animal) or a carbon black solution (1 ml/kg body weight, diluted 1:9 using 0.9% NaCl; Pelikan, Hannover, Germany) were injected intravenously. Animals were euthanized after 30 min, liver and spleen tissue were snap-frozen in isopentan/liquid nitrogen, and cryosections of 10 μm were prepared. After drying the samples on Superfrost Plus Ultra G 90 microscope slides (Menzel), samples were washed with D-PBS and fixed with 2% PFA for 15 min at 20 °C. Slides were counterstained with Hoechst 33342 (1 μg/ml), mounted in Mowiol 4-88/p-phenylenediamine (9:1, v/v), and analysed by microscopy as described above.

Results

Asialofetuin as a vector

Specific binding and uptake of AF by ASGPR was studied *in vitro* using human hepatoma HepG2 cells. Control experiments (data not shown) confirmed expression of the ASGP receptor by HepG2 cells. Desialated glycoprotein AF was labelled with carboxyfluorescein-NHS. After purification by size exclusion chromatography, the degree of labelling was calculated to be in the range of 3.0 to 4.2 fluorophore molecules per molecule of protein. Incubating HepG2 cells for 20 min with 0.23 μM fluorescent-labelled AF (corresponding to 10 μg/ml) resulted in a particulate fluorescent staining pattern (Figure 1A). This concentration is around 10 000 times lower than the concentration CF starts to self-quench. Therefore, quenching effects were excluded. Competitive inhibition of cellular binding and uptake was achieved in the presence of a 100-fold excess of unlabelled AF (Figure 1A, inset).

Flow cytometry analysis of HepG2 cells incubated with 0.23 μM of fluorescent AF (Figure 1B) confirmed the uptake of labelled AF by the majority of target cells. Specificity of AF binding was demonstrated by competitive inhibition in the presence of unlabelled AF. Uptake rather than binding was confirmed by incubation at lower temperature (4 °C) (Figure 1C) and trypan blue quenching (Figure 1D). AF-CF is not degraded upon prolonged storage (several months at 4 °C) and showed the same results in control experiments (data not shown). In contrast, incubation with fluorescent-labelled galactose resulted in considerably lower fluorescent signals, even at receptor ligand concentrations that were higher by two logarithmic orders (data not shown).

Liposomal preparation

After optimizing the vector for targeting ASGPR on the surface of hepatocytes, AF-conjugated liposomes loaded with

DOI: 10.3109/1061186X.2013.860982

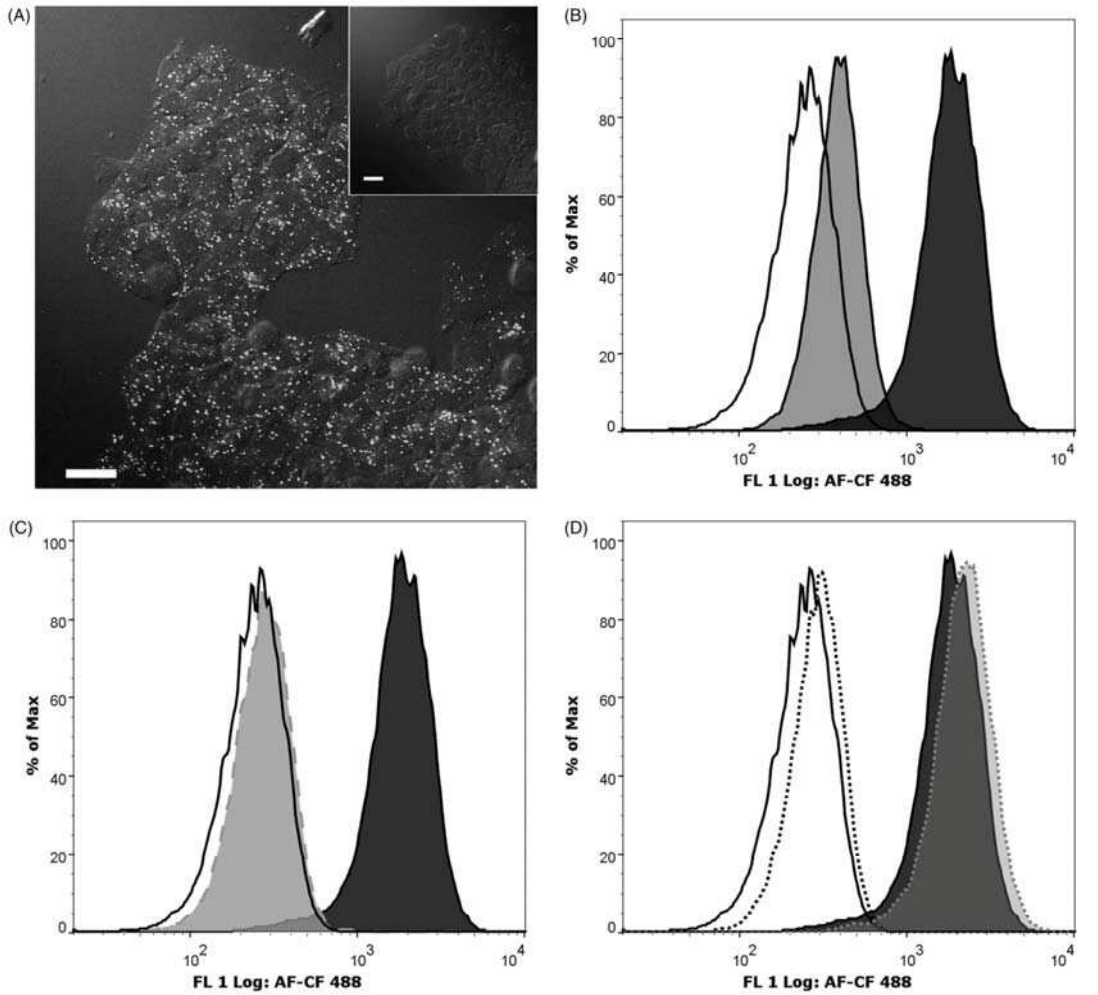

Figure 1. Uptake of fluorescent-labelled AF by HepG2 cells. Panel A: HepG2 cells were incubated for 20 min with carboxyfluorescein-coupled AF and analysed by confocal fluorescence microscopy. An overlay of the fluorescence signal with a differential interference contrast image is shown. Competitive binding inhibition of fluorescent AF was achieved by using a 100-fold excess of unlabelled AF (insert). Scale bars = 20 µm. Panel B/C/D: Flow cytometry analysis of HepG2 cells incubated for 20 min. Incubation with carboxyfluorescein-coupled AF (black histogram) and untreated control cells (white histogram) are shown. Panel B: Competitive inhibition of fluorescent AF binding using a 100-fold excess of unlabelled AF (grey histogram). Panel C: Incubation at 4 °C (grey histogram, dashed line). Panel D: Quenching of surface bound signals with trypan blue for control cells (white histogram, dotted line) and carboxyfluorescein-coupled AF incubated cells (grey histogram, dotted line). Horizontal axis: relative fluorescence intensity of signal collected in FL1 (see Materials and methods). Viable cells were gated based on 7-AAD exclusion.

different fluorescent cargos were prepared to study *in vitro* and *in vivo* targeting strategies. Maleimide-functionalized pegylated phospholipids were incorporated into the liposomal formulation (Figure 2A). Chemical coupling of thiolated AF resulted in the formation of a metabolically stable thioether bond. The size of unilamellar liposomes was adjusted by extrusion through polycarbonate filters with a defined pore size. Depending on the lipid mixture and cargo, vesicles with a particle size between 88 nm and 126 nm were obtained (Table 1). The size distribution of liposomes was narrow as judged by a polydispersity index of less than 0.12. All colloid preparations had a moderate anionic zeta potential (Table 1).

Adding small amounts of pegylated lipids to liposomes resulted in a significantly smaller particle size, compared to their non-pegylated variants. This phenomenon can be attributed to dehydration of the lipid bilayer which enhances the lateral packing of the fatty acid acyl chains [26]. The addition of pegylated phospholipids considerably facilitated the force needed for the extrusion process, increased the apparent stability and was a prerequisite for *in vivo* targeting of hepatocytes. Liposomes loaded with QDs were extruded through a filter with a pore size of 80 nm only. Extrusion through 50 nm filters was not possible, resulting in slightly larger vesicles. Liposomal formulations could be stored for up to 14 months at 4 °C with no increase in mean particle size

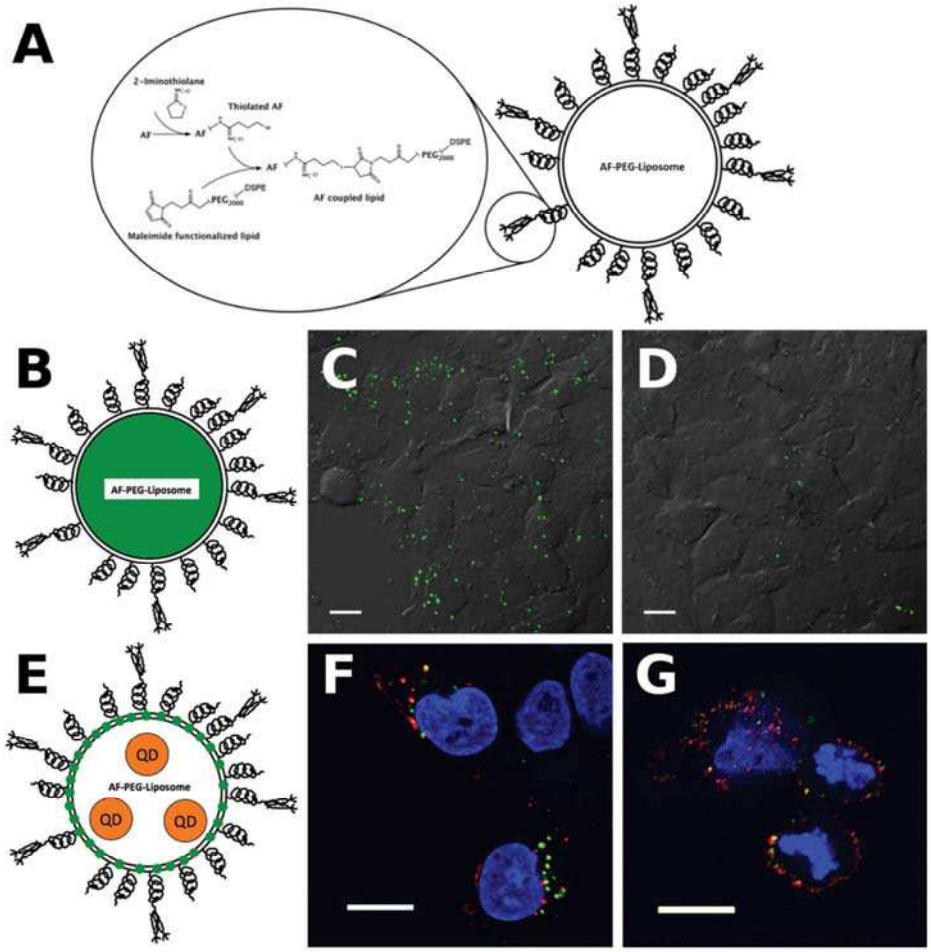

Figure 2. Schematic representation of the AF-PEG-liposome bioconjugation and cellular uptake by HepG2 cells. Panel A: Maleimide-functionalized pegylated DSPE was used as a chemically reactive phospholipid. This linker is an integral part of the liposome membrane. The reaction with thiolated AF gives rise to a metabolically stable thioether linkage. Liposomal cargos included carboxyfluorescein, rhodamine and quantum dots (QDs). Panel B: schematic representation of AF-PEG-liposomes loaded with carboxyfluorescein. Panel C: confocal microscopy analysis of HepG2 cells incubated with fluorescent AF-PEG-liposomes (panel B, green signal). Panel D: competitive inhibition of uptake of fluorescent AF-PEG-liposome (panel C) using unlabelled AF. Panel E: schematic representation of AF-PEG-liposomes loaded with QDs. The liposomal membrane was co-labelled with carboxyfluorescein-conjugated phospholipids. Panel F: HepG2 cells incubated at 37 °C with AF-PEG-liposomes (panel E) loaded with QDs (red signal) and co-labelled with carboxyfluorescein (green signal). Panel G: binding but no cellular uptake of AF-PEG-liposomes (panel F) following incubation at reduced temperature (4 °C). Cell nuclei are visualized using Hoechst 33342 (blue signal). Scale bars = 10 μm.

Table 1. Characterization of liposomes.

Formulation	Mean particle size (nm)	PDI	Zeta potential (mV)
Non-PEG-Liposomes	107 ± 8 ($n = 3$)	0.112 ± 0.055 ($n = 3$)	-11.6 ± 3.3 ($n = 3$)
PEG-Liposomes	88 ± 1 ($n = 3$)	0.044 ± 0.014 ($n = 3$)	-17.8 ± 6.9 ($n = 3$)
AF-PEG-Liposomes	97 ± 3 ($n = 6$)	0.060 ± 0.032 ($n = 6$)	-11.8 ± 4.6 ($n = 5$)
AF-PEG-Liposomes/QD	126 ± 10 ($n = 7$)	0.060 ± 0.019 ($n = 7$)	-13.1 ± 2.8 ($n = 7$)

Analysis of liposomal preparations by dynamic and electrophoretic light scattering. Samples were considered to be monodisperse as indicated by a polydispersity index (PDI) < 0.2. Values are means $\pm$ SD.

and only marginal changes with respect to polydispersity (data not shown).

For thiolation of AF, a molecular excess (200 times) of 2-iminothiolane was used. This resulted in an average of two sulfhydryl groups per molecule of AF, as analysed by Ellman's reaction. The amount of AF bound per vesicle was in the range of 30 to 270 molecules, based on the assumption that a 100-nm liposome contains approximately

DOI: 10.3109/1061186X.2013.860982

80 000 phospholipid molecules [27]. The average coupling efficiency was 20% of the used thiolated AF. Total amount of bound ligand was calculated based on the comparison of peak integrals from the corresponding size exclusion chromatograms, the amount of AF bound to the liposomal surface as determined by the CBQCA protein assay, and the amount of lipids determined by a modified Stewart assay. For *in vitro* studies, carboxyfluorescein was loaded inside the liposomes as a solution (Figure 2B), or incorporated into the liposomal membrane by using carboxyfluorescein-labelled phospholipids in combination with QDs (Figure 2E).

In vitro targeting of liposomes using asialofetuin as a vector

To visualize cellular interactions of AF-conjugated liposomes, a self-quenching solution of the fluorescent dye CF was passively loaded into liposomes. After a 30-min incubation of AF-PEG-liposomes with HepG2 cells, a distinct intracellular fluorescent staining pattern was obtained. Pre-incubation of cells with an excess of unlabelled AF led to competitive inhibition of cellular binding and uptake (Figure 2, panels C and D).

QDs were incorporated into liposomes as alternative fluorescent dyes to improve the fluorescent signal-to-noise ratio and to explore targeting strategies for nanosized particles. Liposome-encapsulated QDs had to be photoactivated by UV-irradiation at a wavelength of 490 nm for 3 min. Longer irradiation of the cells did not result in an increase in signal strength. Incubation of the sample at lower wavelength, even for a short period (15 s), resulted in a strong background signal from the cells and made detection of QDs difficult (data not shown). Emission spectra of QDs after their cellular uptake by HepG2 cells were investigated to demonstrate the presence of QDs within the target cells. The emission maximum of QDs shifted from 625 nm to 610 nm after liposomal incorporation. A lambda scan of HepG2-cell–associated QDs confirmed a narrow and characteristic emission peak at 610 nm which was not affected by prolonged exposure of cells to UV light. HepG2 cells were incubated for 40 min with QDs incorporated in AF-PEG-liposomes. The liposomal membrane was additionally labelled with CF to track the liposome separately from its cargo. Distribution and co-localization were investigated after uptake or binding at 37 °C and 4 °C, respectively (Figure 2, panels F and G). While the QDs and liposomes accumulated intracellularly at 37 °C, indicating cellular uptake and accumulation within the endosomal or lysosomal compartments, a distinct distribution on the cell surface was visible at 4 °C.

In vivo targeting of rat hepatocytes

In a first set of *in vivo* experiments, the uptake of AF-PEG-liposomes and non-pegylated liposomes in liver and spleen was determined in rats 30 min after i.v. injection via indwelling catheters implanted into the jugular vein (Figure 3). The uptake of fluorescent liposomes in liver and spleen for targeted and non-pegylated liposomes showed completely different uptake patterns. Non-pegylated liposomes showed an accumulation in the spleen (Figure 3D), whereas AF-PEG-liposomes accumulated in the liver (Figure 3A). The cellular localization of conventional, non-pegylated fluorescent liposomes in the liver was determined in rats 30 min after i.v. injection (Figure 4, panels A–C). Liposomes were co-administered with carbon black (i.e. a marker for hepatic Kupffer cells [28]). Analysis of liver cryosections revealed a distinct distribution pattern of carbon black and rhodamine, indicating co-localization of carbon black and non-pegylated liposomes within Kupffer cells (Figure 4C). In contrast to non-pegylated vesicles that accumulated in Kupffer cells, AF-PEG-liposomes accumulated within hepatocytes (Figure 4, panels D and E). In these experiments, rhodamine-labelled liposomes were injected i.v., and liver cryosections were analysed after 30 min (Figure 4D). Homogenous distribution of fluorescent liposomes was observed throughout the liver parenchyma, corresponding to the ubiquitous presence of hepatocytes. Competitive inhibition was achieved using an excess of free AF (Figure 4E).

Discussion

The ASGPR is a C-type lectin receptor predominantly and abundantly expressed on the surface of liver parenchymal cells (i.e. hepatocytes). Binding of terminal galactosyl residues induces clathrin-mediated endocytosis [1]. This project aimed to exploit this physiological uptake mechanism to implement a hepatocyte-specific drug targeting strategy. Liposomal drug carriers were thereby covalently linked to an ASGPR ligand promoting hepatocyte binding and cellular uptake of the nanoparticles. This work is the first to employ AF covalently coupled to the surface of pegylated liposomes. Thereby, PEG had a dual role. First, pegylation of liposomal carriers prevents their interactions with phagocytic cells of the RES including spleen and hepatic Kupffer cells [29]. Systemic plasma clearance of liposomes is therefore reduced resulting in an enhanced apparent terminal half-life of liposomes in human from minutes to days [6]. As a consequence, the area under the time versus plasma concentration curve increases, which is a prerequisite for the implementation of drug targeting strategies *in vivo*. Second, PEG with a molecular weight of 2000 Da was used as a tether to attach AF to the surface of the liposome. AF is thereby linked to the tip of the PEG chain. Thus, the targeting vector extends from the hydrophilic PEG-corona and can freely interact with the ASGPR.

As an alternative to monoclonal antibodies, cell-specific receptors can be targeted with artificial or naturally occurring ligands. Gal or GalNAc bind to ASGPR [15] and can be used as robust, cheap and widely available vectors. In the past, various nanoparticles have been linked to Gal to deliver different cargos to hepatocytes with variable success and specificity [30,31]. High surface concentrations of Gal are thereby needed because naturally occurring, high-affinity ligands of the ASGPR contain multi-antennary glycan residues. It can thus be argued that clusters of Gal residues attached to a liposome are necessary to mimic a high-affinity, multi-antennary glycan. If we take into consideration that the optimal distance for tri-antennary binding of the terminal Gal to the ASGPR lies between 1.5 nm and 2.5 nm [11] and the Gal residues are evenly distributed on the liposomal surface, we would need an average of 5000 to 14 000 terminal Gal

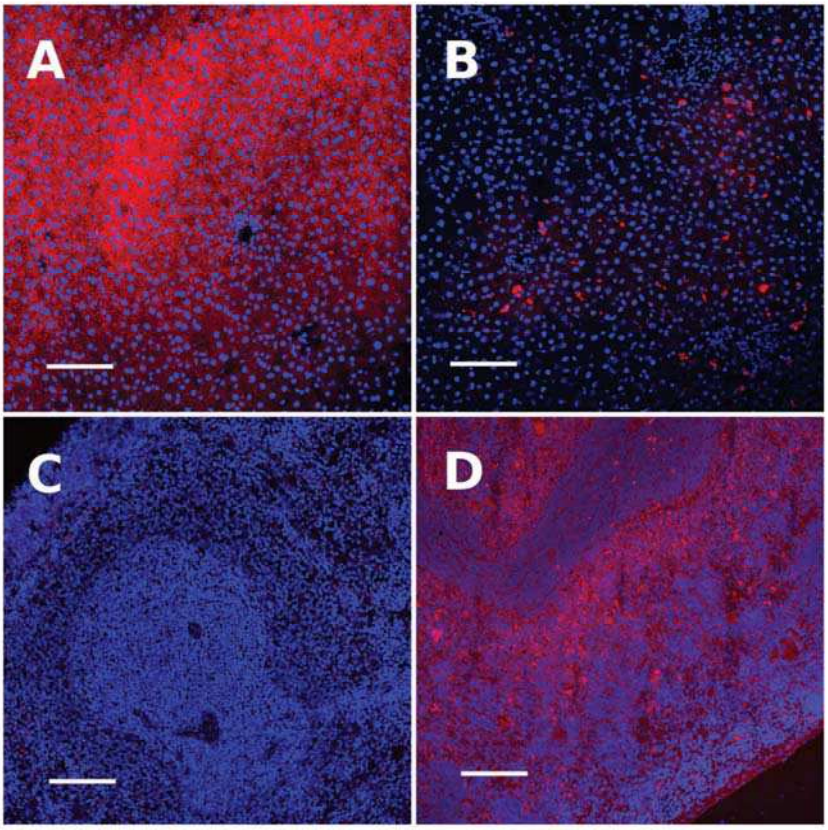

Figure 3. *In vivo* accumulation of AF-PEG-liposomes and non-pegylated liposomes in rat liver and spleen. Analysis by confocal fluorescence microscopy of representative rat liver (panel A/B) and rat spleen (panel C/D) cryosections 30 min after i.v. injection of rhodamine-labelled AF-PEG-liposomes (panel A/C) and non-pegylated liposomes (panel B/D) (red signal). Cell nuclei are visualized using Hoechst 33342 (blue signal). Scale bars = 100 µm (liver); 200 µm (spleen). $n = 3$ animals per experiment.

residues for a liposome with a diameter of 100 nm, which means that approximately 6% to 17% of the 80 000 phospholipids in a 100-nm liposome must carry a Gal [27]. However, an excess of surface-bound terminal Gal leads to an unspecific uptake of particles by Kupffer cells despite the protective properties of PEG. This detrimental effect was observed by Shimada et al., who used up to 20 mol% galactosylated lipids on the surface of pegylated liposomes, leading to a preferential uptake by Kupffer cells [14].

In view of these problems, we decided to select a desialated glycoprotein (i.e. AF) with multi-antennary Gal-terminated residues as an alternative for targeting the ASGPR. With its bi- and tri-antennary N-linked glycans, AF is specifically taken up in the liver by hepatocytes through the ASGPR [32]. Furthermore, it is recognized by hepatocytes from different species, is commercially available, and can be easily modified to be non-immunogenic for use in humans. To this end, multi-antennary glycan residues can be isolated from AF, or the whole protein can be replaced with the human analogue α-2-HS-glycoprotein [33]. AF was modified by a reaction with fluorescent NHS esters or 2-iminothiolane which react with the α-amine at the N-terminus and the ε-amines of lysine side chains to form a stable amide bond (Figure 2A). This derivatization of AF did not interfere with ASGPR binding. Thus, a modification of the protein backbone to enable a subsequent coupling to nanoparticles is not critical, since the oligosaccharides mediating ASGPR interactions are not affected. In contrast to experiments with fluorescent-labelled Gal (data not shown), binding of AF could be inhibited with an excess of free AF, demonstrating specific cellular uptake by the ASGPR (Figure 1). At 4 °C, no cellular uptake of fluorescent-labelled AF was observed. This finding confirms an active and energy-dependent uptake mechanism for AF at 37 °C (Figure 1C). Additionally, trypan blue quenching did not change the relative fluorescence intensity at 37 °C (Figure 1D). This confirms the intracellular localization of AF-CF because trypan blue only quenches free or surface-bound fluorescent dye [25]. It should be noted that the characteristics of binding to and uptake by hepatocytes differed markedly between different AF batches. Batch-to-batch differences were caused by incomplete removal of sialic acid from fetuin during processing by the manufacturer. This could be demonstrated by a mobility shift of AF in SDS-PAGE after treatment with sialidase (data not shown).

DOI: 10.3109/1061186X.2013.860982

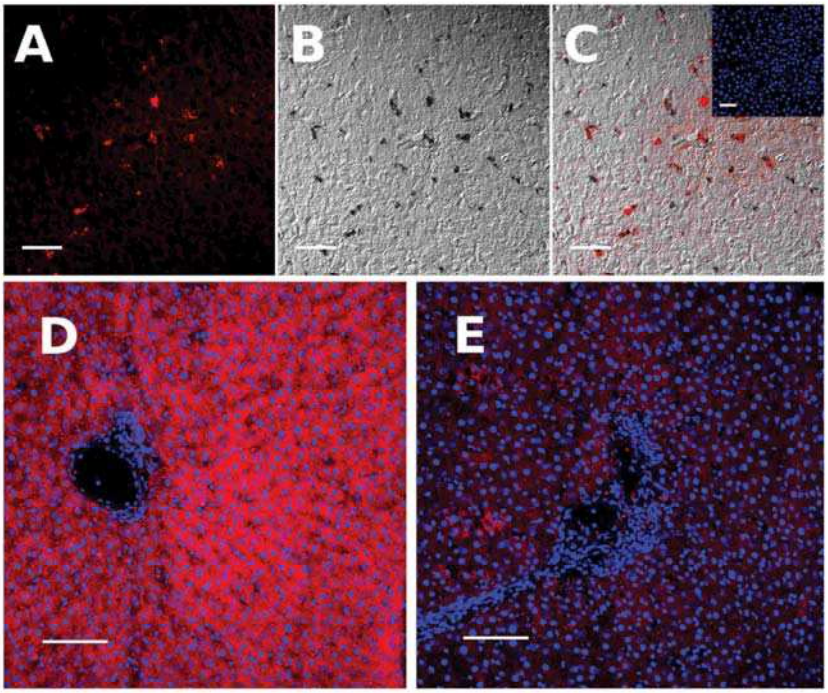

Figure 4. *In vivo* accumulation of non-pegylated liposomes in Kupffer cells and AF-PEG-liposomes in rat hepatocytes. Panel A: Analysis by confocal fluorescence microscopy of representative rat liver cryosections 30 min after i.v. injection of rhodamine-labelled non-pegylated liposomes (red signal). Panel B: Non-pegylated liposomes were administered together with colloidal carbon, a marker for Kupffer cells (black signal, differential interference contrast microscopy). Panel C: overlay of panels A and B. Insert panel C: nuclear staining using Hoechst 33342 (blue) of the same specimen. Panel D: Analysis by confocal fluorescence microscopy of rat liver cryosections 30 min after i.v. administration of rhodamine-labelled AF-PEG-liposomes (red signal). Panel E: Competitive inhibition of *in vivo* uptake of rhodamine-labelled AF-PEG-liposomes by co-injection of unbound AF. Nuclei were stained with Hoechst 33342 (blue signal). Scale bars = 40 μm. $n = 3$ animals per experiment.

All liposomal formulations used in this study were judged to be monodisperse with a particle size below 130 nm. Access to the space of Disse (perisinusoidal space) is therefore granted [31]. Liposomes were prepared using a mixture of 53:44 (mol%) DSPC/Chol. This lipid composition is important, because a higher phosphatidylcholine content of galactosylated liposomes may limit their hepatic extravasation and uptake [34].

In this study, the amount of surface-conjugated AF on liposomes covered a range between 30 to 270 molecules of glycoprotein per liposome. However, the density of receptor ligands on the surface of liposomes had no apparent impact on the results. Although this variability was shown to be of no concern, a post-insertion technique might be a more manageable approach to control the final amount of surface-coupled vectors per liposome. In addition to classical fluorescent dyes, QDs were used to load liposomes. QDs are inorganic nanocrystals composed of specific semiconductors, such as CdSe. Although the diameter of the QDs, including the ZnS shell and polymer coating, is stated by the supplier to be around 10 nm, it was not possible to produce liposomes of a size below 100 nm by filter extrusion, in contrast to liposomes containing organic dyes (Table 1). The quantum yield of QDs is lower than that of organic dyes. But the higher absorption rate and increased photostability result in a brighter fluorescent signal, which opens up new possibilities to track the delivery of nanoparticles *in vitro* and *in vivo*. In fluorescence microscopy, the large Stockes shift and narrow emission spectra facilitate differentiation of the fluorochrome from the background [35]. Various applications of QDs as bioconjugates and their use in live cell imaging were extensively reviewed elsewhere [36,37]. However, QDs have to be photoactivated to overcome non-linear fluorescent properties, intermittent fluorescence emission (blinking) and extensive quenching of the fluorescent signal within cells [38]. In addition, the shell surrounding the core of the nanocrystal plus the overlaying coating determines not only the solubility and intracellular stability of QDs, but also their optical properties [36]. These limitations of QDs precluded quantitative evaluation of cellular uptake and the use of rapid analytical technologies, such as FACS analysis.

Many desialated glycoproteins, including AF, are taken up specifically by hepatocytes rather Kupffer cells [39]. Consequently, AF-mediated drug targeting is expected to be specific for hepatocytes. Two lines of evidence support this notion. First, a strong and specific interaction with HepG2 liver hepatocellular carcinoma cells of fluorescent AF and AF-PEG-liposomes was demonstrated *in vitro*. Binding and cellular uptake were competitively inhibited by free AF. Binding, but not uptake, was observed at 4 °C, indicating an

energy-dependent, endocytotic process. Second, AF-PEG-liposomes accumulated in the majority of cells within the liver after i.v. injection and not in other organs, as demonstrated by the tissue staining patterns. Competitive inhibition of liver tissue accumulation *in vivo* was achieved by co-injection of free AF. This confirms a specific interaction with the ASGP receptor and the absence of receptor oversaturation by AF-PEG-liposomes. Observed effects were different from those resulting from accumulation of nanoparticles within the RES, i.e. Kupffer cells. In contrast, non-pegylated liposomes showed a strong accumulation in the spleen (Figure 3D). Uptake by liver-resident macrophages was demonstrated in control experiments using fluorescent non-pegylated liposomes or colloidal carbon (Figure 4, panels A–C), a marker for Kupffer cells [40]. In these experiments, liver cryosections displayed well-defined, single spots of accumulated fluorescent liposomes together with co-localized carbon. Liposome- and carbon-stained cells represented only a minority of total cells. This pattern applied to an approximately 10% fraction of the cell population, which corresponds to figures reported for the proportion of Kupffer cells in the liver [28]. Because non-pegylated liposomes co-localized with colloidal carbon (Figure 4, panels A–C), it is reasonable to assume that these particles accumulated mostly in the Kupffer cells, while the targeted vesicles were taken up by the liver parenchymal cells.

In view of the batch-to-batch differences of AF, an alternative to this natural receptor ligand would be of interest. In principle, AF can be replaced with the desialated derivative of the human α-1-acid glycoprotein (also known as orosomucoid), which carries bi- and tetra-antennary glycan residues [10,11]. Another possibility is to isolate the multi-antennary glycan residue from AF by specifically cleaving the N-linked glycosylations or by fragmenting the protein backbone with proteases, leaving only the oligosaccharides linked to a short non-immunogenic peptide. The isolated glycans can be coupled to the distal end of pegylated liposomes (glycoliposomes), thus constituting an alternative to the whole glycoprotein [41]. More recently, synthetic carbohydate mimetics were designed as ASGPR ligands [42].

In this study, AF-conjugated pegylated liposomes were used for the first time to implement a hepatocyte-specific drug targeting strategy. Direct targeting of hepatocytes avoids interactions with hepatic Kupffer cells as well as accumulation in the spleen. By this strategy, the risk of potential side effects can be reduced. To optimize this approach and compare it to alternative liver targeting strategies, further *in vivo* experiments are needed to quantify accumulated liposomes in different organs and specific cell populations, such as liver parenchymal and non-parenchymal cells.

Acknowledgements

We thank Dr. Silvia Rogers for editorial assistance.

Declaration of interest

The authors have no conflicting financial interests.

Pascal Detampel was supported by a public grant for a Ph.D. thesis project awarded by the Senglet Foundation (Basel, Switzerland). The Olympus confocal microscope used in the present study was purchased with financial support by the Swiss National Science Foundation (SNSF).

References

1. Poelstra K, Prakash J, Beljaars L. Drug targeting to the diseased liver. J Control Release 2012;161:188–97.
2. Casey LC, Lee WM. Hepatitis C therapy update. Curr Opin Gastroenterol 2012;28:188–92.
3. Lampertico P, Liaw YF. New perspectives in the therapy of chronic hepatitis B. Gut 2012;61 Suppl 1:i18–24.
4. Siebler J, Galle PR. Treatment of nonalcoholic fatty liver disease. World J Gastroenterol 2006;12:2161–7.
5. Aravalli RN, Cressman ENK, Steer CJ. Cellular and molecular mechanisms of hepatocellular carcinoma: an update. Arch Toxicol 2013;87:227–47.
6. Huwyler J, Drewe J, Krähenbuhl S. Tumor targeting using liposomal antineoplastic drugs. Int J Nanomed 2008;3:21–9.
7. Milla P, Dosio F, Cattel L. PE Gylation of proteins and liposomes: a powerful and flexible strategy to improve the drug delivery. Curr Drug Metab 2012;13:105–19.
8. Halm U, Etzrodt G, Schiefke I, et al. A phase II study of pegylated liposomal doxorubicin for treatment of advanced hepatocellular carcinoma. Ann Oncol 2000;11:113–14.
9. Janssen HLA, Reesink HW, Lawitz EJ, et al. Treatment of HCV infection by targeting microRNA. N Engl J Med 2013;368: 1685–94.
10. Schwartz AL. The hepatic asialoglycoprotein receptor. CRC Crit Rev Biochem 1984;16:207–33.
11. Stockert RJ. The asialoglycoprotein receptor: relationships between structure, function, and expression. Physiol Rev 1995;75: 591–609.
12. Wu J, Nantz MH, Zern MA. Targeting hepatocytes for drug and gene delivery: emerging novel approaches and applications. Front Biosci 2002;7:d717–25.
13. Managit C, Kawakami S, Nishikawa M, et al. Targeted and sustained drug delivery using PEGylated galactosylated liposomes. Int J Pharm 2003;266:77–84.
14. Shimada K, Kamps JA, Regts J, et al. Biodistribution of liposomes containing synthetic galactose-terminated diacylglyceryl-poly(ethyleneglycol)s. Biochim Biophys Acta 1997;1326: 329–41.
15. Wang S, Xu H, Xu J, et al. Sustained liver targeting and improved antiproliferative effect of doxorubicin liposomes modified with galactosylated lipid and PEG-lipid. AAPS PharmSciTech 2010;11: 870–7.
16. Connolly DT, Townsend RR, Kawaguchi K, et al. Binding and endocytosis of cluster glycosides by rabbit hepatocytes. Evidence for a short-circuit pathway that does not lead to degradation. J Biol Chem 1982;257:939–45.
17. Neue K, Mormann M, Peter-Katalinić J, Pohlentz G. Elucidation of glycoprotein structures by unspecific proteolysis and direct nanoESI mass spectrometric analysis of ZIC-HILIC-enriched glycopeptides. J Proteome Res 2011;10:2248–60.
18. Dasí F, Benet M, Crespo J, et al. Asialofetuin liposome-mediated human alpha1-antitrypsin gene transfer in vivo results in stationary long-term gene expression. J Mol Med 2001;79: 205–12.
19. Gregoriadis G, Neerunjun ED. Homing of liposomes to target cells. Biochem Biophys Res Commun 1975;65:537–44.
20. Hara T, Aramaki Y, Tsuchiya S, et al. Specific incorporation of asialofetuin-labeled liposomes into hepatocytes through the action of galactose-binding protein. Biopharm Drug Dispos 1987;8: 327–39.
21. Hara T, Ishihara H, Aramaki Y, Tsuchiya S. Specific uptake of asialofetuin-labeled liposomes by isolated hepatocytes. Int J Pharm 1988;42:69–75.
22. Tros de Ilarduya C. Serum-resistant lipoplexes in the presence of asialofetuin. Methods Mol Biol 2010;605:425–34.
23. Huwyler J, Wu D, Pardridge WM. Brain drug delivery of small molecules using immunoliposomes. Proc Natl Acad Sci USA 1996; 93:14164–9.
24. Stewart JC. Colorimetric determination of phospholipids with ammonium ferrothiocyanate. Anal Biochem 1980;104:10–14.

DOI: 10.3109/1061186X.2013.860982

25. Kettiger H, Schipanski A, Wick P, Huwyler J. Engineered nanomaterial uptake and tissue distribution: from cell to organism. Int J Nanomedicine 2013;8:3255–69.
26. Garbuzenko O, Barenholz Y, Priev A. Effect of grafted PEG on liposome size and on compressibility and packing of lipid bilayer. Chem Phys Lipids 2005;135:117–29.
27. Hansen CB, Kao GY, Moase EH, et al. Attachment of antibodies to sterically stabilized liposomes: evaluation, comparison and optimization of coupling procedures. Biochim Biophys Acta 1995; 1239:133–44.
28. Cowper KB, Currin RT, Dawson TL, et al. A new method to monitor Kupffer-cell function continuously in the perfused rat liver. Dissociation of glycogenolysis from particle phagocytosis. Biochem J 1990;266:141–7.
29. Allen TM, Hansen CB. Pharmacokinetics of stealth versus conventional liposomes: effect of dose. Biochim Biophys Acta 1991;1068:133–41.
30. Managit C, Kawakami S, Yamashita F, Hashida M. Uptake characteristics of galactosylated emulsion by HepG2 hepatoma cells. Int J Pharm 2005;301:255–61.
31. Pathak A, Vyas SP, Gupta KC. Nano-vectors for efficient liver specific gene transfer. Int J Nanomed 2008;3:31–49.
32. Tolleshaug H, Berg T, Nilsson M, Norum KR. Uptake and degradation of 125I-labelled asialo-fetuin by isolated rat hepatocytes. Biochim Biophys Acta 1977;499:73–84.
33. Rice KG, Rao NB, Lee YC. Large-scale preparation and characterization of N-linked glycopeptides from bovine fetuin. Anal Biochem 1990;184:249–58.
34. Murao A, Nishikawa M, Managit C, et al. Targeting efficiency of galactosylated liposomes to hepatocytes in vivo: effect of lipid composition. Pharm Res 2002;19:1808–14.
35. Wu X, Liu H, Liu J, et al. Immunofluorescent labeling of cancer marker Her2 and other cellular targets with semiconductor quantum dots. Nat Biotechnol 2003;21:41–6.
36. Medintz IL, Uyeda HT, Goldman ER, Mattoussi H. Quantum dot bioconjugates for imaging, labelling and sensing. Nat Mater 2005; 4:435–46.
37. Michalet X, Pinaud FF, Bentolila LA, et al. Quantum dots for live cells, in vivo imaging, and diagnostics. Science 2005;307: 538–44.
38. Generalov R, Kavaliauskiene S, Westrøm S, et al. Entrapment in phospholipid vesicles quenches photoactivity of quantum dots. Int J Nanomed 2011;6:1875–88.
39. Morell AG, Gregoriadis G, Scheinberg IH, et al. The role of sialic acid in determining the survival of glycoproteins in the circulation. J Biol Chem 1971;246:1461–7.
40. Neyrinck AM, De Wispelaere LD, Vanhulle VP, et al. Are Kupffer cells involved in the metabolic adaptation of the liver to dietary carbohydrates given after fasting? Biochim Biophys Acta 2000; 1475:238–44.
41. Nilsson B, Svensson S. A new method for degradation of the protein part of glycoproteins: isolation of the carbohydrate chains of asialofetuin. Carbohydr Res 1979;72:183–90.
42. Stokmaier D, Khorev O, Cutting B, et al. Design, synthesis and evaluation of monovalent ligands for the asialoglycoprotein receptor (ASGP-R). Bioorg Med Chem 2009;17:7254–64.

Chapter V

"Isolation of Multiantennary *N*-Glycans from Glycoproteins for Hepatocyte specific Targeting via the Asialoglycoprotein Receptor"

Witzigmann D, Detampel P, Porta F, Huwyler J.

RSC Advances. 2016 Oct 07; 2016, 6, 97636-97640.
doi: 10.1039/C6RA18297F

http://pubs.rsc.org/en/content/articlelanding/2016/ra/c6ra18297f#!divAbstract

Highlights: Complex multivalent carbohydrates from glycoproteins offer a huge potential to specifically target parenchymal liver cells via the asialoglycoprotein receptor (ASGPR). Natural *N*-glycans are expected to be superior to multivalent glycomimetics with respect to ease of preparation, geometrical arrangement of the antennary carbohydrates, and biocompatible properties. In this study, an enzymatic isolation strategy for multiantennary, desialylated asparagine-linked carbohydrates from fetuin followed by conjugation to a fluorescent dye using reductive amination is described. These glycan-conjugates were successfully used to actively target the ASGPR on human hepatocellular carcinoma cells *in vitro*. In the future, isolated *N*-glycans might be ideal candidates for further development of ASGPR targeting strategies to guide drugs to the key pathogenic cell type and mediate endocytosis into parenchymal liver cells.

RSC Advances

COMMUNICATION

View Article Online
View Journal | View Issue

Cite this: *RSC Adv.*, 2016, **6**, 97636

Received 18th July 2016
Accepted 7th October 2016

DOI: 10.1039/c6ra18297f

www.rsc.org/advances

Isolation of multiantennary *N*-glycans from glycoproteins for hepatocyte specific targeting *via* the asialoglycoprotein receptor†

Dominik Witzigmann, Pascal Detampel, Fabiola Porta and Jörg Huwyler*

The asialoglycoprotein receptor (ASGPR) expressed on parenchymal liver cells specifically binds multivalent carbohydrates from desialylated glycoproteins. This feature offers a huge potential for hepatocyte specific drug targeting. In this study, multiantennary *N*-glycans from asialofetuin have been isolated to actively target the asialoglycoprotein receptor on human hepatocellular carcinoma cells *in vitro*.

Hepatic diseases are an increasing health burden and efficient and curative treatments are still missing. Targeted therapies to the key pathogenic cells offer promising options to address limitations of current therapeutic interventions.[1] Especially nanomedicines and siRNA therapeutics benefit from targeted cell delivery and enhanced cellular uptake. During the last decade, the asialoglycoprotein receptor (ASGPR) has proven to be the target receptor of choice to enhance the therapeutic effect of medicines for hepatocyte-derived diseases including metabolic and genetic disorders.[2] The ASGPR is highly expressed on the sinusoidal membrane of human hepatocytes, mediating the internalization of the receptor–ligand complex *via* a clathrin-mediated pathway.[3] This offers an excellent option to guide drugs to the key pathogenic cell type and mediate endocytosis into parenchymal liver cells.[4–6] Several recent studies have exploited ASGPR specific interactions for hepatocyte specific drug delivery and imaging.[7–11]

The ASGPR is a heterooligomeric C-type lectin, consisting of two subunits (*i.e.* H1/H2), which are recognizing desialylated glycans with terminal galactose (Gal) or *N*-acetyl galactosamine (GalNAc) residues.[12] Endogenous ligands are glycoproteins with complex-type desialylated glycans, such as asialofetuin A (desialylated alpha-2-HS-glycoprotein) or asialoorosomucoid (desialylated alpha-1-acid-glycoprotein).[13] The linked multivalent carbohydrates bind with high specificity to the hepatic lectin. To facilitate the binding of targeted medicines or diagnostics to hepatocytes, several research groups have developed monovalent glycomimetics.[14–16] In addition, complex multivalent glycans were developed for ASGPR specific targeting.[17–19] The affinity of these ligands increases with increasing number of carbohydrates simultaneously binding to multiple receptor subunits.[20] This multivalency effect (*i.e.* "cluster glycoside effect") is important to overcome the weak and unspecific binding of monovalent sugars and to increase avidity.[21] Several factors are influencing the specificity and binding affinity of these ligands, including the terminal sugar (GalNAc > Gal), the antennary structure (*i.e.* multivalency), as well as the spatial arrangement of the carbohydrates (*e.g.* linker length). Recently, we have proposed a liposomal drug delivery system for ASGPR targeting using a natural and readily available glycoprotein, bovine asialofetuin, as a ligand.[22] Asialofetuin is a glycoprotein with several bi- and tri-antennary glycans, which specifically bind to the ASGPR. However, a shortcoming of asialofetuin is a possible immunogenicity and batch-to-batch variations. Since only the multivalent carbohydrates are important for lectin binding, we decided to explore whether multivalent glycans can be isolated from asialofetuin and used as ligands to target human hepatocytes. It was thus the aim of the present study to develop an enzymatic isolation strategy for multiantennary, desialylated asparagine-linked carbohydrates (*N*-glycans) from fetuin A followed by conjugation to a fluorescent dye using reductive amination. This ligand–dye conjugate was then tested for its targeting ability *in vitro* using qualitative and quantitative methods (Scheme 1). Natural *N*-glycans are expected to be superior to multivalent glycomimetics with respect to ease of preparation. In addition, receptor specificity and affinity can be considered to be very high due to an ideal geometrical arrangement of the antennary carbohydrates (*i.e.* the desialylated *N*-linked glycan). By the use of isolated *N*-glycans, limitations imposed by immunogenic protein or peptide residues can be overcome.

Abundant natural sources for the isolation of *N*-glycans are bovine fetuin or desialylated fetuin (*i.e.* asialofetuin). In the

Division of Pharmaceutical Technology, Department of Pharmaceutical Sciences, University of Basel, Klingelbergstrasse 50, Basel CH-4056, Switzerland. E-mail: joerg.huwyler@unibas.ch

† Electronic supplementary information (ESI) available. See DOI: 10.1039/c6ra18297f

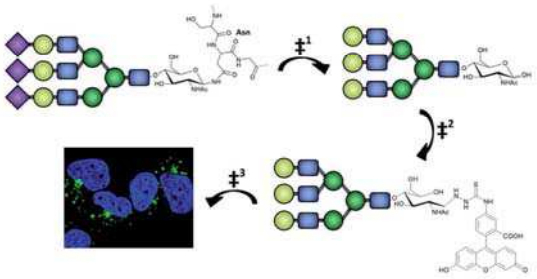

Scheme 1 Different steps for the preparation of asialoglycoprotein receptor targeted multiantennary glycan-conjugates: (‡1) enzymatic cleavage of asparagine-linked *N*-glycans (NA3) using peptide-*N*-glycosidase F and sialidase, followed by an isolation using a combined extraction–separation strategy. (‡2) Fluorescent labelling of *N*-glycans with fluorescein-5-thiosemicarbazide *via* reductive amination. (‡3) Targeting of the human hepatocellular carcinoma cell line HepG2. Analysis using confocal microscopy (blue: nuclei; green: fluorescent *N*-glycans). ◆ = sialic acid; ○ = galactose (Gal); ■ = GlcNAc; ● = mannose.

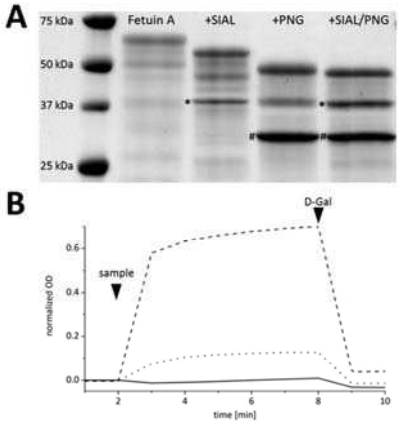

Fig. 1 (A) SDS-PAGE analysis followed by Coomassie blue staining of native fetuin A before and after enzymatic digestion using sialidase (SIAL, protein band indicated with *) and PNGase F (PNG, protein band indicated with #). Upper two bands in each row represent fetuin A and its deglycosylated form, respectively. The mobility shift after enzymatic digestion corresponds to the removal of sialic acid modifications or *N*-glycans (B) *Ricinus communis* agglutinin aggregation assay of fetuin A (solid line), and its desialylated form asialofetuin, after digestion using sialidase for one hour (dotted line) and after total digestion (dashed line). Black triangles: in presence of desialylated glycoprotein (sample), aggregation is induced; competitive de-aggregation by a 100-fold excess of free D-galactose (D-Gal).

present study, fetuin was used as a starting material since commercially available asialofetuin shows considerable batch-to-batch variability with respect to electrophoretic mobility (Fig. S1†) and reactivity in the *Ricinus communis* agglutinin (RCA_{120}) agglutinin aggregation assay (Fig. S2†). Detailed experimental procedures for the isolation of *N*-glycans from fetuin are provided in the ESI.† Bovine fetuin A has 359 amino acids and bears various mono- and multivalent glycosylations. Bi- or tri-antennary carbohydrates are linked to asparagines of the protein at amino acid positions 99, 156, and 176.[23,24] Therefore, several bands were detected in the SDS-PAGE analysis including the full glycosylated form with its *N*- and *O*-glycans (main band). The molecular weight shift after digestion corresponds to the removal of specific glycans. Enzymatic digest of fetuin using sialidase and PNGase F was monitored by SDS-PAGE (Fig. 1A). Neuraminidase (sialidase) specifically cleaves terminal sialic acids from glycans, whereas peptide-*N*-glycosidase F (PNGase F) selectively cuts the bond between asparagine and *N*-linked complex carbohydrates. The underlying chemical reaction mediated by PNGase F is shown in Fig. S3.† The significant shift in electrophoretic mobility of fetuin A confirms the cleavage of sialic acid residues (*i.e.* resulting in asialofetuin) and removal of *N*-linked glycans (corresponding to a molecular weight shift of 9.8 kDa) (Fig. 1A). Based on its amino-acid sequence, fetuin A has a molecular weight of 38.4 kDa (*i.e.* protein backbone). The published molecular weight of 48.4 kDa (*i.e.* glycoprotein) is in line with our result. Enzymatic removal of sialic acid was monitored using the RCA_{120} aggregation assay (Fig. 1B): incubation of the bivalent RCA_{120} lectin with glycoproteins bearing multiantennary glycans (Gal1-4GlcNAc sequences) results in aggregation.[25] An excess of galactose (D-Gal) reduces the lectin crosslinking and thus competitively reverts aggregation (Fig. 1B). Approximately 10–15% of the glycoprotein mass consists of *N*-glycans depending on the glycosylation pattern. For the isolation of complex carbohydrates, we used a preparative approach, combining liquid–liquid extraction and size exclusion chromatography (Scheme 1, step 1).[26] Fetuin A was enzymatically digested. *N*-Glycans were precipitated using 80% acetone and thereby separated from proteins and detergents. The pH was adjusted to 5.5 and *N* glycans were extracted using 60% methanol. The different *N* glycan fractions with a molecular mass between 1600 and 2000 Da were separated by gel filtration chromatography (Superdex 30 Prep Grade column). For size calibration, Met5Enkephalin, vitamine B12 and Magainin II (MW range from 500 Da to 2000 Da) were used.

Chromatographic fractions containing purified *N*-glycans were identified by two different colorimetric reactions (Fig. 2). To confirm that *N*-glycans were isolated, a phenol sulfuric acid assay (PSAA, *i.e.* total carbohydrate assay)[27] was combined with a modified BCA assay to determine fractions with reducing potential. In general, the BCA assay is used to analyse proteins. However, a modified version with enhanced sensitivity can also determine reducing sugars.[28,29] Multiantennary *N*-glycans, which are bound to proteins, do not possess reducing potential. As soon as glycans are cleaved off, the terminal sugar contains a free anomeric carbon with reducing properties amendable to reductive amination. A protein assay was used to confirm separation of *N*-glycans from cleaved protein (Bradford assay; Fig. S5†).

This rapid and convenient extraction–separation-procedure resulted in successful isolation of bi- and tri-antennary *N*-linked glycans from fetuin. In average, 82 μg of multivalent *N*-glycans were isolated per 1 mg fetuin. This corresponds to an isolation yield of 49–60% depending on the glycosylation of the starting material. A matrix-assisted laser desorption ionization

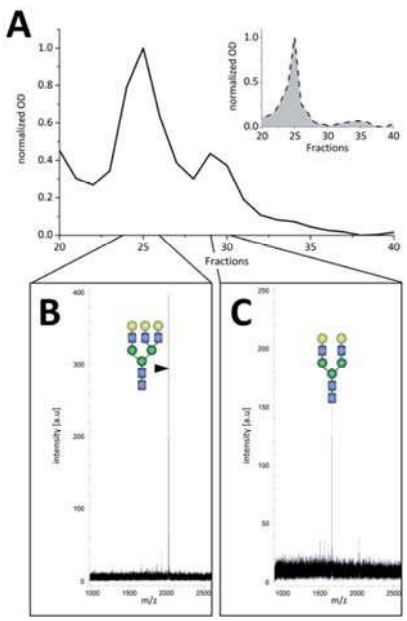

Fig. 2 Size exclusion chromatography of enzymatically digested fetuin A. Fractions including *N*-glycans were analysed with respect to reducing sugars (panel (A); modified BCA assay) and total carbohydrate content (insert of panel (A); phenol sulfuric acid assay PSAA, grey area). Indicated glycan fractions were analysed by MALDI-TOF-MS to identify (B) tri- and (C) bi-valent glycan samples. Complex glycans are detected as sodium adducts.

time of flight mass spectrometer (MALDI-TOF-MS) was used to characterize the isolated *N*-glycans. In brief, fractions were mixed with the matrix solution (2,5-dihydroxy benzoic acid; DHB) in a 1 : 1 ratio and analysed using a MALDI-TOF-MS. As expected, tri- (NA3, Fig. 2B) and bi-antennary glycans (NA2, Fig. 2C) were detected with molecular masses $[M + Na]^+$ of 2029 Da and 1664 Da, respectively. In the MALDI spectrum each of these glycans are typically detected as sodium adducts of the molecular ion $[M + Na]^+$.[30,31]

Several lines of evidence indicate that bi- and tri-antennary *N*-glycans were successfully isolated. First, the used enzymes are highly specific for *N*-linked glycans. Second, the PSAA assay confirms that the isolated structures are carbohydrates. Third, the BCA components react with the reducing end of isolated sugars. Fourth, the molecular masses of the isolated sugars correspond to published results on the structural elucidation of the *N*-linked carbohydrate fraction of fetuin.[24] A detailed summary of the MALDI-TOF analysis is provided in Table S1 in the ESI.†

Isolated *N*-glycans were then conjugated with a model compound, fluorescein-5-thiosemicarbazide (FTSC), *via* reductive amination (Scheme 1, step 2). The detailed chemical steps are represented in Fig. S4.† FTSC has the advantage of a high fluorescence quantum yield in comparison to commonly used glycan-mapping-tags such as 2-aminobenzoic acid (2-AA) or 2-aminobenzamide (2-AB). In an optimized one-pot synthesis, FTSC chemoselectively reacted with the free anomeric carbon of the terminal sugar (reducing end) to form a stable thiosemicarbazone bond. In brief, glycans were dissolved in a mixture of DMSO/HOAc (pH = 5.0) and FTSC was added in DMF. The reducing agent ($NaBH_3CN$) was added and the reaction was stirred for another 2 h at 70 °C. Since the equilibrium of the reducing carbohydrate moiety is shifted to the acetal form, elevated temperature and sodium cyano borohydride have been used. Therefore, the open-chain aldehyde intermediate is formed more efficiently and the conjugation reaction is driven to completion. During the reaction, the fluorescence properties of the FTSC linked-compound decreased, most probably due to the excess of reducing agent as reported recently for Rhodamine 110.[32] Therefore, an aqueous potassium hexacyanoferrate solution was added at the end of the reaction to oxidize the dihydro derivate and to fully restore fluorescence.[32] Finally, the glycan–fluorophore-conjugate was isolated by gel filtration chromatography (Sephadex G10 column) eluting with phosphate buffered saline (pH 7.4). The excess, non-conjugated dye (4.75× molar excess) was completely removed from the glycan–fluorophore-conjugate because of the high affinity to the stationary phase. To determine the recovery of fluorescent *N*-glycans in the collected fractions, a total carbohydrate assay was performed.

The targeting ability of the FTSC-labelled multivalent *N*-glycans were investigated using the human hepatocellular carcinoma cell line HepG2 (Scheme 1, step 3). Recently, we have shown that this cell line is an excellent model to study targeting strategies *via* the ASGPR.[12] HepG2 cells have a high expression level of around 250 000 ASGP receptors per cell. This is comparable to the expression level in human liver hepatocytes. For uptake experiments, HepG2 cells were incubated with 300 nM fluorescent *N*-glycans for 30 min before qualitative analysis using confocal laser scanning microscopy (Fig. 3 and S6†). The nuclei were counterstained using Hoechst 33342. Cells were excited at 405 nm (Hoechst) and 488 nm (FTSC–glycans).

FTSC–glycans were internalized within 30 min resulting in a particulate intracellular fluorescence signal (Fig. 3; FTSC–glycan). The staining pattern suggests uptake and intracellular processing of FTSC–glycans by receptor mediated endocytosis. In order to confirm specificity of internalization *via* the ASGPR, uptake was inhibited using a 100× molar excess of asialofetuin (Fig. 3, CI-AF) or a 1000× molar excess of *N*-acetyl galactosamine (Fig. 3, CI-GalNAc). Since binding affinity of monovalent sugars is weak, a higher molar excess of GalNAc was needed for competitive inhibition as compared to multivalent asialofetuin. Both methods resulted in a significant decrease of *N*-glycan uptake, indicating a highly specific ASGPR-mediated endocytosis. To confirm that the *N*-glycan internalization is an energy dependent process, the uptake experiment was also performed at 4 °C (Fig. 3, 4 °C). No uptake was observed at low temperature confirming active transport.

In order to quantify fluorescent signals, we performed a flow cytometry analysis (Fig. 4). HepG2 cells incubated for 30 min with *N*-glycan-conjugates showed a three-fold shift of mean fluorescence intensity (Fig. 4A). Inhibition of this strong and fast uptake was observed in competitive inhibition experiments.

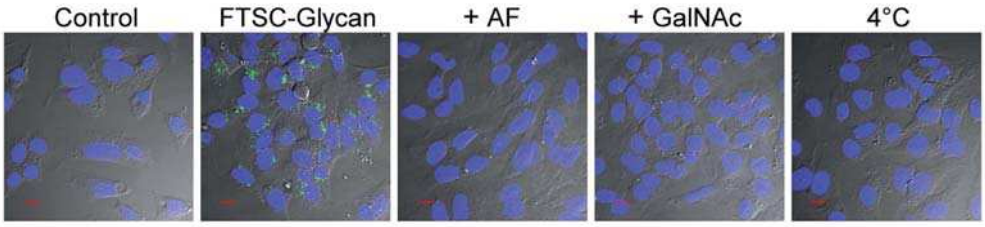

Fig. 3 Confocal laser scanning microscopy analysis of HepG2 cells incubated for 30 min with PBS (control) or FTSC-labelled multivalent *N*-glycans (green signal). Cellular uptake of *N*-glycans was competitively inhibited using an excess of asialofetuin (+AF) or *N*-acetyl galactosamine (+GalNAc). Cellular uptake was blocked at low temperature (4 °C). Nuclei are stained using Hoechst 33342 (blue signal). Differential interference contrast (DIC) images are combined with fluorescence signals from cell nuclei and fluorescent *N*-glycans. Scale bars: 20 μm. Single fluorescence channel signals are provided in the ESI (Fig. S6†).

Incubation in presence of an excess of free asialofetuin (Fig. 4B) or GalNAc (Fig. 4C) reduced the uptake of fluorescent *N*-glycans by 65% and 94%, respectively. Incubation at 4 °C completely blocked cellular uptake (Fig. 4D). These experiments confirm active and specific uptake of fluorescent-tagged, multivalent, isolated *N*-glycans by human liver cells *via* the ASGPR (Fig. 4).

In summary, this proof-of-concept study shows that multi-antennary *N*-glycans can be successfully isolated from glycoproteins (*i.e.* fetuin) and conjugated to model compounds (*i.e.* fluorophore) *via* reductive amination. We show that this approach is a convenient and efficient strategy to generate ligand-conjugates for hepatocyte specific targeting *via* the ASGPR. Current and future projects will focus on the implementation of glycan based ASGPR targeting strategies. First, the glycans will be linked to nanoparticles to guide encapsulated drugs (*i.e.* small molecules or nucleic acids) specifically to hepatocytes. This offers the possibility to overcome limitations of conventional therapeutics such as off target effects or drug degradation. Second, the *N*-glycans will be used to develop a diagnostic tool to determine the ASGPR expression level of parenchymal liver cells and thus preselect patients for a targeted therapy. This strategy might significantly increase the success rate of ASGPR targeted therapeutics for the treatment of hepatic disorders.

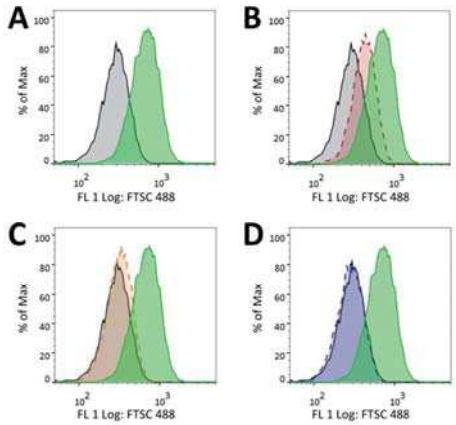

Fig. 4 Flow cytometry analysis of HepG2 cells incubated with (A) PBS (gray; solid line) and fluorescent *N*-glycans (green; solid line). Competitive inhibition using an excess of free asialofetuin (red; dashed line) or GalNAc (orange; dashed line) is shown in panel (B) and (C), respectively. Incubation at 4 °C completely inhibited the uptake (blue; dashed line; panel (D)).

Acknowledgements

The authors thank Dr Simon Sieber for scientific input and Darryl Borland for editorial assistance. Dominik Witzigmann acknowledges the financial support from the "Novartis University Basel Excellence Scholarship for Life Sciences".

Notes and references

1 A. Wicki, D. Witzigmann, V. Balasubramanian and J. Huwyler, *J. Controlled Release*, 2015, **200**, 138–157.
2 A. A. D'Souza and P. V. Devarajan, *J. Controlled Release*, 2015, **203**, 126–139.
3 M. D. Bider and M. Spiess, *FEBS Lett.*, 1998, **434**, 37–41.
4 S. E. Barrett, R. S. Burke, M. T. Abrams, C. Bason, M. Busuek, E. Carlini, B. A. Carr, L. S. Crocker, H. Fan, R. M. Garbaccio, E. N. Guidry, J. H. Heo, B. J. Howell, E. A. Kemp, R. A. Kowtoniuk, A. H. Latham, A. M. Leone, M. Lyman, R. G. Parmar, M. Patel, S. Y. Pechenov, T. Pei, N. T. Pudvah, C. Raab, S. Riley, L. Sepp-Lorenzino, S. Smith, E. D. Soli, S. Staskiewicz, M. Stern, Q. Truong, M. Vavrek, J. H. Waldman, E. S. Walsh, J. M. Williams, S. Young and S. L. Colletti, *J. Controlled Release*, 2014, **183**, 124–137.
5 D. B. Rozema, D. L. Lewis, D. H. Wakefield, S. C. Wong, J. J. Klein, P. L. Roesch, S. L. Bertin, T. W. Reppen, Q. Chu, A. V. Blokhin, J. E. Hagstrom and J. A. Wolff, *PNAS*, 2007, **104**, 12982–12987.
6 A. Akinc, W. Querbes, S. De, J. Qin, M. Frank-Kamenetsky, K. N. Jayaprakash, M. Jayaraman, K. G. Rajeev, W. L. Cantley, J. R. Dorkin, J. S. Butler, L. Qin, T. Racie, A. Sprague, E. Fava, A. Zeigerer, M. J. Hope, M. Zerial, D. W. Sah, K. Fitzgerald, M. A. Tracy, M. Manoharan,

V. Koteliansky, A. de Fougerolles and M. A. Maier, *Mol. Ther.*, 2010, **18**, 1357–1364.
7 S. Matsuda, K. Keiser, J. K. Nair, K. Charisse, R. M. Manoharan, P. Kretschmer, C. G. Peng, A. V. Kel'in, P. Kandasamy, J. L. S. Willoughby, A. Liebow, W. Querbes, K. Yucius, T. Nguyen, S. Milstein, M. A. Maier, K. G. Rajeev and M. Manoharan, *ACS Chem. Biol.*, 2015, **10**, 1181–1187.
8 K. G. Rajeev, J. K. Nair, M. Jayaraman, K. Charisse, N. Taneja, J. O'Shea, J. L. S. Willoughby, K. Yucius, T. Nguyen, S. Shulga-Morskaya, S. Milstein, A. Liebow, W. Querbes, A. Borodovsky, K. Fitzgerald, M. A. Maier and M. Manoharan, *ChemBioChem*, 2015, **16**, 903–908.
9 Y. K. Dhande, B. S. Wagh, B. C. Hall, D. Sprouse, P. B. Hackett and T. M. Reineke, *Biomacromolecules*, 2016, **17**, 830–840.
10 T. Yamamoto, M. Sawamura, F. Wada, M. Harada-Shiba and S. Obika, *Bioorg. Med. Chem.*, 2016, **24**, 26–32.
11 Z. Guo, M. Gao, M. Song, Y. Li, D. Zhang, D. Xu, L. You, L. Wang, R. Zhuang, X. Su, T. Liu, J. Du and X. Zhang, *Adv. Mater.*, 2016, **28**, 5898–5906.
12 D. Witzigmann, L. Quagliata, S. H. Schenk, C. Quintavalle, L. M. Terracciano and J. Huwyler, *Hepatol. Res.*, 2015, **46**, 686–696.
13 M. D. Bider, R. Cescato, P. Jenö and M. Spiess, *Eur. J. Biochem.*, 1995, **230**, 207–212.
14 S. K. Mamidyala, S. Dutta, B. A. Chrunyk, C. Préville, H. Wang, J. M. Withka, A. McColl, T. A. Subashi, S. J. Hawrylik, M. C. Griffor, S. Kim, J. A. Pfefferkorn, D. A. Price, E. Menhaji-Klotz, V. Mascitti and M. G. Finn, *J. Am. Chem. Soc.*, 2012, **134**, 1978–1981.
15 D. Stokmaier, O. Khorev, B. Cutting, R. Born, D. Ricklin, T. O. G. Ernst, F. Böni, K. Schwingruber, M. Gentner, M. Wittwer, M. Spreafico, A. Vedani, S. Rabbani, O. Schwardt and B. Ernst, *Bioorg. Med. Chem.*, 2009, **17**, 7254–7264.
16 A. G. Majouga, Y. A. Ivanenkov, M. S. Veselov, A. V. Lopuhov, S. V. Maklakova, E. K. Beloglazkina, N. L. Klyachko, Y. B. Sandulenko, N. Y. Galkina and V. E. Koteliansky, *Curr. Drug Delivery*, 2016, 13.
17 O. Khorev, D. Stokmaier, O. Schwardt, B. Cutting and B. Ernst, *Bioorg. Med. Chem.*, 2008, **16**, 5216–5231.
18 P. C. N. Rensen, S. H. van Leeuwen, L. A. J. M. Sliedregt, T. J. C. van Berkel and E. A. L. Biessen, *J. Med. Chem.*, 2004, **47**, 5798–5808.
19 M. Monestier, P. Charbonnier, C. Gateau, M. Cuillel, F. Robert, C. Lebrun, E. Mintz, O. Renaudet and P. Delangle, *ChemBioChem*, 2016, **17**, 590–594.
20 R. T. Lee and Y. C. Lee, *Glycoconjugate J.*, 2000, **17**, 543–551.
21 J. J. Lundquist and E. J. Toone, *Chem. Rev.*, 2002, **102**, 555–578.
22 P. Detampel, D. Witzigmann, S. Krähenbühl and J. Huwyler, *J. Drug Targeting*, 2014, **22**, 232–241.
23 J. U. Baenziger and D. Fiete, *J. Biol. Chem.*, 1979, **254**, 789–795.
24 E. D. Green, G. Adelt, J. U. Baenziger, S. Wilson and H. V. Halbeek, *J. Biol. Chem.*, 1988, **263**, 18253–18268.
25 A. M. Wu, J. H. Wu, T. Singh, L.-J. Lai, Z. Yang and A. Herp, *Mol. Immunol.*, 2006, **43**, 1700–1715.
26 M. F. Verostek, C. Lubowski and R. B. Trimble, *Anal. Biochem.*, 2000, **278**, 111–122.
27 T. Masuko, A. Minami, N. Iwasaki, T. Majima, S.-I. Nishimura and Y. C. Lee, *Anal. Biochem.*, 2005, **339**, 69–72.
28 A. E. Manzi, L. D. Powell and A. Varki, in *Current Protocols in Molecular Biology*, John Wiley & Sons, Inc., 2001.
29 S. Kongruang, M. J. Han, C. I. G. Breton and M. H. Penner, *Appl. Biochem. Biotechnol.*, 2004, **113–116**, 213–231.
30 W. Morelle and J.-C. Michalski, *Nat. Protoc.*, 2007, **2**, 1585–1602.
31 L. Han and C. E. Costello, *Biochemistry*, 2013, **78**, 710–720.
32 S. Ijiri, K. Todoroki, H. Yoshida, T. Yoshitake, H. Nohta and M. Yamaguchi, *Electrophoresis*, 2011, **32**, 3499–3509.

RSC Advances

SUPPORTING INFORMATION

Isolation of multiantennary *N*-glycans from glycoproteins for hepatocyte specific targeting via the asialoglycoprotein receptor

Received 2016
Accepted 2016

DOI: 10.1039/x0xx00000x

www.rsc.org/

Dominik Witzigmann,[a] Pascal Detampel,[a] Fabiola Porta,[a] and Jörg Huwyler [a]*

Experimental - Supporting Information

Enzymatic digestion

Fetuin A from fetal calf serum was purchased from Sigma-Aldrich (F3004, Lot-No. 109K7425V, Buchs, Switzerland). Fetuin A has an average molecular weight (MW) of 48.4 kDa (full glycoprotein) including a constant protein part (38.4 kDa) and a variable glycosylation pattern (*N*- and *O*-glycosylations). In the SDS-PAGE analysis fetuin A showed a main band of 63.2 kDa corresponding to the full glycoprotein. It has been reported that the molecular mass varies depending on the carbohydrate content. [1] A standard logMW versus Rf blot was used for the molecular weight determination. For the enzymatic digestion Peptide-*N*-Glycosidase F (PNGase F; 36 kDa) and α2-3,6,8 neuraminidase (Sialidase; 43 kDa) (Fig. S3) were used. Enzymes were obtained from New England BioLabs (Ontario, Canada). Fetuin A was dissolved in ddH_2O containing 0.5% SDS and 40 mM DTT. This solution was heated to 94 °C for 10 min in order to denature the glycoprotein. Phosphate buffer (final concentration 50 mM; pH 7.5), 1% NP40 (detergent), PNGase F (5.37 mU/1 mg fetuin A), sialidase (35U/1 mg fetuin A), and ddH_20 were added to a final fetuin A concentration of 10 mg/mL. Enzymatic digest was for 72 h at 37 °C.

Electrophoretic mobility assay

SDS containing polyacrylamide gels (10%) were prepared using a standard protocol. Samples containing the digested glycoprotein were mixed with reducing sample buffer containing SDS and *β*-mercaptoethanol, heated to 94 °C for 5 min, loaded onto the gel and separated using a current of 30 mA. Proteins were stained using Coomassie blue.

RCA aggregation assay

The Ricinus communis agglutinin (RCA) aggregation assay was performed as described previously. [2,3] In brief, the UV absorbance at 450 nm of 1 mg/mL RCA_{120} (Vector Laboratories, Peterborough, UK) in Dulbecco`s phosphate buffered saline pH 7.4 (Sigma-Aldrich) was measured for 2 min to establish a baseline using a SpectraMax M2 spectrophotometer (Molecular Devices, Sunnyvale, USA). Glycoprotein was added to initiate lectin aggregation. After 6 min, a galactose solution (10 mg/mL) was added to reverse the aggregation process.

[a] *Division of Pharmaceutical Technology, Department of Pharmaceutical Sciences, University of Basel, Klingelbergstrasse 50, Basel CH-4056, Switzerland.*
**E-mail: joerg.huwyler@unibas.ch*

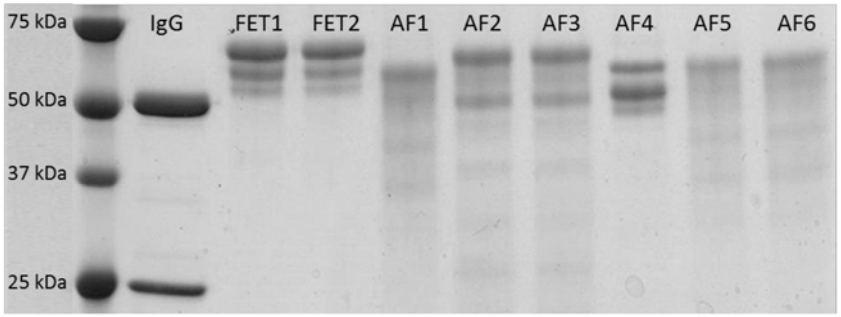

Fig. S1: Analysis of electrophoretic mobility of different fetuin A (FET) and asialofetuin (AF) batches using SDS-PAGE. Proteins were stained using Coomassie blue.

Liquid-liquid extraction

Liquid-liquid extraction of *N*-glycans was performed as described previously with minor modifications. [4] The pH of the digestion mixture was adjusted to 5.5 using an aq.phosphoric acid soln. (8.5%). Acetone was added and the sample was kept for 1 h at -20 °C to precipitate glycans and proteins. The sample was centrifuged for 20 min at 13000 g and 2 °C and the supernatant was discarded. The pellet was resuspended using 1 mL of an aq. methanol soln. (60%) at -20 °C and the sample was left for 1 h at -20 °C to precipitate proteins. Finally, the sample was centrifuged for 5 min at 13000 g and 2 °C and the supernatant containing the *N*-glycans was collected. The methanol extraction procedure was repeated twice.

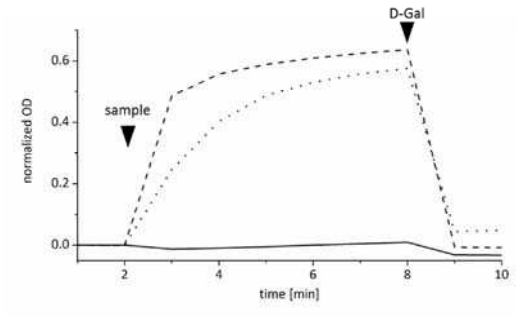

Fig. S2: Ricinus communis agglutinin aggregation assay of fetuin A (solid line), and two different asialofetuin batches (dashed and dotted line). Black triangles: in presence of desialylated glycoprotein (sample), aggregation is induced; competitive de-aggregation by a 100-fold excess of free D-galactose (D-Gal).

Size exclusion chromatography

Isolated *N*-glycans were separated from protein residuals and fractionated using a Superdex 30 Prep Grade column (XK 16/70, GE Healthcare, Glattbrugg, Switzerland) eluting with an aq. phosphate buffer (10 mM, pH 7.4). Collected fractions were dried under nitrogen.

BCA assay

Multiantennary glycan fractions containing terminal sugars with a free and reducing anomeric carbon were identified using a modified bicinchoninic acid (BCA) assay (ThermoFisher Scientific, Zug, Switzerland). [5,6] In brief, samples were mixed with the working reagent (50:1, reagent A:B) in a 1:1 ratio. Samples were heated for 30 min at 65 °C using a water bath, allowed to cool down to room temperature and analysed by UV absorbance measurement at 562 nm.

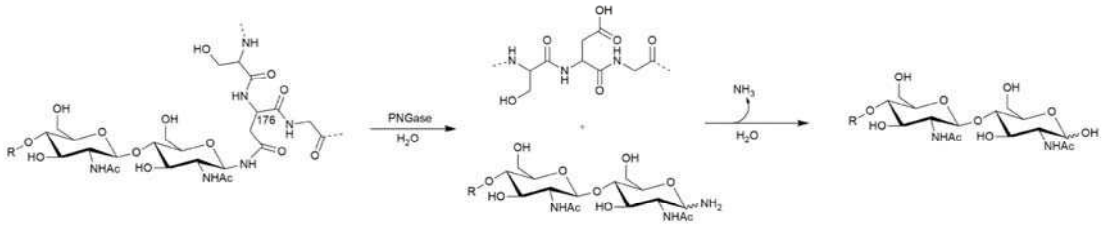

Fig. S3: Enzymatic digestion of bovine fetuin A using Peptide-*N*-Glycosidase F (PNGase) leading to deglycosylation at the representative amino acid position 176. PNGase F selectively cleaves the bond between asparagine and *N*-linked complex carbohydrates. Terminal sialic acid on multiantennary *N*-glycans was cleaved by sialidase.

Bradford assay

Proteins were detected using the Bradford assay (Bio-Rad Laboratories). Samples (160 µl) were mixed with 40 µl dye reagent containing Coomassie blue, methanol, and phosphoric acid. After 10 min incubation at room temperature, the absorbance at 595 nm was determined.

PSAA assay

To detect carbohydrates, the phenol–sulfuric acid assay (PSAA) was used. [7] In brief, the sample was mixed with a threefold volume of concentrated sulfuric acid. Then, an aq. phenol soln. (5%) was added and the mixture was incubated for 5 min at 90 °C. Absorbance was measured at 490 nm.

MALDI-TOF-MS

Fractions containing *N*-glycans were prepared for matrix-assisted laser desorption ionization time of flight mass spectrometer (MALDI-TOF-MS) analysis as follows: The 2,5-dihydroxy benzoic acid (DHB) matrix was spotted onto a MALDI-TOF-MS target plate and allowed to dry. Samples were added to each spot and allowed to dry before analysis. Mass spectra were recorded using a Bruker Ultraflex MALDI-TOF-MS (Bruker, Bremen, Germany). Spectra were analysed using the Bruker Daltonics flex analysis software.

Fluorescent labelling

In order to label isolated *N*-glycans with fluorescein-5-thiosemicarbazide (FTSC; Sigma-Aldrich), a carbohydrate sample (250 µg) was dissolved in 400 µL of a mixture of DMSO and aq. 0.1 M acetic acid soln. (7:3), FTSC (0.25 mg) dissolved in DMF (20 µL) was added and the mixture was stirred for 30 min. To reduce the hydrazone bond and to stabilize the conjugate, an excess of sodium cyanoborhydride was added (500 mM final concentration). The mixture was stirred for 2 h at 70 °C and 700 rpm. Finally, potassium hexacyanoferrate (20 mg) was added to quench the excess of cyanoborhydride and to increase the fluorescence of the fluorophore. The mixture was stirred for 60 min at room temperature. Figure S4 shows the chemical reaction of fluorescent labelling of isolated *N*-glycans. The FTSC-labelled *N*-glycans were purified by gel filtration chromatography (Sephadex G10; GE Healthcare, Glattbrugg, Switzerland; mobile phase of 0.01 M phosphate buffered saline (PBS), pH 7.4).

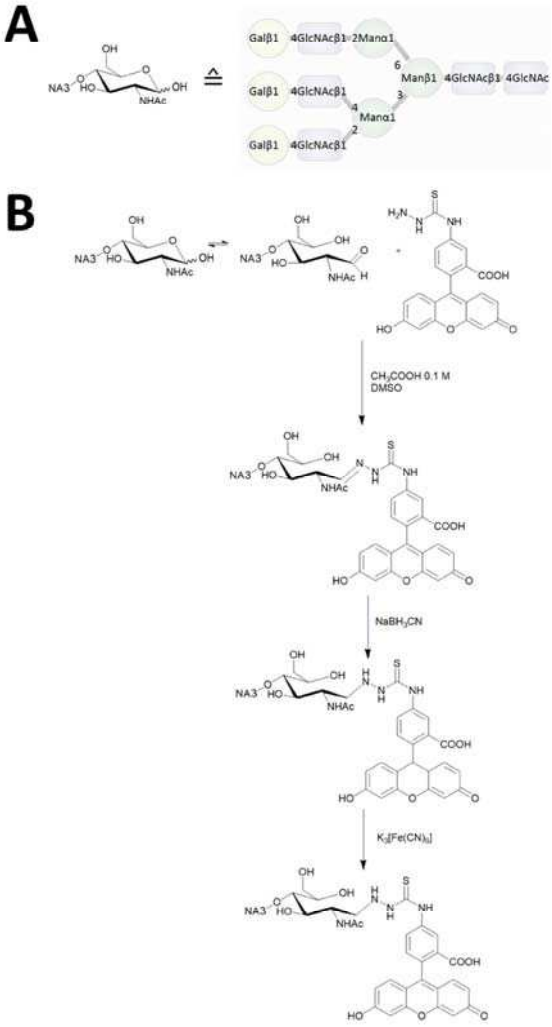

Fig. S4: Fluorescent labelling of complex carbohydrates. (A) Representation of a desialylated triantennary *N*-glycan (NA3) cleaved from asparagine 176 of bovine fetuin A. (B) Chemical reactions for fluorescent labelling of isolated *N*-glycans with fluorescein-5-thiosemicarbazide (FTSC) via reductive amination. Gal: galactose; Man: mannose; GlcNAc: *N*-acetyl glucosamine.

Uptake experiment

Human hepatocellular carcinoma cells (HepG2) were kindly provided by Prof. Dr. Dietrich von Schweinitz (University Hospital Basel, Switzerland). Cells were cultured at 37 °C in a 5% CO_2 atmosphere. All cell culture reagents were purchased from ThermoFisher Scientific (Zug, Switzerland). Dulbecco`s modified Eagle`s culture medium (4.5 g/L glucose) was supplemented with 10% fetal calf serum (FCS), penicillin (100 units/mL) and streptomycin (100 µg/mL). For uptake experiments, HepG2 cells were washed with PBS, detached using accutase and then seeded into 12-well plates at a

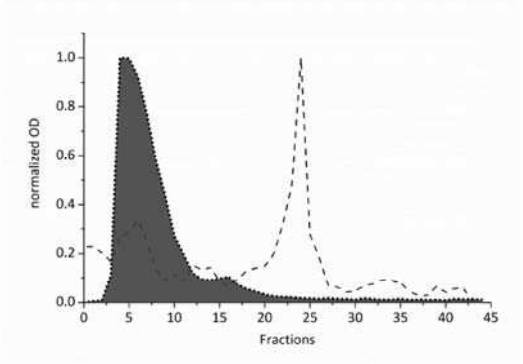

Fig. S5: Size exclusion chromatography fractions of enzymatically digested fetuin A were analysed using different colorimetric assays. The Bradford assay (dotted line, grey) represents the protein residues. The phenol–sulfuric acid assay (dashed line, white) detects carbohydrates. A baseline separation of proteins and free glycans was achieved.

density of 10^5 cells/well. They were allowed to adhere for 24 h. For confocal laser scanning microscopy experiments, cells were cultured on poly-D-lysine coated glass cover slips. Uptake experiments were performed as described previously. [8] In brief, HepG2 cells were incubated with 300 nM fluorescent glycans for 30 min at 37 °C in DMEM without FCS. As a control, cells were co-incubated with asialofetuin (30 µM) or GalNAc (300 µM) or incubations were carried out at 4 °C. Confocal laser scanning microscopy and flow cytometry were used for qualitative and quantitative analysis of uptake, respectively.

Confocal laser scanning microscopy analysis

Cell nuclei were counterstained using 1.0 µg/mL Hoechst 33342 (Sigma-Aldrich). Cells were washed with PBS and then embedded using ProLong Gold antifading reagent (Invitrogen Life Technologies, Zug, Switzerland). Confocal laser scanning microscopy analysis was performed using an Olympus FV-1000 inverted microscope (Olympus Ltd., Tokyo, Japan), equipped with a 60x PlanApo N oil-immersion objective (numerical aperture 1.40). Hoechst 33342 and FTSC-glycans were visualized using excitation at 405 nm and 488 nm and emission at 425-475 nm and 500-600 nm, respectively.

Flow cytometry analysis

For flow cytometry analysis, cells were washed with PBS and detached using 0.25% trypsin/EDTA. Cells were washed twice and then re-suspended in FACS buffer (PBS containing 1% FCS, 0.05% NaN_3, and 2.5 mM EDTA). A FACS Canto II flow cytometer (Becton Dickinson, San Jose, USA) was used for the analysis of 10`000 cells per setting. Cells were excited at 488 nm and the emission was detected in FL1 (505LP - 530/30). To evaluate the uptake rate of FTSC-glycans, Flow Jo VX software (TreeStar, Ashland, OR) was used.

Table S1: Most abundant complex carbohydrates detected after isolation procedure using MALDI-TOF-MS.

Detected Signal $[M+Na]^+$	Attached to	Glycan structure	Reference
1664	ASN-99 and ASN-156	[NA2], e.g. Gal(b1-4)GlcNAc(b1-2)Man(a1-3)[Gal(b1-4)GlcNAc(b1-2)Man(a1-6)]Man(b1-4)GlcNAc(b1-4)GlcNAc	9–11
2029	ASN-99, ASN-156 (major) AND ASN-176	[NA3], e.g. Gal(b1-4)GlcNAc(b1-2)[Gal(b1-4)GlcNAc(b1-4)]Man(a1-3)[Gal(b1-4)GlcNAc(b1-2)Man(a1-6)]Man(b1-4)GlcNAc(b1-4)GlcNAc	9–11
2029	ASN-99, ASN-156 AND ASN-176 (major)	[NA3], e.g. Gal(b1-3)GlcNAc(b1-4)[Gal(b1-4)GlcNAc(b1-2)]Man(a1-3)[Gal(b1-4)GlcNAc(b1-2)Man(a1-6)]Man(b1-4)GlcNAc(b1-4)GlcNAc	9–11

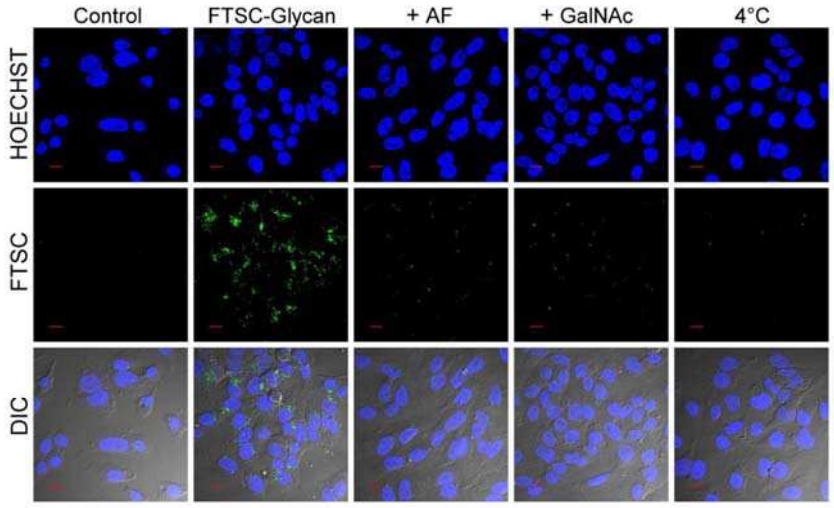

Fig. S6: Confocal laser scanning microscopy analysis of HepG2 cells incubated for 30 min with PBS (control) or FTSC-labelled multivalent N-glycans (green signal). Cellular uptake of N-glycans was competitively inhibited using an excess of asialofetuin (+ AF) or N-acetyl galactosamine (+ GalNAc). Cellular uptake was blocked at low temperature (4 °C). Nuclei are stained using Hoechst 33342 (blue signal). Differential interference contrast (DIC) images are combined with fluorescence signals from cell nuclei and fluorescent N-glycans. Scale bars: 20 µm.

Results - Supporting Information

Electrophoretic mobility batch control

Different batches of fetuin A (FET) and asialofetuin (AF) purchased from Sigma-Aldrich were compared by analysis of their electrophoretic mobility. Figure S1 shows variations in electrophoretic mobility for different asialofetuin batches. Asialofetuin batches AF2 and AF3 show a decreased mobility as compared to other AF batches. These two AF batches have shown a decreased aggregation in the RCA aggregation assay confirming incomplete desialylation of linked glycans (Fig. S2). After a glycan digest using sialidase, the electrophoretic mobility of asialofetuin batches AF2/AF3 was increased and RCA aggregation could be induced. We conclude, that commercial AF (in contrast to fetuin A) shows considerable batch-to-batch differences and that enzymatic treatment (in contrast to chemical processing) of fetuin A leads to better results with respect to completeness of desialylation (AF4). It was therefore decided to use fetuin A as a starting material for further investigations.

RCA aggregation assay batch control

The ricininus communis agglutinin aggregation assay was used as a tool to compare different asialofetuin batches. Figure S2 shows the variation in complexation kinetics of different asialofetuin batches. An excess of galactose (D-Gal) reduces the lectin crosslinking and thus the aggregation.

Analysis of size exclusion chromatography fractions

Size exclusion chromatography was used to separate the different components (i.e. proteins and glycans) of enzymatically digested fetuin. Fractions were analysed

using three different microplate assays (Fig. S5). A Bradford assay was performed to determine the protein content (Fig. S5). As expected, not all proteins have been removed using the liquid-liquid extraction. However, the phenol sulfuric acid assay (PSAA, i.e. total carbohydrate assay) verified, that isolated glycans have successfully been separated from the protein residuals (Fig. S5).

MALDI-TOF-MS

Table S1 summarizes the signals from the MALDI-TOF analysis and published glycosylations reported on unicarbkb.org for bovine fetuin A (Accession number: P12763). [9–11] In total there are 46 associated glycan structures reported with its major glycosylations linked to asparagines at amino acid positions 99, 156, and 176.

Confocal laser scanning microscopy analysis of cellular uptake

The uptake experiments confirm active and specific uptake of fluorescent-tagged, multivalent, isolated *N*-glycans (Fig. S6).

Notes and references - Supporting Information

1 A. M. Sakwe, R. Koumangoye, S. J. Goodwin and J. Ochieng, *J Biol Chem*, 2010, **285**, 41827–41835.
2 C. Managit, S. Kawakami, F. Yamashita and M. Hashida, *J Pharm Sci*, 2005, **94**, 2266–2275.
3 K. Morimoto, M. Nishikawa, S. Kawakami, T. Nakano, Y. Hattori, S. Fumoto, F. Yamashita and M. Hashida, *Mol. Ther.*, 2003, **7**, 254–261.
4 M. F. Verostek, C. Lubowski and R. B. Trimble, *Anal. Biochem.*, 2000, **278**, 111–122.
5 A. E. Manzi, L. D. Powell and A. Varki, in *Current Protocols in Molecular Biology*, John Wiley & Sons, Inc., 2001.
6 S. Kongruang, M. J. Han, C. I. G. Breton and M. H. Penner, *Appl. Biochem. Biotechnol.*, 2004, **113–116**, 213–231.
7 T. Masuko, A. Minami, N. Iwasaki, T. Majima, S.-I. Nishimura and Y. C. Lee, *Anal. Biochem.*, 2005, **339**, 69–72.
8 P. Detampel, D. Witzigmann, S. Krähenbühl and J. Huwyler, *Journal of Drug Targeting*, 2014, **22**, 232–241.
9 J. S. Rohrer, G. A. Cooper and R. R. Townsend, *Anal. Biochem.*, 1993, **212**, 7–16.
10 K. G. Rice, N. B. Rao and Y. C. Lee, *Anal. Biochem.*, 1990, **184**, 249–258.
11 T. Tamura, M. S. Wadhwa and K. G. Rice, *Anal. Biochem.*, 1994, **216**, 335–344.

Chapter VI

"Formation of Lipid and Polymer-based Gold Nanohybrids Using a Nanoreactor Approach"

Witzigmann D, Sieber S, Porta F, Grossen P, Bieri A, Strelnikova N, Pfohl T, Baschong C, Huwyler J.

RSC Advances. 2015 Aug 25; 5(91):74320-28. doi: 10.1039/c5ra13967h

http://pubs.rsc.org/en/Content/ArticleLanding/2015/RA/C5RA13967H#!divAbstract

Highlights: The analysis of nanocarrier uptake and their intracellular fate is of great interest in biomedical research. Bioimaging tools to determine subcellular localization of nanocarriers are increasingly needed. This publication highlights the development of a novel and versatile strategy to encapsulate gold nanoparticles into nanocarriers. This approach is applicable to different nanomaterials as well as various preparation techniques with high reproducibility. The unique optical properties of gold loaded nanocarriers were used to visualize cellular uptake *in vitro* demonstrating the promising applicability as a bioimaging tool for intracellular trafficking. In the future, this technology will be instrumental to develop a better understanding of the complex cellular uptake processes and intracellular trafficking of nanocarriers.

RSC Advances

PAPER

View Article Online
View Journal | View Issue

Cite this: *RSC Adv.*, 2015, **5**, 74320

Formation of lipid and polymer based gold nanohybrids using a nanoreactor approach†

Dominik Witzigmann,[a] Sandro Sieber,[a] Fabiola Porta,[a] Philip Grossen,[a] Andrej Bieri,[b] Natalja Strelnikova,[c] Thomas Pfohl,[c] Cristina Prescianotto-Baschong[d] and Jörg Huwyler*[a]

Received 15th July 2015
Accepted 24th August 2015

DOI: 10.1039/c5ra13967h

www.rsc.org/advances

Nanocarriers encapsulating gold nanoparticles (AuNPs) hold tremendous promise for numerous biomedical applications. So far only a few fabrication strategies have been investigated and efficient processes for the manufacturing of gold nanohybrids (AuNHybs) are still missing. We encapsulated a tetrachloroaurate/citrate mixture within nanocarriers and initiated the AuNP formation after self-assembly of the nanomaterial by a temperature shift. This nanoreactor approach was successfully combined with the film-rehydration, nanoprecipitation, or microfluidics method. Different nanomaterials were validated including phospholipids and copolymers and the process was optimized towards encapsulation efficiency and physico-chemical homogeneity of AuNHybs. Our nanoreactor technology is versatile, efficient, and highly reproducible. Dynamic light scattering and electron microscopy techniques confirmed that generated lipid and polymer based AuNHybs were of uniform size below 130 nm and contained a single AuNP. The AuNHyb solutions had a deep-red color and exhibited the specific surface plasmon absorption of AuNPs. The unique optical properties of AuNHybs were used to visualize cellular uptake of nanocarriers *in vitro* demonstrating the promising applicability of AuNHybs as a bioimaging tool.

1. Introduction

Gold nanoparticles (AuNPs) have attracted great interest since Michael Faraday first described them in 1857.[1,2] The application of AuNPs in the field of imaging and therapy were based on their unique properties, which include; (I) advantageous physico-chemical characteristics, (II) non-toxic and inert properties, (III) facile preparation of monodisperse AuNPs, and (IV) various modification options.[3–5] Different methods for the synthesis of AuNPs have been described.[6,7] The most widely used approach is the chemical reduction of gold salt (Au^{3+}) such as tetrachloroaurate ($HAuCl_4$) to metallic gold (Au^0) using the Turkevich[8,9] or Brust-Schiffrin[10] method. Moreover, synthesis methods using microwaves, UV irradiation, microfluidics, or biologic approaches were examined.[3,11] Ultimately, AuNPs have to be modified with capping agents to avoid aggregation, provide solubility in aqueous media, and improve stability.[12]

Encapsulation of AuNPs into different nanocarriers such as liposomes or polymeric nanoparticles is an interesting option for a wide range of applications such as smart drug delivery, imaging, or photothermal therapy.[13–18] In recent decades, great progress has been made in the field of hybrid nanocarriers using AuNPs and several strategies for their synthesis have been investigated. For example, lipid based gold nanohybrids (lipid-AuNHybs) have been prepared using the following methods: improved cholate dialysis,[19] incorporation of hydrophobic AuNPs,[20–22] physical absorption,[23,24] or precipitation of gold within liposomes using either, glycerol including formation or reverse-phase evaporation.[25,26]

However, these strategies exhibited marked variability in homogeneity, reproducibility, size distribution, and morphology of gold nanohybrids (AuNHybs). To overcome these challenges, we developed a novel and versatile strategy to encapsulate AuNPs into different nanocarriers with high reproducibility using a nanoreactor approach. The goal of the present study was, (I) the encapsulation of a tetrachloroaurate/citrate mixture within nanocarriers and (II) the initiation of AuNP formation after self-assembly of the nanomaterial. Selected nanomaterials (*i.e.* lipid and polymer based) were validated and the encapsulation efficiency, homogeneity, and robustness of our approach were optimized. Nanocarriers loaded with AuNPs were prepared by three different methods depending on the physico-chemical properties of the nanocarrier material.

[a]*Division of Pharmaceutical Technology, Department of Pharmaceutical Sciences, University of Basel, Klingelbergstrasse 50, Basel CH-4056, Switzerland. E-mail: joerg.huwyler@unibas.ch*

[b]*Center for Cellular Imaging and NanoAnalytics (C-CINA), Biozentrum, University of Basel, Mattenstrasse 26, Basel CH-4058, Switzerland*

[c]*Department of Chemistry, University of Basel, Klingelbergstrasse 80, Basel CH-4056, Switzerland*

[d]*Biozentrum, University of Basel, Klingelbergstrasse 70, Basel CH-4056, Switzerland*

† Electronic supplementary information (ESI) available. See DOI: 10.1039/c5ra13967h

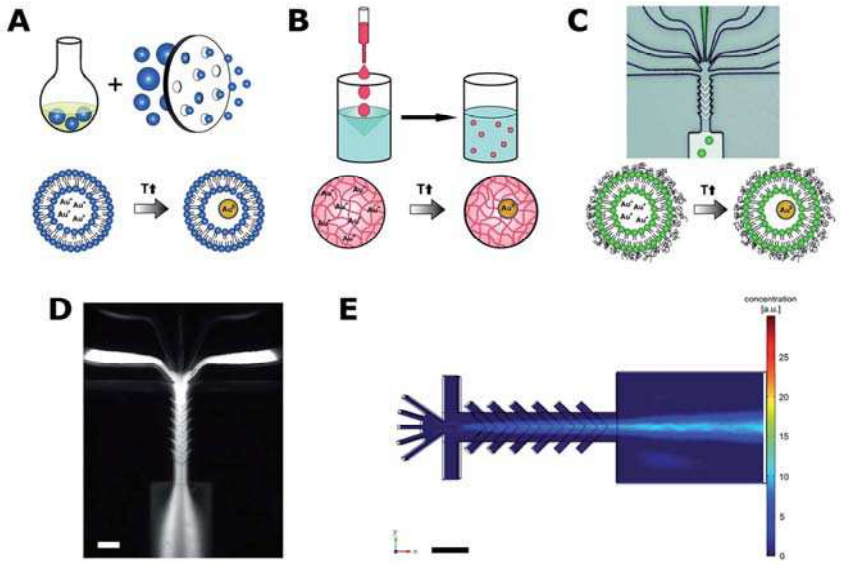

Fig. 1 Different methods for the preparation of gold nanohybrids. Schematic representation of the, (A) film-rehydration–extrusion method for lipids with T_m < room temperature (RT), (B) nanoprecipitation method for the di-block copolymer PEG–PCL, and (C) microfluidics platform for lipids with T_m > RT. The formation of gold nanoparticles inside the nanocarriers was initiated by temperature increase after self-assembly. (C) The microfluidics device had seven inlet channels converging to a single staggered herringbone micromixer. (D) Microfluidic streams were visualized using the fluorescence dye fluorescein. (E) Computational fluid dynamics simulation of concentration gradients (in a.u.) in the microfluidics device. Scale bars indicate 100 μm.

The film-rehydration–extrusion method[27] was used for conventional (non-PEGylated) liposomes, the nanoprecipitation method[28] was used for di-block copolymer nanoparticles, and the microfluidics method[29,30] was used for PEGylated (sterically stabilized) liposomes (Fig. 1). The most important feature of our nanoreactor approach is the production of nanocarriers at room temperature (RT), which avoids the formation of AuNPs before self-assembly. AuNP formation is subsequently initiated by a temperature shift. The applicability of the AuNHybs as bioimaging tool was demonstrated *in vitro* using HepG2 human hepatocellular carcinoma cells.

2. Experimental section

2.1 AuNP synthesis

AuNPs were synthesized following a modified Turkevich method.[7] Optimization of AuNP synthesis using a 2^3 full factorial design of experiment (DoE) [Stavex 5.2, Aicos Technologies, Basel, Switzerland] is described in detail in the ESI (Table S1†). Briefly, ddH_2O with 1 mM tetrachloroaurate (Sigma-Aldrich, Buchs, Switzerland) were heated to 70 °C for 20 min under vigorous stirring. To start the formation of AuNPs, citrate solution (170 mM; 50 mg mL^{-1}) was added as a reducing and capping reagent. The $HAuCl_4$/citrate gold reaction mixture (AuR-solution) was stirred at 70 °C for 10 min until the solution had a deep-red color.

2.2 AuNHyb formation using film rehydration

The film rehydration method was used for lipids with a transition temperature (T_m) below RT with modifications described elsewhere.[31] Liposomes were produced at a temperature which inhibits the AuNP formation. In brief, 1-palmitoyl-2-oleoyl-*sn-glycero*-3-phosphocholine (15 μmol) [POPC] (Avanti Polar-Lipids, Alabaster, USA) and 1-palmitoyl-2-oleoyl-*sn-glycero*-3-phospho-1′-*rac*-glycerol (5 μmol) [POPG] (Avanti Polar-Lipids, Alabaster, USA) were dissolved in chloroform/methanol (2 : 1, v/v) and a homogenous dry lipid film was prepared using a Rotavapor A-134 (Büchi, Flawil, Switzerland). The lipid film was rehydrated with a freshly prepared AuR-solution ($HAuCl_4$: citrate ratio – 1 : 4) at RT and 120 rpm for 10 min with 3 g glass beads (diameter 5 mm). Different lipid (20 mM) to AuR-solution ratios were tested starting from 1 mM $HAuCl_4$/4.1 mM citrate up to 8 mM $HAuCl_4$/32.8 mM citrate.

The resulting multilamellar vesicles were subjected to three freeze–thaw cycles and extruded through polycarbonate membranes with two different pore sizes using a barrel extruder (Lipex; Northern Lipids, Vancouver; Canada). Liposomes were extruded at RT 3 times through a 200 nm polycarbonate membrane and 11 times through a membrane with a pore size of 100 nm (VWR International, Dietikon, Switzerland). AuNPs, which were formed during the extrusion procedure, bind to the filter membranes. Finally, the unilamellar liposomes were heated to 70 °C for 10 min to start the formation of AuNPs. To separate liposomes from free AuNPs, the sample was purified by FPLC using a Superose 6 prep column (GE Healthcare,

Glattbrugg, Switzerland) eluting with 0.01 M phosphate buffered saline (PBS) containing 150 mM sodium chloride, pH 7.4 (Sigma-Aldrich, Buchs, Switzerland).

2.3 AuNHyb formation using nanoprecipitation

A nanoprecipitation method was used for the di-block copolymer polyethyleneglycol–polycaprolactone [PEG–PCL] (Sigma-Aldrich, Buchs, Switzerland). The polymer (5 mg) was dissolved in THF (50 μL) [Sigma-Aldrich, Buchs, Switzerland] under constant stirring with a magnetic bar (750 rpm). The AuR-solution ($HAuCl_4$: citrate ratio – 1 : 4) was added dropwise (one drop per five seconds). The mixture was stirred for 10 min at 750 rpm followed by 10 min on a thermomixer at 70 °C and 300 rpm. Different polymer to AuR-solution ratios were tested starting from 1 mM $HAuCl_4$/4.1 mM citrate up to 8 mM $HAuCl_4$/32.8 mM citrate. To separate the PEG–PCL–AuNHybs from free AuNPs, a FPLC purification step was used (see above).

2.4 Microfluidics device design and fabrication

The microfluidics device was fabricated with 0.05 mm thick polystyrene foil (GoodFellow, Huntingdon, UK) and NOA 81 (Norland, Cranberry, USA) using standard soft-lithography techniques according to the procedure described previously.[32,33] The microfluidics device had seven inlet channels converging to a single staggered herringbone micromixer. The rectangular cross-section had dimensions of 468 μm length, 80 μm width, and 40 μm/200 μm height (Fig. 1C). Detailed experimental procedures are given in the ESI.†

2.5 Flow visualization and computational fluid dynamics simulation

Detailed experimental procedures are given in the ESI.†

2.6 AuNHyb formation using microfluidics

The microfluidics method was used for lipids with a transition temperature above RT (55 °C). Therefore, the AuNP formation during the liposome production was hampered due to decreased temperature. 1,2-Distearoyl-*sn-glycero*-3-phosphocholine (DSPC) [5.75 μmol] (Avanti Polar-Lipids, Alabaster, USA), cholesterol [4 μmol] (Sigma-Aldrich, Buchs, Switzerland), and 1,2-distearoyl-*sn-glycero*-3-phosphoethanolamine-*N*-(methoxy(polyethylene glycol)-2000) (DSPE-PEG2000) [0.25 μmol] (Avanti Polar-Lipids, Alabaster, USA) were dissolved in ethanol. The microfluidics device was primed with water for the outer streams and with ethanol for the central inlet (1 μL s^{-1}) using syringe pumps.

Afterwards four different syringes were connected: (I) double-distilled water, (II) citrate solution (4.1 mM–32.8 mM), and (III) tetrachloroaurate ($HAuCl_4$) solution (1 mM–8 mM) were connected to the outer streams (always with a $HAuCl_4$: citrate ratio of 1 : 4) and (IV) lipids in ethanol (5 mM) were connected to the central inlet. The speed was set to 4 μL s^{-1} for syringe I, 2 μL s^{-1} for syringe II/III and 1 μL s^{-1} for syringe IV. The sample was collected at the outlet. Finally, the liposomes were heated to 70 °C for 10 min to start the formation of AuNPs. To separate lipid-AuNHybs from free AuNPs, the sample was purified by FPLC using a Superose 6 prep column eluting with 0.01 M PBS pH 7.4.

2.7 Size analysis using dynamic light scattering

Dynamic light scattering (DLS) measurements of AuNPs and all lipid- and polymer-AuNHybs were conducted using a Delsa Nano C Particle Analyzer (Beckman Coulter, Nyon, Switzerland). The laser was adjusted to 658 nm and scattered light was detected at a 165° angle. Data was converted using CONTIN particle size distribution analysis. The AuNHyb size was analyzed three times in PBS at RT.

2.8 UV-Vis and fluorescence measurements

Ultraviolet-visible (UV-Vis) absorption from 260 nm to 750 nm (step size one nm) of different samples was measured using a SpectraMax M2 (Molecular Devices, Sunnyvale, USA). Fluorescence of lipid-AuNHybs containing rhodamine labelled phospholipids (Rho-PE) [Avanti Polar-Lipids, Alabaster, USA] was analyzed by excitation at 560 nm and detection between 572 nm to 750 nm.

2.9 Transmission electron microscopy of gold nanohybrids

Size and shape of the AuNPs and AuNHybs were analyzed by transmission electron microscopy (TEM) using a CM-100 (Philips, Eindhoven, Netherlands) operating at 80 kV. Samples were prepared by deposition onto a 400-mesh carbon-coated copper grid (Polysciences Inc., Eppelheim, Germany). Prior to sample deposition, the grid was exposed to plasma for 10 seconds to increase sample binding. Grids were washed with double-distilled water to prevent precipitation of uranyl salts by phosphate ions. Then the samples were negatively stained using a 2% uranylacetate solution (Sigma-Aldrich, Buchs, Switzerland), the excess of uranylacetate was removed using filter paper, and the samples were dried at RT overnight. Nanocarrier integrity was preserved by this procedure as confirmed by Cryo-EM analysis using sample vitrification (see below). To characterize the size of AuNPs inside of AuNHybs, the diameter of at least 100 AuNPs was determined.

2.10 Cryo-TEM of gold nanohybrids

Aliquots (4 μL) of AuNHybs were adsorbed onto holey-carbon supported grids (Quantifoil, Glossloebichau, Germany), blotted with Whatman 1 filter papers, and vitrified in liquid nitrogen-cooled liquid ethane using a Vitrobot IV (FEI Company, Eindhoven, Netherland). Cryo-electron imaging was performed with a Philips CM200-FEG electron microscope operated at an acceleration voltage of 200 kV. Micrographs were recorded with a 4k × 4k TemCam-F416 CMOS camera (TVIPS, Gauting, Germany).

2.11 Preparation of fluorescent lipid based AuNHybs

Detailed experimental procedures are given in the ESI.†

2.12 Passive uptake of AuNPs and AuNHybs in HepG2 cells

HepG2 cells were seeded on a 10 cm plate and cultured in 10 mL Dulbecco's modified Eagle's culture medium high glucose supplemented with 10% fetal calf serum (FCS), 100 units mL^{-1} penicillin, and 100 μg mL^{-1} of streptomycin (DMEM comp). All cell culture media components were purchased from Sigma-Aldrich (Buchs, Switzerland). Cells were allowed to adhere for 24 h before the AuNPs or AuNHybs were added. After incubation at 37 °C for 18 h, the tissue culture plate was washed three times with DMEM comp (37 °C). Afterwards, the cells were fixed with DMEM containing 3% formaldehyde (Sigma-Aldrich, Buchs, Switzerland) and 0.3% glutaraldehyde (Sigma-Aldrich, Buchs, Switzerland) for two hours at RT and stored overnight at 4 °C. The following day, cells were scraped, pelleted, and washed three times with water, and then incubated with 2% uranylacetate for two hours at 4 °C in the dark. The sample was washed, dehydrated by series of methanol, and infiltrated with LR-gold resin (London Resin, London, UK) according to the manufacturer's instructions. Polymerization was performed at −10 °C by UV light for one day. Sections of about 70 nm were collected on carbon-coated Formvar-Ni-grids (EMS, Hatfield, USA) and stained for 15 min with 4% uranylacetate followed by two minutes in Reynolds lead citrate solution. Sections were viewed using a Phillips CM-100 electron microscope.

3. Results and discussion

3.1 Film rehydration (conventional liposomes)

For the preparation of AuNP loaded liposomes, the most direct approach is the rehydration of a lipid film with presynthesized AuNPs. The well-characterized method developed by Turkevich and Frens is ideal to synthesize AuNPs with diameters of approximately 20 nm (see ESI† for experimental details).[7,34,35] However, the AuNP encapsulation approach has several issues. The AuNPs often form aggregates up to several hundred nanometers (Fig. 2A), which results in low encapsulation efficiency (Fig. 2D) and renders extrusion impossible due to blocked filter membranes. Therefore, we developed an alternative strategy and combined the film-rehydration method with a 'nanoreactor approach'. We rehydrated the lipid film with the Turkevich reaction mixture consisting of tetrachloroaurate and citrate. Then the formation of AuNPs was initiated inside the core of preassembled liposomes by a shift in temperature [70 °C, 10 min] (Fig. 1A).

To prevent the formation of AuNPs during the preparation of liposomes, we selected lipids that are characterized by a low transition temperature (T_m). The lipid composition consisted of POPC and POPG, which provides a T_m of −2 °C. The lipid film was rehydrated with a tetrachloroaurate and citrate reaction solution in different ratios and the liposomes were extruded at RT before initiation of AuNP formation. The final AuNHyb sample exhibited the characteristic ruby-red color resulting from the surface plasmon resonance of encapsulated AuNPs.[36] To test if the temperature affected the efficiency of the process, the entire procedure was also carried out at 4 °C. However, there was no difference between AuNHybs prepared at RT or at lower temperatures. TEM showed that the AuNPs were encapsulated inside the AuNHybs (Fig. 2B). Encapsulation efficiency (*i.e.* the ratio between liposomes encapsulating AuNPs and liposomes that were empty) was significantly higher using the nanoreactor approach compared with either extrusion at high temperature (data not shown) or use of preformed AuNPs (Fig. 2D). The latter condition lead to the formation of AuNP aggregates in the medium surrounding the liposomes (Fig. 2D). In contrast, the nanoreactor approach resulted in the encapsulation of a single AuNP in the inner liposomal core.

POPC/POPG–AuNHybs were also analyzed by Cryo-TEM (Fig. 2C). Under these conditions, the native, hydrated state of the lipid formulation is presented.[37] Cryo-TEM showed that lipid-AuNHybs were spherical, mainly unilamellar, and efficiently loaded with AuNPs (Fig. 2C). AuNPs were located in the hydrophilic core of the liposomes (Fig. 2C), consistent with TEM analysis (Fig. 2B). Interestingly, some AuNPs were located in close proximity to the lipid bilayer. This could be either an artefact from the drying process during the TEM grid preparation or an interaction of the AuNPs with one of the phospholipids. The number of AuNPs encapsulated was dependent on the concentration of the AuR-solution. The highest AuNP encapsulation efficiency was achieved with 4 mM tetrachloroaurate, 16.3 mM citrate, and 20 mM lipids. Higher AuR-solution to lipid ratios resulted in the formation of AuNP agglomerates outside of the liposomes. On the other hand, lower AuR-solution to lipid ratios led to a significant amount of empty nanocarriers. Interestingly, TEM analysis revealed that the AuNPs, which were synthesized inside liposomes were significantly smaller than AuNPs synthesized without lipids (approximately 12.0 nm *vs.* 21.5 nm) (Fig. 2A *vs.* Fig. 2B). It is tempting to speculate that the limited amount of tetrachloroaurate and citrate available inside the nanocarriers is limiting the maximum size of the AuNPs. The POPC/POPG–AuNHybs were analyzed by DLS. The size of POPC/POPG–AuNHybs (104.7 nm ± 5.2 nm) was similar to the size of empty liposomes (Fig. 3A). Thus, AuNPs did not influence the nanocarrier diameter. In Fig. 4A, the absorption spectra of empty POPC/POPG liposomes (negative control), AuNPs (positive control), and POPC/POPG–AuNHybs are compared. As expected no absorption maximum was observed for empty POPC/POPG liposomes in the wavelength range from 500 nm to 600 nm. In contrast, AuNPs and POPC/POPG–AuNHybs showed a distinct surface plasmon absorbance peak at 525 nm. This indicates the successful encapsulation of AuNPs inside POPC/POPG liposomes.

3.2 Nanoprecipitation (di-block copolymer nanoparticles)

To demonstrate the broad applicability of our nanoreactor approach, we investigated the formation of polymer-AuNHybs using nanoprecipitation (Fig. 1B). For this method, the AuR-solution was added dropwise to the di-block copolymer PEG–PCL dissolved in THF (see ESI† for experimental details). Similar to the lipid-AuNHybs, the addition of preformed AuNPs to the polymer resulted in low encapsulation efficiency (Fig. S1A†). In contrast, high encapsulation efficiency with one

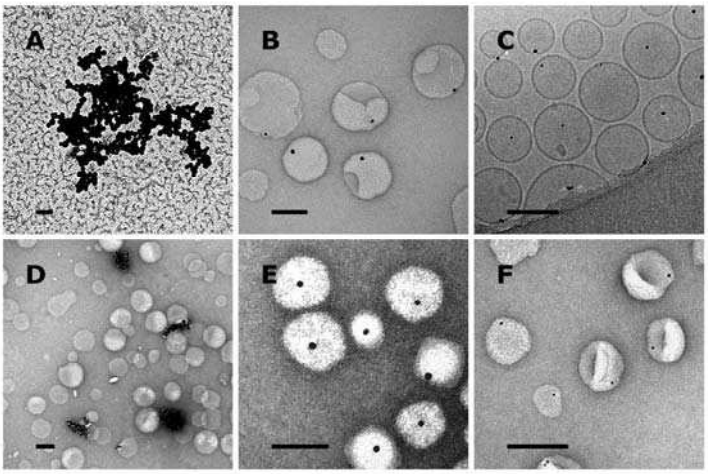

Fig. 2 Characterization of gold nanoparticles (AuNPs) and gold nanohybrids (AuNHybs). Representative transmission electron microscopy (TEM) (A/B, D–F) and Cryo-TEM (C) images are shown. (A) AuNPs were synthesized using a modified Turkevich method. (B) POPC/POPG–AuNHybs were analyzed by TEM and (C) Cryo-TEM. (D) The film-rehydration method for a lipid formulation with preformed AuNPs resulted in agglomerates. (E) PEG–PCL–AuNHybs prepared by nanoprecipitation and (F) PEG–liposome–AuNHybs after microfluidics platform preparation contain a single AuNP. Scale bars indicate 100 nm.

AuNP per polymeric nanocarrier was achieved using the nanoreactor approach (Fig. 2E). Cryo-TEM analysis confirmed that AuNPs with a size of 14.1 nm ± 3.1 nm were located inside the polymer-AuNHybs (Fig. S1B†).

Polymer-AuNHybs consisting of PEG–PCL presented a spherical morphology in which polymer chains self-assemble as solid polymeric nanoparticles. Thus, the hydrophilic parts of the di-block copolymer are exposed towards the outer buffer environment (Fig. S1B†). Recently, this was also shown for other polymeric nanoparticles.[38] DLS analysis showed a monodisperse formulation of polymer-AuNHybs (polydispersity index = 0.088) with a diameter of 77.5 nm ± 3.9 nm (Fig. 3B). Additionally, the polymer-AuNHybs showed a characteristic surface plasmon band at 527 nm due to the unique optical properties of AuNPs (Fig. 4B).

3.3 Microfluidics (PEGylated liposomes)

Recently, it has been demonstrated that rapid microfluidic mixing offers a controlled method to produce lipid nanocarriers.[39] Defined interfacial forces between the nanomaterial components result in a controllable and highly reproducible self-assembly process.[40] To facilitate the production of AuNP loaded PEGylated liposomes, we developed a microfluidics platform for the preparation of lipid-AuNHybs using lipids with a transition temperature above RT. Briefly, PEGylated lipid based gold nanohybrids (PEG–Lipo–AuNHybs) were synthesized by rapid mixing of an ethanolic lipid solution (5 mM, consisting of DSPC, cholesterol, and DSPE-PEG2000) and the aqueous Turkevich AuR-solution. In the last step of the process, the PEGylated liposomes were heated to 70 °C to start the formation of the AuNPs inside the liposomes.

In more detail, our microfluidics device consisted of seven inlet channels which converged into a single staggered-herringbone micromixer (see ESI†). At the junction of the inlets, the center stream was hydrodynamically focused to improve the mixing. To illustrate the nanomanufacturing process, we simulated the flow patterns and visualized them with a fluorescent dye (Fig. 1D/E; ESI Fig. S2†). Liposomes are formed at the interface between the hydrodynamically focused lipid stream and the AuR-solution. The mechanism of controlled, focused, and rapid mixing[41] is visible both in the experimental setting (Fig. 1D) and the computer simulation (Fig. 1E). The central inlet was used for the model ethanolic lipid solution [5 mM] (Fig. S2B†). The other six, outer inlets were used for tetrachloroaurate (Fig. S2C†), citrate (Fig. S2D†), and water (two inlets for each solution). Syringe pumps were used with flow rates up to 4 μL s^{-1}. The reagents were supplied by separate inlets because the use of tetrachloroaurate and citrate in the same inlet resulted in premature AuNP formation in the herringbone micromixer (Fig. S3D†).[40] In addition, the use of preformed AuNPs resulted in a low encapsulation efficiency, as observed for the film-rehydration and nanoprecipitation method with preformed AuNPs (Fig. S3E†). Therefore, the best results were achieved using a microfluidics platform with seven different inlets (Fig. 1C–E).

Water (4 μL s^{-1}) was used to improve the hydrodynamic flow focusing of the lipid stream and to decrease the final ethanol concentration. Furthermore, we used a higher flow rate for the outer inlets to increase the water to ethanol ratio. This is important to prevent the destabilization of liposomes caused by elevated ethanol concentrations.[42] Microfluidics parameters were adjusted to optimize encapsulation efficiency and size distribution. A continuous and efficient production was achieved with 2 mM tetrachloroaurate/8.2 mM citrate solution

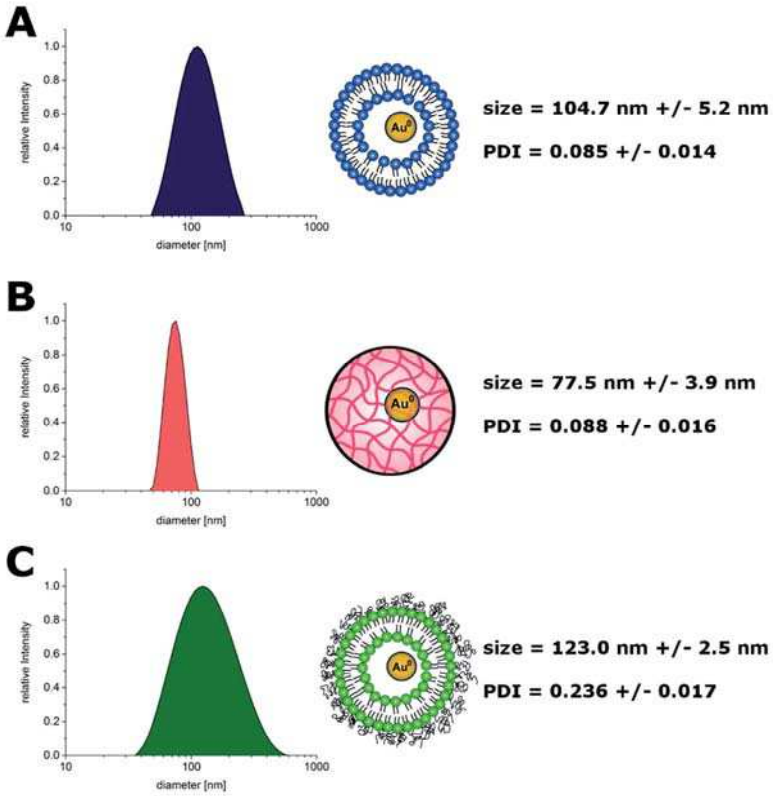

Fig. 3 Dynamic light scattering analysis of gold nanohybrids (AuNHybs). Intensity distribution of (A) POPC/POPG–AuNHyb, (B) PEG–PCL–AuNHyb, and (C) PEGylated liposome–AuNHyb. Mean values of size and polydispersity index (PDI) are given ± SD ($n = 5$).

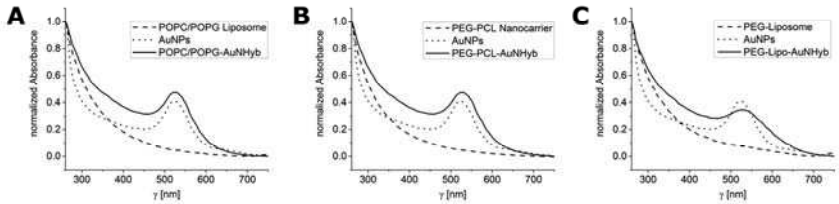

Fig. 4 UV spectra of empty nanocarriers, gold nanoparticles (AuNPs), and gold nanohybrids (AuNHybs). Relative UV-Vis absorption from 260 nm to 750 nm (step size one nm) was measured for (A) POPC/POPG, (B) PEG–PCL, and (C) PEG–lipid based nanocarriers. Spectra were normalized to an OD_{260} of 1.0. All AuNHybs showed a characteristic surface plasmon band at approximately 525 nm.

(for 5 mM lipids); and flow rates of 2 μL s^{-1} for the AuR-solutions, and 1 μL s^{-1} for the lipid solution. The absolute production speed was 420 μL min^{-1} (Fig. S2A†). Increasing the concentration of the AuR-solution for the microfluidics manufacturing resulted in an increased number of encapsulated AuNPs per AuNHyb (Fig. S3A–C†) until agglomerates were observed. AuNHybs with several encapsulated AuNPs mostly resulted in Janus-like vesicle structures (*i.e.* asymmetrical loading) as recently shown for Janus magnetic liposomes.[43] DLS and TEM showed that the size of PEG–Lipo–AuNHybs was similar to that of empty PEGylated liposomes (Fig. 2F and 3C). PEG–Lipo–AuNHybs with a mean hydrodynamic diameter of 123 nm ± 2.5 nm (*Z*-average) and a monodisperse size distribution were obtained (Fig. 3C). Each liposome incorporated one AuNP with a diameter of 6.8 nm ± 1.5 nm as shown by TEM (Fig. 2F). A characteristic plasmon absorption at 525 nm was observed using UV-Vis spectroscopy (Fig. 4C).

3.4 Characterization of nanoreactor approach

We showed that our nanoreactor approach is applicable for a wide range of nanomaterials, as well as different preparation methods. The film rehydration method can be used for lipids

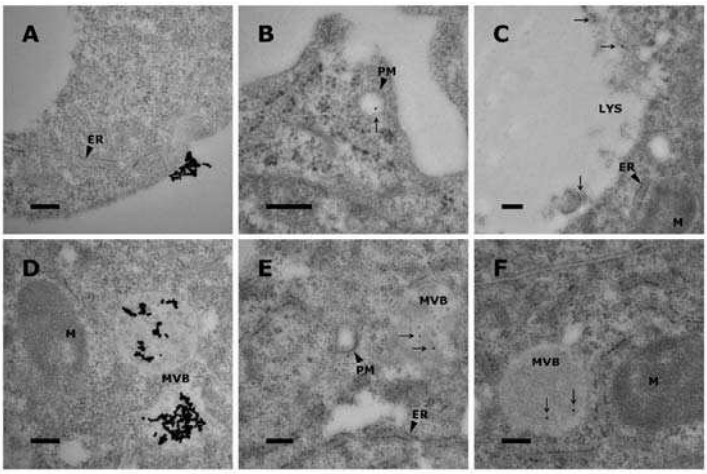

Fig. 5 Uptake experiments of gold nanoparticles (AuNPs) and gold nanohybrids (AuNHybs) in HepG2 cells. (A) AuNPs localized at the cell surface or (D) inside the cell. Representative uptake images of (B/E) POPC/POPG–AuNHybs and (C/F) PEG–PCL–AuNHybs (arrows). ER = endoplasmatic reticulum; LYS = lysosome; M = mitochondria; MVB = multi vesicular body; PM = plasma membrane. Scale bars indicate 200 nm.

with a transition temperature below RT, whereas the nanoprecipitation method is suitable for several polymer nanomaterials.[28,44] The microfluidics method is especially designed for lipids with a transition temperature above RT. However, this technique is suitable for all nanomaterials, that need highly controlled nanomanufacturing.[40]

The most important step of our nanoreactor approach is the speed of the nanocarrier production. The nanocarrier formation needs to be faster than AuNP aggregate formation. Therefore, the AuNP formation inside the nanocarriers is initiated by a temperature shift after self-assembly. AuNP aggregates formed outside of the self-assembled nanocarrier are removed by size exclusion chromatography. During this step, the outer buffer can be exchanged to a physiological compatible medium such as PBS. Several publications have shown that a difference in tonicity between the nanocarrier lumen and the outer buffer environment is not affecting the stability or morphology of nanocarriers.[45–47]

All tested combinations resulted in efficient and reproducible formation of AuNHybs. Moreover, DLS, TEM, and Cryo-TEM analysis showed that the final AuNHybs preserved the initial dimensions of the empty nanocarriers. Four distinct observations indicate that the AuNPs were encapsulated inside the nanocarriers. Firstly, the AuNHybs passed easily through the size exclusion chromatography medium (Superose 6 prep) whereas non-encapsulated AuNPs showed a high affinity for the chromatography medium, which was recently also shown for quantum dots.[48] Secondly, the AuNHybs exhibited an improved stability in PBS and aggregation was prevented as compared to free AuNPs. Thirdly, electron microscopy analysis showed a single AuNP entrapped per nanocarrier and no clusters of AuNPs were observed. Finally, the deep-red AuNHyb solutions exhibited a specific surface plasmon absorption peak at 525 nm, and a low 650 nm/530 nm ratio, which is characteristic for non-agglomerated AuNPs.[49]

3.5 Cellular uptake experiments

To demonstrate the use of AuNHybs for bioimaging, we performed uptake experiments with the AuNHybs in HepG2 cells exploiting the unique optical properties of AuNPs. The electron-density of AuNPs was used for further TEM analysis of cells (Fig. 5) as shown recently for surface-modified AuNPs.[50] Due to the high quality and uniform size of AuNPs, TEM observations were possible without silver enhancement. Using this approach, fundamental insights about nanocarrier uptake and intracellular fate can be obtained. For example, proteins covering the surface of nanocarriers after administration to biological medium can influence cellular uptake. However, formation of a protein corona and opsonisation can be minimized using PEGylated nanocarriers (*i.e.* PEG–PCL nanoparticles or PEGylated liposomes).[51,52] It remains to be elucidated to which degree protein adsorption onto non-modified nanocarriers such as conventional liposomes has to be taken into account for biomedical applications.[53,54]

The interaction of free AuNPs with HepG2 cells is shown in Fig. 5A and D. Free AuNPs formed aggregates which were located on the cellular plasma membrane (Fig. 5A) or taken up into the cell (Fig. 5D). These observations are in agreement with published results.[50,55] Fig. 5 shows the interaction with cells of lipid (panel B/E) or polymer based AuNHybs (panel C/F). In contrast to the uptake of free AuNPs, no AuNP aggregates were detected using AuNHybs. Different internalization steps were observed. An early stage in the cellular uptake mechanism was indicated by parts of the cellular plasma membrane around endosomes located near the cellular membrane (Fig. 5B). Compartments filled with more than one AuNP are most likely caused during maturation of different AuNHyb-filled vesicles (Fig. 5E/F).

AuNHybs could thus be used to examine nanoparticle–cell-interactions and the intracellular fate of the nanocarriers

inside the cells using TEM, a technique which offers greater resolution compared to confocal microscopy. It should be noted that liposomes encapsulating AuNPs can act simultaneously as a carrier for fluorescent dyes (see ESI† for experimental details). For example rhodamine labelled phospholipids (Rho-PE) can be used to fluorescence label AuNHybs (Fig. S4b†). This offers the possibility to image fluorescent AuNHybs by confocal fluorescence microscopy or to quantify them with flow cytometry analysis.

4. Conclusions

In conclusion, we have developed a novel strategy for the preparation of lipid and polymer based AuNHybs. After encapsulation of the required reagents inside nanocarriers, formation of AuNPs was triggered by a temperature shift. In future, a similar approach could be used for the preparation of alternative metal nanohybrids such as silver nanoparticles. Different preparation techniques were used in combination with various nanomaterials. To the best of our knowledge, this nanoreactor approach is unique and was not used previously. The high reproducibility and versatility of our nanoreactor approach is unprecedented and makes this technology suitable for many nanomaterials. Microfluidics offers the possibility for an efficient and large scale production.

The produced AuNHybs have a size of 70 nm to 130 nm, which makes them ideal for bioimaging applications.[56] In addition, AuNHybs can be stored over a prolonged period of time (*i.e.* >3 months/4 °C) maintaining their initial size and monodispersity.

In order to target specific cells or tissues, AuNHybs can be easily modified using surface-conjugated receptor ligands.[57] Our nanoreactor approach will be instrumental to develop a better understanding of cellular uptake and intracellular trafficking of targeted nanocarriers.

Acknowledgements

The authors declare no conflicting financial interest. Funding of the Stiftung zur Förderung des pharmazeutischen Nachwuchses in Basel is acknowledged. C. P.-B. was supported by the Swiss National Science Foundation (31003A-125423). D. W. thanks Lisa Stoltenburg for her support during this project. The authors thank Dr Adam Lister for editorial and Andrea Fehrenbach for graphical assistance. In addition, we thank Dr Susanne H. Schenk for her feedback on the manuscript, Dr Timothy Sharpe for his scientific input, and Prof. Henning Stahlberg (Director of C-CINA, Centre for Cellular Imaging and NanoAnalytics) and the Microscopy Center of the Biozentrum Basel for their support with electron microscopy techniques.

Notes and references

1 A. S. Thakor, J. Jokerst, C. Zavaleta, T. F. Massoud and S. S. Gambhir, *Nano Lett.*, 2011, **11**, 4029–4036.
2 D. F. Moyano, B. Duncan and V. M. Rotello, *Methods Mol. Biol.*, 2013, **1025**, 3–8.
3 D. Kumar, N. Saini, N. Jain, R. Sareen and V. Pandit, *Expert Opin. Drug Delivery*, 2013, **10**, 397–409.
4 R. Cao-Milán and L. M. Liz-Marzán, *Expert Opin. Drug Delivery*, 2014, **11**, 741–752.
5 L. C. Kennedy, L. R. Bickford, N. A. Lewinski, A. J. Coughlin, Y. Hu, E. S. Day, J. L. West and R. A. Drezek, *Small*, 2011, **7**, 169–183.
6 E. Oh, K. Susumu, R. Goswami and H. Mattoussi, *Langmuir*, 2010, **26**, 7604–7613.
7 C. Li, D. Li, G. Wan, J. Xu and W. Hou, *Nanoscale Res. Lett.*, 2011, **6**, 440.
8 S. K. Sivaraman, S. Kumar and V. Santhanam, *J. Colloid Interface Sci.*, 2011, **361**, 543–547.
9 J. Kimling, M. Maier, B. Okenve, V. Kotaidis, H. Ballot and A. Plech, *J. Phys. Chem. B*, 2006, **110**, 15700–15707.
10 P. J. G. Goulet and R. B. Lennox, *J. Am. Chem. Soc.*, 2010, **132**, 9582–9584.
11 L. L. Lazarus, A. S.-J. Yang, S. Chu, R. L. Brutchey and N. Malmstadt, *Lab Chip*, 2010, **10**, 3377–3379.
12 W. Wang, Q.-Q. Wei, J. Wang, B.-C. Wang, S. Zhang and Z. Yuan, *J. Colloid Interface Sci.*, 2013, **404**, 223–229.
13 D. Pornpattananangkul, S. Olson, S. Aryal, M. Sartor, C.-M. Huang, K. Vecchio and L. Zhang, *ACS Nano*, 2010, **4**, 1935–1942.
14 D. V. Volodkin, A. G. Skirtach and H. Möhwald, *Angew. Chem., Int. Ed. Engl.*, 2009, **48**, 1807–1809.
15 M. R. Preiss and G. D. Bothun, *Expert Opin. Drug Delivery*, 2011, **8**, 1025–1040.
16 A. K. Rengan, M. Jagtap, A. de, R. Banerjee and R. Srivastava, *Nanoscale*, 2014, **6**, 916–923.
17 G. von White, Y. Chen, J. Roder-Hanna, G. D. Bothun and C. L. Kitchens, *ACS Nano*, 2012, **6**, 4678–4685.
18 J. Nam, Y. S. Ha, S. Hwang, W. Lee, J. Song, J. Yoo and S. Kim, *Nanoscale*, 2013, **5**, 10175–10178.
19 H. Minematsu, T. Otani, T. Oohashi, M. Hirai, K. Oie, K. Igarashi and A. Ohtsuka, *J. Electron Microsc.*, 2011, **60**, 95–99.
20 M. R. Rasch, E. Rossinyol, J. L. Hueso, B. W. Goodfellow, J. Arbiol and B. A. Korgel, *Nano Lett.*, 2010, **10**, 3733–3739.
21 S.-H. Park, S.-G. Oh, J.-Y. Mun and S.-S. Han, *Colloids Surf., B*, 2006, **48**, 112–118.
22 L. Paasonen, T. Sipilä, A. Subrizi, P. Laurinmäki, S. J. Butcher, M. Rappolt, A. Yaghmur, A. Urtti and M. Yliperttula, *J. Controlled Release*, 2010, **147**, 136–143.
23 C. Kojima, Y. Hirano, E. Yuba, A. Harada and K. Kono, *Colloids Surf., B*, 2008, **66**, 246–252.
24 T. K. Sau, A. S. Urban, S. K. Dondapati, M. Fedoruk, M. R. Horton, A. L. Rogach, F. D. Stefani, J. O. Rädler and J. Feldmann, *Colloids Surf., A*, 2009, **342**, 92–96.
25 R. Genç, G. Clergeaud, M. Ortiz and C. K. O'Sullivan, *Langmuir*, 2011, **27**, 10894–10900.
26 K. Hong, D. S. Friend, C. G. Glabe and D. Papahadjopoulos, *Biochim. Biophys. Acta*, 1983, **732**, 320–323.
27 J. Huwyler, D. Wu and W. M. Pardridge, *Proc. Natl. Acad. Sci. U. S. A.*, 1996, **93**, 14164–14169.
28 T. Govender, S. Stolnik, M. C. Garnett, L. Illum and S. S. Davis, *J. Controlled Release*, 1999, **57**, 171–185.

29 Y. Kim, B. Lee Chung, M. Ma, W. J. M. Mulder, Z. A. Fayad, O. C. Farokhzad and R. Langer, *Nano Lett.*, 2012, **12**, 3587–3591.
30 L. Y. Yeo, H.-C. Chang, P. P. Y. Chan and J. R. Friend, *Small*, 2011, **7**, 12–48.
31 P. Detampel, D. Witzigmann, S. Krähenbühl and J. Huwyler, *J. Drug Targeting*, 2013, **22**, 232–241.
32 S. Deshpande and T. Pfohl, *Biomicrofluidics*, 2012, **6**, 34120.
33 M. E. Brennich, J.-F. Nolting, C. Dammann, B. Nöding, S. Bauch, H. Herrmann, T. Pfohl and S. Köster, *Lab Chip*, 2011, **11**, 708–716.
34 J. Turkevich, P. C. Stevenson and J. Hillier, *Discuss. Faraday Soc.*, 1951, **11**, 55–75.
35 G. Frens, *Nature (London), Phys. Sci.*, 1973, **241**, 20–22.
36 E. Casals, T. Pfaller, A. Duschl, G. J. Oostingh and V. Puntes, *ACS Nano*, 2010, **4**, 3623–3632.
37 S. Mornet, O. Lambert, E. Duguet and A. Brisson, *Nano Lett.*, 2005, **5**, 281–285.
38 E. Jäger, A. Jäger, T. Etrych, F. C. Giacomelli, P. Chytil, A. Jigounov, J.-L. Putaux, B. Říhová, K. Ulbrich and P. Štěpánek, *Soft Matter*, 2012, **8**, 9563–9575.
39 I. V. Zhigaltsev, N. Belliveau, I. Hafez, A. K. K. Leung, J. Huft, C. Hansen and P. R. Cullis, *Langmuir*, 2012, **28**, 3633–3640.
40 A. Jahn, W. N. Vreeland, M. Gaitan and L. E. Locascio, *J. Am. Chem. Soc.*, 2004, **126**, 2674–2675.
41 P. M. Valencia, P. A. Basto, L. Zhang, M. Rhee, R. Langer, O. C. Farokhzad and R. Karnik, *ACS Nano*, 2010, **4**, 1671–1679.
42 N. Maurer, K. F. Wong, H. Stark, L. Louie, D. McIntosh, T. Wong, P. Scherrer, S. C. Semple and P. R. Cullis, *Biophys. J.*, 2001, **80**, 2310–2326.
43 C. Bonnaud, C. A. Monnier, D. Demurtas, C. Jud, D. Vanhecke, X. Montet, R. Hovius, M. Lattuada, B. Rothen-Rutishauser and A. Petri-Fink, *ACS Nano*, 2014, **8**, 3451–3460.
44 U. Bilati, E. Allémann and E. Doelker, *Eur. J. Pharm. Sci.*, 2005, **24**, 67–75.
45 D. D. Lasic, B. Ceh, M. C. Stuart, L. Guo, P. M. Frederik and Y. Barenholz, *Biochim. Biophys. Acta*, 1995, **1239**, 145–156.
46 B. Ceh and D. D. Lasic, *J. Colloid Interface Sci.*, 1997, **185**, 9–18.
47 A. Fritze, F. Hens, A. Kimpfler, R. Schubert and R. Peschka-Süss, *Biochim. Biophys. Acta, Biomembr.*, 2006, **1758**, 1633–1640.
48 M. Camblin, P. Detampel, H. Kettiger, D. Wu, V. Balasubramanian and J. Huwyler, *Int. J. Nanomed.*, 2014, **9**, 2287–2298.
49 C.-C. Huang, Y.-F. Huang, Z. Cao, W. Tan and H.-T. Chang, *Anal. Chem.*, 2005, **77**, 5735–5741.
50 P. Nativo, I. A. Prior and M. Brust, *ACS Nano*, 2008, **2**, 1639–1644.
51 D. Pozzi, V. Colapicchioni, G. Caracciolo, S. Piovesana, A. L. Capriotti, S. Palchetti, S. D. Grossi, A. Riccioli, H. Amenitsch and A. Laganà, *Nanoscale*, 2014, **6**, 2782–2792.
52 M. Lundqvist, J. Stigler, T. Cedervall, T. Berggård, M. B. Flanagan, I. Lynch, G. Elia and K. Dawson, *ACS Nano*, 2011, **5**, 7503–7509.
53 M. Lundqvist, J. Stigler, G. Elia, I. Lynch, T. Cedervall and K. A. Dawson, *Proc. Natl. Acad. Sci. U. S. A.*, 2008, **105**, 14265–14270.
54 M. Hadjidemetriou, Z. Al-Ahmady, M. Mazza, R. F. Collins, K. Dawson and K. Kostarelos, *ACS Nano*, 2015, **9**, 8142–8156.
55 B. D. Chithrani, A. A. Ghazani and W. C. W. Chan, *Nano Lett.*, 2006, **6**, 662–668.
56 H. Kettiger, A. Schipanski, P. Wick and J. Huwyler, *Int. J. Nanomed.*, 2013, **8**, 3255–3269.
57 A. Wicki, D. Witzigmann, V. Balasubramanian and J. Huwyler, *J. Controlled Release*, 2015, **200**, 138–157.

RSC Advances

SUPPLEMENTARY INFORMATION

Formation of lipid and polymer based gold nanohybrids using a nanoreactor approach†

Dominik Witzigmann,[a] Sandro Sieber,[a] Fabiola Porta,[a] Philip Grossen,[a] Andrej Bieri,[b] Natalja Strelnikova,[c] Thomas Pfohl,[c] Cristina Prescianotto-Baschong[d] and Jörg Huwyler*[a]

** Author for correspondence:*
Prof. Dr. Jörg Huwyler
Phone: +41 (0)61 267 15 13
E-mail: joerg.huwyler@unibas.ch

1. Supplementary Information Experimental Section

1.1 Gold nanoparticle (AuNP) synthesis

The AuNP synthesis was optimized using a 2^3 full factorial design of experiment (DoE) [Stavex 5.2, Aicos Technologies, Basel, Switzerland]. Variables are listed in Table S1. All glass equipment was cleaned with aqua regia to prevent the formation of gold seeds. The best condition (smallest AuNPs and mild reaction condition) from our screening was used for further AuNHyb preparations (1.0 mM $HAuCl_4$ / 4.1 mM citrate; 1:4 molar ratio).

Table S1: AuNP synthesis screening using Turkevich method. Variations of citrate or tetrachloroaurate concentration, pH, and temperature.

Sample	c ($HAuCl_4$) [mM]	c (Citrate) [mM]	c (NaOH) [mM]	T [°C]	Size [nm]
Factorial Design (Mild Conditions)					
A	0.5	2.0	-	70	20.2
B	1.0	2.0	-	70	24.3
C	0.5	4.1	-	70	43.1
D	1.0	4.1	-	70	16.6
E	0.5	2.0	-	85	20.8
F	1.0	2.0	-	85	19.8
G	0.5	4.1	-	85	17.0
H	1.0	4.1	-	85	17.8
Other Approaches [1–4]					
I	0.5	2.0	-	boiling	18.7
K	1.0	4.1	-	boiling	19.3
L	2.5	5.1	5.0	70	26.6
M	2.5	5.1	6.6	85	19.6

1.2 Microfluidics device design and fabrication

For the master fabrication, SU8 (Microchem, Newton, USA) spin coated silicon wafers (Si-Mat, Kaufering, Germany) were used. To produce a master with a staggered herringbone micromixer, multi-layer photolithography was carried out using appropriate photomasks (JD Pho-tools, Oldham, UK) and a MJB4 mask aligner (SUSS MicroTec AG, Garching, Germany).

The first layer was made of SU8-3025 and the second one of SU8-3050 negative photoresists. PDMS and cross-linker (Sylgard 184, Dow Corning GmbH, Wiesbaden, Germany) were mixed in the mass ratio of 10:1, degassed, and poured on the masters followed by overnight curing. Cured PDMS stamp was peeled off from the wafer.

To prepare a 3D channel device, two sides (bottom side and top side) of polystyrene foil/NOA 81 were prepared as follows. A drop of NOA 81 was pipetted onto the structure of the PDMS stamp. Then a piece of polystyrene foil was placed on the NOA 81 and pressed down until the polystyrene foil touches elevated channel on the PDMS stamp that the channels were only laterally defined by NOA 81. NOA 81 was cured under UV-light for 3 min (366 nm, 2 x 8 W, Camag, Muttenz, Switzerland). The second side of the device was prepared the same way. Additionally, 0.75 mm holes were punched for tubing connection (Harris Unicore). Both polystyrene foil/NOA 81 sides were aligned, gently pressed, and cured under UV-light for 10 min.

1.3 Flow visualization

Deionized water, ethanol, and a fluorescein solution were used to visualize the flow patterns of the microfluidics device (Figure 1D). Images were taken using an Olympus IX81 inverted microscope (Olympus, Tokyo, Japan) equipped with fluorescence illumination (X-Cite Series 120 Q).

1.4 Computational Fluid Dynamics Simulation

For the numerical computational fluid dynamics (CFD) simulations we used the CFD module of the software COMSOL 4.3a (COMSOL Inc, Burlington, USA). The microfluidics device was modeled in 3D using 792,779 finite elements solving the incompressible Navier-Stokes-equation and advection-diffusion equation. The stationary flow field was calculated and in a second step the material transport of the diluted species were calculated using the beforehand-obtained stationary flow fields. We assumed a Newtonian fluid having the properties of water at room temperature.[5] Flow rates and inflow concentrations were specified at the seven inlets and the following diffusion coefficients were assumed: $D_{lipids} = 5 \cdot 10^{-11}$ m^2 s^{-1}, $D_{citrate} = 8.9 \cdot 10^{-10}$ m^2 s^{-1} and $D_{AuCL4} = 5.6 \cdot 10^{-10}$ m^2 s^{-1}.

1.5 Preparation of fluorescent lipid based gold nanohybrids (AuNHybs)

To broaden the application spectrum of AuNHybs for bioimaging purposes, we introduced an additional fluorescence marker, namely Rho-PE (Avanti Polar-Lipids, Alabaster, USA), into lipid based nanocarriers. Rho-PE was post inserted into preformed 75mol% POPC, 25mol% POPG liposomes as described elsewhere.[6] The modified liposomes possessed specific absorption properties based on the encapsulated AuNPs and an additional fluorescence based on the post-insertion of Rho-PE. The non-Rho-PE liposomes showed neither an absorption peak between 260 nm and 750 nm, nor a fluorescence after excitation at 560 nm. In contrast, the Rho-PE containing liposomes possessed a strong fluorescence with a maximum at 596 nm after they were excited near their absorption maximum at 560 nm. Compared with lipid-AuNHybs, the Rho-PE containing AuNHybs showed an additional absorption peak and were fluorescent after they were excited at 560 nm.

2. Supplementary Information Figures

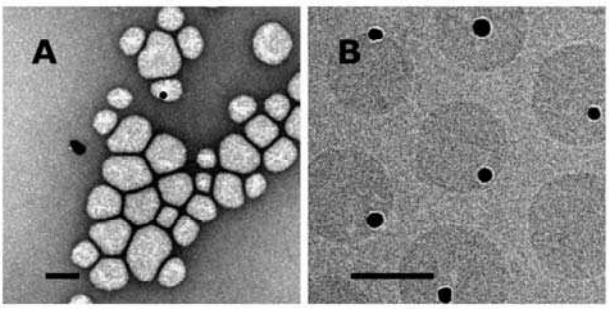

Figure S1. Electron microscopy analysis of PEG-PCL-gold nanohybrids (AuNHybs). Representative transmission electron microscopy (TEM) and Cryo-TEM images of solid polymeric nanoparticles are shown. (A) Preparation of PEG-PCL-AuNHybs using preformed AuNPs results in low encapsulation efficiency. (B) Cryo-TEM analysis of PEG-PCL-AuNHybs prepared via nanoreactor approach. Scale bars indicate 50 nm.

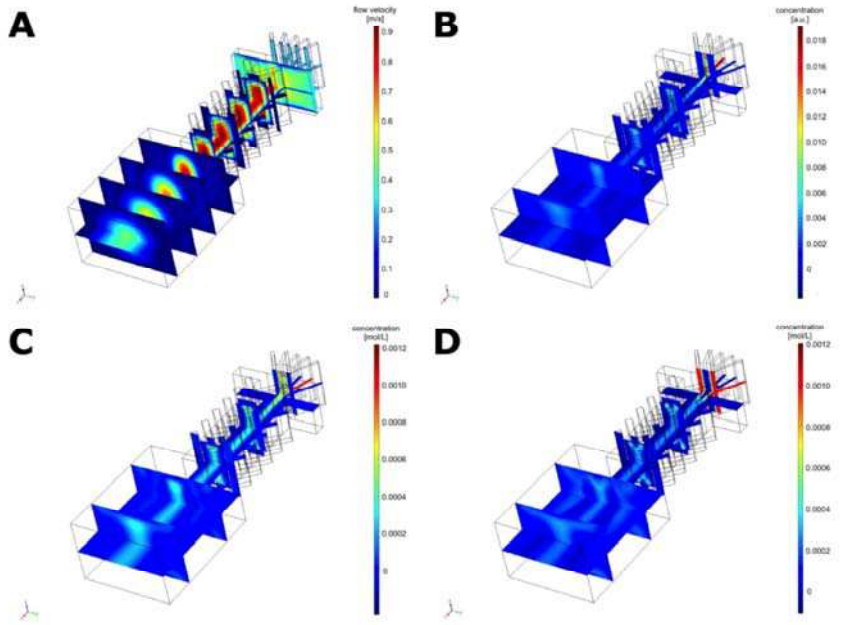

Figure S2. Computational fluid dynamics (CFD) simulations. (A) CFD simulation of the flow rate (m/s) of all seven inlet channels converging to a single micromixer is shown. Simulation of concentration gradients of (B) ethanol (in a.u.), (C) tetrachloroaurate (in mol/L), and (D) citrate (in mol/L) solution are presented.

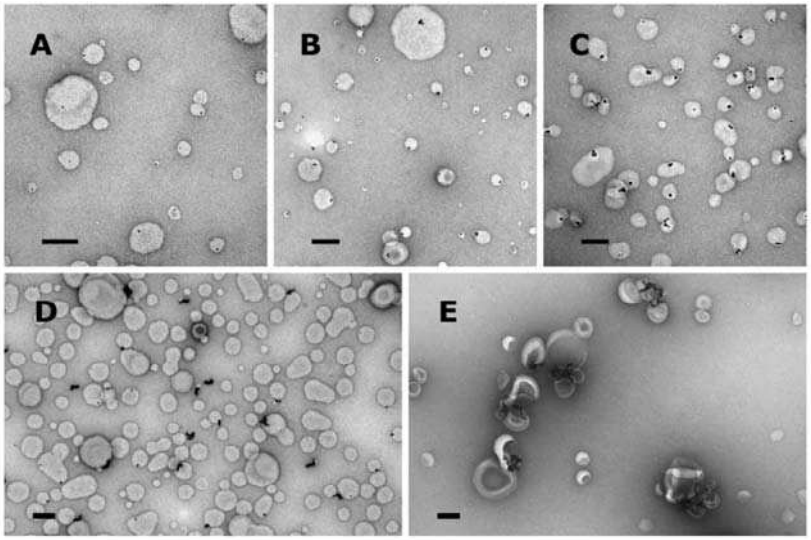

Figure S3. Preparation of gold nanohybrids (AuNHybs) using microfluidics. Representative transmission electron microscopy (TEM) images are shown. Increasing concentration of the reaction solutions (1x = 1 mM $HAuCl_4$ / 4.1 mM citrate) for the nanoreactor approach resulted in an increased number of AuNPs per nanocarrier. (A) 2x, (B) 4x, and (C) 8x reaction solutions were used. (D) Preparation of AuNHybs with one combined reaction solution in the same inlet resulted in AuNP formation during microfluidics procedure. (E) Direct use of AuNPs resulted in agglomerates and low encapsulation efficiency. Scale bars indicate 100 nm.

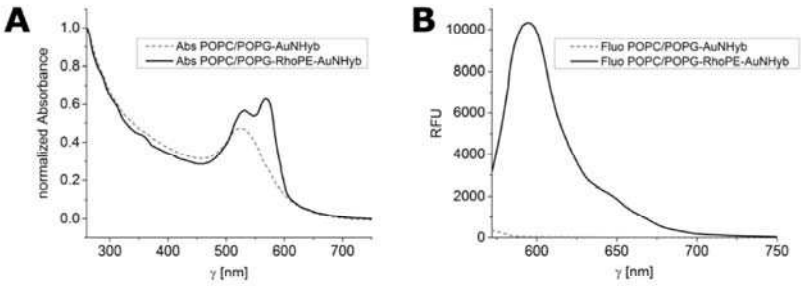

Figure S4. UV-Vis and fluorescence spectra of gold nanohybrids (AuNHybs) with and without fluorescent lipid (Rho-PE). (A) UV-Vis absorption from 260 nm to 750 nm (step size one nm) was measured. Spectra were normalized to an OD_{260} of 1.0. Fluorescently labelled AuNHybs showed two absorbance maxima, i.e. characteristic surface plasmon band and absorbance maximum of Rho-PE. (B) Fluorescence spectra of AuNHybs between 572 nm to 750 nm after excitation at 560 nm. POPC/POPG-RhoPE-AuNHybs showed strong fluorescence (RFU = relative fluorescence units), whereas POPC/POPG-AuNHybs were not fluorescent.

Supplementary Information References

1 E. Oh, K. Susumu, R. Goswami and H. Mattoussi, *Langmuir*, 2010, **26**, 7604–7613.
2 C. Li, D. Li, G. Wan, J. Xu and W. Hou, *Nanoscale Res. Lett.*, 2011, **6**, 440.
3 S. K. Sivaraman, S. Kumar and V. Santhanam, *J. Colloid Interface Sci.*, 2011, **361**, 543–547.
4 J. Kimling, M. Maier, B. Okenve, V. Kotaidis, H. Ballot and A. Plech, *J. Phys. Chem. B*, 2006, **110**, 15700–15707.
5 Y. Kim, B. Lee Chung, M. Ma, W. J. M. Mulder, Z. A. Fayad, O. C. Farokhzad and R. Langer, *Nano Lett.*, 2012, **12**, 3587–3591.
6 T. M. Allen, P. Sapra and E. Moase, *Cell. Mol. Biol. Lett.*, 2002, **7**, 889–894.

Chapter VII

"Biocompatible Polymer-Peptide Hybrid-Based DNA Nanoparticles for Gene Delivery"

Witzigmann D, Wu D*, Schenk SH, Balasubramanian V, Meier W, Huwyler J.*

ACS Appl Mater Interfaces. 2015 May 20; 7(19):10446-56.

doi: 10.1021/acsami.5b01684. (**contributed equally)*

http://pubs.acs.org/doi/abs/10.1021/acsami.5b01684

Highlights: The delivery of nucleic acids is one of the most interesting areas in nanomedicine research. In this publication, the development of a novel polymer-peptide hybrid system for gene delivery is highlighted. A biocompatible and protein repellent synthetic polymer (i.e., PMOXA) was combined with a biocleavable peptide block, namely PASP. This polymer-peptide hybrid system was modified with diethylenetriamine to allow for plasmid DNA complexation and delivery. Transfection of target cells was achieved *in vitro* with high efficiency. PMOXA-*b*-PASP(DET) nanoparticles had a slightly negative zeta potential and were not cytotoxic. These unique properties set this block copolymer apart from established polycationic DNA delivery systems. In the future, this versatile and biocompatible polymer might find a widespread use in the field of targeted gene therapy.

ACS APPLIED MATERIALS & INTERFACES

Research Article

www.acsami.org

Biocompatible Polymer–Peptide Hybrid-Based DNA Nanoparticles for Gene Delivery

Dominik Witzigmann,[†] Dalin Wu,[‡] Susanne H. Schenk,[†] Vimalkumar Balasubramanian,[†,§] Wolfgang Meier,[‡] and Jörg Huwyler*[,†]

[†]Division of Pharmaceutical Technology, Department of Pharmaceutical Sciences, University of Basel, Klingelbergstrasse 50, Basel CH-4056, Switzerland

[‡]Department of Chemistry, University of Basel, Klingelbergstrasse 80, Basel CH-4056, Switzerland

[§]Division of Pharmaceutical Chemistry and Technology, Faculty of Pharmacy, University of Helsinki, Viikinkaari 5E, Helsinki FI-00014, Finland

Supporting Information

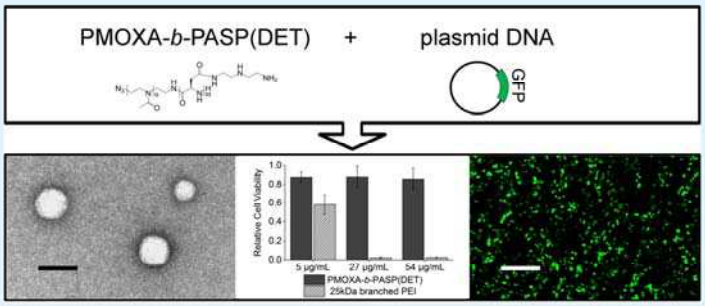

ABSTRACT: Currently, research on polymers to be used as gene delivery systems is one of the most important directions in both polymer science and biomedicine. In this report, we describe a five-step procedure to synthesize a novel polymer–peptide hybrid system for gene transfection. The block copolymer based on the biocompatible polymer poly(2-methyl-2-oxazoline) (PMOXA) was combined with the biocleavable peptide block poly(aspartic acid) (PASP) and finally modified with diethylenetriamine (DET). PMOXA-*b*-PASP(DET) was produced in high yield and characterized by ^{1}H NMR and FT-IR. Our biopolymer complexed plasmid DNA (pDNA) efficiently, and highly uniform nanoparticles with a slightly negative zeta potential were produced. The polymer–peptide hybrid system was able to efficiently transfect HEK293 and HeLa cells with GFP pDNA *in vitro*. Unlike the commonly used polymer, 25 kDa branched poly(ethylenimine), our biopolymer had no adverse effects on cell growth and viability. In summary, the present work provides valuable information for the design of new polymer–peptide hybrid-based gene delivery systems with biocompatible and biodegradable properties.

KEYWORDS: *polymer–peptide hybrid system, transfection, gene delivery, nanoparticles, toxicity, biodegradability*

INTRODUCTION

Gene therapy is one of the most rapidly growing areas in nanomedicine research.[1] In general, gene delivery systems are classified into two major groups, i.e., viral and nonviral.[2] Viral vectors, such as retroviruses or adenoviruses, are characterized by high transfection efficacies, but their major drawback is the concern about biosafety and cytocompatibility.[3] Nonviral systems, such as lipids or polymers, have gained attention especially because of their lower cytotoxicity and easier production.[4] In particular, polymers have great potential for gene therapy because of their chemical versatility.[5,6]

Many groups developed polymers or polymer conjugates with linear, branched, or cyclic molecule structure for gene delivery to express exogenous proteins.[3,7−14] To be translated into a protein, pDNA needs to overcome two barriers. First, pDNA has to cross the cell membrane, and second, it must overcome the nuclear membrane. In the nucleus, pDNA will be transcribed into mRNA, and the protein of interest will be expressed.

Polycations are the major type of nonviral polymeric gene nanocarriers. The most widely used transfection polymer is 25 kDa branched poly(ethylenimine) (bPEI).[15] However, bPEI as well as several other polymers including poly(L-lysine) (PLL), poly(propylenimine) (PPI), and poly(2-dimethylamino ethyl methacrylate) (PDMAEMA) have cytotoxic side effects.[16−18] Therefore, developments are focusing on gene vectors with

Received: February 24, 2015
Accepted: April 24, 2015
Published: April 24, 2015

DOI: 10.1021/acsami.5b01684
ACS Appl. Mater. Interfaces 2015, 7, 10446−10456

ACS Applied Materials & Interfaces Research Article

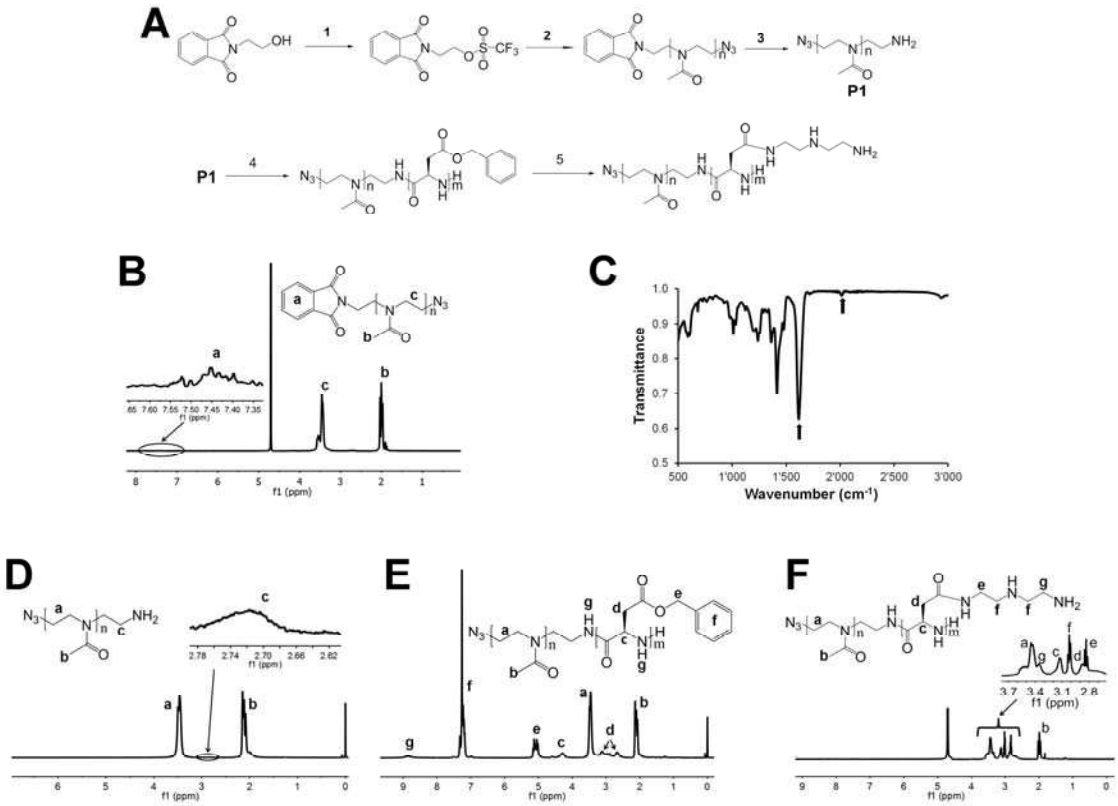

Figure 1. Synthesis and characterization of PMOXA-*b*-PASP(DET). (A) Schematic diagram illustrating the synthesis of PMOXA-*b*-PASP(DET): (1) triflic anhydride, TEA, DCM, −20 °C; (2) 2-methyl-2-oxazoline, acetonitrile, 80 °C, NaN_3; (3) $NH_2-NH_2{\cdot}H_2O$, ethanol, RT; (4) β-Benzyl L-aspartate anhydride, DMF, RT; (5) DMF, DET, 40 °C. (B) ^1H NMR spectrum of N_3-PMOXA-Ph in $CDCl_3$. (C) FT-IR spectrum of N_3-PMOXA-Ph. Stretching vibration of C═O (1616 cm^{-1}). Azide group (2010 cm^{-1}). (D) ^1H NMR spectrum of N_3-PMOXA-NH_2 in $CDCl_3$. (E) ^1H NMR spectrum of N_3-PMOXA-*b*-PBLA in $CDCl_3$. (F) ^1H NMR spectrum of N_3-PMOXA-*b*-PASP(DET) in D_2O.

improved transfection efficiency as well as decreased cytotoxicity. Several approaches have already been investigated, e.g., ternary complexes consisting of PLL, pDNA, and a functional polymer;[19,20] single cyclic knot polymer structures;[21] or highly branched degradable copolymers.[22]

The main objective of the present work was the development of a novel polymer−peptide hybrid (PPH)-based gene delivery system with minimal cytotoxicity, improved biocompatibility, and advantageous physicochemical characteristics. PPH systems have recently attracted great attention because this type of block copolymers combines the excellent safety and biocompatibility profiles of both synthetic polymers and natural peptides.[3,7,10,23] We synthesized a block copolymer by ring-opening polymerization of 2-methyl-2-oxazoline and β-benzyl-L-aspartate *N*-carboxy anhydride (BLA-NCA), using the synthetic polymer poly(2-methyl-2-oxazoline) (PMOXA) and the peptide block poly(aspartic acid) (PASP).

PMOXA is a hydrophilic polymer with stealth[24] and protein-repellent properties,[25] which is an advantage for biomedical application.[26] *In vivo*, the circulation half-life is prolonged, and immunogenicity of the gene delivery system is reduced.[27] Recently, Pidhatika et al. demonstrated that, under physiological conditions, PMOXA is more stable than polyethylene glycol (PEG).[28] This suggests that PMOXA might be an excellent alternative to PEG. Thus, we used PMOXA as a biocompatible and protein-repellent backbone of the gene delivery system. To the best of our knowledge, our biopolymer is the first PMOXA-based PPH for gene delivery.

PASP is a biocompatible and biodegradable polypeptide that can be used for further functionalization of the copolymer.[29,30] In order to deliver nucleic acids with our PPH, the peptide block was easily modified with the amine-containing unit, diethylenetriamine (DET). Flanking primary and secondary amines allow for electrostatic interactions with the negatively charged backbone of nucleic acids.[31] This is necessary to complex pDNA and to form nanoparticles. Transfection efficiency of our tailor-made PPH PMOXA-*b*-PASP(DET) in mammalian cells was assessed using pDNA encoding green fluorescence protein (GFP). In addition, we evaluated the biocompatibility of our PPH *in vitro* as well as *in vivo* in a preliminary safety study.

EXPERIMENTAL SECTION

Materials. Agarose and sodium dodecyl sulfate (SDS) were purchased from Bio-Rad Laboratories (Cressier, Switzerland), and 3-(4,5-dimethylthiazole-2-yl)-2,5-diphenyltetrazolinium bromide (MTT) and 1% ethidium bromide solution were obtained from Carl

DOI: 10.1021/acsami.5b01684
ACS Appl. Mater. Interfaces 2015, 7, 10446−10456

Roth (Karlsruhe, Germany). Opti-MEM and 0.25% trypsin-EDTA were obtained from Invitrogen, Life Technologies (Zug, Switzerland). Cell media and all other chemicals were purchased from Sigma (Buchs, Switzerland): *N*-(2-hydroxyethyl)phthalimide (99%), trifluoromethanesulfonic anhydride (≥99%), triethylamine (≥99%), 2-methyl-2-oxazoline (98%), sodium azide (≥99.5%), hydrazine monohydrate (98%), β-benzyl-L-aspartate (98%), triphosgene (98%), DET (99%), calcium hydride (95%), acetonitrile (≥99.8%), dichloromethane (≥99.8%), ethanol (99.8%), *N*,*N*-dimethylformamide (≥99.8%), and tetrahydrofuran (≥99.9%). Triethylamine, dichloromethane, 2-methyl-2-oxazoline, and acetonitrile were separated from CaH_2, and tetrahydrofuran was separated from $LiAlH_4$ by distillation. Other chemicals and solvents were used without additional purification.

Synthesis and Characterization of PMOXA-*b*-PASP(DET). The PPH PMOXA-*b*-PASP(DET) was synthesized via a five-step procedure (Figure 1A). A ^{1}H NMR was recorded on a Bruker DPX-400 MHz spectrometer in $CDCl_3$ and D_2O and was analyzed using MestReNova software. The molecular weight of our PPH was assessed using ^{1}H NMR. Due to poor solubility of our PPH in THF, a reliable determination of the molecular weight using gel permeation chromatography (GPC) was not possible. Fourier transform infrared spectroscopy (FT-IR) (PerkinElmer Spectrum 100 FT-IR spectrometer) was used to characterize the presence of specific chemical groups. Polymer samples were measured with 256 scans and 2 cm^{-1} resolution. The spectra were measured from 400 to 3000 cm^{-1}.

Phthalimidoethyl Triflate. *N*-(2-Hydroxyethyl)phthalimide (0.63 g, 3.30 mmol) and trimethylamine (TEA, 0.60 mL, 4.30 mmol) were first dissolved in 20 mL of distilled dichloromethane (DCM) at −20 °C. Afterward, trifluoromethanesulfonic anhydride (0.67 mL, 4.0 mmol) was mixed with another 5 mL of distilled DCM and then dropped slowly into the solution under argon. The final solution was stirred for 3 h at −20 °C under argon atmosphere. After washing with cold saturated $NaHCO_3$ aqueous solution and brine, the organic phase was dried by water-free $MgSO_4$. After filtration of $MgSO_4$, the solvent was evaporated, and the residues were dried in high vacuum for 2 h before further use.

N_3-PMOXA-Ph. The initiator, phthalimidoethyl triflate (0.97 g, 3.0 mmol), was dissolved in 30 mL of distilled acetonitrile, and then distilled 2-methyl-2-oxazoline (22 mL, 259 mmol) was added. Finally, the polymerization medium was heated to 80 °C for 24 h under argon. The medium was cooled down to room temperature (RT), and a 10-fold excess of NaN_3 was added to the medium to quench the polymerization and introduce the azide functional group. The medium was stirred for 24 h at RT. NaN_3 was removed by filtration, and the solvent was evaporated. The final product was purified by dialysis against water for 48 h. N_3-PMOXA-Ph (20 g) was obtained by freeze-drying as a colorless powder. The yield was 91%. ^{1}H NMR (400 MHz, δ, $CDCl_3$): 2.0 ppm (m, O═C—CH_3, H_b), 3.44−3.54 ppm (m, CH_2—CH_2, H_c), 7.35−7.60 ppm (m, C_6H_4, H_a).

N_3-PMOXA-NH_2. N_3-PMOXA-Ph (4.25 g, 0.55 mmol) was dissolved in ethanol (100 mL). Hydrazine monohydrate (400 mL) was added, and the solution was stirred overnight under argon at RT. After evaporation of the solvent, the polymer was redissolved in MeOH and precipitated twice in cold diethyl ether. The polymer was then redissolved in water and dialyzed against water for 48 h. N_3-PMOXA-NH_2 (3.8 g) was obtained by freeze-drying as a colorless powder; the yield was 89%. ^{1}H NMR (400 MHz, δ, $CDCl_3$): 1.91 ppm (m, O═C—CH_3, H_b), 3.38−3.50 ppm (m, CH_2—CH_2, H_c).

N_3-PMOXA-PBLA-NH_2. N_3-PMOXA-NH_2 (0.90 g, 0.12 mmol) was dissolved in water-free DMF. β-Benzyl L-aspartate anhydride (2.9 g, 11.62 mmol) was added, and the reaction medium was continually stirred for 24 h at RT under argon atmosphere. The reaction medium was precipitated twice in cold diethyl ether to get 3 g of a colorless solid. The yield was 79%. ^{1}H NMR (400 MHz, δ, $CDCl_3$): 2.10 ppm (m, O═C—CH_3, Hb), 2.66 ppm (broad, CH_2—C═O, Hd), 3.11 ppm (br, CH_2—C═O, Hd), 3.45 ppm (m, CH_2—CH_2, Ha), 4.28 ppm (br, CH—NH, Hc), 5.09 ppm (m, CH_2—C_6H_5, He), 7.25 ppm (m, C_6H_5, Hf), 8.87 ppm (br, O═C—NH, Hg).

N_3-PMOXA-PASP(DET)-NH_2. N_3-PMOXA-PBLA-NH_2 (0.052 g, 0.0029 mmol) was dissolved in water-free DMF (4 mL), and then DET (0.75 mL, 6.9 mmol) was added. The reaction was carried out at 40 °C under argon for 36 h. The reaction medium was added to 20 mL of acetic acid aqueous solution (10%) and then dialyzed against a 0.01 N HCl aqueous solution for 48 h. A slightly yellow solid powder (50 mg) was obtained after lyophilization. The yield was 98%. ^{1}H NMR (400 MHz, δ, D_2O): 1.99 ppm (m, O═C—CH_3, Hb), 2.83 ppm (m, O═C—NH—CH_2, He), 2.90 ppm (br, CH_2—C═O, Hd), 3.02 ppm (m, CH_2—NH—CH_2, Hf), 3.13 ppm (br, O═C—CH—NH, Hc), 3.36 ppm (br, CH_2—NH_2, Hg), 3.43−3.53 ppm (m, CH_2—CH_2—N, Ha).

Cell Culture. Human embryonic kidney (HEK293) cells and the human epithelial carcinoma cell line HeLa were cultured at 37 °C under 5% CO_2 and saturated humidity in Dulbecco's modified Eagle's culture medium high glucose (DMEM) supplemented with 10% fetal calf serum (FCS), penicillin (100 units/mL), and streptomycin (100 μg/mL). HEK293 cells stably expressing GFP for growth characteristic studies were produced by single-cell sorting and were cultured in DMEM containing 10% FCS and 0.5 mg/mL Geneticin (G418, Invitrogen, Life Technologies). Transfection assays were performed using the mammalian expression plasmid pTagGFP-N (Evrogen) with a size of 4.7 kb. The pDNA vector is encoding the enhanced GFP and comprises the immediate early promotor of cytomegalovirus (CMV).

pDNA Complexation. To form polymer-pDNA complexes, PMOXA-*b*-PASP(DET) or bPEI was mixed with pDNA in 100 μL of complexation medium in defined nitrogen to phosphate (N/P) ratios and incubated for 30 min at RT. As complexation medium we tested Opti-MEM (pH 7.4), acetate buffer (pH 5.5), and tris-buffered saline (TBS; pH 8.0). The resulting polymer-pDNA complexes were used for further experiments. For the N/P ratio calculations, we assumed a mass of 179 g/mol for each amine-containing unit of our PPH, 43.1 g/mol for each amine-containing unit of bPEI, and 330 g/mol for each phosphate-containing unit of the pDNA.

Gel Retardation Assay. Freshly prepared PMOXA-*b*-PASP(DET)-pDNA complexes with N/P ratios of 0.5−300 were analyzed by gel retardation assay. Samples containing either pDNA only or PMOXA-*b*-PASP(DET) only (mock control) were used as controls. For tracking, a loading buffer (15% Ficoll 400 in tris/borate/EDTA buffer [TBE]) containing bromophenol blue (0.1%) was added to each sample. All samples were separated on a 0.8% agarose gel containing 0.05 mg/mL ethidium bromide (EtBr) at 80 V for 45 min using TBE buffer. A gel documentation system (GelDoc-It TS2 Imager, UVP, Cambridge, U.K.) was used to visualize pDNA migration.

PPH-pDNA-Nanocomplex Characterization. *Morphology.* Particle size and morphology of nanocomplexes were analyzed using transmission electron microscopy (TEM). Samples were loaded on a carbon-coated grid and stained negatively with 2% uranylacetate solution. Excess of uranylacetate was removed, and the samples were dried at RT overnight. TEM analysis was performed with a CM-100 electron microscope (Philips, Eindhoven, Netherlands).

Size. Tunable resistive pulse sensing (TRPS) analysis was performed using the qNano (Izon Science, Christchurch, New Zealand). Particle size, size distribution, and concentration of PPH-pDNA-nanoparticles at N/P ratios of 100 and 300 were analyzed. The nanoparticles were passed through a tunable nanopore with size designation np300. Calibration was performed with 115.0 nm carboxylated polystyrene nanoparticles. Degree of membrane stretch (46.05 mm) and applied voltage (0.70 V) were tuned to optimize the resolution for each preparation.

Zeta Potential. Zeta potential of the polymer-pDNA nanocomplexes (PPH or bPEI) was measured using a Delsa Nano C Particle Analyzer (Beckman Coulter, Nyon, Switzerland). The laser wavelength was 658 nm, and the measurement angle was 15°. Samples were measured in D-PBS at RT by electrophoretic light scattering. Data were converted using the Smoluchowski equation (Delsa Nano V3.73/2.30, Beckman Coulter Inc., Brea, CA).

Stability. Stability of PMOXA-*b*-PASP(DET)-pDNA nanocomplexes was assessed using TEM analysis. Freshly prepared nanocomplexes were compared to nanocomplexes stored for 2 weeks in

DOI: 10.1021/acsami.5b01684
ACS Appl. Mater. Interfaces 2015, 7, 10446−10456

complexation medium at 4 °C. Sample preparation was performed as described before.

GFP pDNA Transfection. To assess the functionality of our PPH-based system, transfection assays were performed. In a 24-well plate, 120 000 HEK293 or HeLa cells were seeded and cultured in 1 mL of DMEM. Cells were allowed to adhere for 24 h. Then, 100 μL of freshly prepared PMOXA-*b*-PASP(DET)-pDNA complexes (N/P ratios 0−300) was added to each well. Controls (0% transfection) were defined as incubation of cells with DMEM and complexation buffer (Opti-MEM) only. Additionally, cells were incubated with pDNA alone to assess transfection efficiency without any transfection reagent. Autofluorescence of cells was determined by incubation of cells with the PPH only. GFP expression was analyzed qualitatively by confocal laser scanning microscopy (CLSM) or quantitatively by flow cytometry 48 h after transfection (see below).

GFP Expression Analysis. *Confocal Laser Scanning Microscopy.* For qualitative analysis of GFP expression, cells were washed with D-PBS and cultured in DMEM without phenol red. Live cell imaging was performed using an Olympus FV-1000 inverted confocal fluorescence microscope (Olympus Ltd., Tokyo, Japan) and a 10× objective (numerical aperture 0.40). Excitation and emission wavelengths were 488 and 516 nm, respectively. Surface area of GFP-positive cells was assessed using ImageJ 1.46 software (National Institutes of Health).

Flow Cytometry. For quantitative analysis of GFP expression, cells were washed with cold D-PBS (4 °C) and detached using 0.25% trypsin/EDTA. After two additional washing steps with D-PBS, cells were resuspended in staining buffer containing D-PBS, 1% FCS, 0.05% NaN_3, and 2.5 mM EDTA. Flow cytometry analysis of 10 000 cells was carried out using a FACS Canto II flow cytometer (Becton Dickinson, San Jose, CA). The cells were excited at 488 nm, and doublets were excluded. The fluorescence signal of GFP was detected in FL1 (505LP-530/30). To evaluate the transfection efficacies (% of GFP-positive cells), Flow Jo VX software (TreeStar, Ashland, OR) was used.

Cell Viability Assay. To evaluate the cytotoxic effect of PMOXA-*b*-PASP(DET) and bPEI, native or in complex with pDNA, an MTT assay was performed as described previously.[32] In brief, HEK293 or HeLa cells were incubated for 24 h with different concentrations of the test compounds. Afterward, the cells were incubated with MTT reagent at 37 °C and 5% CO_2 for 4 h. In order to solubilize the reduced MTT for the readout, the culture medium was discarded, and a solution containing 20 μL of 3% (v/v) sodium dodecyl sulfate in water and 100 μL of 40 mM hydrochloric acid in isopropanol was added. The water insoluble formazan dye crystals were dissolved in the dark for 2 h at RT by shaking. Finally, the optical density at 570 nm was measured using a Spectramax M2 microplate reader (Molecular Devices, Sunnyvale, CA). The results are given as relative cell viability (RCV) compared to control cells (complexation medium only). Interference controls were performed to exclude the influence of PMOXA-*b*-PASP(DET) on the outcome of the assay.

Analysis of Morphology and Cell Growth. To assess the influence of PMOXA-*b*-PASP(DET) or bPEI on cell growth characteristics, HEK293 cells stably expressing GFP were seeded at a density of 10 000 cells/well in a 96-well plate. GFP-expressing HEK293 cells were used to improve the visibility of growth difference compared to nontreated control cells. Opti-MEM, PMOXA-*b*-PASP(DET), or bPEI was added 24 h after seeding. After an additional 48 h, CLSM analysis was performed to assess morphological changes and cell growth. GFP-expressing HEK293 cells were analyzed by CLSM as described above. For quantitative analysis of growth area of cells, ImageJ 1.46 software was used.

Statistical Analysis. Statistical analysis of transfection experiments, MTT assays, and safety studies was performed by one-way analysis of variance (ANOVA) followed by a Bonferroni *posthoc* test using OriginPro 9.1 (OriginLab Corporation; Northampton, MA) software. All data represent means ±SD of at least $n = 3$ independent sets of experiments.

Transfection efficiency of our PPH was optimized using a 2^3 full factorial design of experiment (DoE) (Stavex 5.2 software, Aicos Technologies, Basel, Switzerland). The studied variables included the following: (a) Opti-MEM (pH 7.4) or TBS (pH 8.0) as complexation medium, (b) N/P ratio 20 or 100, and (c) type of transfection protocol (i.e., direct application of transfection mix onto cells versus dilution of transfection mix in DMEM prior to addition).

RESULTS AND DISCUSSION

Synthesis and Characterization of PMOXA-*b*-PASP-(DET). The main goal of the present work was to synthesize a novel, biocompatible PPH system for gene delivery. Phthalimidoethyl triflate was used as an educt for the chemical synthesis (Figure 1A).[33] Ring-opening polymerization of 2-methyl-2-oxazoline was quenched using NaN_3. According to the ^{1}H NMR calculation, the degree of polymerization index was 90 (Table 1).

Table 1. Characterization of PMOXA-*b*-PASP(DET)

	^{1}H NMR	
sample	DP[a]	M_n
N_3-PMOXA$_n$-NH_2	90	7700
N_3-PMOXA$_n$-PASP(DET)$_m$-NH_2	90:50	18100

[a]DP, degree of polymerization index; M_n, average molecular weight.

Finally, the azide functional group was connected to PMOXA (Figure 1A). The appearance of chemical shift signals from 7.35 to 7.55 ppm on ^{1}H NMR of N_3-PMOXA-Ph proved the existence of phthalimide (Figure 1B), indicating that there was no side reaction occurring between this protection group and 2-methyl-2-oxazoline during polymerization. In addition, absorbance at 2010 nm in the FT-IR proved the successful connection of the azide group on the polymer (Figure 1C).[34] The azide function offers the possibility to connect special targeting ligands through a click chemistry reaction.

The phthalimide group can be deprotected in the presence of hydrazine monohydrate to afford the primary amine.[35] The chemical shift at the position of 1.91 and 3.38 ppm in the ^{1}H NMR spectra of N_3-PMOXA-NH_2 demonstrated that the PMOXA backbone was kept intact in the presence of hydrazine monohydrate during the reaction (Figure 1D).

N_3-PMOXA-NH_2 was used as the macroinitiator to initiate ring-opening polymerization of β-benzyl L-aspartate anhydride in DMF solution. The new peaks with chemical shifts of 2.66, 3.11, 4.28, 5.09, and 7.25 ppm in the ^{1}H NMR demonstrated the successful synthesis of N_3-PMOXA-*b*-PBLA with around 50 repeating units (Figure 1E). To avoid intermolecular aminolysis reaction, N_3-PMOXA-*b*-PBLA was treated with a 2500-fold excess of DET. Disappearance of the benzyl group peaks and appearance of DET on chemical shift 2.83, 3.02, and 3.36 ppm in the ^{1}H NMR spectrum proved the successful modification of N_3-PMOXA-*b*-PBLA with high density of DET (Figure 1F and Table 1). This functionality is needed to form a complex with negatively charged pDNA. In conclusion, PMOXA-*b*-PASP-(DET) was successfully synthesized in high yield using a versatile five-step procedure. The different steps could be easily modified to change the physicochemical characteristics of the biopolymer.

Physicochemical Characterization of PMOXA-*b*-PASP-(DET) as Gene Delivery System. Gene delivery systems have to meet a number of criteria for successful expression of proteins. These include the following: (I) efficient nucleic acid packaging, (II) entry into cell by endocytosis, (III) endosomal escape, (IV) intracellular DNA/carrier release, and (V) entry into the cell nucleus.[17,36,37] The first step for efficient

DOI: 10.1021/acsami.5b01684
ACS Appl. Mater. Interfaces 2015, 7, 10446−10456

transfection is complete complexation of pDNA by electrostatic interactions. PMOXA-*b*-PASP(DET) has several protonable amino groups with pK_a values of 9.1 (secondary amine) and 6.3 (primary amine), resulting in a cationic charge at physiological pH (7.4).[38] In order to assess the complexation power of the PPH, we performed a gel retardation assay analysis (Figure 2 and Supporting Information Figure S1). The positive charge of PMOXA-*b*-PASP(DET) compensates for the negative charge of the pDNA, resulting in a polymer-pDNA nanocomplex with decreased charge. In addition, the PPH forms nanocomplexes with pDNA which are too big to migrate in the agarose gel.

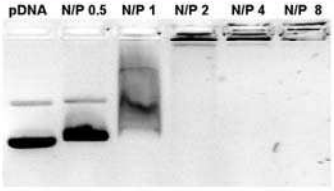

Figure 2. Gel retardation assay. Migration of pDNA (4.7 kb), either native or complexed with increasing concentrations of PMOXA-*b*-PASP(DET). Different N/P ratios are shown. The samples were separated by electrophoresis on a 0.8% agarose gel in the presence of ethidium bromide. pDNA (lane 1) migrates as two bands, i.e., supercoiled and relaxed circular plasmid. An extended version of this figure showing that the complexation of pDNA with PMOXA-*b*-PASP(DET) is pH independent is given in the Supporting Information (Figure S1).

Migration of nanocomplexes in the agarose gel slowed with increasing pDNA complexation (Figure 2 and Supporting Information Figure S1A–C). At N/P ratios of 4, we observed complete complexation and thus slowed migration of the pDNA in the agarose gel. Notably, this observation was independent of the pH (Supporting Information Figure S1A–C). Thus, we conclude that transfection experiments should be performed using an N/P ratio of at least 4. PMOXA-*b*-PASP(DET) stored for a long period (nine months) in Opti-MEM (2 mg/mL) no longer showed an ability to complex pDNA (Supporting Information Figure S1D). Thus, PPH solutions were always prepared freshly.

bPEI generally condenses pDNA completely already at N/P ratios of 1.5–2.0.[18] This difference can be explained by the fact that nitrogens in the PMOXA backbone of our PPH are part of amide bonds. Therefore, they cannot interact with pDNA by electrostatic interactions. The relative number of charged amino groups is lower compared to bPEI which consists only of a polycationic polymer.

TEM analysis of PPH-pDNA complexes formed at different N/P ratios between 0.5 and 300 was performed (Figure 3). At an N/P ratio of 20, PPH-pDNA complexes started to form filamentous and ring-like morphologies (Figure 3A). However, starting at an N/P ratio of 50, the PPH formed spherical

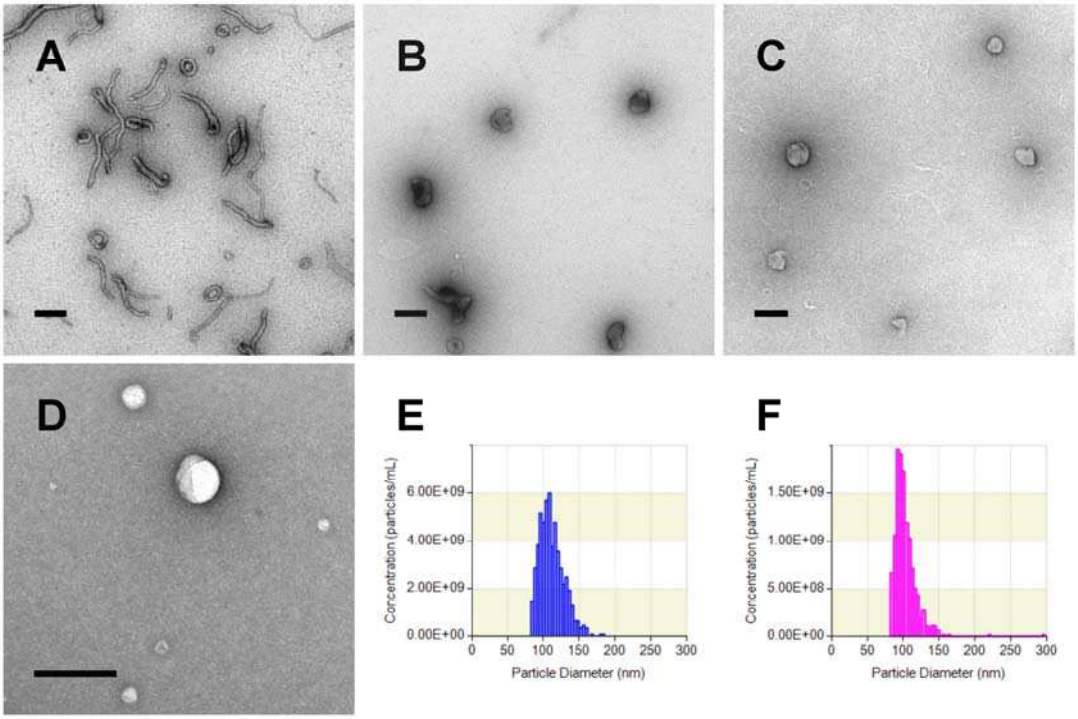

Figure 3. Characterization of nanoparticles with transmission electron microscopy (TEM) and tunable resistive pulse sensing (TRPS). Representative TEM images of PPH-pDNA complexes at N/P ratios of 20 (A), 50 (B), 100 (C), and 300 (D). Scale bars = 200 nm. Additional images of PPH-pDNA nanoparticles at an N/P ratio of 300 are given in the Supporting Information (Figure S2). Size analysis of PPH-pDNA nanoparticles at N/P ratios of 100 (E) and 300 (F) using TRPS.

DOI: 10.1021/acsami.5b01684
ACS Appl. Mater. Interfaces 2015, 7, 10446–10456

ACS Applied Materials & Interfaces Research Article

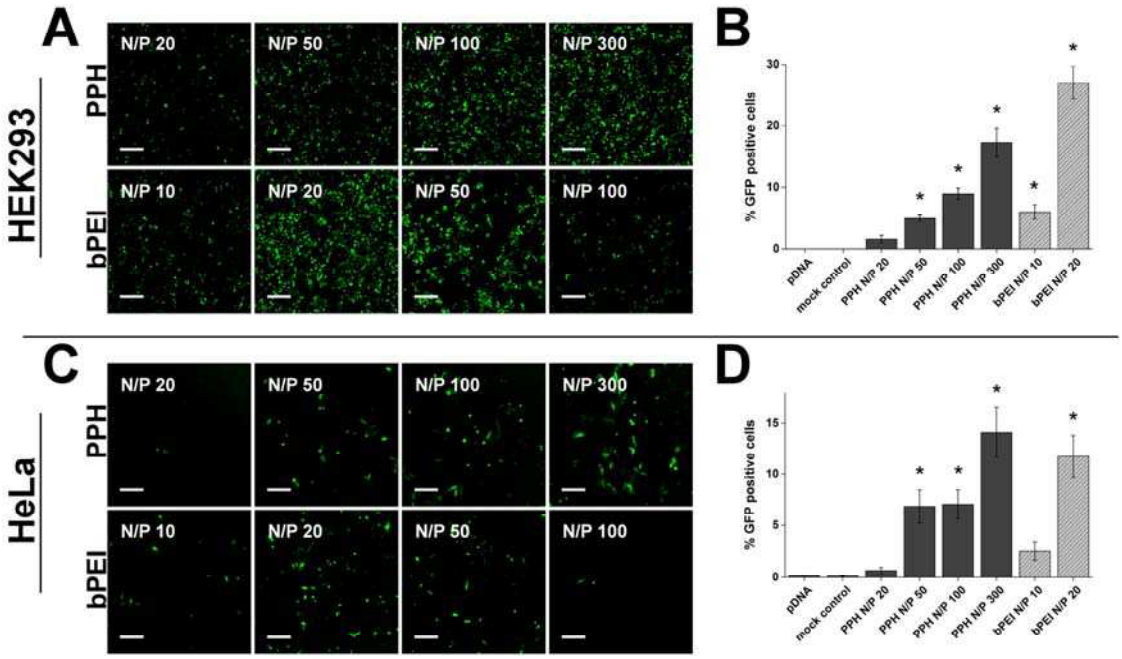

Figure 4. HEK293 and HeLa cells transfected with pDNA encoding for green fluorescence protein (GFP). Confocal laser scanning microscopy (CLSM) analysis of (A) HEK293 and (C) HeLa cells transfected with 1 μg of pDNA complexed with our polymer−peptide hybrid (PPH) system PMOXA-*b*-PASP(DET) or with bPEI. Representative images after transfection at different N/P ratios are shown. Scale bars = 200 μm. Percentages of GFP-positive (B) HEK293 and (D) HeLa cells of the same preparations were quantified using flow cytometry. Only N/P ratios, which did not show any cytotoxic effects in the CLSM analysis, were analyzed. Values are means ± SD of four independent experiments per setting. Level of significance compared to pDNA control and corrected for multiple comparisons: * indicates $P < 0.001$.

structures with a diameter below 200 nm (Figure 3B−D and Supporting Information Figure S2). Interestingly, increasing N/P ratios decreased the size of the resulting PPH-pDNA nanoparticles. After 2 weeks in complexation medium, the PPH-pDNA complexes kept their initial, spherical morphology (Supporting Information Figure S2). It should be noted that TEM analysis is a qualitative method, which cannot provide precise information on size distribution. This can be attributed to the fact that only a limited number of nanoparticles can be analyzed by TEM. Therefore, we used TRPS as a quantitative, precise, and very sensitive method. Mean particle diameter of the nanoparticles determined by TRPS was 109.8 nm at an N/P ratio of 100 and 101.2 nm at an N/P ratio of 300, confirming the corresponding TEM analysis (Figure 3E,F). The d90/d10 values of 1.5 (N/P 100) and 1.4 (N/P 300) were indicative of a narrow and monodisperse size distribution of both nanoparticle types. Nanoparticles in this size range are considered to be optimal for DNA transfection and drug delivery since they can easily undergo endocytosis.[39,40]

The zeta potential of the PPH-pDNA nanoparticles increased with increasing N/P ratios, ranging from −28.0 ± 1.6 mV (N/P 50) to −11.4 ± 2.0 mV (N/P 100), and −5.4 ± 3.4 mV (N/P 300). With increasing amounts of PMOXA-*b*-PASP(DET), the negative charge of pDNA was compensated to a larger degree. The PMOXA block in our PPH might stabilize the nanoparticles by steric repulsion overcoming lowered electrostatic repulsion. In contrast, bPEI-pDNA complexes at N/P ratios of 50, 100, and 300 showed positive zeta potentials (14.4 ± 2.0, 15.7 ± 3.1, and 14.8 ± 2.6 mV, respectively).

The slightly negative zeta potential of our PPH-pDNA nanoparticles is favorable for biomedical applications *in vitro* as well as *in vivo*. Our results demonstrate that the slightly negative charge of our PPH-pDNA nanoparticles does not interfere with *in vitro* cell transfection. We therefore did not use higher N/P ratios since negatively charged nanoparticles are known to be less cytotoxic and less prone to activate the immune system.[41] In addition, it is tempting to speculate that *in vivo* our slightly negative nanoparticles will be characterized by low volume of distribution and a long half-life in the circulation. In contrast, *in vivo* use of cationic nanoparticles is not possible due to their unspecific interaction with plasma membranes and their resulting rapid sequestration in the lung after intravenous administration.[42]

Use of PMOXA-*b*-PASP(DET) as Gene Delivery System. Our nanoparticle characterization data suggest that the PPH should be used at N/P ratios above 20. Therefore, we performed a 2^3 full factorial DoE to evaluate the effect of N/P ratio, complexation medium, and transfection method on transfection efficiency. Our model provided a good fit (R^2 = 0.9822). The complexation medium and N/P ratio were considered as important. The N/P ratio had a significant impact on transfection efficiency (P = 0.0002) followed by the complexation medium (P = 0.0145). Interestingly, the transfection method had no statistically significant impact on transfection efficiency.

In the gel retardation assay we did not observe any difference in pDNA complexation of our PPH at different pH values (Supporting Information Figure S1). Since it was recently

DOI: 10.1021/acsami.5b01684
ACS Appl. Mater. Interfaces 2015, 7, 10446−10456

ACS Applied Materials & Interfaces Research Article

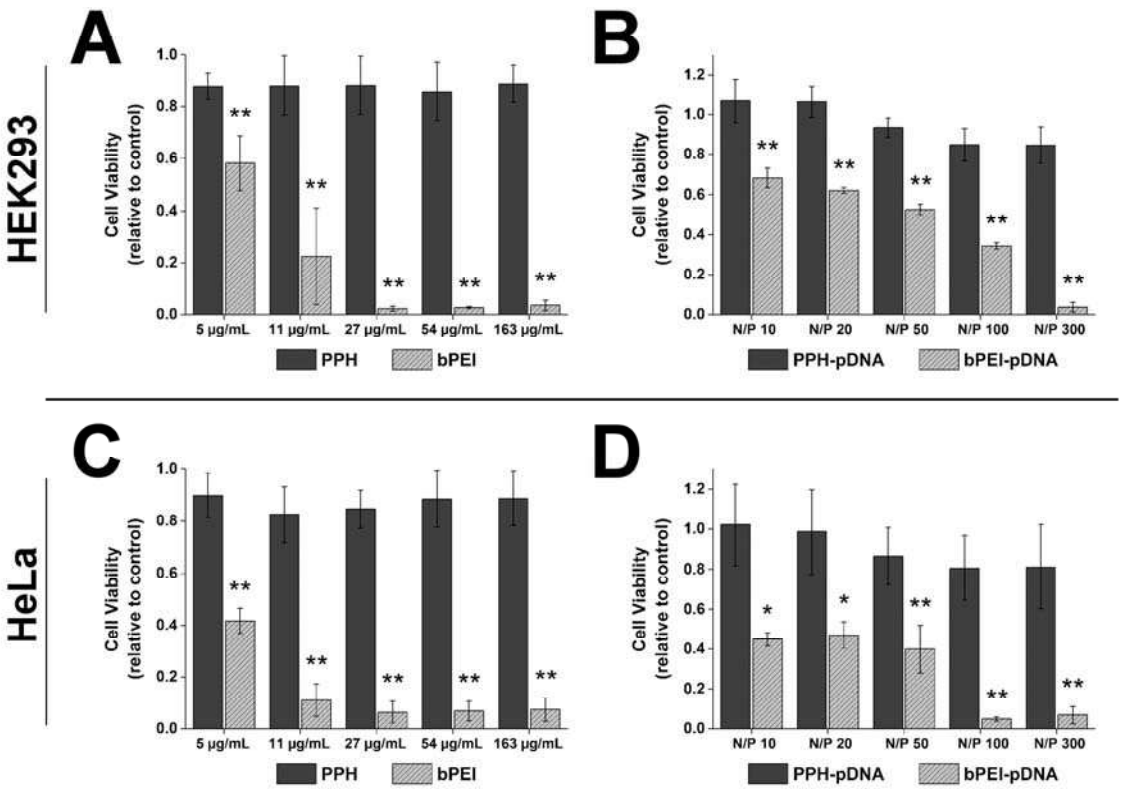

Figure 5. Cell viability assay of HEK293 and HeLa cells determined by MTT assay. (A) HEK293 and (C) HeLa cells were incubated with different amounts of our polymer−peptide hybrid (PPH) PMOXA-*b*-PASP(DET) or with bPEI for 24 h. For better comparability with transfection experiments, the amounts of PPH needed to complex a hypothetical amount of 1 μg/mL pDNA were tested. Analysis of cell viability of (B) HEK293 and (D) HeLa cells incubated with polymer-pDNA nanocomplexes (PPH or bPEI) at different N/P ratios are shown. Values are means ± SD of three independent experiments per setting. Level of significance compared to control (complexation medium only) and corrected for multiple comparisons: * indicates $P < 0.01$; ** indicates $P < 0.001$.

reported that tris buffer enhances the transfection efficiency of polyplex solutions, we used TBS for our 2^3 full factorial DoE.[43] However, we observed that transfection using TBS (pH 8.0) was less efficient compared to Opti-MEM with a pH of 7.4. At lower pH, more amine groups of the PPH are protonated allowing better complex formation of pDNA and PPH. It is important to note that a physiological pH is favorable with respect to biocompatibility and evaluation of the nanoparticles in cell culture or *in vivo*. In conclusion, the best combination from our DoE model was the use of a physiological complexation medium and an N/P ratio of 100.

For qualitative analysis of GFP expression in HEK293 and HeLa cells we used CLSM (Figure 4A,C). Respective polymer-pDNA complexes were always freshly prepared for each experiment to minimize the effect of nucleases, especially because we observed a decreased amount of nanoparticles after storage for 2 weeks in complexation medium. As expected, cells treated with pDNA alone or cells treated with PMOXA-*b*-PASP(DET) alone (mock control) did not express GFP, while cells transfected with PMOXA-*b*-PASP(DET)-pDNA complexes showed GFP expression (Figure 4A,C). The number of GFP-positive cells increased with increasing N/P ratios (20–300). In contrast, HEK293 and HeLa cells transfected with bPEI/pDNA showed the highest number of GFP-positive cells at an N/P ratio of 20 (Figure 4A,C). When the N/P ratios were increased even more, the total number of cells decreased, indicative of cytotoxic effects of bPEI (Figure 4A,C).

To underline our observation, we performed an image analysis of surface area of GFP-positive cells (%) as an indicator for the total number of transfected cells. In fact, the image analysis revealed that the surface area of GFP-positive cells decreased for higher bPEI N/P ratios. Increasing the N/P ratio from 20 to 50 decreased the surface area of GFP-positive cells approximately 40%. There was no indication of PPH-pDNA complex-induced cell toxicity despite the use of higher amounts of transfection reagent. In both human cell lines the surface area of GFP-positive cells increased significantly with increasing N/P ratios from 20 to 300.

For an exact quantification of transfection efficiency, we performed a flow cytometry analysis using N/P ratios not showing any cellular toxicity in CLSM studies. Neither PPH alone nor pDNA alone resulted in transfection of cells (Figure 4B,D). bPEI (N/P = 20) yielded a transfection efficiency of 27.0% ± 2.7% and 11.7% ± 2.1% using the same amount of pDNA and the same transfection method as for the PHH in HEK293 and HeLa cells, respectively. Using PPH-pDNA

DOI: 10.1021/acsami.5b01684
ACS Appl. Mater. Interfaces 2015, 7, 10446−10456

complexes, the percentage of GFP-expressing cells increased significantly with increasing N/P ratios (Figure 4B,D). The highest N/P ratio of PMOXA-*b*-PASP(DET)/pDNA used in our study (N/P = 300) showed a GFP-transfection efficiency of 17.3% ± 2.3% in HEK293 cells and 14.1% ± 2.4% in HeLa cells. Thus, our PPH resulted in a GFP expression level comparable to the one induced by bPEI (Figure 4B,D). These results are comparable to findings from other recently developed polymer conjugates such as cyclodextrin-cored starlike carriers[44] or PPH systems based on PLL.[45−47] However, it should be noted that a comparison of published results is difficult. Transfection efficiency depends on various factors such as cell line, pDNA promotor, or encoded protein.

Cytocompatibility of PMOXA-*b*-PASP(DET) as Gene Delivery System. Transfection of cells with cationic reagents is often linked to cytotoxic effects since excessive positive charges destabilize the cell membrane. In general, high molecular weight cationic polymers show higher cytotoxicity compared to low molecular polycations.[48] This interaction is more likely when the polyplex dissociates *in vivo* and the free polycation interacts with cell membranes.[49] *In vivo*, accumulation of the compound in specific organs can lead to long-term side effects. Therefore, we used the MTT assay to evaluate cytotoxicity of bPEI and PMOXA-*b*-PASP(DET) in the presence (Figure 5B,D) and more importantly in the absence (Figure 5A,C) of pDNA in two human cell lines.

bPEI resulted in strong cytotoxic effects (Figure 5). A significant decrease in cell viability of more than 90% was detected for 163 μg/mL bPEI ($P < 0.001$) in both cell lines (Figure 5A,C). This effect was even seen at low concentrations of 5 μg/mL bPEI with RCV of 0.58 ± 0.10 in HEK293 and 0.42 ± 0.05 in HeLa cells. Similar results were observed for bPEI-pDNA complexes (Figure 5B,D). With increasing N/P ratios, the cell viability decreased significantly compared to control cells up to 96.3% ± 2.4% in HEK293 and 93.1% ± 4.3% in HeLa cells for N/P 300. Importantly, also N/P ratios used in transfection experiments (N/P 10 and N/P 20) resulted in significantly reduced cell viability.

In sharp contrast, our PPH resulted in high cell viability at all concentrations in absence and presence of pDNA (Figure 5). In both cell lines no significant difference in cell viability compared to control cells was observed. There was no concentration-dependent effect, and even high concentrations or high N/P ratios were well-tolerated (Figure 5). Concentrations of 163 μg/mL (corresponding to an N/P ratio of 300 used for the transfection assay) resulted in excellent cell viability with an RCV of 0.89 ± 0.07 in HEK293 and 0.89 ± 0.10 in HeLa cells (Figure 5A,C). Cells treated with PPH-pDNA nanoparticles showed superior cytocompatibility compared to bPEI at all N/P ratios (Figure 5B,D).

Our findings are consistent with other PMOXA-based copolymer studies that also showed high cytocompatibility.[32] The PPH might benefit from the biocompatible features of the PMOXA block.[50] In addition, peptide-based polymer hybrids are biodegradable resulting in improved long-term cytocompatibility as also shown by other groups.[51]

The results of the MTT assay were confirmed by cell growth analysis (Figure 6). Transfection reagents are commonly used for pDNA delivery *in vitro*. However, they may interfere with cell replication and cell growth. Fischer et al. reported that polycations, such as bPEI, induce necrotic cell reactions.[16] Thus, we performed a CLSM study to analyze the effect of bPEI and our PPH on cell growth and morphology (Figure 6A + Supporting Information Figure S3). bPEI had a strong influence on the growth characteristics. Cells grew slowly and in clusters. This result was confirmed by analyzing the growth area of cells after 48 h. bPEI decreased the growth of cells substantially, leading to a reduction of the overgrown area to only 2.0% ± 0.9% at a concentration of 11 μg/mL compared to that of control cells (Figure 6). Furthermore, bPEI caused characteristic apoptotic features such as roundness, detachment, cytoplasmic blebbing, and debris (Supporting Information Figure S3).

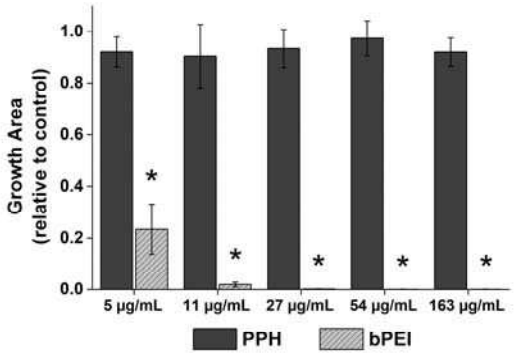

Figure 6. Cell growth analysis. Cell growth analysis of GFP-expressing HEK293 cells 48 h after addition of our polymer−peptide hybrid (PPH) PMOXA-*b*-PASP(DET) or bPEI at different concentrations. Mean values of growth region of GFP-positive cells (%) compared to control conditions (complexation medium only) are given ± SD (n = 4). Level of significance compared to control and corrected for multiple comparisons: * indicates $P < 0.001$. Representative images are shown in the Supporting Information (Figure S3).

In sharp contrast, growth of cells cultured in medium containing our PPH was not impaired. Even at the highest concentrations of our PPH, the relative growth area of 92.0% ± 5.5% was not significantly different from that obtained for the control (Figure 6A and Supporting Information Figure S3). The highest concentration of 163 μg/mL corresponds to an N/P ratio of 300. We conclude that our PPH (but not the commonly used transfection reagent bPEI) is not cytotoxic nor does it impair cell growth. These results are in line with the findings from the transfection experiments (Figure 4). In addition, a pilot study in a vertebrate model, namely, the zebrafish embryo model,[52−54] was performed to assess the safety of PPH *in vivo*. In accordance to OECD guidelines, zebrafish embryos were dechorionated before the incubation with test compounds due to the high molecular weight of the polymers. Zebrafish embryos incubated with our PPH showed a significantly increased survival rate as compared to bPEI ($P < 0.001$): Concentrations of 27 μg/mL bPEI resulted in 100% mortality of zebrafish embryos after incubation for 24 h. In sharp contrast, our PPH (27 μg/mL) was much better tolerated, and the zebrafish embryos showed a survival rate of 48.9% ± 3.8%. These results are consistent with other recently published nanotoxicity studies using the zebrafish embryo assay.[55] Toxicity of bPEI was attributed to its cationic properties.

In summary, our PPH is characterized by a surprisingly high transfection efficiency despite a negative zeta potential and the protein-repellent properties of PMOXA.[56] Cell membranes have a negative surface charge predominantly because of the

DOI: 10.1021/acsami.5b01684
ACS Appl. Mater. Interfaces 2015, 7, 10446−10456

highly anionic glycosaminoglycans (GAGs). Therefore, interactions with the cell membrane are more pronounced if the nanocomplex has free positively charged groups leading to increased cell uptake. In this respect, the incubation conditions in cell culture do not precisely reflect the *in vivo* situation. In our experiments, cells are exposed for a long time (e.g., 48 h) to high concentrations of nanoparticles. Under these conditions, a forced and unspecific uptake of nanoparticles may occur. *In vivo*, sophisticated targeting strategies will be needed to promote a comparable cellular uptake. On the other hand, highly cationic polymers, such as bPEI, may destabilize cellular membranes leading to toxic side effects.

Thus, the better biocompatibility of our PPH may compensate for reduced transfection efficiency. A factor facilitating cell transfection using our PPH might be nanoparticle morphology. A small particle size (i.e., 100 nm) and narrow size distribution favor pDNA delivery into cells.[57−59]

To further increase transfection efficiency using our PPH, the amino functionality of the PPH could be varied. This modification might improve the interaction with the cell membrane and/or enhance endosomal escape of internalized nanoparticles. A long-term perspective of our platform technology is the use for *in vivo* gene therapy. To this end, nanoparticles have to be modified with a targeting ligand to direct them to diseased tissues or organs in the body. Thus, a next generation of targeted nanoparticles will be needed to achieve this goal. The azide function of the PPH could be used for conjugation of targeting ligands via click chemistry. A possible *in vivo* application might be targeting of hepatocytes via the asialoglycoprotein receptor.[60,36] Therapeutic regimens for genetic diseases such as α1-antitrypsin deficiency[61] as well as strategies against hepatocellular carcinoma[62] might profit significantly from such a targeted gene therapy approach.

■ CONCLUSION

The present paper describes the synthesis of a novel PPH system, namely, PMOXA-*b*-PASP(DET), which efficiently complexed pDNA. The PPH formed nanocomplexes with different morphologies. At high N/P ratios, highly uniform PPH-pDNA nanoparticles (d90/10 = 1.4) with a mean diameter around 100 nm were produced. The zeta potential of the resulting nanoparticles was slightly negative. Our PPH system showed excellent cytocompatibility. The pDNA transfection ability in HEK293 and HeLa cells was comparable to that of bPEI.

In conclusion, the combination of the biocompatible PMOXA backbone with the biodegradable PASP block is a novel and promising PPH system for efficient pDNA delivery without significant cytotoxic drawbacks. Additionally, our PPH system offers many possibilities for chemical modification. These interesting properties might be beneficial for *in vivo* applications, such as targeted gene delivery.

■ ASSOCIATED CONTENT

Supporting Information

Complexation of pDNA with PMOXA-*b*-PASP(DET) under different pH conditions (Figure S1), stability test of PPH-pDNA-nanoparticles using TEM analysis (Figure S2), and representative images of GFP expressing HEK293 cells 48 h after addition of PMOXA-*b*-PASP(DET) or bPEI at different concentrations (Figure S3). The Supporting Information is available free of charge on the ACS Publications website at DOI: 10.1021/acsami.5b01684.

■ AUTHOR INFORMATION

Corresponding Author

*E-mail: joerg.huwyler@unibas.ch. Phone: +41 (0)61 267 15 13.

Author Contributions

D. Witzigmann and D. Wu contributed equally to this work. All authors contributed to the contents of this manuscript, and all of them gave their approval to the final version.

Notes

The authors declare no competing financial interest.

■ ACKNOWLEDGMENTS

We acknowledge the financial support of the Swiss Centre of Applied Human Toxicology (SCAHT), Swiss National Science Foundation, and Swiss Nanoscience Institute (SNI). We thank the China Scholarship Council for supporting D. Wu. In addition, the authors thank Dr. Fabiola Porta and Stefan Siegrist for experimental support with the zebrafish embryo study, Prof. Markus Affolter for access to the zebrafish facility, Hubertus Kohler for support in the production of GFP expressing HEK 293 cells, and Izon Science (Oxford, U.K.) for assistance with TRPS measurements. Furthermore, we thank Dr. Silvia Rogers for editorial assistance.

■ ABBREVIATIONS

bPEI, branched poly(ethylenimine)
CLSM, confocal laser scanning microscopy
DCM, dichloromethane
DMEM, Dulbecco's modified Eagle's culture medium
DET, diethylenetriamine
FCS, fetal calf serum
FT-IR, Fourier transform infrared spectroscopy
GFP, green fluorescence protein
HEK293 cells, human embryonic kidney cells
N/P, nitrogen to phosphate
PASP, poly(aspartic acid)
pDNA, plasmid DNA
PEG, polyethylene glycol
PMOXA, poly(2-methyl-2-oxazoline)
PPH, polymer−peptide hybrid
RT, room temperature
TBE, tris/borate/EDTA buffer
TBS, tris-buffered saline
TEA, trimethylamine
TEM, transmission electron microscopy
TRPS, tunable resistive pulse sensing

■ REFERENCES

(1) Gene Therapy Clinical Trials Worldwide Home Page. http://www.abedia.com/wiley/phases.php (accessed Oct 3, 2014).
(2) Wicki, A.; Witzigmann, D.; Balasubramanian, V.; Huwyler, J. Nanomedicine in Cancer Therapy: Challenges, Opportunities, and Clinical Applications. *J. Controlled Release* **2015**, *200*, 138−157.
(3) Dey, D.; Inayathullah, M.; Lee, A. S.; LeMieux, M. C.; Zhang, X.; Wu, Y.; Nag, D.; De Almeida, P. E.; Han, L.; Rajadas, J. Efficient Gene Delivery of Primary Human Cells Using Peptide Linked Polyethylenimine Polymer Hybrid. *Biomaterials* **2011**, *32*, 4647−4658.
(4) Pack, D. W.; Hoffman, A. S.; Pun, S.; Stayton, P. S. Design and Development of Polymers for Gene Delivery. *Nat. Rev. Drug Discovery* **2005**, *4*, 581−593.
(5) Palivan, C. G.; Fischer-Onaca, O.; Delcea, M.; Itel, F.; Meier, W. Protein-Polymer Nanoreactors for Medical Applications. *Chem. Soc. Rev.* **2012**, *41*, 2800−2823.

DOI: 10.1021/acsami.5b01684
ACS Appl. Mater. Interfaces 2015, 7, 10446−10456

(6) Kataoka, K.; Harada, A.; Nagasaki, Y. Block Copolymer Micelles for Drug Delivery: Design, Characterization and Biological Significance. *Adv. Drug Delivery Rev.* **2012**, *64*, 37−48.
(7) Mei, Y.; Beers, K. L.; Byrd, H. C. M.; VanderHart, D. L.; Washburn, N. R. Solid-Phase ATRP Synthesis of Peptide-Polymer Hybrids. *J. Am. Chem. Soc.* **2004**, *126*, 3472−3476.
(8) Zhong, Z.; Song, Y.; Engbersen, J. F. J.; Lok, M. C.; Hennink, W. E.; Feijen, J. A Versatile Family of Degradable Non-Viral Gene Carriers Based on Hyperbranched Poly(ester Amine)s. *J. Controlled Release* **2005**, *109*, 317−329.
(9) Kim, T.; Ou, M.; Lee, M.; Kim, S. W. Arginine-Grafted Bioreducible Poly(disulfide Amine) for Gene Delivery Systems. *Biomaterials* **2009**, *30*, 658−664.
(10) Klok, H.-A. Peptide/Protein-Synthetic Polymer Conjugates: Quo Vadis. *Macromolecules* **2009**, *42*, 7990−8000.
(11) Zhang, S.; Zhao, Y.; Zhao, B.; Wang, B. Hybrids of Nonviral Vectors for Gene Delivery. *Bioconjugate Chem.* **2010**, *21*, 1003−1009.
(12) Mahato, M.; Kumar, P.; Sharma, A. K. Amphiphilic Polyethylenimine Polymers Mediate Efficient Delivery of DNA and siRNA in Mammalian Cells. *Mol. BioSyst.* **2013**, *9*, 780−791.
(13) Zhang, Q.-F.; Yu, Q.-Y.; Geng, Y.; Zhang, J.; Wu, W.-X.; Wang, G.; Gu, Z.; Yu, X.-Q. Ring-Opening Polymerization for Hyperbranched Polycationic Gene Delivery Vectors with Excellent Serum Tolerance. *ACS Appl. Mater. Interfaces* **2014**, *6*, 15733−15742.
(14) Kim, H. J.; Miyata, K.; Nomoto, T.; Zheng, M.; Kim, A.; Liu, X.; Cabral, H.; Christie, R. J.; Nishiyama, N.; Kataoka, K. siRNA Delivery from Triblock Copolymer Micelles with Spatially-Ordered Compartments of PEG Shell, siRNA-Loaded Intermediate Layer, and Hydrophobic Core. *Biomaterials* **2014**, *35*, 4548−4556.
(15) Winter, J.; Link, S.; Witzigmann, D.; Hildenbrand, C.; Previti, C.; Diederichs, S. Loop-miRs: Active microRNAs Generated from Single-Stranded Loop Regions. *Nucleic Acids Res.* **2013**, *41*, 5503−5512.
(16) Fischer, D.; Li, Y.; Ahlemeyer, B.; Krieglstein, J.; Kissel, T. In Vitro Cytotoxicity Testing of Polycations: Influence of Polymer Structure on Cell Viability and Hemolysis. *Biomaterials* **2003**, *24*, 1121−1131.
(17) Wong, S. Y.; Pelet, J. M.; Putnam, D. Polymer Systems for Gene Delivery-Past, Present, and Future. *Prog. Polym. Sci.* **2007**, *32*, 799−837.
(18) Zhu, Y.; Tang, G.-P.; Xu, F.-J. Efficient poly(N-3-Hydroxypropyl)aspartamide-Based Carriers via ATRP for Gene Delivery. *ACS Appl. Mater. Interfaces* **2013**, *5*, 1840−1848.
(19) Zhou, D.; Li, C.; Hu, Y.; Zhou, H.; Chen, J.; Zhang, Z.; Guo, T. PLL/pDNA/P(His-Co-DMAEL) Ternary Complexes: Assembly, Stability and Gene Delivery. *J. Mater. Chem.* **2012**, *22*, 10743−10751.
(20) Zhou, D.; Li, C.; Hu, Y.; Zhou, H.; Chen, J.; Zhang, Z.; Guo, T. The Effects of a Multifunctional Oligomer and Its Incorporation Strategies on the Gene Delivery Efficiency of poly(L-Lysine). *Chem. Commun.* **2012**, *48*, 4594−4596.
(21) Newland, B.; Zheng, Y.; Jin, Y.; Abu-Rub, M.; Cao, H.; Wang, W.; Pandit, A. Single Cyclized Molecule versus Single Branched Molecule: A Simple and Efficient 3D "Knot" Polymer Structure for Nonviral Gene Delivery. *J. Am. Chem. Soc.* **2012**, *134*, 4782−4789.
(22) Zhao, T.; Zhang, H.; Newland, B.; Aied, A.; Zhou, D.; Wang, W. Significance of Branching for Transfection: Synthesis of Highly Branched Degradable Functional Poly(dimethylaminoethyl Methacrylate) by Vinyl Oligomer Combination. *Angew. Chem.* **2014**, *126*, 6209−6214.
(23) Hentschel, J.; Bleek, K.; Ernst, O.; Lutz, J.-F.; Boerner, H. G. Easy Access to Bioactive Peptide-Polymer Conjugates via RAFT. *Macromolecules* **2008**, *41*, 1073−1075.
(24) Hoogenboom, R. Poly(2-Oxazoline)s: A Polymer Class with Numerous Potential Applications. *Angew. Chem., Int. Ed.* **2009**, *48*, 7978−7994.
(25) Konradi, R.; Pidhatika, B.; Mühlebach, A.; Textor, M. Poly-2-Methyl-2-Oxazoline: A Peptide-like Polymer for Protein-Repellent Surfaces. *Langmuir* **2008**, *24*, 613−616.
(26) Viegas, T. X.; Bentley, M. D.; Harris, J. M.; Fang, Z.; Yoon, K.; Dizman, B.; Weimer, R.; Mero, A.; Pasut, G.; Veronese, F. M. Polyoxazoline: Chemistry, Properties, and Applications in Drug Delivery. *Bioconjugate Chem.* **2011**, *22*, 976−986.
(27) Fishburn, C. S. The Pharmacology of PEGylation: Balancing PD with PK to Generate Novel Therapeutics. *J. Pharm. Sci.* **2008**, *97*, 4167−4183.
(28) Pidhatika, B.; Rodenstein, M.; Chen, Y.; Rakhmatullina, E.; Mühlebach, A.; Acikgöz, C.; Textor, M.; Konradi, R. Comparative Stability Studies of poly(2-Methyl-2-Oxazoline) and Poly(ethylene Glycol) Brush Coatings. *Biointerphases* **2012**, *7*, 1.
(29) Canalle, L. A.; Löwik, D. W. P. M.; van Hest, J. C. M. Polypeptide-Polymer Bioconjugates. *Chem. Soc. Rev.* **2010**, *39*, 329−353.
(30) Morell, M.; Puiggali, J. Hybrid Block Copolymers Constituted by Peptides and Synthetic Polymers: An Overview of Synthetic Approaches, Supramolecular Behavior and Potential Applications. *Polymers* **2013**, *5*, 188−224.
(31) Osada, K.; Kataoka, K. Drug and Gene Delivery Based on Supramolecular Assembly of PEG-Polypeptide Hybrid Block Copolymers. In *Peptide Hybrid Polymers*; Klok, H. A., Schlaad, H., Eds.; Springer-Verlag: Berlin, 2006; Vol. *202*, pp 113−153.
(32) Camblin, M.; Detampel, P.; Kettiger, H.; Wu, D.; Balasubramanian, V.; Huwyler, J. Polymersomes Containing Quantum Dots for Cellular Imaging. *Int. J. Nanomed.* **2014**, *9*, 2287−2298.
(33) Smicius, R.; Engels, J. W. Preparation of Zwitterionic Ribonucleoside Phosphoramidites for Solid-Phase siRNA Synthesis. *J. Org. Chem.* **2008**, *73*, 4994−5002.
(34) Vinson, N.; Gou, Y.; Becer, C. R.; Haddleton, D. M.; Gibson, M. I. Optimised "click" Synthesis of Glycopolymers with Mono/di- and Trisaccharides. *Polym. Chem.* **2010**, *2*, 107−113.
(35) Osby, J. O.; Martin, M. G.; Ganem, B. An Exceptionally Mild Deprotection of Phthalimides. *Tetrahedron Lett.* **1984**, *25*, 2093−2096.
(36) Kettiger, H.; Schipanski, A.; Wick, P.; Huwyler, J. Engineered Nanomaterial Uptake and Tissue Distribution: From Cell to Organism. *Int. J. Nanomed.* **2013**, *8*, 3255−3269.
(37) Hu, Y.; Zhu, Y.; Yang, W. T.; Xu, F. J. New Star-Shaped Carriers Composed of B-Cyclodextrin Cores and Disulfide-Linked Poly(glycidyl Methacrylate) Derivative Arms with Plentiful Flanking Secondary Amine and Hydroxyl Groups for Highly Efficient Gene Delivery. *ACS Appl. Mater. Interfaces* **2013**, *5*, 703−712.
(38) Miyata, K.; Oba, M.; Nakanishi, M.; Fukushima, S.; Yamasaki, Y.; Koyama, H.; Nishiyama, N.; Kataoka, K. Polyplexes from Poly(aspartamide) Bearing 1,2-Diaminoethane Side Chains Induce pH-Selective, Endosomal Membrane Destabilization with Amplified Transfection and Negligible Cytotoxicity. *J. Am. Chem. Soc.* **2008**, *130*, 16287−16294.
(39) Xu, A.; Yao, M.; Xu, G.; Ying, J.; Ma, W.; Li, B.; Jin, Y. A Physical Model for the Size-Dependent Cellular Uptake of Nanoparticles Modified with Cationic Surfactants. *Int. J. Nanomed.* **2012**, *7*, 3547−3554.
(40) Jiang, S.; Eltoukhy, A. A.; Love, K. T.; Langer, R.; Anderson, D. G. Lipidoid-Coated Iron Oxide Nanoparticles for Efficient DNA and siRNA Delivery. *Nano Lett.* **2013**, *13*, 1059−1064.
(41) Karmali, P. P.; Simberg, D. Interactions of Nanoparticles with Plasma Proteins: Implication on Clearance and Toxicity of Drug Delivery Systems. *Expert Opin. Drug Delivery* **2011**, *8*, 343−357.
(42) Ishiwata, H.; Suzuki, N.; Ando, S.; Kikuchi, H.; Kitagawa, T. Characteristics and Biodistribution of Cationic Liposomes and Their DNA Complexes. *J. Controlled Release* **2000**, *69*, 139−148.
(43) Iwai, R.; Haruki, R.; Nemoto, Y.; Nakayama, Y. Enhanced Transfection Efficiency of poly(N,N-Dimethylaminoethyl Methacrylate)-Based Deposition Transfection by Combination with Tris(hydroxymethyl)aminomethane. *Bioconjugate Chem.* **2013**, *24*, 159−166.
(44) Li, R. Q.; Niu, Y. L.; Zhao, N. N.; Yu, B. R.; Mao, C.; Xu, F. J. Series of New B-Cyclodextrin-Cored Starlike Carriers for Gene Delivery. *ACS Appl. Mater. Interfaces* **2014**, *6*, 3969−3978.

DOI: 10.1021/acsami.5b01684
ACS Appl. Mater. Interfaces 2015, 7, 10446−10456

(45) Von Erlach, T.; Zwicker, S.; Pidhatika, B.; Konradi, R.; Textor, M.; Hall, H.; Lühmann, T. Formation and Characterization of DNA-Polymer-Condensates Based on poly(2-Methyl-2-Oxazoline) Grafted poly(L-Lysine) for Non-Viral Delivery of Therapeutic DNA. *Biomaterials* **2011**, *32*, 5291−5303.
(46) Fukushima, S.; Miyata, K.; Nishiyama, N.; Kanayama, N.; Yamasaki, Y.; Kataoka, K. PEGylated Polyplex Micelles from Triblock Catiomers with Spatially Ordered Layering of Condensed pDNA and Buffering Units for Enhanced Intracellular Gene Delivery. *J. Am. Chem. Soc.* **2005**, *127*, 2810−2811.
(47) Cai, X.; Dong, C.; Dong, H.; Wang, G.; Pauletti, G. M.; Pan, X.; Wen, H.; Mehl, L; Li, Y.; Shi, D. Effective Gene Delivery Using Stimulus-Responsive Catiomer Designed with Redox-Sensitive Disulfide and Acid-Labile Imine Linkers. *Biomacromolecules* **2012**, *13*, 1024−1034.
(48) Car, A.; Baumann, P.; Duskey, J. T.; Chami, M.; Bruns, N.; Meier, W. pH-Responsive PDMS-B-PDMAEMA Micelles for Intracellular Anticancer Drug Delivery. *Biomacromolecules* **2014**, *15*, 3235−3245.
(49) Kircheis, R.; Wightman, L.; Wagner, E. Design and Gene Delivery Activity of Modified Polyethylenimines. *Adv. Drug Delivery Rev.* **2001**, *53*, 341−358.
(50) Isaacman, M. J.; Corigliano, E. M.; Theogarajan, L. S. Stealth Polymeric Vesicles via Metal-Free Click Coupling. *Biomacromolecules* **2013**, *14*, 2996−3000.
(51) Lynn, D. M.; Langer, R. Degradable Poly(β-Amino Esters): Synthesis, Characterization, and Self-Assembly with Plasmid DNA. *J. Am. Chem. Soc.* **2000**, *122*, 10761−10768.
(52) Fako, V. E.; Furgeson, D. Y. Zebrafish as a Correlative and Predictive Model for Assessing Biomaterial Nanotoxicity. *Adv. Drug Delivery Rev.* **2009**, *61*, 478−486.
(53) Hu, Y.-L.; Qi, W.; Han, F.; Shao, J.-Z.; Gao, J.-Q. Toxicity Evaluation of Biodegradable Chitosan Nanoparticles Using a Zebrafish Embryo Model. *Int. J. Nanomed.* **2011**, *6*, 3351−3359.
(54) Duan, J.; Yu, Y.; Li, Y.; Yu, Y.; Sun, Z. Cardiovascular Toxicity Evaluation of Silica Nanoparticles in Endothelial Cells and Zebrafish Model. *Biomaterials* **2013**, *34*, 5853−5862.
(55) Rizzo, L. Y.; Golombek, S. K.; Mertens, M. E.; Pan, Y.; Laaf, D.; Broda, J.; Jayapaul, J.; Möckel, D.; Subr, V.; Hennink, W. E.; Storm, G.; Simon, U.; Jahnen-Dechent, W.; Kiessling, F.; Lammers, T. In Vivo Nanotoxicity Testing Using the Zebrafish Embryo Assay. *J. Mater. Chem. B* **2013**, *1*, 3918−3925.
(56) Byeon, J. H.; Kim, H.-K.; Thompson, D. H.; Roberts, J. T. Aerosol-Based Fabrication of Modified Chitosans and Their Application for Gene Transfection. *ACS Appl. Mater. Interfaces* **2014**, *6*, 4597−4602.
(57) Van de Wetering, P.; Moret, E. E.; Schuurmans-Nieuwenbroek, N. M. E.; van Steenbergen, M. J.; Hennink, W. E. Structure−Activity Relationships of Water-Soluble Cationic Methacrylate/Methacrylamide Polymers for Nonviral Gene Delivery. *Bioconjugate Chem.* **1999**, *10*, 589−597.
(58) Zhang, S.; Li, J.; Lykotrafitis, G.; Bao, G.; Suresh, S. Size-Dependent Endocytosis of Nanoparticles. *Adv. Mater.* **2009**, *21*, 419−424.
(59) Lu, F.; Wu, S.-H.; Hung, Y.; Mou, C.-Y. Size Effect on Cell Uptake in Well-Suspended, Uniform Mesoporous Silica Nanoparticles. *Small* **2009**, *5*, 1408−1413.
(60) Detampel, P.; Witzigmann, D.; Krähenbühl, S.; Huwyler, J. Hepatocyte Targeting Using Pegylated Asialofetuin-Conjugated Liposomes. *J. Drug Targeting* **2013**, *22*, 232−241.
(61) Stoller, J. K.; Aboussouan, L. S. Alpha1-Antitrypsin Deficiency. *Lancet* **2005**, *365*, 2225−2236.
(62) Peng, D.-J.; Sun, J.; Wang, Y.-Z.; Tian, J.; Zhang, Y.-H.; Noteborn, M. H. M.; Qu, S. Inhibition of Hepatocarcinoma by Systemic Delivery of Apoptin Gene via the Hepatic Asialoglycoprotein Receptor. *Cancer Gene Ther.* **2007**, *14*, 66−73.

DOI: 10.1021/acsami.5b01684
ACS Appl. Mater. Interfaces 2015, 7, 10446−10456

ACS APPLIED MATERIALS & INTERFACES

Research Article

www.acsami.org

SUPPORTING INFORMATION

Biocompatible Polymer–Peptide Hybrid-Based DNA Nanoparticles for Gene Delivery

Dominik Witzigmann,[†] Dalin Wu,[‡] Susanne H. Schenk,[†] Vimalkumar Balasubramanian,[†,§] Wolfgang Meier,[‡] and Jörg Huwyler*[,†]

[†]Division of Pharmaceutical Technology, Department of Pharmaceutical Sciences, University of Basel, Klingelbergstrasse 50, Basel CH-4056, Switzerland

[‡]Department of Chemistry, University of Basel, Klingelbergstrasse 80, Basel CH-4056, Switzerland

[§]Division of Pharmaceutical Chemistry and Technology, Faculty of Pharmacy, University of Helsinki, Viikinkaari 5E, Helsinki FI-00014, Finland

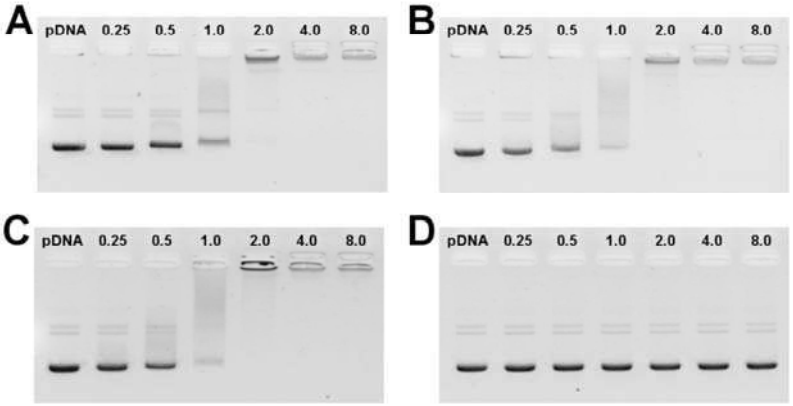

Figure S1. Complexation of pDNA under Different Conditions. Migration of pDNA (4.7 kb), either native or complexed with increasing concentrations of PMOXA-*b*-PASP(DET) in (A) Opti-MEM - physiological pH, (B) acetate buffer - pH 5.5, (C) tris-buffered saline - pH 8.0, or (D) with PMOXA-*b*-PASP(DET) stored for nine months in Opti-MEM. Numbers indicate the different N/P ratios. The samples were separated by electrophoresis on a 0.8% agarose gel in the presence of ethidium bromide. pDNA (lane 1) migrates as three bands, i.e. supercoiled (major band) and relaxed circular/linear plasmid (minor bands).

ACS Applied Materials & Interfaces Research Article

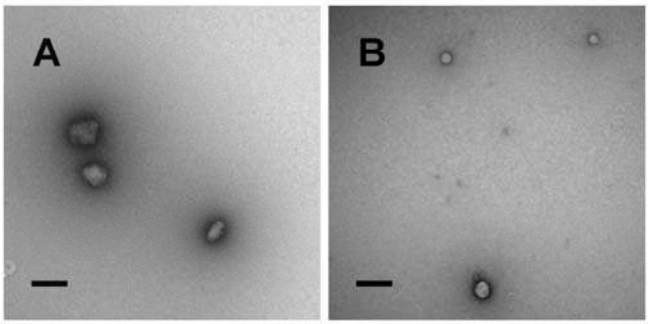

Figure S2. Stability of Polymer Peptide Hybrid (PPH) pDNA nanoparticles. Representative TEM images of (A) freshly prepared PPH-pDNA nanoparticles at N/P ratio of 300 and (B) after storage for 14 days at 4°C. Scale bars = 200 nm.

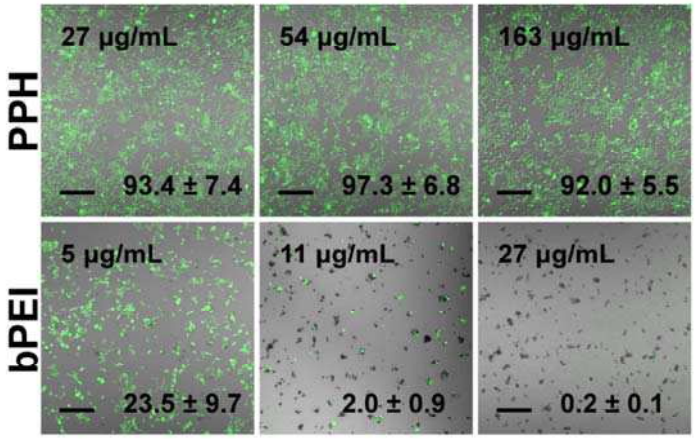

Figure S3. Cell growth analysis of GFP-expressing HEK293 cells. Representative fluorescence images of GFP expressing HEK293 cells 48 h after addition of PMOXA-*b*-PASP(DET) or bPEI at different concentrations. Cells were excited at 488 nm and fluorescence was measured at 516 nm. Mean values of growth region of GFP-positive cells (%) compared to control conditions (buffer only) are given ± SD (n=4).

DISCUSSION AND CONCLUSION

In the context of this PhD thesis on "Hepatocyte-specific drug delivery using active targeted nanomedicines" various drug delivery and drug targeting strategies to parenchymal liver cells were developed. This "Discussion and Conclusion" paragraph brings all research achievements into a larger context. Active targeting strategies are summarized and new targets are evaluated. In addition, the development of a gene delivery system is elaborated.

I. Active Targeting Strategy And Its Analysis

1. Hepatocyte-specific Drug Targeting

1.1. Importance of Targeting Approach

(i) The liver is characterized by a high metabolic rate, (ii) many drugs and nanoparticles passively accumulate in the liver, (iii) and liver parenchymal cells represent approximately 80% of all hepatic cells. These statements can lead to a misconception and thus raise the question why hepatocyte-specific targeting approaches are needed. The answer can be found in the biodistribution and subsequent drug accumulation. Most conventional drugs and nanoparticles do not accumulate in the correct cell type. Mostly, they passively accumulate in tissue-resident Kupffer cells. These members of the mononuclear phagocyte system comprise more than 80% of the total population of macrophages in the body and lead to a fast clearance of administered therapeutics. Active targeting strategies are the prerequisite to decrease the exposure of non-diseased cells and at the same time

reach sufficient concentrations at the side of action (i.e., inside the key pathogenic cell type). Therefore, drug targeting of parenchymal liver cells not only includes organ-specific targeting (i.e., liver), but also avoidance of tissue-resident macrophages, and distinction between different hepatic cell types. Avoidance of Kupffer cells is essential to prevent unspecific and rapid accumulation of nanoparticles in the liver and other tissues characterized by a high activity of the mononuclear phagocyte system (e.g., spleen). Therefore, nanocarriers have to be modified with a hydrophilic polymer (i.e., PEG or PMOXA) in order to prevent opsonization *in vivo*. Active targeting ligands are necessary to guide the nanocarrier to the correct cell type (i.e., hepatocytes) and trigger endocytosis. In particular, this is obligatory for compounds which pharmacological effect depends on internalization, such as nucleic acid therapeutics.

During this PhD project, different ligands were evaluated and various hepatocyte-targeted drug delivery systems were successfully tested *in vitro* as well as *in vivo*. These optimally designed hepatocyte-specific targeting technologies might be promising alternatives to conventional therapeutics.

2. ASGPR-specific Targeting

2.1. Target Receptor

For hepatocyte-specific drug targeting, the abundant and exclusive expression of a target receptor on the surface of parenchymal liver cells is necessary. In this PhD project, the ASGPR was successfully evaluated (**Chapter III**) for the development of active targeted nanocarriers. In healthy tissue specimens, the ASGPR is abundantly expressed on the sinusoidal membrane of parenchymal liver cells. Hence, the ASGPR-specific drug targeting strategy can be used for patients without parenchymal damage (Table 2). By contrast, the ASGPR expression is decreased with increasing

HCC grade. Interestingly, the ASGPR is upregulated in cirrhotic tissue. This might be interesting for an early treatment option of chronic liver infections. However, the pathological changes including enhanced fibrotic matrix deposition in the space of Disse might decrease the targeting ability. Diagnostic tools to assess the targeting ability of parenchymal liver cells in different patients offer a promising approach. Thus, a preselection of responders could help to enhance the clinical outcome.

2.2. ASGPR-specific Ligands

Hepatocyte-specific drug delivery via the ASGPR can be achieved using glycan-derived targeting ligands (i.e., glycoproteins, multiantennary carbohydrates, or monovalent sugars) as well as antibodies against the ASGPR (Figure 7). During this PhD project, several different targeting ligands were evaluated. Table 3 summarizes the advantages and disadvantages of these approaches.

Firstly, a glycoprotein (i.e., bovine asialofetuin) which contains various multiantennary *N*-glycans was successfully used to guide stealth liposomes specifically to hepatocytes (**Chapter IV**). In order to overcome the main disadvantage of bovine asialofetuin, immunogenicity, either the human analogue or isolated *N*-glycans should be used. The latter approach was investigated *in vitro* to specifically trigger the internalization into hepatocytes (**Chapter V**). The use of these multivalent glycan ligands might be a promising and efficacious strategy *in vivo*. The main advantages are the high affinity, enhanced specificity, small size and biocompatibility.

In addition, to the targeting ligands explicitly described and discussed in the "Results" section, various other targeting approaches were assessed during this PhD project. The use of synthetic ligands including multiantennary glycan conjugates or monovalent glycomimetics was considered. Ernst and colleagues synthesized several different high affinity ligands. [149,164] However, the availability of sufficient amounts needed for the development of nanoparticulate drug delivery systems was restricted due to the complex chemical synthesis.

Table 3: Expert opinion on ASGPR-specific targeting ligands. The advantages and disadvantages of different ligands for ASGPR-specific drug targeting are summarized. Synthetic glycans, natural glycans and protein-based ligands are evaluated separately. In each group the complexity and ASGPR affinity of ligands decreases from top to bottom.

Ligand Type	Advantages	Disadvantages	Ref.
Synthetic Glycan Ligands			
. Multivalent Glycans	high affinity, chemical variability	expensive, complex synthesis, sub-optimal geometrical arrangement, availability	149,167,169
. Monovalent Glycans	medium affinity, chemically defined	expensive, lower affinity	163,164
Natural Glycan Ligands			
. Glycoproteins (e.g., asialofetuin)	highest affinity (several multivalent glycans), cheap, high amount	immunogenic, batch-to-batch differences	103,158,159
. Glycopeptides	high affinity, lower immunogenicity	glycan variability, several production steps necessary	162
. Multivalent Glycans (e.g., NA3)	high affinity, no synthesis, ideal geometrical arrangement	isolation necessary, yield low, reproducibility/quality dependent on starting material	
. Monovalent Glycans (e.g., GalNAc)	cheap, easy to use, improvement of avidity using surface of nanocarriers	low affinity/specificity, density on nanocarriers influences outcome	165,166,168
Protein-based Ligands			
. Antibodies	high specificity	species dependent, immunogenic, expensive	157,190

An alternative strategy to mimic multivalency of natural *N*-glycans is the conjugation of monovalent sugars onto the surface of nanocarriers. This approach has also been evaluated during this PhD project using stealth liposomes. Based on the fluidity of the lipid bilayer, ligands conjugated to a lipid bilayer-standing anchor (i.e., DSPE-PEG2000) should self-assemble in clusters and therefore mimic a multivalent ligand. [191] Custom synthesized monovalent GalNAc moieties (i.e., β-GalNAc-PEG_2-SH) were conjugated to the surface of pegylated liposomes to increase their specificity and avidity, and thus enhance the uptake rate in hepatocytes.

However, cellular uptake experiments showed no difference in uptake rate of GalNAc-conjugated liposomes as compared to stealth liposomes. The absent targeting ability can be

attributed to the amount of sugar moieties needed to exactly mimic the optimal spatial arrangement of multiantennary glycans. To reach the ideal geometrical distance of sugar moieties, up to 20mol% of DSPE-PEG would be necessary. Already starting at 10mol% we observed the formation of micelles (electron microscopy analysis). Therefore, the optimal concentration of ligands on the nanocarrier surface cannot be achieved. Furthermore, the influence on biodistribution for future *in vivo* applications has to be considered. A high rate of modification might interact with stealth properties and cell type specificity *in vivo*. Shimada and colleagues showed that 20mol% galactosylated lipids significantly increased the uptake rate in Kupffer cells at the expense of parenchymal liver cells. [168]

Finally, the use of antibodies for ASGPR-specific drug targeting was evaluated. Several research projects from our group have successfully shown that antibodies can be used to guide liposomal drug delivery systems to specific tissues. [192–196] In terms of immunogenicity, single-chain antibody fragments (scFv) are advantageous for *in vivo* applications as compared to full-length antibodies. Recently, Trahtenherts and colleagues isolated a scFv against the ASGPR from a phage display library to facilitate the internalization of a highly effective immunotoxin. [157] Therefore, this targeting ligand was investigated for nanoparticulate drug delivery. However, preliminary experiments showed that the applicability as a ligand for nanocarriers was limited. Due to its low affinity, further investigations using this scFv were not performed.

In conclusion, pegylated liposomes for ASGPR-specific targeting should be combined with glycoproteins or multiantennary glycans. These approaches were successfully tested during this PhD project *in vitro* as well as *in vivo*. Alternatively, other receptors for hepatocyte-specific targeting approaches should be evaluated in the future (see below and exemplified in the "Future Perspective" section).

3. Alternative Targeting Approaches

Since the ASGPR is significantly downregulated in some pathological liver diseases such as hepatocellular carcinoma, other surface proteins on hepatocytes should be evaluated in the future. Interestingly, viruses also use active targeting approaches to enter parenchymal liver cells. The following paragraph summarizes three receptors interesting for the development of active targeted nanomedicine therapeutics, which are also used by viruses to enter hepatocytes.

First, the **low-density lipoprotein receptor (LDLR)** is highly expressed on hepatocytes. Natural ligands such as apolipoprotein E (ApoE) are internalized after receptor binding. Interestingly, this receptor (among several others) is utilized by the hepatitis C virus as an entry pathway. [197,198] During the last decade, this strategy has also been evaluated for nanoparticulate drug delivery systems. Akinc and colleagues showed *in vivo* that siRNA loaded lipid nanoparticles spontaneously absorb ApoE on their surface after systemic administration. [182] This allows specific binding of the "endogenous ligand-modified nanocarriers" to the hepatic LDL receptor and mediation of cellular uptake. Interestingly, this technology is already in clinical trials for the therapy of genetic liver diseases. [65] Patisiran is tested in a phase 3 clinical trial for the treatment of transthyretin-mediated amyloidosis (NCT 01960348, ALN-TTR02). However, the LDLR is not exclusively expressed on hepatocytes. Targeting strategies to pass the blood-brain-barrier also take advantage of this approach. [199–201] Therefore, the specificity of LDL-targeted nanocarriers is limited and off-target effects have to be kept in mind.

Second, the **coxsackie-adenovirus receptor (CAR)** on hepatocytes is utilized by adenoviruses to accumulate in parenchymal liver cells. [100] This approach has been evaluated for viral gene therapy approaches. [202,203] However, safety concerns due to immunogenicity, gene transduction, and off-target effects prevent the widespread use. [204,205]

Third, the **sodium-taurocholate cotransporting polypeptide (NTCP/SLC10A1)** on parenchymal liver cells might be an interesting target. The hepatitis B virus has a strong affinity to hepatocytes. However, for a long time the exact mechanism of this highly efficient hepatotropism was unknown. Recently, Yan and colleagues discovered that the human hepatitis B virus binds with high affinity to the hNTCP. [85] To specify the exact requirements for this strong binding, Urban *et al.* performed a fine mapping of the HBV surface protein (HBVpreS) sequence. [206] This approach revealed a highly essential peptide sequence (NPLGFFP) in the HBV envelope proteins specific for the hNTCP. [84] The discovery resulted in the first HBV/HDV entry inhibitor (IC_{50} = 80 pM), namely Mycludex B. [207]

The development of a novel nanoparticulate drug targeting approach to the human NTCP and its implementation is carefully elaborated in the "Future Perspective" section as an alternative to ASGPR-specific targeting strategies.

II. Gene Delivery

Nanoparticulate drug delivery systems offer the unique opportunity to transport complex biomolecules including nucleic acids. Therefore, it is possible to implement gene therapy approaches for systemic administration. During this PhD project the feasibility of such an approach was evaluated and a stealth polymeric nanomaterial was tested *in vitro*. This "Discussion and Conclusion" section elaborates the use of non-targeted gene delivery systems including commercially available transfection reagents and the developed sterically stabilized plasmid DNA nanocarrier. In addition, further improvements necessary for a targeted gene delivery *in vivo* are emphasized.

1. Passive Gene Delivery

1.1. Transfection Reagents

Commercially available transfection reagents such as Lipofectamine 2000, FuGene HD, or jetPEI profit from high transfection efficiencies *in vitro*. These positively charged lipid or polymer mixtures electrostatically interact with negatively charged nucleic acids, thus forming cationic lipo- or polyplexes. The positive surface charge enhances the interaction with negatively charged cell membranes, thus enhancing cellular uptake. Intracellularly, the nucleic acid-nanocarrier complexes are released via endosomal escape mechanisms and thus allow for gene expression.

In particular, for *in vitro* experiments these transfection reagents are favorable. However, they suffer from major drawbacks. First, the high positive charge of the complexes results in increased cytotoxicity. Second, the *in vivo* application is limited. After systemic administration positive complexes are rapidly sequestered in the lung. Therefore, only a local administration such as intratumoral injection is possible thereby decreasing patient compliance and acceptance.

1.2. Advanced Transfection Reagent

An advanced transfection reagent would offer possibilities to complex nucleic acids during formulation (low pH) and result in a neutral or negative surface charge at physiological pH (pH = 7.4). In addition, advanced gene delivery systems should be sterically stabilized. This would offer possibilities to envision a systemic administration.

During this PhD project, a novel, biocompatible, and stealth polymer-peptide hybrid nanomaterial was developed. The general physico-chemical properties of the resulting pDNA-polymer nanoparticles are ideal for the development of a hepatocyte-directed gene therapy. The nanoparticle size was less than 120 nm, they had a monodisperse size distribution and a slightly

negative zeta potential. Importantly, passive transfection of cells *in vitro* was achieved without cytotoxic drawbacks. In order to increase the transfection efficiency further modification is necessary.

First, targeting ligands attached to the surface of these nanocarriers might increase cellular uptake and thus gene delivery. Second, the nanomaterial should be optimized in regard to pDNA encapsulation and efficient intracellular release. The development of novel lipid-based nanomaterials is described in the "Future Perspective" section.

2. Active Targeted Gene Delivery

The pharmacological effect of nucleic acids (i.e., plasmid DNA, mRNA, siRNA, miRNA) is dependent on internalization. In order to facilitate the uptake of negatively charged nucleic acids across the negatively charged cell membrane, nanoparticulate delivery systems are necessary. As mentioned above, neutral or slightly negative nanocarriers are needed for systemic application. However, this hampers the uptake of nanocarriers. Therefore, targeting ligands are required to guide the nanocarriers to a defined cell type and enhance cellular uptake (Figure 8). During this PhD project, several targeting ligands were evaluated. This knowledge should be used in the future to develop a hepatocyte-specific gene delivery system.

III. Conclusion

Despite the improved therapeutic options for many diseases, incidence rates of hepatic disorders are further increasing and millions of people are affected around the globe. In the context of this PhD thesis, drug delivery and drug targeting strategies to parenchymal liver cells should be evaluated and developed.

During this PhD project the four core aspects of hepatocyte-specific drug delivery were evaluated: (i) nanocarrier systems, (ii) target receptors, (iii) targeting ligands, (iv) *in vitro*/*in vivo* models. First, various nanomaterials and drug delivery systems were evaluated regarding their clinical application (**Chapter I/II**). Several stealth nanoparticulate drug delivery systems were developed accordingly. Second, the use of the ASGPR as target receptor for hepatocyte-specific drug delivery was assessed. ASGR1 expression levels in human liver specimens and several liver-derived cell lines were investigated (**Chapter III**). Third, various ASGPR-specific targeting ligands were evaluated. Glycoproteins and glycans were tested for their targeting ability and ASGPR-specificity *in vitro* as well as *in vivo* (**Chapter IV/V**). Furthermore, technologies to investigate the uptake mechanisms and intracellular fate of nanocarriers were established (**Chapter VI**). Fourth, all *in vitro* and *in vivo* tests were performed in suitable model systems (**Chapter III/IV/V**). Finally, the first steps towards the development of a hepatocyte-specific gene delivery system were made (**Chapter VII**).

In conclusion, future projects should use the acquired technologies for the development of novel hepatocyte-targeted gene delivery systems. This is of great interest for therapeutic interventions of various liver disorders. The idea and concept of a possible research project is described in detail in the "Future Perspectives" section.

FUTURE PERSPECTIVES

Nanomedicines for the delivery of therapeutic genes have the potential to overcome the lack of satisfactory and alternative treatment options for hepatic disorders. Therefore, future projects should focus on the design of functional nanomedicines for targeted nucleic acid delivery to liver parenchymal cells.

To implement such targeting strategies, the following steps are necessary: (I) Identification of an alternative, highly selective and specific targeting ligand, (II) development of novel ionizable nanomaterials to assist in the formulation of expression plasmids, (III) combination of targeting strategy and gene delivery technology to address unmet medical needs *in vivo*.

I. Novel Targeting Strategy

So far, hepatocyte-specific targeting strategies have been based on ASGPR-specific drug carriers. However, as outlined in this PhD thesis, the ASGPR showed variable expression levels and altered expression patterns in different patients as well as different liver disorders. In addition, targeting vectors based on "asialofetuin" have important shortcomings including batch-to-batch differences and possible immunogenicity. In view of these problems, alternative hepatocyte-specific targeting strategies should be evaluated.

The most promising target to implement such an approach is the sodium/bile acid cotransporter hNTCP (sodium-taurocholate cotransporting polypeptide), which is highly expressed on parenchymal liver cells.

1. Active Targeting of hNTCP

In close collaboration with the Molecular Virology Division at the University of Heidelberg (Group of Prof. Dr. Stephan Urban), a novel hepatitis B virus (HBV) entry inhibitor should be tested as targeting ligand. The HBV entry inhibitor **Myrcludex B** was developed by Urban and colleagues and is at present being tested in clinical phase IIa studies (NCT02637999). Interestingly, Myrcludex B is characterized by a strong tropism towards hepatocytes. The polypeptide-lipid conjugate binds with high affinity to the hNTCP thereby effectively blocking HBV entry and infection (Figure 9). Myrcludex B is a lipid-conjugated polypeptide identified by epitope mapping of the preS1 domain of the N-terminal extension of the large surface glycoprotein of HBV (Figure 9).

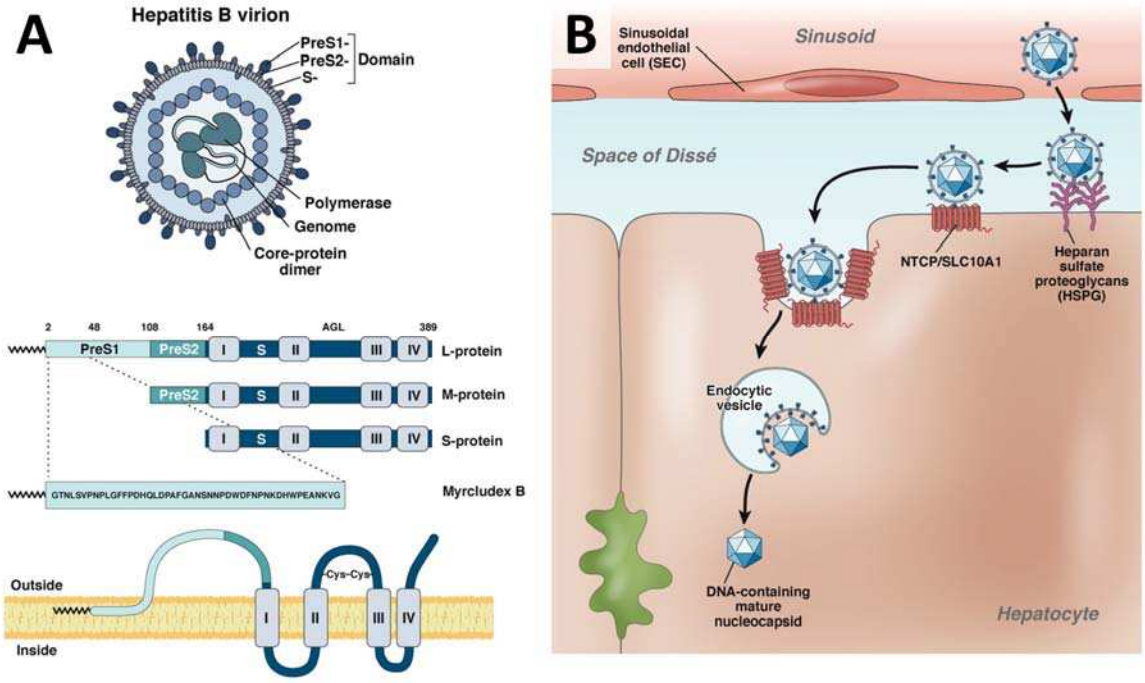

Figure 9: Hepatitis B Virus (HBV) structure and cell entry. (A) Structure of HBV with envelope consisting of different surface proteins. Important for hepatocyte-specific binding is the myristoylated preS1 domain. Myrcludex B is the first HBV entry inhibitor blocking the hNTCP tested in clinical trials. (B) Route of hepatocyte uptake is shown. The HBV passes the hepatic sinusoids to enter the space of Disse, where it interacts with proteoglycans. The specific binding to the NTCP results in endocytosis. Intracellular processes are initiated for the replication inside hepatocytes. Figures are adapted from Urban *et al.* [88]

In order to implement a novel targeting strategy to hepatocytes, Myrcludex B-modified pegylated liposomes should be developed and tested *in vitro* as well as *in vivo*. Liposomes should be modified with different variations of Myrcludex B (e.g., truncated peptide sequences and various fatty acid modifications), to test their effect on liposome formulation, physico-chemical liposome characteristics, and targeting ability. Specificity of cellular binding, uptake mechanism and its efficiency as well as intracellular transport should be investigated in several human cell lines *in vitro*. *In vivo* experiments will be necessary to analyze the biodistribution of the nanoparticulate drug delivery system on an organ as well as cellular level and to verify hepatocyte specificity. [208] *In vivo* imaging in mice will be performed in collaboration with the Radiopharmaceutical Chemistry Division at the University of Heidelberg (Group of Prof. Dr. W. Mier) using established protocols. [209,210]

With this approach, it will be possible to develop a novel and ASGPR-alternative nanoparticle-based drug delivery platform to deliver small molecules or nucleic acids efficiently and with high specificity to hepatocytes.

II. Plasmid DNA-based Gene Delivery

There is an increasing interest in non-viral gene delivery systems. Future projects should focus on the development of a novel nanoparticle platform to deliver nucleic acids efficiently and with low cytotoxicity to hepatocytes. An ideal nucleic acid delivery system for biomedical applications should fulfill following criteria: small size (<120 nm), neutral or slightly negative zeta potential, high nucleic acid encapsulation, efficient cellular uptake and endosomal release, biocompatibility, and easy manufacturing process. [102] Most approaches described in literature for cellular delivery of nucleic acids suffer from major drawbacks.

First, the synthesis route of many polymers used for the design of nanomaterials is complex and offers limited control over polymerization.[184] Second, commonly used nanoparticle preparation techniques such as the film-rehydration method are time-consuming, not amendable to scale up, and characterized by poor encapsulation efficiency. [211] So far, these systems are not being used in clinical applications, largely because of their complex design leading to technical challenges with respect to GMP manufacturing and product registration. Finally, many developed gene delivery systems have a positive charge (i.e., needed for the pDNA complexation). [212] This leads to unspecific cellular uptake and rapid sequestration in the lung after i.v. injection. [120] Thus, systemic administration *in vivo* is not possible. One solution to this problem are pH responsive delivery systems. [213] Ionizable groups offer the possibility to formulate nanoparticles at low pH thus enhancing intravesicular pDNA complexation. At physiological pH in circulation the nanoparticle surface has a neutral charge thus offering optimal physico-chemical properties for a systemic administration (Figure 8).

1. Novel Nanomaterials: Ionizable Amino-lipids

Among the various nanomaterials, liposomal formulations can be considered to be safe, biocompatible and non-immunogenic. Therefore, these delivery systems are a promising alternative to viral vectors for gene therapy. In general, neutral and pegylated phospholipids in combination with cholesterol are used for the formation of liposomes. Such sterically stabilized liposomes were shown previously to be ideal candidates to implement targeted drug delivery strategies. [103] However, for efficient loading of expression plasmids, cationic helper lipids are needed.

Therefore, a **novel ionizable amino-lipid library** should be synthetized to facilitate pDNA encapsulation within liposomal carriers as well as to enhance endosomal escape, intracellular release and transgene expression. The ionizable lipids are supposed to have a high buffering capacity in the

pH range between 5.0 and 6.0 and therefore induce rupture of endosomal membranes via "proton sponge" mechanism enabling endosomal escape. Screening of the lipid library will help to identify lead structures, which can be further optimized by chemical methods. This part of the project will be carried out in cooperation with the Division of Chemical Lipidology at the University of Fribourg (Group of Prof. Dr. Andreas Zumbühl).

In order to establish a versatile platform technology, efficient technologies are needed to prepare liposomal carriers and to load them with pDNA. **Microfluidics** is a recent technology, which facilitates this process (Figure 10). It allows the rapid and highly controlled mixing of the nanomaterial (i.e., amino-lipids or phospholipids) with nucleic acids (i.e., plasmid DNA). [214–216] Batch sizes range from a few hundred microliters to production scale volumes. This technology is thus amendable to industrial scale production under GMP conditions.

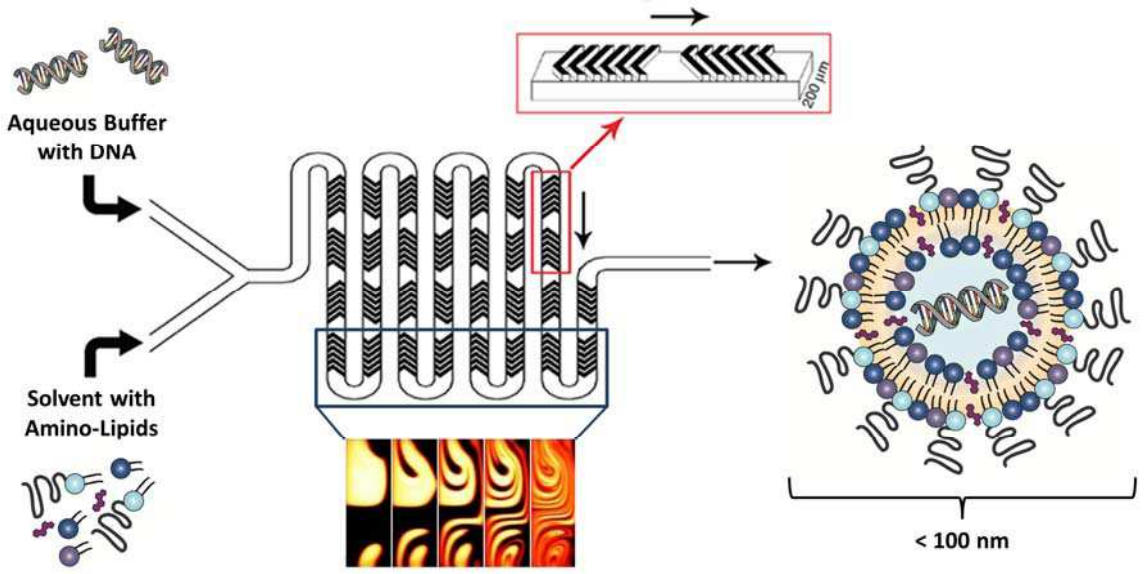

Figure 10: Schematic illustration of microfluidics approach. Nucleic acid loaded nanoparticles are prepared using microfluidics. The microfluidics device has two inlet channels converging to a single staggered herringbone micromixer. The lipid mix (ethanol) and pDNA (formulation buffer) solution are injected simultaneously. In the micromixer the components are mixed and pDNA loaded nanoparticles are formed. This process is controllable and highly reproducible. Figures are adapted from Rungta *et al*. and Stroock *et al*. [199,214]

Finally, the developed nanoparticles should be tested *in vitro* for their **cytocompatibility** and **transfection efficiency**. Several assays should be used to uncover potential safety issues including general cytotoxicity, reactive oxidative species (ROS) and superoxide production, apoptosis, or hemolysis. To investigate mechanisms of intracellular pDNA release from the endosomal compartment and its nuclear translocation, labeled nanocarriers should be used. To explore the transfection efficiency of amino-lipid containing formulations *in vitro*, expression of reporter genes such as green fluorescent protein (GFP) or of the very sensitive marker luciferase can be studied.

The design of next-generation nanoparticles and the mechanistic insights from such an research project will not only be instrumental to optimize gene targeting strategies but will also contribute to ongoing efforts in this field of research to better control expression of transfected genes on a cellular level.

III. Combination of Targeting and Gene Delivery Approach

For the implementation of gene therapy approaches, targeted nucleic acid loaded nanoparticles are needed. These delivery systems should fulfill following criteria: efficient nucleic acid loading, stealth properties, small size, specific target-binding and uptake, endosomal escape, intracellular pDNA release (Figure 11). In addition, these systems should be safe and non-immunogenic.

To develop such a targeted gene delivery approach, the above mentioned targeting strategy (**Section I**) should be combined with novel gene delivery nanomaterials (**Section II**). This offers the possibility to enhance cellular uptake and promote intracellular release.

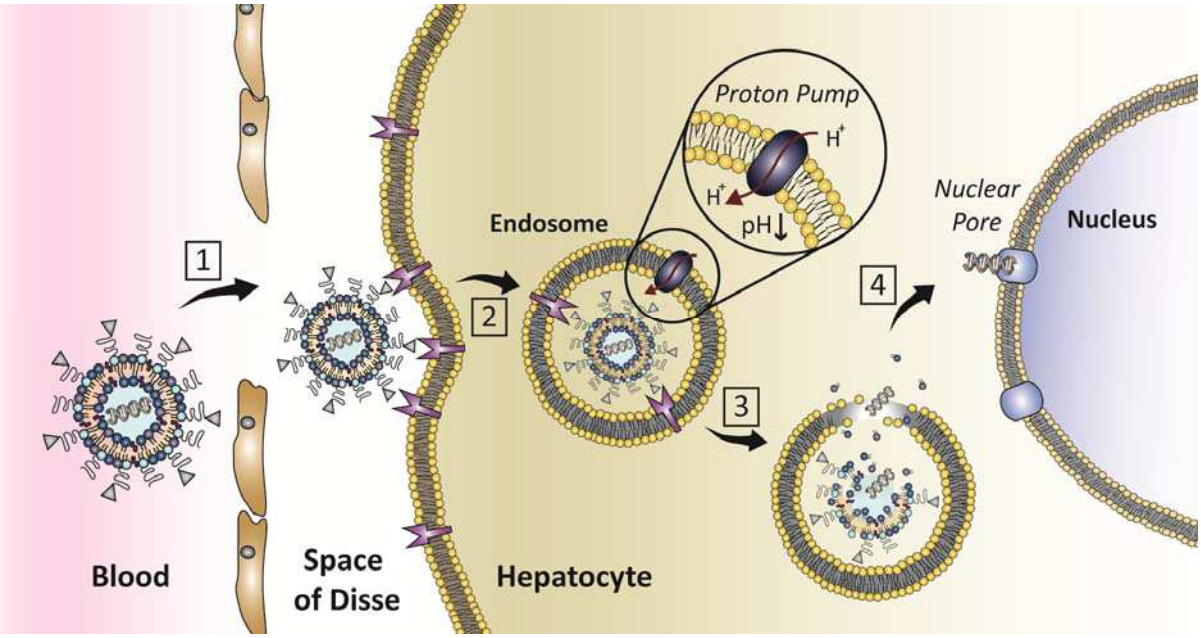

Figure 11: Hepatocyte-specific gene delivery. Ligand-modified DNA lipid nanoparticles circulate in the blood stream. (1) After passage of the hepatic sinusoids, the nanoparticles specifically bind to hepatocyte membrane receptors. This interaction triggers internalization. (2) The pH in endosomes decreases due to proton pumps. (3) Acidification of endosome results in protonation of ionizable lipids which finally causes endosomal escape of plasmid DNA via proton sponge effect. (4) Via the nuclear pore the nucleic acid enters the nucleus. The delivered gene gets transcribed and finally leads to the translation of an exogenous protein.

1. Targeted Gene Delivery

In the last phase of the project, the potential of the novel targeted gene delivery system will be confirmed *in vitro* and possible future clinical applications will be explored *in viv*o. The targeted gene delivery system will be optimized with respect to physico-chemical features for an *in vivo* application (e.g., stability, increased circulation half-life, or biocompatibility). Optimal lipid compositions will be identified based on expression levels of the transfected protein of interest.

Thus, it is the aim of these experiments to obtain a gene delivery system, which is optimized both with respect to cell-specific targeting as well as cellular uptake, intracellular release and subsequent gene expression of the delivered pDNA.

IV. Future Clinical Applications

In **conclusion**, this research project aims to close the gap of efficient therapeutics with the development of an innovative and functional platform technology for the expression of therapeutic genes specifically in hepatocytes. A highly selective targeting ligand will be combined with optimized nanomaterials for gene delivery. With this novel therapeutic strategy, we have the possibility to address unmet medical needs. The proposed technology can potentially be used for several clinical applications.

First, the delivery of larger nucleic acids could open the door to promising **gene editing** approaches such as the CRISPR/Cas9 or zinc-finger technology for *in vivo* applications. [217] Second, the expression of **oncotoxic proteins** is a promising approach to treat hepatocellular carcinoma more efficiently [218]. The treatment options for advanced stages of HCC are limited and the use of small molecule therapeutics is often limited due to the development of resistance. Gene therapy would offer new possibilities to overcome these limitations. An interesting strategy is the expression of oncotoxic proteins inside tumor cells. For instance, the parvovirus-H1 derived non-structural protein (NS1) induces tumor-selective apoptosis. [219] Several endogenous proteins are redirected by NS1 resulting in ROS production, DNA damage, actin skeleton rearrangement, cathepsin B release, or caspase activation and finally tumor cell death. [220] Due to its various induced toxicity pathways, the development of resistance to NS1 is not possible. Thus, cancer cells produce their own suicide protein. Finally, patients with **orphan monogenetic liver disorders** (i.e., rare diseases) would highly benefit from novel therapeutic options, which replace the mutated enzyme by delivery of their encoding DNA sequences [61,221]. For instance, an UGT1A1 gene-replacement therapy for patients with hereditary Crigler-Najjar syndrome would offer an interesting treatment strategy, which outperforms all existing therapeutic options.

ABBREVIATIONS

ADC	Antibody Drug Conjugate
ApoE/B	Apolipoprotein E/B
ARG	Arginase
ASGPR	Asialoglycoprotein receptor
ASL	Argininosuccinate lyase
ASS	Argininosuccinate synthetase
BCLC	Barcelona Clinic Liver Cancer
CAR	Coxsackie-adenovirus receptor
Cas9	CRISPR-associated
CPS	Carbamoylphosphate synthetase
CRD	Carbohydrate Recognition Domain
CRISPR	Clustered Regularly Interspaced Short Palindromic Repeats
DNA	Deoxyribonucleic acid
DSPC	1,2-Distearoyl-sn-glycero-3-phosphocholine
DSPE	1,2-Distearoyl-sn-glycero-3-phosphoethanolamine
FAH	Fumarylacetoacetate hydrolase
FAP	Familial Amyloid Polyneuropathy
G6PD	Glucose-6-phosphate dehydrogenase
Gal	Galactose
GalNAc	N-acetylgalactosamine
GFP	Green Fluorescent Protein
GMP	Good Manufacturing Practice
GSD	Glycogen Storage Diseases
HBV	Hepatitis B Virus
HC	Hepatocytes
HCC	Hepatocellular carcinoma
HCV	Hepatitis C Virus
KC	Kupffer Cells
LDLR	Low-Density Lipoprotein Receptor
MPS	Mononuclear Phagocyte System
NAGS	N-acetyl glutamate synthetase
NDDS	Nanoparticulate drug delivery system
NS1	Non-structural protein
NTCP	Sodium-Taurocholate Cotransporting Polypeptide
OTC	Ornithine transcarbamylase
PBS	Phosphate Buffered Saline
PCSK9	Proprotein Convertase Subtilisin/Kexin type 9
PDGF	Platelet-Derived Growth Factor
pDNA	plasmid DNA
PEG	Polyethylene glycol
PMOXA	Poly(2-methyloxazoline)
RES	Reticuloendothelial system
RFA	Radiofrequency Ablation
RNA	Ribonucleic acid
RNAi	RNA interference
ROS	Reactive Oxidative Species
SAXS	Small-Angle X-ray Scattering
SC	Stellate Cells
scFv	Single-chain (variable fragment) antibody
SEC	Sinusoidal Endothelial Cells
siRNA	small interfering RNA
TACE	Transarterial chemoembolization
TEM	Transmission Electron Microscopy
TFR	Transferrin receptor
TGF	Transforming Growth Factor
TIMP	Tissue inhibitors of matrix metalloproteinases
TTR	Transthyretin
UGT1A1	UDP-glucuronosyltransferase 1A1

BIBLIOGRAPHY

1. Mosby. *Mosby's Medical Dictionary*.
2. Lau, A. H., Szabo, G. & Thomson, A. W. Antigen-presenting cells under the influence of alcohol. *Trends in Immunology* **30,** 13–22 (2009).
3. Guengrich, F. P. Cytochrome P-450 3A4: Regulation and role in drug metabolism. *Annu. Rev. Pharmacol. Toxicol.* **39,** 1–17 (1999).
4. Brown, M., Kovanen, P. & Goldstein, J. Regulation of Plasma-Cholesterol by Lipoprotein Receptors. *Science* **212,** 628–635 (1981).
5. Harrison, P. M. & Arosio, P. Ferritins: Molecular properties, iron storage function and cellular regulation. *Biochim. Biophys. Acta-Bioenerg.* **1275,** 161–203 (1996).
6. McCuskey, R. in *Zakim and Boyer's Hepatology (Sixth Edition)* (ed. Sanyal, T. D. B. P. M. J.) 3–19 (W.B. Saunders, 2012).
7. Mishra, N. *et al.* Efficient Hepatic Delivery of Drugs: Novel Strategies and Their Significance. *Biomed Res Int* **2013,** (2013).
8. Sørensen, K. K., Simon-Santamaria, J., McCuskey, R. S. & Smedsrød, B. in *Comprehensive Physiology* (John Wiley & Sons, Inc., 2011).
9. Maurel, P. in *Hepatocytes: Methods and Protocols* **640,** (2010).
10. Braet, F. & Wisse, E. Structural and functional aspects of liver sinusoidal endothelial cell fenestrae: a review. *Comp Hepatol* **1,** 1 (2002).
11. Braet, F., Fraser, R. & McCuskey, R. S. Thirty-five years of liver sinusoidal cells: Eddie Wisse in retirement. *Hepatology* **38,** 1056–1058 (2003).
12. Wisse, E. An electron microscopic study of the fenestrated endothelial lining of rat liver sinusoids. *J. Ultrastruct. Res.* **31,** 125–150 (1970).
13. Braet, F. *et al.* Three-dimensional organization of fenestrae labyrinths in liver sinusoidal endothelial cells. *Liver Int.* **29,** 603–613 (2009).
14. Braet, F. & Wisse, E. AFM imaging of fenestrated liver sinusoidal endothelial cells. *Micron* **43,** 1252–1258 (2012).

15. Mori, T. *et al.* Defenestration of the sinusoidal endothelial cell in a rat model of cirrhosis. *Hepatology* **17,** 891–897 (1993).
16. Wisse, E., De Zanger, R. B., Charels, K., Van Der Smissen, P. & McCuskey, R. S. The liver sieve: considerations concerning the structure and function of endothelial fenestrae, the sinusoidal wall and the space of Disse. *Hepatology* **5,** 683–692 (1985).
17. Gaumet, M., Vargas, A., Gurny, R. & Delie, F. Nanoparticles for drug delivery: the need for precision in reporting particle size parameters. *Eur J Pharm Biopharm* **69,** 1–9 (2008).
18. Horn, T., Christoffersen, P. & Henriksen, J. H. Alcoholic liver injury: defenestration in noncirrhotic livers--a scanning electron microscopic study. *Hepatology* **7,** 77–82 (1987).
19. Fraser, R., Clark, S. A., Day, W. A. & Murray, F. E. Nicotine decreases the porosity of the rat liver sieve: a possible mechanism for hypercholesterolaemia. *Br J Exp Pathol* **69,** 345–350 (1988).
20. Steffan, A. M., Gendrault, J. L. & Kirn, A. Increase in the number of fenestrae in mouse endothelial liver cells by altering the cytoskeleton with cytochalasin B. *Hepatology* **7,** 1230–1238 (1987).
21. Wright, P. L., Smith, K. F., Day, W. A. & Fraser, R. Small liver fenestrae may explain the susceptibility of rabbits to atherosclerosis. *Arteriosclerosis* **3,** 344–348 (1983).
22. Moghimi, S. M., Hunter, A. C. & Murray, J. C. Long-circulating and target-specific nanoparticles: theory to practice. *Pharmacol. Rev.* **53,** 283–318 (2001).
23. Caliceti, P. & Veronese, F. M. Pharmacokinetic and biodistribution properties of poly(ethylene glycol)-protein conjugates. *Adv. Drug Deliv. Rev.* **55,** 1261–1277 (2003).
24. Takakura, Y., Mahato, R. & Hashida, M. Extravasation of macromolecules. *Adv. Drug Deliv. Rev.* **34,** 93–108 (1998).
25. Wadenvik, H. & Kutti, J. The spleen and pooling of blood cells. *Eur. J. Haematol.* **41,** 1–5 (1988).
26. Moghimi, S. M. Exploiting bone marrow microvascular structure for drug delivery and future therapies. *Advanced Drug Delivery Reviews* **17,** 61–73 (1995).
27. Seymour, L. W. Passive tumor targeting of soluble macromolecules and drug conjugates. *Crit Rev Ther Drug Carrier Syst* **9,** 135–187 (1992).
28. Hobbs, S. K. *et al.* Regulation of transport pathways in tumor vessels: role of tumor type and microenvironment. *Proc. Natl. Acad. Sci. U.S.A.* **95,** 4607–4612 (1998).
29. Jain, R. K. Barriers to drug delivery in solid tumors. *Sci. Am.* **271,** 58–65 (1994).

30. Arfors, K. E., Rutili, G. & Svensjö, E. Microvascular transport of macromolecules in normal and inflammatory conditions. *Acta Physiol Scand Suppl* **463,** 93–103 (1979).
31. Clark, S. A. *et al.* Defenestration of hepatic sinusoids as a cause of hyperlipoproteinaemia in alcoholics. *Lancet* **2,** 1225–1227 (1988).
32. Naito, M., Hasegawa, G., Ebe, Y. & Yamamoto, T. Differentiation and function of Kupffer cells. *Med Electron Microsc* **37,** 16–28 (2004).
33. Bilzer, M., Roggel, F. & Gerbes, A. L. Role of Kupffer cells in host defense and liver disease. *Liver Int.* **26,** 1175–1186 (2006).
34. Kolios, G., Valatas, V. & Kouroumalis, E. Role of Kupffer cells in the pathogenesis of liver disease. *World J. Gastroenterol.* **12,** 7413–7420 (2006).
35. Sleyster, E. C. & Knook, D. L. Relation between localization and function of rat liver Kupffer cells. *Lab. Invest.* **47,** 484–490 (1982).
36. Toth, C. A. & Thomas, P. Liver endocytosis and Kupffer cells. *Hepatology* **16,** 255–266 (1992).
37. Van Rooijen, N., Kors, N., vd Ende, M. & Dijkstra, C. D. Depletion and repopulation of macrophages in spleen and liver of rat after intravenous treatment with liposome-encapsulated dichloromethylene diphosphonate. *Cell Tissue Res.* **260,** 215–222 (1990).
38. Yamamoto, T. *et al.* Repopulation of murine Kupffer cells after intravenous administration of liposome-encapsulated dichloromethylene diphosphonate. *Am. J. Pathol.* **149,** 1271–1286 (1996).
39. Cormack, D.H. *Ham's Histology.* (1987).
40. Vollmar, B. & Menger, M. D. The Hepatic Microcirculation: Mechanistic Contributions and Therapeutic Targets in Liver Injury and Repair. *Physiological Reviews* **89,** 1269–1339 (2009).
41. Electron Miscroscopy. Available at: http://missinglink.ucsf.edu/lm/approach_to_histo/electronmicroscopy.htm. (Accessed: 16th February 2016)
42. Blomhoff, R. & Wake, K. Perisinusoidal stellate cells of the liver: important roles in retinol metabolism and fibrosis. *FASEB J.* **5,** 271–277 (1991).
43. Moreira, R. K. Hepatic stellate cells and liver fibrosis. *Arch. Pathol. Lab. Med.* **131,** 1728–1734 (2007).
44. Sato, M., Suzuki, S. & Senoo, H. Hepatic stellate cells: unique characteristics in cell biology and phenotype. *Cell Struct. Funct.* **28,** 105–112 (2003).

45. Williams, R. *et al.* Addressing liver disease in the UK: a blueprint for attaining excellence in health care and reducing premature mortality from lifestyle issues of excess consumption of alcohol, obesity, and viral hepatitis. *Lancet* **384,** 1953–1997 (2014).
46. Pellicoro, A., Ramachandran, P., Iredale, J. P. & Fallowfield, J. A. Liver fibrosis and repair: immune regulation of wound healing in a solid organ. *Nat Rev Immunol* **14,** 181–194 (2014).
47. Orphanet. Available at: http://www.orpha.net/consor/cgi-bin/index.php. (Accessed: 20th February 2016)
48. El-Serag, H. B. & Rudolph, K. L. Hepatocellular carcinoma: epidemiology and molecular carcinogenesis. *Gastroenterology* **132,** 2557–2576 (2007).
49. El-Serag, H. B. Hepatocellular carcinoma. *N. Engl. J. Med.* **365,** 1118–1127 (2011).
50. Forner, A., Llovet, J. M. & Bruix, J. Hepatocellular carcinoma. *Lancet* **379,** 1245–1255 (2012).
51. Bouchard, M. J. & Navas-Martin, S. Hepatitis B and C virus hepatocarcinogenesis: lessons learned and future challenges. *Cancer Lett.* **305,** 123–143 (2011).
52. Chisari, F. V., Isogawa, M. & Wieland, S. F. Pathogenesis of hepatitis B virus infection. *Pathol. Biol.* **58,** 258–266 (2010).
53. Liaw, Y.-F. & Chu, C.-M. Hepatitis B virus infection. *Lancet* **373,** 582–592 (2009).
54. Trépo, C., Chan, H. L. Y. & Lok, A. Hepatitis B virus infection. *Lancet* **384,** 2053–2063 (2014).
55. Lavanchy, D. Evolving epidemiology of hepatitis C virus. *Clin. Microbiol. Infect.* **17,** 107–115 (2011).
56. Galinski, M. R. & Barnwell, J. W. Plasmodium vivax: who cares? *Malar. J.* **7 Suppl 1,** S9 (2008).
57. Price, R. N. *et al.* Vivax malaria: neglected and not benign. *Am. J. Trop. Med. Hyg.* **77,** 79–87 (2007).
58. Murambiwa, P., Masola, B., Govender, T., Mukaratirwa, S. & Musabayane, C. T. Anti-malarial drug formulations and novel delivery systems: a review. *Acta Trop.* **118,** 71–79 (2011).
59. Wells, T. N. C., Burrows, J. N. & Baird, J. K. Targeting the hypnozoite reservoir of Plasmodium vivax: the hidden obstacle to malaria elimination. *Trends Parasitol.* **26,** 145–151 (2010).
60. Bosma, P. J. Inherited disorders of bilirubin metabolism. *J. Hepatol.* **38,** 107–117 (2003).
61. van Dijk, R., Beuers, U. & Bosma, P. J. Gene replacement therapy for genetic hepatocellular jaundice. *Clin Rev Allergy Immunol* **48,** 243–253 (2015).
62. Fagiuoli, S., Daina, E., D'Antiga, L., Colledan, M. & Remuzzi, G. Monogenic diseases that can be cured by liver transplantation. *J. Hepatol.* **59,** 595–612 (2013).

63. Bergmann, K. R. *et al.* Late-Onset Ornithine Transcarbamylase Deficiency: Treatment and Outcome of Hyperammonemic Crisis. *Pediatrics* **133,** E1072–E1076 (2014).
64. Hawkins, P. N. *et al.* Evolving landscape in the management of transthyretin amyloidosis. *Ann. Med.* **47,** 625–638 (2015).
65. Suhr, O. B. *et al.* Efficacy and safety of patisiran for familial amyloidotic polyneuropathy: a phase II multi-dose study. *Orphanet J Rare Dis* **10,** 109 (2015).
66. Hoppe, B. An update on primary hyperoxaluria. *Nat. Rev. Nephrol.* **8,** 467–475 (2012).
67. Raal, F. J. & Santos, R. D. Homozygous familial hypercholesterolemia: Current perspectives on diagnosis and treatment. *Atherosclerosis* **223,** 262–268 (2012).
68. Seidah, N. G., Awan, Z., Chretien, M. & Mbikay, M. PCSK9: A Key Modulator of Cardiovascular Health. *Circ.Res.* **114,** 1022–1036 (2014).
69. Kay, M. A. State-of-the-art gene-based therapies: the road ahead. *Nat. Rev. Genet.* **12,** 316–328 (2011).
70. High, K. A. Gene therapy for haemophilia: a long and winding road. *J. Thromb. Haemost.* **9,** 2–11 (2011).
71. Bereczky, Z., Kovacs, K. B. & Muszbek, L. Protein C and protein S deficiencies: similarities and differences between two brothers playing in the same game. *Clin. Chem. Lab. Med.* **48,** S53–S66 (2010).
72. Qi, X. *et al.* Prevalence of inherited antithrombin, protein C, and protein S deficiencies in portal vein system thrombosis and Budd-Chiari syndrome: A systematic review and meta-analysis of observational studies. *J. Gastroenterol. Hepatol.* **28,** 432–442 (2013).
73. Flotte, T. R. & Mueller, C. Gene therapy for alpha-1 antitrypsin deficiency. *Hum. Mol. Genet.* **20,** R87–R92 (2011).
74. Stoller, J. K. & Aboussouan, L. S. A Review of alpha(1)-Antitrypsin Deficiency. *Am. J. Respir. Crit. Care Med.* **185,** 246–259 (2012).
75. Rosencrantz, R. & Schilsky, M. Wilson Disease: Pathogenesis and Clinical Considerations in Diagnosis and Treatment. *Semin. Liver Dis.* **31,** 245–259 (2011).
76. Purchase, R. The treatment of Wilson's disease, a rare genetic disorder of copper metabolism. *Science Progress* **96,** 19–32 (2013).
77. Pietrangelo, A. Hereditary Hemochromatosis: Pathogenesis, Diagnosis, and Treatment. *Gastroenterology* **139,** 393–408 (2010).

78. Babitt, J. L. & Lin, H. Y. The Molecular Pathogenesis of Hereditary Hemochromatosis. *Semin. Liver Dis.* **31,** 280–292 (2011).
79. Nobili, V. *et al.* Tyrosinemia Type 1: Metastatic Hepatoblastoma With a Favorable Outcome. *Pediatrics* **126,** E235–E238 (2010).
80. Kitagawa, T. Hepatorenal tyrosinemia. *Proc. Jpn. Acad. Ser. B-Phys. Biol. Sci.* **88,** 192–200 (2012).
81. Ozen, H. Glycogen storage diseases: new perspectives. *World J. Gastroenterol.* **13,** 2541–2553 (2007).
82. Byrne, B. J. *et al.* Pompe disease gene therapy. *Hum. Mol. Genet.* **20,** R61–R68 (2011).
83. Ni, Y. Characterization of the infectivity determinants of the envelope proteins of Hepatitis B Virus. (2010). Available at: http://archiv.ub.uni-heidelberg.de/volltextserver/10698/. (Accessed: 7th March 2016)
84. Ni, Y. *et al.* Hepatitis B and D viruses exploit sodium taurocholate co-transporting polypeptide for species-specific entry into hepatocytes. *Gastroenterology* **146,** 1070–1083 (2014).
85. Yan, H. *et al.* Sodium taurocholate cotransporting polypeptide is a functional receptor for human hepatitis B and D virus. *eLife Sciences* **1,** e00049 (2012).
86. Uhl, P., Fricker, G., Haberkorn, U. & Mier, W. Current status in the therapy of liver diseases. *Int J Mol Sci* **15,** 7500–7512 (2014).
87. Zoulim, F. Hepatitis B virus resistance to antiviral drugs: where are we going? *Liver Int.* **31 Suppl 1,** 111–116 (2011).
88. Urban, S., Bartenschlager, R., Kubitz, R. & Zoulim, F. Strategies to inhibit entry of HBV and HDV into hepatocytes. *Gastroenterology* **147,** 48–64 (2014).
89. Prudêncio, M., Rodriguez, A. & Mota, M. M. The silent path to thousands of merozoites: the Plasmodium liver stage. *Nat. Rev. Microbiol.* **4,** 849–856 (2006).
90. Baird, J. K. Resistance to therapies for infection by Plasmodium vivax. *Clin. Microbiol. Rev.* **22,** 508–534 (2009).
91. Baird, J. K. & Rieckmann, K. H. Can primaquine therapy for vivax malaria be improved? *Trends Parasitol.* **19,** 115–120 (2003).
92. Hill, D. R. *et al.* Primaquine: report from CDC expert meeting on malaria chemoprophylaxis I. *Am. J. Trop. Med. Hyg.* **75,** 402–415 (2006).
93. Miranda, P. S. M. & Bosma, P. J. Towards liver-directed gene therapy for Crigler-Najjar syndrome. *Curr Gene Ther* **9,** 72–82 (2009).

94. Bortolussi, G. *et al.* Life-long correction of hyperbilirubinemia with a neonatal liver-specific AAV-mediated gene transfer in a lethal mouse model of Crigler-Najjar Syndrome. *Hum. Gene Ther.* **25,** 844–855 (2014).
95. Schmitt, F. *et al.* Lentiviral vectors that express UGT1A1 in liver and contain miR-142 target sequences normalize hyperbilirubinemia in Gunn rats. *Gastroenterology* **139,** 999–1007, 1007.e1–2 (2010).
96. van der Wegen, P. *et al.* Successful treatment of UGT1A1 deficiency in a rat model of Crigler-Najjar disease by intravenous administration of a liver-specific lentiviral vector. *Mol. Ther.* **13,** 374–381 (2006).
97. Maestri, N. E., Brusilow, S. W., Clissold, D. B. & Bassett, S. S. Long-term treatment of girls with ornithine, transcarbamylase deficiency. *N. Engl. J. Med.* **335,** 855–859 (1996).
98. Rivera-Barahona, A. *et al.* Functional characterization of the spf/ash splicing variation in OTC deficiency of mice and man. *PLoS ONE* **10,** e0122966 (2015).
99. Viecelli, H. M. *et al.* Liver Directed Gene Therapy Using Non-Viral Minicircle-DNA Vector for Ornithine Transcarbamylase Deficiency (OTCD). *Mol. Ther.* **23,** S60–S60 (2015).
100. Poelstra, K., Prakash, J. & Beljaars, L. Drug targeting to the diseased liver. *J Control Release* **161,** 188–197 (2012).
101. Reddy, L. H. & Couvreur, P. Nanotechnology for therapy and imaging of liver diseases. *J. Hepatol.* **55,** 1461–1466 (2011).
102. Wicki, A., Witzigmann, D., Balasubramanian, V. & Huwyler, J. Nanomedicine in cancer therapy: challenges, opportunities, and clinical applications. *J Control Release* **200,** 138–157 (2015).
103. Detampel, P., Witzigmann, D., Krähenbühl, S. & Huwyler, J. Hepatocyte targeting using pegylated asialofetuin-conjugated liposomes. *Journal of Drug Targeting* **22,** 232–241 (2014).
104. Witzigmann, D. *et al.* Biocompatible Polymer–Peptide Hybrid-Based DNA Nanoparticles for Gene Delivery. *ACS Appl. Mater. Interfaces* **7,** 10446–10456 (2015).
105. Witzigmann, D. *et al.* Formation of lipid and polymer based gold nanohybrids using a nanoreactor approach. *RSC Adv.* **5,** 74320–74328 (2015).
106. Gregoriadis, G. & Ryman, B. E. Liposomes as carriers of enzymes or drugs: a new approach to the treatment of storage diseases. *Biochem. J.* **124,** 58P (1971).
107. Bangham, A. D., Standish, M. M., Watkins, J. C. & Weissmann, G. The diffusion of ions from a phospholipid model membrane system. *Protoplasma* **63,** 183–187 (1967).

108. Deamer, D. W. From 'banghasomes' to liposomes: a memoir of Alec Bangham, 1921-2010. *FASEB J.* **24,** 1308–1310 (2010).
109. Allen, T. M. & Cullis, P. R. Liposomal drug delivery systems: from concept to clinical applications. *Adv. Drug Deliv. Rev.* **65,** 36–48 (2013).
110. McIntosh, T. J. The effect of cholesterol on the structure of phosphatidylcholine bilayers. *Biochim. Biophys. Acta* **513,** 43–58 (1978).
111. Torchilin, V. P. Recent advances with liposomes as pharmaceutical carriers. *Nat Rev Drug Discov* **4,** 145–160 (2005).
112. Huwyler, J., Drewe, J. & Krähenbuhl, S. Tumor targeting using liposomal antineoplastic drugs. *Int J Nanomedicine* **3,** 21–29 (2008).
113. Al-Jamal, W. T. & Kostarelos, K. Liposomes: from a clinically established drug delivery system to a nanoparticle platform for theranostic nanomedicine. *Acc. Chem. Res.* **44,** 1094–1104 (2011).
114. Peer, D. *et al.* Nanocarriers as an emerging platform for cancer therapy. *Nat Nanotechnol* **2,** 751–760 (2007).
115. Witzigmann, D., Camblin, M., Huwyler, J. & Balasubramanian, V. in *Biomedical Polymers and Polymer Biomaterials* **8,** 5364–5378 (2015).
116. Elsabahy, M. & Wooley, K. L. Design of polymeric nanoparticles for biomedical delivery applications. *Chem Soc Rev* **41,** 2545–2561 (2012).
117. Kumari, A., Yadav, S. K. & Yadav, S. C. Biodegradable polymeric nanoparticles based drug delivery systems. *Colloids Surf B Biointerfaces* **75,** 1–18 (2010).
118. Mora-Huertas, C. E., Fessi, H. & Elaissari, A. Polymer-based nanocapsules for drug delivery. *Int J Pharm* **385,** 113–142 (2010).
119. He, C., Hu, Y., Yin, L., Tang, C. & Yin, C. Effects of particle size and surface charge on cellular uptake and biodistribution of polymeric nanoparticles. *Biomaterials* **31,** 3657–3666 (2010).
120. Ishiwata, H., Suzuki, N., Ando, S., Kikuchi, H. & Kitagawa, T. Characteristics and biodistribution of cationic liposomes and their DNA complexes. *J Control Release* **69,** 139–148 (2000).
121. Rothkopf, C., Fahr, A., Fricker, G., Scherphof, G. L. & Kamps, J. a. a. M. Uptake of phosphatidylserine-containing liposomes by liver sinusoidal endothelial cells in the serum-free perfused rat liver. *Biochim. Biophys. Acta* **1668,** 10–16 (2005).
122. Xiao, K. *et al.* The effect of surface charge on in vivo biodistribution of PEG-oligocholic acid based micellar nanoparticles. *Biomaterials* **32,** 3435–3446 (2011).

123. Karmali, P. P. & Simberg, D. Interactions of nanoparticles with plasma proteins: implication on clearance and toxicity of drug delivery systems. *Expert Opin. Drug Deliv.* **8,** 343–357 (2011).
124. van Furth, R. *et al.* The mononuclear phagocyte system: a new classification of macrophages, monocytes, and their precursor cells. *Bull. World Health Organ.* **46,** 845–852 (1972).
125. Milla, P., Dosio, F. & Cattel, L. PEGylation of proteins and liposomes: a powerful and flexible strategy to improve the drug delivery. *Curr. Drug Metab.* **13,** 105–119 (2012).
126. Kamaly, N., Xiao, Z., Valencia, P. M., Radovic-Moreno, A. F. & Farokhzad, O. C. Targeted polymeric therapeutic nanoparticles: design, development and clinical translation. *Chem. Soc. Rev.* **41,** 2971–3010 (2012).
127. Lammers, T., Kiessling, F., Hennink, W. E. & Storm, G. Drug targeting to tumors: Principles, pitfalls and (pre-) clinical progress. *J. Control. Release* **161,** 175–187 (2012).
128. Witzigmann, D. *et al.* Variable asialoglycoprotein receptor 1 expression in liver disease: Implications for therapeutic intervention. *Hepatol. Res.* (2015). doi:10.1111/hepr.12599
129. Lammers, T., Aime, S., Hennink, W. E., Storm, G. & Kiessling, F. Theranostic nanomedicine. *Acc. Chem. Res.* **44,** 1029–1038 (2011).
130. Rizzo, L. Y., Theek, B., Storm, G., Kiessling, F. & Lammers, T. Recent progress in nanomedicine: therapeutic, diagnostic and theranostic applications. *Curr. Opin. Biotechnol.* **24,** 1159–1166 (2013).
131. Theek, B., Rizzo, L. Y., Ehling, J., Kiessling, F. & Lammers, T. The Theranostic Path to Personalized Nanomedicine. *Clin Transl Imaging* **2,** 66–76 (2014).
132. Gu, F. *et al.* Precise engineering of targeted nanoparticles by using self-assembled biointegrated block copolymers. *PNAS* **105,** 2586–2591 (2008).
133. Alexis, F., Pridgen, E., Molnar, L. K. & Farokhzad, O. C. Factors Affecting the Clearance and Biodistribution of Polymeric Nanoparticles. *Mol Pharm* **5,** 505–515 (2008).
134. Bertrand, N., Wu, J., Xu, X., Kamaly, N. & Farokhzad, O. C. Cancer nanotechnology: the impact of passive and active targeting in the era of modern cancer biology. *Adv. Drug Deliv. Rev.* **66,** 2–25 (2014).
135. Ashwell, G. & Harford, J. Carbohydrate-specific receptors of the liver. *Annu. Rev. Biochem.* **51,** 531–554 (1982).
136. Morell, A. G., Irvine, R. A., Sternlieb, I., Scheinberg, I. H. & Ashwell, G. Physical and chemical studies on ceruloplasmin. V. Metabolic studies on sialic acid-free ceruloplasmin in vivo. *J. Biol. Chem.* **243,** 155–159 (1968).

137. Drickamer, K. Two distinct classes of carbohydrate-recognition domains in animal lectins. *J. Biol. Chem.* **263,** 9557–9560 (1988).
138. Kilpatrick, D. C. Animal lectins: a historical introduction and overview. *Biochim. Biophys. Acta* **1572,** 187–197 (2002).
139. Stockert, R. J. The asialoglycoprotein receptor: relationships between structure, function, and expression. *Physiol. Rev.* **75,** 591–609 (1995).
140. Baenziger, J. U. & Maynard, Y. Human hepatic lectin. Physiochemical properties and specificity. *J. Biol. Chem.* **255,** 4607–4613 (1980).
141. Bider, M. D., Cescato, R., Jenö, P. & Spiess, M. High-affinity ligand binding to subunit H1 of the asialoglycoprotein receptor in the absence of subunit H2. *Eur. J. Biochem.* **230,** 207–212 (1995).
142. Spiess, M. The asialoglycoprotein receptor: a model for endocytic transport receptors. *Biochemistry* **29,** 10009–10018 (1990).
143. Breitfeld, P. P., Simmons, C. F., Strous, G. J., Geuze, H. J. & Schwartz, A. L. Cell biology of the asialoglycoprotein receptor system: a model of receptor-mediated endocytosis. *Int. Rev. Cytol.* **97,** 47–95 (1985).
144. Geffen, I. & Spiess, M. Asialoglycoprotein receptor. *Int. Rev. Cytol.* **137B,** 181–219 (1992).
145. Schwartz, A. L., Geuze, H. J. & Lodish, H. F. Recycling of the asialoglycoprotein receptor: biochemical and immunocytochemical evidence. *Philos. Trans. R. Soc. Lond., B, Biol. Sci.* **300,** 229–235 (1982).
146. Mu, J. Z., Gordon, M., Shao, J. S. & Alpers, D. H. Apical expression of functional asialoglycoprotein receptor in the human intestinal cell line HT-29. *Gastroenterology* **113,** 1501–1509 (1997).
147. Park, J.-H., Kim, K. L. & Cho, E.-W. Detection of surface asialoglycoprotein receptor expression in hepatic and extra-hepatic cells using a novel monoclonal antibody. *Biotechnol. Lett.* **28,** 1061–1069 (2006).
148. Seow, Y. T., Tan, M. G. K. & Woo, K. T. Expression of a functional asialoglycoprotein receptor in human renal proximal tubular epithelial cells. *Nephron* **91,** 431–438 (2002).
149. Khorev, O., Stokmaier, D., Schwardt, O., Cutting, B. & Ernst, B. Trivalent, Gal/GalNAc-containing ligands designed for the asialoglycoprotein receptor. *Bioorg. Med. Chem.* **16,** 5216–5231 (2008).

150. Andersen, C. B. F. & Moestrup, S. K. How calcium makes endocytic receptors attractive. *Trends Biochem. Sci.* **39,** 82–90 (2014).
151. Piccinotti, S., Kirchhausen, T. & Whelan, S. P. J. Uptake of rabies virus into epithelial cells by clathrin-mediated endocytosis depends upon actin. *J. Virol.* **87,** 11637–11647 (2013).
152. Lee, R. T. & Lee, Y. C. Affinity enhancement by multivalent lectin-carbohydrate interaction. *Glycoconj. J.* **17,** 543–551 (2000).
153. Lundquist, J. J. & Toone, E. J. The cluster glycoside effect. *Chem. Rev.* **102,** 555–578 (2002).
154. Lee, Y. C. *et al.* Binding of synthetic oligosaccharides to the hepatic Gal/GalNAc lectin. Dependence on fine structural features. *J. Biol. Chem.* **258,** 199–202 (1983).
155. Rensen, P. C. N. *et al.* Determination of the Upper Size Limit for Uptake and Processing of Ligands by the Asialoglycoprotein Receptor on Hepatocytesin Vitro and in Vivo. *J. Biol. Chem.* **276,** 37577–37584 (2001).
156. Poelstra, K., Prakash, J. & Beljaars, L. Drug targeting to the diseased liver. *J Control Release* **161,** 188–197 (2012).
157. Trahtenherts, A. & Benhar, I. An internalizing antibody specific for the human asialoglycoprotein receptor. *Hybridoma (Larchmt)* **28,** 225–233 (2009).
158. Dasí, F., Benet, M., Crespo, J., Crespo, A. & Aliño, S. F. Asialofetuin liposome-mediated human alpha1-antitrypsin gene transfer in vivo results in stationary long-term gene expression. *J. Mol. Med.* **79,** 205–212 (2001).
159. Farinha, D., Pedroso de Lima, M. C. & Faneca, H. Specific and efficient gene delivery mediated by an asialofetuin-associated nanosystem. *Int J Pharm* **473,** 366–374 (2014).
160. Singh, M. & Ariatti, M. Targeted gene delivery into HepG2 cells using complexes containing DNA, cationized asialoorosomucoid and activated cationic liposomes. *J Control Release* **92,** 383–394 (2003).
161. Wu, J., Liu, P., Zhu, J. L., Maddukuri, S. & Zern, M. A. Increased liver uptake of liposomes and improved targeting efficacy by labeling with asialofetuin in rodents. *Hepatology* **27,** 772–778 (1998).
162. Kallinteri, P., Liao, W. Y., Antimisiaris, S. G. & Hwang, K. H. Characterization, stability and in-vivo distribution of asialofetuin glycopeptide incorporating DSPC/CHOL liposomes prepared by mild cholate incubation. *J Drug Target* **9,** 155–168 (2001).
163. Mamidyala, S. K. *et al.* Glycomimetic ligands for the human asialoglycoprotein receptor. *J. Am. Chem. Soc.* **134,** 1978–1981 (2012).

164. Stokmaier, D. *et al.* Design, synthesis and evaluation of monovalent ligands for the asialoglycoprotein receptor (ASGP-R). *Bioorg. Med. Chem.* **17,** 7254–7264 (2009).
165. Managit, C., Kawakami, S., Yamashita, F. & Hashida, M. Effect of galactose density on asialoglycoprotein receptor-mediated uptake of galactosylated liposomes. *J Pharm Sci* **94,** 2266–2275 (2005).
166. Morille, M., Passirani, C., Letrou-Bonneval, E., Benoit, J.-P. & Pitard, B. Galactosylated DNA lipid nanocapsules for efficient hepatocyte targeting. *Int J Pharm* **379,** 293–300 (2009).
167. Rensen, P. C. N., van Leeuwen, S. H., Sliedregt, L. A. J. M., van Berkel, T. J. C. & Biessen, E. A. L. Design and synthesis of novel N-acetylgalactosamine-terminated glycolipids for targeting of lipoproteins to the hepatic asialoglycoprotein receptor. *J. Med. Chem.* **47,** 5798–5808 (2004).
168. Shimada, K. *et al.* Biodistribution of liposomes containing synthetic galactose-terminated diacylglyceryl-poly(ethyleneglycol)s. *Biochim. Biophys. Acta* **1326,** 329–341 (1997).
169. Sliedregt, L. A. *et al.* Design and synthesis of novel amphiphilic dendritic galactosides for selective targeting of liposomes to the hepatic asialoglycoprotein receptor. *J. Med. Chem.* **42,** 609–618 (1999).
170. Wang, H.-X., Xiong, M.-H., Wang, Y.-C., Zhu, J. & Wang, J. N-acetylgalactosamine functionalized mixed micellar nanoparticles for targeted delivery of siRNA to liver. *J Control Release* **166,** 106–114 (2013).
171. Westerlind, U. *et al.* Ligands of the asialoglycoprotein receptor for targeted gene delivery, part 1: Synthesis of and binding studies with biotinylated cluster glycosides containing N-acetylgalactosamine. *Glycoconj. J.* **21,** 227–241 (2004).
172. Zhou, X. *et al.* Lactosylated liposomes for targeted delivery of doxorubicin to hepatocellular carcinoma. *Int J Nanomedicine* **7,** 5465–5474 (2012).
173. Fitzgerald, K. *et al.* Effect of an RNA interference drug on the synthesis of proprotein convertase subtilisin/kexin type 9 (PCSK9) and the concentration of serum LDL cholesterol in healthy volunteers: a randomised, single-blind, placebo-controlled, phase 1 trial. *Lancet* **383,** 60–68 (2014).
174. Sehgal, A. *et al.* An RNAi therapeutic targeting antithrombin to rebalance the coagulation system and promote hemostasis in hemophilia. *Nat. Med.* **21,** 492–497 (2015).
175. Wooddell, C. I. *et al.* Hepatocyte-targeted RNAi therapeutics for the treatment of chronic hepatitis B virus infection. *Mol. Ther.* **21,** 973–985 (2013).
176. Mulligan, R. C. The basic science of gene therapy. *Science* **260,** 926–932 (1993).

177. Gene Therapy Clinical Trials Worldwide Home Page. *Retrieved October 2014* (2014). Available at: http://www.abedia.com/wiley/phases.php.
178. Niidome, T. & Huang, L. Gene therapy progress and prospects: nonviral vectors. *Gene Ther.* **9,** 1647–1652 (2002).
179. Kanasty, R., Dorkin, J. R., Vegas, A. & Anderson, D. Delivery materials for siRNA therapeutics. *Nat Mater* **12,** 967–977 (2013).
180. Lorenzer, C., Dirin, M., Winkler, A.-M., Baumann, V. & Winkler, J. Going beyond the liver: progress and challenges of targeted delivery of siRNA therapeutics. *J Control Release* **203,** 1–15 (2015).
181. Sehgal, A., Vaishnaw, A. & Fitzgerald, K. Liver as a target for oligonucleotide therapeutics. *J. Hepatol.* **59,** 1354–1359 (2013).
182. Akinc, A. *et al.* Targeted delivery of RNAi therapeutics with endogenous and exogenous ligand-based mechanisms. *Mol. Ther.* **18,** 1357–1364 (2010).
183. Barrett, S. E. *et al.* Development of a liver-targeted siRNA delivery platform with a broad therapeutic window utilizing biodegradable polypeptide-based polymer conjugates. *J Control Release* **183,** 124–137 (2014).
184. Rozema, D. B. *et al.* Dynamic PolyConjugates for targeted in vivo delivery of siRNA to hepatocytes. *Proc. Natl. Acad. Sci. U.S.A.* **104,** 12982–12987 (2007).
185. Scholz, C. & Wagner, E. Therapeutic plasmid DNA versus siRNA delivery: common and different tasks for synthetic carriers. *J Control Release* **161,** 554–565 (2012).
186. Bardita, C., Predescu, D. & Predescu, S. Long-term silencing of intersectin-1s in mouse lungs by repeated delivery of a specific siRNA via cationic liposomes. Evaluation of knockdown effects by electron microscopy. *J Vis Exp* (2013). doi:10.3791/50316
187. Dehousse, V., Garbacki, N., Colige, A. & Evrard, B. Development of pH-responsive nanocarriers using trimethylchitosans and methacrylic acid copolymer for siRNA delivery. *Biomaterials* **31,** 1839–1849 (2010).
188. Varkouhi, A. K., Scholte, M., Storm, G. & Haisma, H. J. Endosomal escape pathways for delivery of biologicals. *J Control Release* **151,** 220–228 (2011).
189. Liang, W. & W. Lam, J. K. in *Molecular Regulation of Endocytosis* (ed. Ceresa, B.) (InTech, 2012).
190. Shimada, M. *et al.* A monoclonal antibody to rat asialoglycoprotein receptor that recognizes an epitope specific to its major subunit. *Hepatol. Res.* **26,** 55–60 (2003).

191. Stahn, R. & Zeisig, R. Cell adhesion inhibition by glycoliposomes: effects of vesicle diameter and ligand density. *Tumour Biol.* **21,** 176–186 (2000).
192. Schnyder, A., Krähenbühl, S., Drewe, J. & Huwyler, J. Targeting of daunomycin using biotinylated immunoliposomes: pharmacokinetics, tissue distribution and in vitro pharmacological effects. *J Drug Target* **13,** 325–335 (2005).
193. Schnyder, A., Krähenbühl, S., Török, M., Drewe, J. & Huwyler, J. Targeting of skeletal muscle in vitro using biotinylated immunoliposomes. *Biochem. J.* **377,** 61–67 (2004).
194. Schnyder, A. & Huwyler, J. Drug transport to brain with targeted liposomes. *NeuroRx* **2,** 99–107 (2005).
195. Huwyler, J., Yang, J. & Pardridge, W. M. Receptor mediated delivery of daunomycin using immunoliposomes: pharmacokinetics and tissue distribution in the rat. *J. Pharmacol. Exp. Ther.* **282,** 1541–1546 (1997).
196. Huwyler, J., Wu, D. & Pardridge, W. M. Brain drug delivery of small molecules using immunoliposomes. *Proc. Natl. Acad. Sci. U.S.A.* **93,** 14164–14169 (1996).
197. Agnello, V., Abel, G., Elfahal, M., Knight, G. B. & Zhang, Q. X. Hepatitis C virus and other flaviviridae viruses enter cells via low density lipoprotein receptor. *Proc. Natl. Acad. Sci. U.S.A.* **96,** 12766–12771 (1999).
198. Ujino, S. *et al.* Hepatitis C virus utilizes VLDLR as a novel entry pathway. *Proc. Natl. Acad. Sci. U.S.A.* **113,** 188–193 (2016).
199. Rungta, R. L. *et al.* Lipid Nanoparticle Delivery of siRNA to Silence Neuronal Gene Expression in the Brain. *Mol Ther Nucleic Acids* **2,** e136 (2013).
200. Kreuter, J. Nanoparticulate systems for brain delivery of drugs. *Adv. Drug Deliv. Rev.* **47,** 65–81 (2001).
201. Rempe, R., Cramer, S., Qiao, R. & Galla, H.-J. Strategies to overcome the barrier: use of nanoparticles as carriers and modulators of barrier properties. *Cell Tissue Res.* **355,** 717–726 (2014).
202. Herzog, R. W. Recent advances in hepatic gene transfer: more efficacy and less immunogenicity. *Curr Opin Drug Discov Devel* **8,** 199–206 (2005).
203. Nguyen, T. H. & Ferry, N. Liver gene therapy: advances and hurdles. *Gene Ther.* **11 Suppl 1,** S76–84 (2004).

204. Descamps, D. & Benihoud, K. Two key challenges for effective adenovirus-mediated liver gene therapy: innate immune responses and hepatocyte-specific transduction. *Curr Gene Ther* **9,** 115–127 (2009).
205. Haisma, H. J. & Bellu, A. R. Pharmacological interventions for improving adenovirus usage in gene therapy. *Mol. Pharm.* **8,** 50–55 (2011).
206. Schulze, A., Schieck, A., Ni, Y., Mier, W. & Urban, S. Fine mapping of pre-S sequence requirements for hepatitis B virus large envelope protein-mediated receptor interaction. *J. Virol.* **84,** 1989–2000 (2010).
207. Lempp, F. A. & Urban, S. Inhibitors of hepatitis B virus attachment and entry. *Intervirology* **57,** 151–157 (2014).
208. van der Geest, T. *et al.* Comparison of three remote radiolabelling methods for long-circulating liposomes. *J Control Release* **220,** 239–244 (2015).
209. Müller, T. *et al.* Liver imaging with a novel hepatitis B surface protein derived SPECT-tracer. *Mol. Pharm.* **10,** 2230–2236 (2013).
210. Miller, T. *et al.* Premature drug release of polymeric micelles and its effects on tumor targeting. *Int J Pharm* **445,** 117–124 (2013).
211. Yu, B., Lee, R. J. & Lee, L. J. Microfluidic Methods for Production of Liposomes. *Methods Enzymol* **465,** 129–141 (2009).
212. Fischer, D., Li, Y., Ahlemeyer, B., Krieglstein, J. & Kissel, T. In vitro cytotoxicity testing of polycations: influence of polymer structure on cell viability and hemolysis. *Biomaterials* **24,** 1121–1131 (2003).
213. Guidry, E. N. *et al.* Improving the in vivo therapeutic index of siRNA polymer conjugates through increasing pH responsiveness. *Bioconjug. Chem.* **25,** 296–307 (2014).
214. Stroock, A. D. *et al.* Chaotic mixer for microchannels. *Science* **295,** 647–651 (2002).
215. Kastner, E. *et al.* High-throughput manufacturing of size-tuned liposomes by a new microfluidics method using enhanced statistical tools for characterization. *Int J Pharm* **477,** 361–368 (2014).
216. Walsh, C. *et al.* Microfluidic-based manufacture of siRNA-lipid nanoparticles for therapeutic applications. *Methods Mol. Biol.* **1141,** 109–120 (2014).
217. Platt, R. J. *et al.* CRISPR-Cas9 Knockin Mice for Genome Editing and Cancer Modeling. *Cell* **159,** 440–455 (2014).

218. Noteborn, M. H. M. Proteins selectively killing tumor cells. *European Journal of Pharmacology* **625,** 165–173 (2009).

219. Nüesch, J. P. F. & Rommelaere, J. Tumor suppressing properties of rodent parvovirus NS1 proteins and their derivatives. *Adv. Exp. Med. Biol.* **818,** 99–124 (2014).

220. Nüesch, J. P. F., Lacroix, J., Marchini, A. & Rommelaere, J. Molecular pathways: rodent parvoviruses--mechanisms of oncolysis and prospects for clinical cancer treatment. *Clin. Cancer Res.* **18,** 3516–3523 (2012).

221. Wang, L. *et al.* Sustained correction of OTC deficiency in spf ash mice using optimized self-complementary AAV2/8 vectors. *Gene Ther* **19,** 404–410 (2012).

ACKNOWLEDGMENT

A great "**THANK YOU"** to all the people who supported me during my PhD project. You have helped me to perform many experiments, publish excellent papers, develop new ideas, start novel projects, and give my brain a break.

In particular, I would like to thank my doctoral advisor **Prof. Jörg Huwyler** for the opportunity to perform my PhD project under his supervision. It was great to work in his team and I am more than thankful for his support and his trust in all my ideas, projects and collaborations. Thank you for your feedback on the three P, i.e., Publications, Presentations, and Posters. In addition, I am grateful for the opportunity to attend several conferences and seminars to create my own scientific network. Thank you for a great PhD time. I am very much looking forward to our future projects.

For his co-referee of my PhD thesis, for his support in grant applications and the start of a new project, I would like to thank **Prof. Andreas Zumbühl**. I am looking forward to a great collaboration and interesting experiments.

For his chair during my PhD defense, for his support on project ideas, and for the opportunity to attend the "Clinical Pharmacology Seminar", I would like to thank my co-supervisor **Prof. Stephan Krähenbühl**. I have learned many new things and created several ideas during our discussions, especially from a clinical point of view.

Great thanks go to the whole team of the **Pharmaceutical Technology** for all the collaborative work, lab meetings, discussions, lunch and coffee breaks and several social events. In particular, I would like to thank **Philip Grossen**, **Sandro Sieber** and **Stefan Siegrist** for the

"Thirsty Thursdays", private and scientific conversations, and the great time in and outside the lab. Furthermore, I would like to thank **Dr. Susanne Schenk** for her great support, honest feedbacks, and several reviews of my publications and my PhD thesis. There are several **other team members,** who I would to thank for their special help. However, the space in this thesis is limited. I will thank you in person after my defense. Furthermore, I would like to thank some former group members who have influenced my PhD time. **Dr. Pascal Detampel**: Thank you for introducing me into the research topic, for giving me a lot of advice, and for reviewing my PhD thesis. **Dr. Helene Kettiger**: Thank you for many great scientific and social moments. I am looking forward to many more. **Dr. Andrea Allmendinger**: Thank you for the time during student practicals and bringing me to the Bio/Pharma PhD student representatives.

Thanks to all my collaborators from publications: **Dr. Luca Quagliata**, **Dr. Cristina Quintavalle**, and **Prof. Luigi Terracciano** (Molecular Pathology) – thank you for the ASGR1 project. It was a pleasure to work with you. I am looking forward to work with you together in the future. **Dr. Andreas Wicki** (Oncology University Hospital) – thank you for writing together a great, "highly cited" and "most downloaded" review. In addition, thanks for your insights into the oncology field. I am looking forward to work together in the near future. **Natalja Strelnikova** and **Prof. Thomas Pfohl** (Physical Chemistry) – thank you for introducing me to microfluidics. **Dr. Dalin Wu** and **Prof. Wolfgang Meier** (Chemistry, SNI) – Thank you for the chemical synthesis of polymers. **Dr. Vimalkumar Balasubramanian** (Helsinki University) – Thank you for several cooperative projects.

In addition, I would like to thank **Prof. Henriette Meier zu Schwabedissen** for her "open lab policy", her support regarding grant applications, and her encouragement to start the Pharmazentrum PhD Club. In addition, I would like to thank for the collaborative projects with **Daniel Gliesche** and the nice time with the whole "Biopharmacy" group on the 2nd floor.

Prof. Stephan Urban, **Prof. Walter Mier** and **Christina Kaufman** - I would like to thank for a great collaboration on a novel project. I am looking forward to several new experiments and future publications.

Great thanks to **Dr. Andreas Jodal** for being one of my PhD thesis reviewers. Hopefully we have many "Pharma Freiburg Meetings" together with **Dr. Sebastian Wicha** in the future.

I would like to thank the **PhD representatives** of the Biozentrum and the **PhD Club** of the Pharmazentrum for a great time, interesting experiences and many successful events.

Awesome thanks go to the **L´equipe**. Thank you for many great hours, funny evenings, and brilliant holidays. Looking very much forward to mooooore of this!

Great thanks to the **Hochrhein Gang**. Thank you for several funny moments, soccer conversations "GO SCF!" and many enjoyable evenings.

Lovely thanks to my parents (**Edith** and **Hans Witzigmann**), my sister including her family (**Corinna**, **Heiko**, **Mailin** and **Bastian Gloderer**) and my parents in law (**Michael** and **Ulrike Stoltenburg**). Thank you for your tremendous support. It is great to know that I can always count on you.

The greatest thanks go to my **girlfriend Lisa Stoltenburg**. Thank you for your endless support and excellent motivation. It is great to have you by my side. Looking forward to our future.

"This PhD thesis is dedicated to my grandmother…

…I have promised her that she will have a grandchild with a doctor title."